

# Sheffield Hallam University

*The control of metal-NiNGaAs and NiNAIAs interfaces by cryogenic processing.*

CAMMACK, Darren S.

Available from the Sheffield Hallam University Research Archive (SHURA) at:

<http://shura.shu.ac.uk/19420/>

## A Sheffield Hallam University thesis

This thesis is protected by copyright which belongs to the author.

The content must not be changed in any way or sold commercially in any format or medium without the formal permission of the author.

When referring to this work, full bibliographic details including the author, title, awarding institution and date of the thesis must be given.

Please visit <http://shura.shu.ac.uk/19420/> and <http://shura.shu.ac.uk/information.html> for further details about copyright and re-use permissions.

LEARNING CENTRE  
CITY CAMPUS, POND STREET,  
SHEFFIELD, S1 1WB.

101 617 337 7



**REFERENCE**

ProQuest Number: 10694301

All rights reserved

INFORMATION TO ALL USERS

The quality of this reproduction is dependent upon the quality of the copy submitted.

In the unlikely event that the author did not send a complete manuscript and there are missing pages, these will be noted. Also, if material had to be removed, a note will indicate the deletion.



ProQuest 10694301

Published by ProQuest LLC (2017). Copyright of the Dissertation is held by the Author.

All rights reserved.

This work is protected against unauthorized copying under Title 17, United States Code  
Microform Edition © ProQuest LLC.

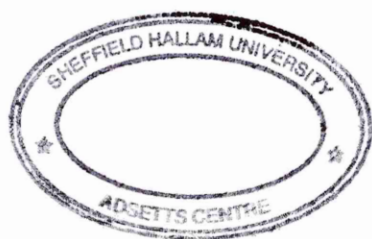
ProQuest LLC.  
789 East Eisenhower Parkway  
P.O. Box 1346  
Ann Arbor, MI 48106 – 1346

**The Control of Metal-nInGaAs and nInAlAs Interfaces by  
Cryogenic Processing**

**Darren S. Cammack**

**A thesis submitted in partial fulfillment of the requirements of  
Sheffield Hallam University for the degree of Doctor of Philosophy**

**August 1999**



# CONTENTS

<b>Abstract</b>	v
<b>Acknowledgements</b>	vi
<b>CHAPTER 1: Introduction</b>	
1.0 General introduction	1
1.1 Aims and objectives	3
1.2 Program of work	3
1.3 The format of this thesis	4
1.4 References	5
<b>CHAPTER 2: Models of Metal-Semiconductor (Schottky) Contacts</b>	
2.0 Introduction	6
2.1 Models for Schottky barrier formation	6
2.1.1 The Schottky-Mott model	6
2.1.2 The Bardeen model (The effect of intrinsic surface states)	8
2.1.3 Intimate contacts	9
2.1.3.1 Metal induced gap states (MIGS)	11
2.1.3.2 The unified defect model (UDM)	12
2.1.3.3 Chemical reactions	12
2.2 Summary	15
2.2.1 Schottky barrier formation	15
2.3 References	16
<b>CHAPTER 3: Theory of Experimental Techniques</b>	
3.0 Introduction	18
3.1 The photoemission process	18
3.2 Photoemission theory	20
3.2.1 The three step model	21
3.3 Photo-ionisation cross section	24
3.4 Surface sensitivity	25
3.4.1 Electron scattering and inelastic mean free path (IMFP)	25
3.4.2 Effective escape depth: Changing the angle of detection	27
3.4.3 Photoelectron diffraction	28
3.5 Core level analysis	28

3.5.1	Structural or surface related shifts	28
3.5.2	Chemical shifts	29
3.5.3	Relaxation	29
3.5.4	Band bending	29
3.5.5	Surface photovoltages	30
3.5.6	Lineshape broadening effects	30
3.5.7	Core level intensities and overlayer growth	31
3.5.8	Spin orbit splitting	32
3.5.9	Assymmetric metal core levels	32
3.5.10	Deconvolution of core level spectra	33
3.6	Low energy electron diffraction (LEED)	34
3.7	Transmission electron microscopy (TEM)	35
3.8	Molecular beam epitaxy (MBE)	36
3.9	Measurement of the Schottky barrier height	37
3.9.1	Photoemission measurements	37
3.10	References	39
<b>CHAPTER 4: Experimental Apparatus and Procedures</b>		
4.0	Introduction	41
4.1	The Daresbury experimental system (Beamline 4.1)	41
4.1.1	The Daresbury synchrotron radiation source	41
4.1.2	Beamline 4.1	42
4.1.3	Beamline 4.1 analysis chamber	44
4.1.4	Sample preparation	46
4.1.5	Metal evaporation sources	47
4.1.6	The Scienta SES energy analyser	49
4.1.7	LEED apparatus	52
4.2	The Sheffield Hallam microlab	53
4.2.1	Sample mounting and heater stage	53
4.2.2	The microlab X-ray sources	54
4.2.3	The Microlab energy analyser	54
4.3	The transmission electron microscope and sample preparation	55
4.4	References	56

## **CHAPTER 5: Arsenic Decapping of The $\text{In}_{0.53}\text{Ga}_{0.47}\text{As}(100)$ Surface**

5.0	Introduction	57
5.1	Arsenic cap sublimation	58
5.1.1	Core level photoemission	59
5.1.2	Clean surface stoichiometry	60
5.2	Summary	61
5.3	References	63

## **CHAPTER 6: Metal- $\text{In}_{0.53}\text{Ga}_{0.47}\text{As}(100)$ Interfaces Formed as a Function of Temperature**

6.0	Introduction	64
6.1	Photoemission studies	65
6.1.1	Introduction	65
6.1.2	Experimental details	66
6.1.3	The clean $(3\times 1)$ reconstructed $\text{In}_{0.53}\text{Ga}_{0.47}\text{As}(100)$ surface	66
6.1.4	$\text{In-In}_{0.53}\text{Ga}_{0.47}\text{As}(100)$ interface formation	69
6.1.5	$\text{Au-In}_{0.53}\text{Ga}_{0.47}\text{As}(100)$ interface formation	76
6.2	Microscopy studies	82
6.2.1	Introduction	82
6.2.2	The $\text{In-In}_{0.53}\text{Ga}_{0.47}\text{As}(100)$ interface	82
6.2.3	The $\text{Au-In}_{0.53}\text{Ga}_{0.47}\text{As}(100)$ interface	83
6.3	Summary	83
6.3.1	The $\text{In-In}_{0.53}\text{Ga}_{0.47}\text{As}(100)$ interface	83
6.3.2	The $\text{Au-In}_{0.53}\text{Ga}_{0.47}\text{As}(100)$ interface	84
6.4	References	85

## **CHAPTER 7: Metal- $\text{In}_{0.52}\text{Al}_{0.48}\text{As}(100)$ Interfaces Formed as a Function of Temperature**

7.0	Introduction	87
7.1	Photoemission studies	87
7.1.1	Introduction	87
7.1.2	Experimental details	88
7.1.3	The Clean $(3\times 1)$ reconstructed $\text{In}_{0.52}\text{Al}_{0.48}\text{As}(100)$ surface	89
7.1.4	$\text{In-In}_{0.52}\text{Al}_{0.48}\text{As}(100)$ interface formation	91
7.1.5	$\text{Au-In}_{0.52}\text{Al}_{0.48}\text{As}(100)$ interface formation	97

7.2	Microscopy studies	102
7.2.1	Introduction	102
7.2.2	The Au-In <sub>0.52</sub> Al <sub>0.48</sub> As(100) interface	102
7.3	Summary	103
7.3.1	In-In <sub>0.52</sub> Al <sub>0.48</sub> As(100) interface formation	103
7.3.2	Au-In <sub>0.52</sub> Al <sub>0.48</sub> As(100) interface formation	104
7.4	References	105
<b>CHAPTER 8: Discussion and Conclusions</b>		
8.0	Introduction	107
8.1	Summary of experimental results	107
8.2	Discussion: Schottky barrier formation	111
8.3	Conclusions	114
8.4	Future work	115
8.5	References	117

## ABSTRACT

The physical and chemical properties of In- and Au- interfaces with  $\text{In}_{0.53}\text{Ga}_{0.47}\text{As}/\text{InP}(100)$  and  $\text{In}_{0.52}\text{Al}_{0.48}\text{As}(100)$  formed at room and low temperatures have been studied. Current-voltage measurements have indicated that In contacts to  $\text{In}_{0.53}\text{Ga}_{0.47}\text{As}(100)$  formed at 80K exhibit significantly higher Schottky barriers ( $\phi_b = 0.45$  eV) than In diodes formed at 294K ( $\phi_b = 0.30$  eV), whereas Au diodes formed on  $\text{In}_{0.53}\text{Ga}_{0.47}\text{As}(100)$  at either low temperature or room temperature exhibit Ohmic behaviour. The reactions occurring during interface formation at room and low temperatures have been investigated using soft X-ray photoemission spectroscopy (SXPS) and Transmission Electron Microscopy (TEM).

The results presented show that In metallisation of  $\text{In}_{0.53}\text{Ga}_{0.47}\text{As}(100)$  at room temperature results in a predominantly three dimensional mode of growth, accompanied by the out-diffusion of As. Low temperature (125K) metallisation appears to reduce clustering and inhibit As out-diffusion. Examination of the resulting interfaces by TEM confirm the more uniform nature of the metal layers formed at low temperature. Metallisation temperature seems to have little effect on the formation of Au- $\text{In}_{0.53}\text{Ga}_{0.47}\text{As}(100)$  interfaces, other than to reduce the extent of overlayer clustering, with As out-diffusion apparent for both low and room temperature Au deposition.

Interfaces formed between In and  $\text{In}_{0.52}\text{Al}_{0.48}\text{As}(100)$  at both low and room temperature were relatively abrupt with no out-diffusion of substrate species into the metal overlayer. Low temperature metallisation again appeared to reduce overlayer clustering, with TEM studies showing a smaller grain size at low temperature. Au deposition onto  $\text{In}_{0.52}\text{Al}_{0.48}\text{As}(100)$  produced similar interfaces formed at room and low temperature. As diffuses into the Au overlayer to form an Au/As compound at both temperatures, resulting in an interface that is complex and reacted. The degree of overlayer clustering is also thought to be much less pronounced for Au deposition compared to In deposition.

Barrier heights measured by SXPS during the study, show good agreement with reported current-voltage measurements for Au and In diodes formed on both  $\text{In}_{0.53}\text{Ga}_{0.47}\text{As}/\text{InP}(100)$  and  $\text{In}_{0.52}\text{Al}_{0.48}\text{As}(100)$ . Possible mechanisms for the observed adaptation of the pinning position are discussed in the context of current models of Schottky barrier formation.

## Acknowledgements

I would like to start by thanking my Director of Studies, Dr. Simon Clark for all his help, advice and friendship during my PhD. His proof reading along with Dr. I.M. Dharmadasa has been invaluable and is much appreciated. My thanks go also to Dr. Steven Wilks, Dr. Steve Burgess, Min Pan, Mark Pritchard and especially Dr. Peter Dunstan all at Swansea University, for their help and support during the long days and nights at Daresbury. The support of the staff on beamlines 4.1 and 6.1 at CLRC Daresbury is also gratefully acknowledged. Similarly I would like to thank Dr. Francesca Peiró, Dr. Albert Cornet and Juan-Carlos Ferrer at the Universitat de Barcelona for their help with the TEM studies, and for giving me the opportunity to visit their fantastic city.

Many thanks go to all the great friends I made at Sheffield Hallam for making my time there such an enjoyable one. A special note goes to the boys at Edgecumbe namely Dr. Steve McHugh, Dr. Steve Thompson and Dr. Stuart Mills with whom I spent three great years. Cheers.

Finally I would like to thank my parents, family and friends back home in Manchester who have kept me sane and solvent over the past few years. Without you none of this would have been possible. I hope it was worth it.

# Chapter 1

## Introduction

### 1.0 General introduction

Advances in modern technology over the past twenty years have led to a massive change in the way society conducts itself. From business to shopping, leisure to learning, microelectronics now plays a major part in the everyday lives of people all over the world. This is, in part, due to the development of smaller, faster and more efficient electronic devices that are based on the electronic properties of semiconductor materials.

Silicon and Germanium, which come from group IV in the periodic table, were the first semiconducting materials to be employed for solid state devices. However the range of applications for devices incorporating these materials is restricted due to their indirect band gaps and low mobilities. Hence the need for semiconductor materials with a wider range of physical properties (i.e. greater mobilities and direct band gaps) prompted an increase in the research into semiconductor technology. Semiconductor compounds formed by combining elements from group III with elements from group V of the periodic table (“III-V” materials) offer such properties and perhaps the most widely studied of the III-V materials is the binary compound gallium arsenide (GaAs). GaAs has a greater carrier mobility than Si resulting in improved operating frequencies over Si based devices. Furthermore the direct band gap of GaAs ( $E_g = 1.42$  eV at room temperature) lends itself to optoelectronic devices operating in the near infrared region of the electromagnetic spectrum. More recently, ternary compounds such as  $\text{In}_x\text{Ga}_{1-x}\text{As}$  and  $\text{In}_y\text{Al}_{1-y}\text{As}$  have offered a new degree of freedom in that by altering the alloy compositions  $x$  and  $y$ , an even wider range of energy gaps and mobilities can be accessed.

Electronic devices require the use of almost entirely pure semiconductor materials, into which a small amount of foreign dopant atoms can be added to control their electronic properties. The semiconductor must also be in the form of a pure single crystal throughout the device, as its electronic properties depend enormously on the

ordered, periodic nature of the crystal structure. Any crystal imperfections may be detrimental to the device performance. Modern growth techniques such as molecular beam epitaxy (MBE) are capable of growing such high quality ordered structures with the compilation of atomic layer upon atomic layer. Lattice matched  $\text{In}_y\text{Al}_{1-y}\text{As}/\text{In}_x\text{Ga}_{1-x}\text{As}/\text{InP}(100)$  heterostructures ( $x = 0.53$ ,  $y = 0.52$ ) grown by MBE, show great promise in the fabrication of optoelectronic and high frequency devices [1].

These materials are, however, no use in electronic components unless electrical contacts can be made to the devices, through which to apply voltages and collect current. In general, these contacts are made by depositing a metal on to the semiconductor surface and provide electrical connection between the device and the “outside world”. These metal-semiconductor contacts which can be linear, (“Ohmic contacts”) or rectifying, (“Schottky contacts”) can also play an active role in the performance of a semiconductor device. The ideal rectifying contact should exhibit a suitably high Schottky barrier, which restricts current flow to the direction away from the device, low leakage currents and high reliability. The linear contact should be of low resistivity and hence offer no significant barrier to current flow in either direction at the contact. The acquisition of these characteristics for metal-  $\text{In}_y\text{Al}_{1-y}\text{As}$  and  $\text{In}_x\text{Ga}_{1-x}\text{As}$  contacts will depend on the chemical, physical and electronic nature of the metal-semiconductor interface and hence represents a significant challenge to device engineers and physicists.

Metal- $\text{In}_x\text{Ga}_{1-x}\text{As}$  Schottky contacts obtained by conventional room temperature metallisation techniques usually produce low barrier heights ( $\phi_b \approx 0.2$  eV) which renders them unsuitable for non-linear (Schottky) contacts. However recent current-voltage (I-V) studies have shown that the barrier heights at  $\text{In-In}_{0.53}\text{Ga}_{0.47}\text{As}$  contacts can be greatly improved ( $\phi_b \approx 0.45$  eV) if the metallisation process is carried out at greatly reduced temperatures ( $\approx 77\text{K}$ ) [2]. Clearly, this represents a significant advance in  $\text{In}_{0.53}\text{Ga}_{0.47}\text{As}$  processing and should prove to be extremely beneficial to industry for the production of commercial devices. The exact mechanism that produces the barrier height enhancement is however, unclear. Photoemission studies of metal interfaces with As decapped  $\text{GaAs}(100)$  surfaces held at low temperature have indicated that barriers formed at these surfaces are dependent on the chemical reactivity of the metal-semiconductor interface, resulting in a Fermi level that is pinned by the introduction of surface states within the forbidden gap. It was proposed that the use of low temperatures

(~100K) inhibited these chemical reactions producing an unpinned surface with barriers approaching the Schottky limit [3,4]. However the validity of this hypothesis was explored by Wilks *et al.* using the I-V technique for diodes formed on “as grown” GaAs(100) surfaces at room and low temperatures. Here no correlation between  $\phi_b$  and metal work function was observed [5]. These experiments were extended to intimate metal-In<sub>0.53</sub>Ga<sub>0.47</sub>As(100) interfaces by Clark *et al.* who also found no correlation between metal work function and  $\phi_b$  for Schottky barriers formed at low temperature [2].

To date no work has been carried out on the low temperature metallisation of In<sub>y</sub>Al<sub>1-y</sub>As(100). Metal-In<sub>y</sub>Al<sub>1-y</sub>As Schottky contacts formed at room temperature, produce higher barriers ( $\phi_b \approx 0.8-0.9\text{eV}$ ), however, preliminary studies of the interface formation by X-ray photoemission spectroscopy (XPS) indicate that these interfaces are complex and non-abrupt, and that the Fermi level in the semiconductor is pinned before metallisation [6].

## 1.1 Aims and objectives

The aims and objectives of this project are to investigate the basic physics of the reactions that occur during the formation of the metal-In<sub>0.53</sub>Ga<sub>0.47</sub>As and In<sub>0.52</sub>Al<sub>0.48</sub>As/InP(100) interfaces at room and low temperatures, using photoemission spectroscopy and electron microscopy techniques. The aim is that, by correlation with electron transport measurements, a greater understanding of the significance of interface formation temperature with regard to future device processing will be obtained.

## 1.2 Program of work

In figure 1.1, a flow chart describing the various stages of work undertaken in this study is presented. The starting point and motivation behind this study was the previous I-V studies of metal deposition onto In<sub>0.53</sub>Ga<sub>0.47</sub>As(100) at room and low temperatures. A brief decapping study of As capped In<sub>0.53</sub>Ga<sub>0.47</sub>As(100) was then undertaken at Sheffield Hallam University using x-ray photoelectron spectroscopy (XPS). The clean surface achieved after As decapping was investigated more thoroughly by the use of high resolution, surface sensitive soft x-ray photoelectron spectroscopy

(SXPS) and low energy electron diffraction (LEED). Following the characterisation of the clean surface, the formation of the metal-In<sub>0.53</sub>Ga<sub>0.47</sub>As(100) interface was examined by SXPS as a function of metal type and temperature. The resulting metal-In<sub>0.53</sub>Ga<sub>0.47</sub>As(100) interfaces were then characterised by transmission electron microscopy (TEM). The above procedure was then repeated for the metal-In<sub>0.52</sub>Al<sub>0.48</sub>As(100) system.

### 1.3 The format of this thesis

In chapter 2, the various models describing Schottky barrier formation at a metal-semiconductor interface are discussed along with the mechanisms for electron transport across the Schottky barriers formed. Chapters 3 and 4 describe the theory and experimental apparatus used in this study, respectively. The results of a preliminary XPS decapping study of As capped In<sub>0.53</sub>Ga<sub>0.47</sub>As(100) are presented in chapter 5, and following on from this, the formation of intimate In and Au interfaces with clean decapped In<sub>0.53</sub>Ga<sub>0.47</sub>As(100) and In<sub>0.52</sub>Al<sub>0.48</sub>As(100) are examined by SXPS in chapters 6 and 7, respectively. The results are summarised and discussed in chapter 8, in relation to currently understood models for Schottky barrier formation and finally possible areas of future study are considered.

## 1.4 References

- [1] H.J. Lee, W.A. Anderson, H. Hardtdegen and H. Lüth, Appl. Phys. Lett. **63**, 1939, (1993).
- [2] S.A. Clark, S.P. Wilks, A. Kestle, D.I. Westwood and M. Elliott, Surf. Sci. **352-354**, 850 (1996)
- [3] R.E. Vitturo, S. Chang, J.L. Shaw, L.J. Brillson, P.D. Kirchner and J.M. Woodall, J. Vac. Sci. Technol. **B7**, 1007 (1989)
- [4] S.Chang, J.L. Shaw, R.E. Vitturo, L.J. Brillson, P.D. Kirchner and J.M. Woodall, J. Vac. Sci. Technol. **A8**, 3803 (1990)
- [5] S.P. Wilks, J.I. Morris, D.A. Woolf and R.H. Williams, J. Vac. Sci. Technol. **B9(4)**, 2118-2121 (1991).
- [6] S.A. Clark, S.P. Wilks, J.I. Morris, D.A. Woolf and R.H. Williams, J. Appl. Phys., **75(5)**, 2481, (1994).

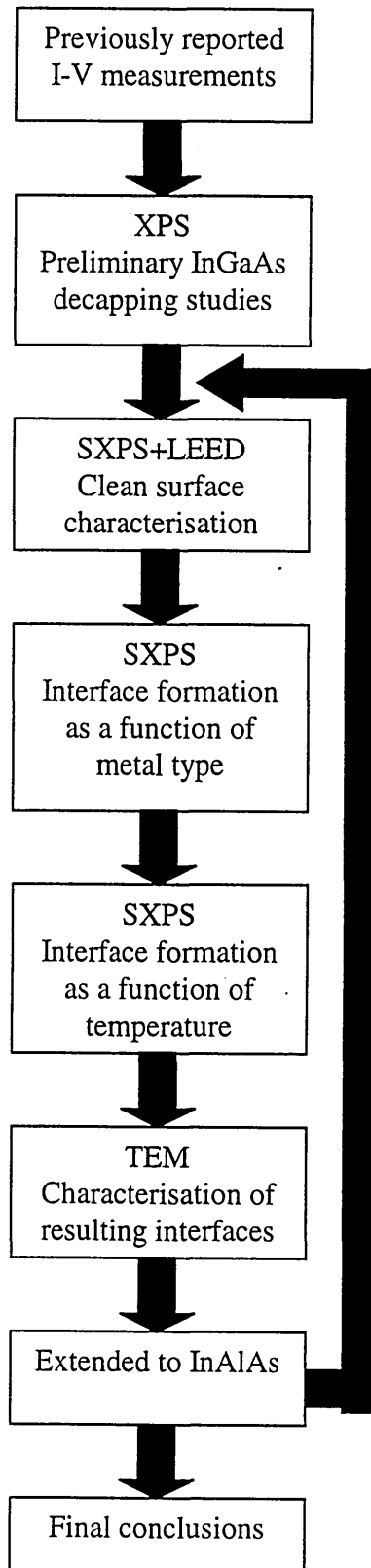


Figure 1.1: A flow chart outlining the program of work undertaken during this study.

# Chapter 2

## Models of metal-semiconductor (Schottky) contacts and electron transport across the potential barrier

### 2.0 Introduction

The contact potential at a metal-semiconductor interface is called a Schottky barrier. The difference in energy between the Fermi level of the metal and the semiconductor conduction band minimum at the interface is defined as the Schottky barrier height  $\phi_b$ .

A variety of models have been proposed to account for various experimentally observed phenomena relating to the formation of Schottky barriers, and these have been reviewed in detail elsewhere [1]. In this chapter, the models most relevant to the present study are described.

As yet,  $\phi_b$  has not been predicted consistently or accurately by any one particular model that has been proposed. This is likely to be due to the fact that many processes contribute to the electronic structure of the interface and hence the value of the Schottky barrier,  $\phi_b$ .

### 2.1 Models for Schottky barrier formation

#### 2.1.1 The Schottky-Mott model

Barriers at metal-semiconductor contacts, which follow the simple Schottky model, are determined by the difference in the work function of the metal ( $\phi_m$ ), and the electron affinity ( $\chi_s$ ), or work function ( $\phi_s$ ), of the semiconductor [2]. The energy-band diagram for an n-type semiconductor and metal that are electrically neutral and separated is shown in Fig. 2.1 (a). In practice, the most important case is when the work function of the semiconductor is less than that of the metal, and we assume that there are no surface states present. When the metal and semiconductor are brought into contact, electrons flow from the semiconductor into the metal until the Fermi levels align. This

produces a region of uncompensated positive donor ions that is depleted of electrons. The electrostatic field associated with this depletion region increases from zero to a maximum, from bulk semiconductor to the metal-semiconductor interface. As a result, the energy bands bend up at the interface.

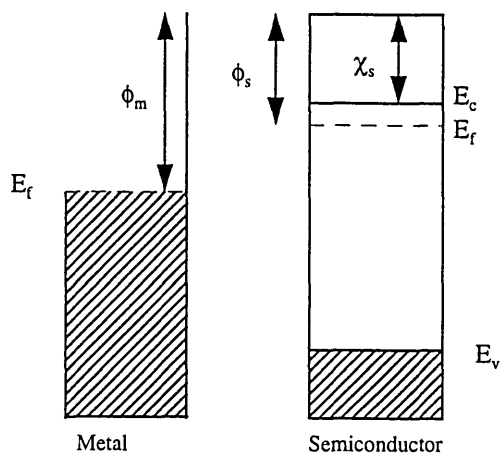
Fig. 2.1 (c) shows the resultant barrier height ( $\phi_b$ ). The barrier height is defined as,

$$\phi_b = \phi_m - \chi_s \quad [2.1]$$

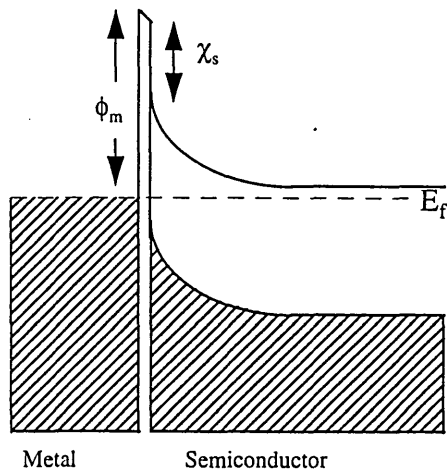
In the case where  $\phi_m > \phi_s$ , electrons have great difficulty overcoming the potential barrier ( $\phi_b$ ) when flowing from the metal to the semiconductor. This is described as a rectifying “Schottky” contact and better rectifying characteristics are acquired if  $\phi_b$  is large and has a wide depletion region. By contrast, if  $\phi_s > \phi_m$ , the bands in the semiconductor will bend down at the interface and the electrons will encounter no potential barrier. There is therefore no resistance to current flow in either direction and the junction is termed “Ohmic”.

Experimental evidence for most semiconductors does not support equation 2.1, due to the fact that it neglects the effects of interface states [1]. Furthermore, the ideal metal-semiconductor junction as shown in Fig. 2.1 (c) is unlikely to be achieved because there is normally a thin insulating layer of oxide on the surface of the semiconductor. This interfacial oxide layer gives rise to a junction more in common to that shown in Fig. 2.1 (b).

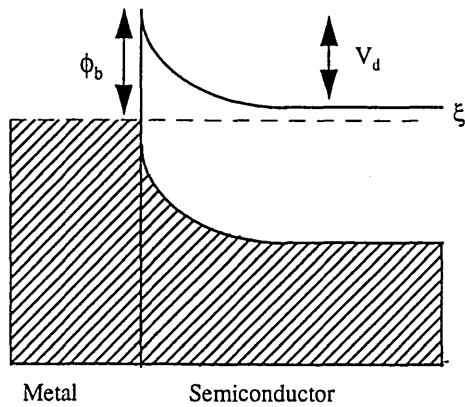
Equation 2.1 was first stated independently by Schottky [3] and Mott [4] and is referred to as the Schottky-Mott limit. The problem with this theory is that it assumes that the difference between surface dipole contributions to  $\phi_m$  and  $\chi_s$  do not change when the metal and semiconductor are brought into contact. It also assumes that there is perfect contact between the metal and semiconductor (i.e. there is no intervening layer) and that there are no localised states on the surface of the semiconductor.



(a)



(b)



(c)

Figure 2.1: Formation of a Schottky barrier between a metal and semiconductor.

(a) Neutral and separated, (b) Separated by an insulating film, (c) in perfect contact.

### 2.1.2 The Bardeen model (The effect of intrinsic surface states)

At the surface of a solid, the bulk periodic potential is abruptly terminated, resulting in a perturbation of the conditions that determine band gaps in the bulk of the semiconductor. Consequently surface states may exist, with wave functions that correspond to the complex values of the wave vector  $\underline{k}$ , which decay exponentially with distance from the surface to the bulk. These states are known as intrinsic surface states as they are a property of the semiconductor and exist on a perfect free surface in an ideal solid. It is possible for these intrinsic surface states to be located in the forbidden gap of the semiconductor.

It has been suggested by Bardeen, that the barrier height does not have such a strong dependence on  $\phi_m$  as equation [2.1] may suggest, and in some cases the barrier height is independent of the choice of metal [5]. This independence of  $\phi_m$  can be explained by the effect of intrinsic surface states, which are assumed to be uniformly distributed throughout the semiconductor band gap with a density  $D_{SS}$ . The main concept of the Bardeen model is that there is a charge neutrality level  $\phi_0$  within the band gap. If the surface states within the gap are filled with electrons up to this level, the charge on the surface will be neutral. Surface states that appear below  $\phi_0$  are known as donor-like states (i.e. positive when empty) and states that occur above are acceptor-like (negative when filled). When a surface is formed, electrons in the conduction band will flow into the preferred lower energy surface states above  $\phi_0$ , producing a depletion region in the semiconductor. The transfer of charge induces a shift in the Fermi level relative to the band edges, and hence the bands will bend producing a potential barrier at the semiconductor surface. This charge transfer will continue until the Fermi level coincides with the highest occupied surface state as shown in figure 2.2 (a-c). The difference in energy between the Fermi level and the charge neutrality level is dependant on  $D_{SS}$ . The Fermi level and the charge neutrality level will be almost coincident for a large density of surface states ( $D_{SS} \rightarrow \infty$ ), and at this point it is said that the Fermi level is pinned due to the high density of surface states.

When a metal comes into contact with the semiconductor, there is a transfer of charge similar to that in the Schottky case, again this transfer of charge continues until the Fermi levels align. If the density of states is sufficiently large, this charge transfer will take place between the metal and the intrinsic surface states, without modifying the

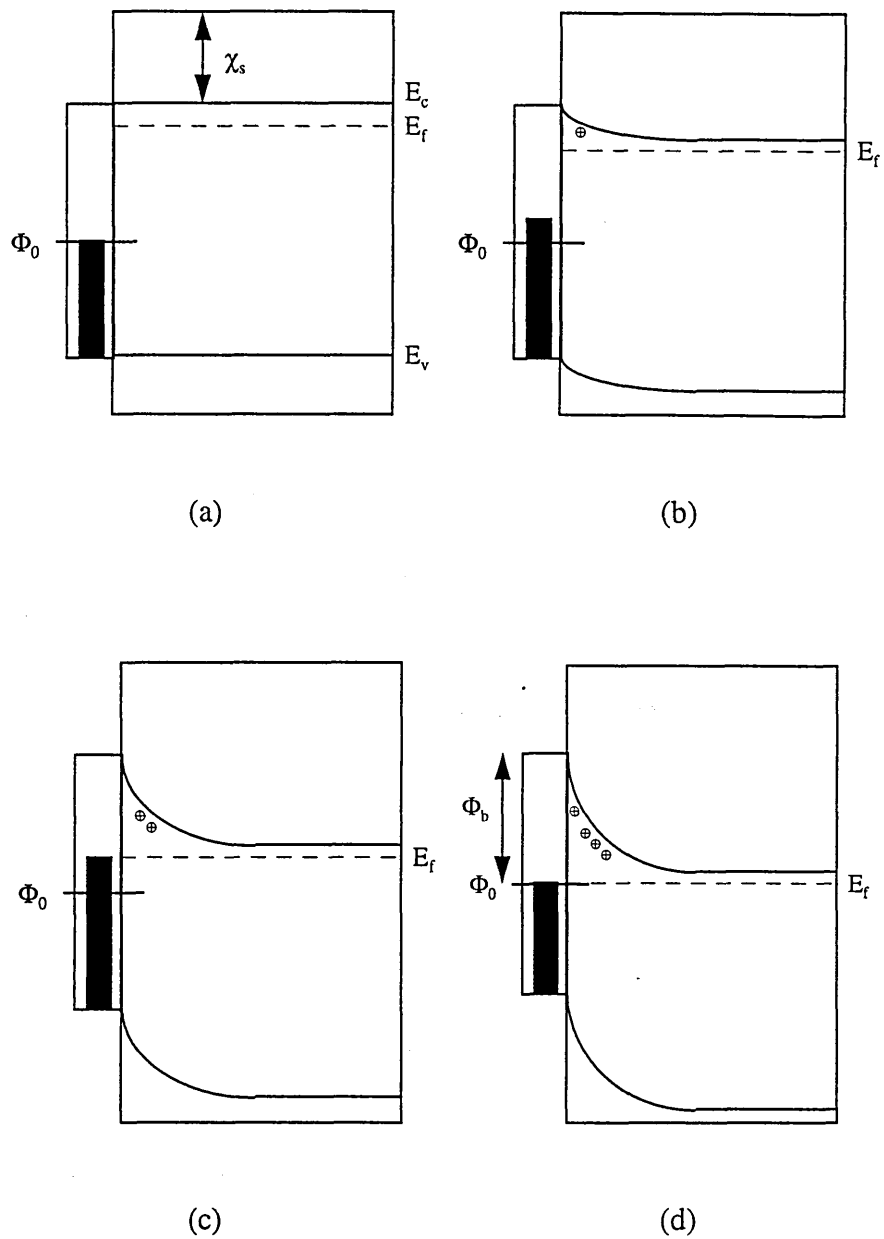


Figure 2.2: The role played by surface states on a clean semiconductor surface; (a) Surface states are filled up to the charge neutrality level  $\phi_0$  for the initial, non equilibrium condition, (b) Still in non-equilibrium, electrons from the conduction band move to fill the surface states above  $\phi_0$ , (c) Equilibrium condition is reached for a semiconductor with a low density of surface states, (d) Equilibrium condition for a semiconductor with a very large density of surface states, as  $D_{ss} \rightarrow \infty$ ,  $E_f \rightarrow \phi_0$ .

space charge region in the semiconductor as shown in figure 2.3. This results in a negligible movement of the semiconductor Fermi level position and the semiconductor is said to be screened from the metal. For the situation where a metal is separated from an n-type semiconductor by a thin insulating layer, Rhoderick and Williams have shown that the pinning of the Fermi level by intrinsic surface states results in a barrier height given by,

$$\phi_b = \gamma(\phi_m - \chi_s) + (1-\gamma)(E_g - \phi_0) \quad [2.2]$$

for an insulating layer of width  $\delta$  ( $\delta \sim$  several Ångströms) and permitivity  $\epsilon$  [1].  $E_g$  is the energy gap, and  $\gamma$  is given by,

$$\gamma = \epsilon / (\epsilon + e\delta D_{SS}) \quad [2.3]$$

Hence for a large density of states,  $D_{SS} \rightarrow \infty$ , and  $\gamma \rightarrow 0$  leading to a barrier height given by,

$$\phi_b = E_g - \phi_0 \quad [2.4]$$

This is known as the Bardeen limit, and the barrier height is seen to be independent of the metal used. The Fermi level is pinned at  $\phi_0$  by the high density of surface states ( $D_{SS} > 10^{13} \text{ cm}^{-2}\text{eV}^{-1}$ ) [1].

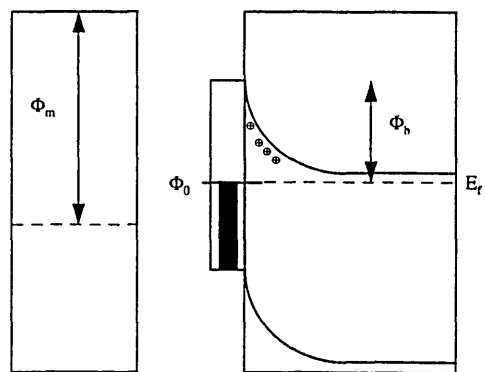
Conversely, when there are no surface states present,  $D_{SS} \rightarrow 0$ , and  $\gamma \rightarrow 1$  leading to a barrier height given by,

$$\phi_b = \phi_m - \chi_s \quad [2.1]$$

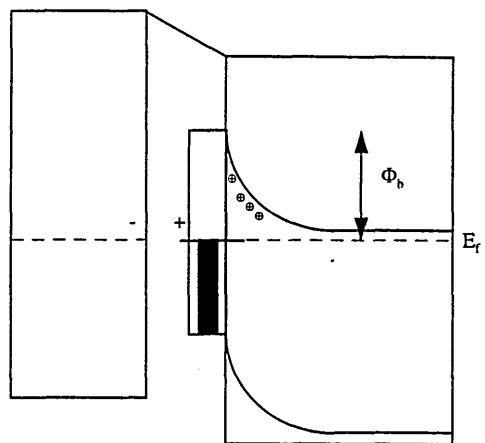
and so the barrier height is again governed by the Schottky limit, and dependent on the metal contact used.

### 2.1.3 Intimate contacts

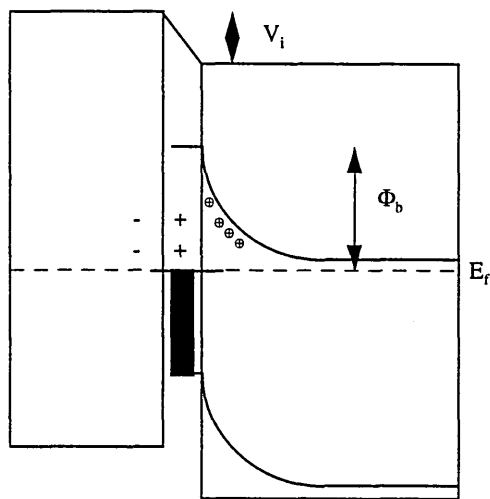
In the case of the Bardeen model a thin insulating layer separates the metal-semiconductor interface. The insulating layer is thin enough to allow electrons to tunnel through it easily, but is also thick enough to assume that the intrinsic states on the semiconductor surface are not affected by the coupling of the semiconductor and the metal.



(a)



(b)



(c)

Figure 2.3: A metal in contact with a semiconductor with a high density of surface states, (a) before contact, (b) electrically connected with transfer of charge between the metal and surface states and (c) large density of surface states shield the semiconductor from the contact potential and  $E_f$  is pinned at  $\phi_0$ .

It is possible that states may be formed as a consequence of interactions between the metal and the semiconductor during the formation of an interface. States formed in this way are described as extrinsic surface states and in sufficient density are also capable of pinning the Fermi level as described by the Bardeen model.

Metal contacts can be deposited onto atomically clean surfaces using ultra high vacuum (UHV) systems. Clean surfaces can be obtained by heating the semiconductor, desorption of a protective cap or by cleaving in UHV. The latter technique has a disadvantage in that cleaving is restricted to a few crystal planes, such as the (110) plane for III-V semiconductors. Interfaces formed on atomically clean surfaces are described as intimate, and the extrinsic surface states at these interfaces can be determined by a number of important factors.

- (a) In the majority of cases, metal films on semiconductors are polycrystalline with the exact nature of the polycrystalline layer dependent on the deposition conditions. It is likely that the distribution of states at the metal-semiconductor interface will be dependent on the structure of the metal overlayer.
- (b) Atoms from the metal may diffuse into the semiconductor adopting substitutional or interstitial positions, leaving the interface non-abrupt and defected. Atoms may also diffuse from the semiconductor into the metal overlayer. Either outcome may adapt the density of interface states present at the interface.
- (c) Many metals will undergo strong chemical reactions when they are deposited on semiconductor surfaces, leading to the formation of a compound layer at the interface. The electronic properties are sensitive to the nature and order of such layers.

Modern surface science techniques such as LEED allow us to probe the structure of thin films, while SXPS lets us investigate chemical reactions and interdiffusion when the metal contact is only a few Ångströms thick. These techniques are described in more detail in chapter 3.

The following section discusses the various sources of extrinsic surface states. It should be noted that the pinning process may be a factor of several mechanisms mentioned in this section, with one or more being dominant under differing conditions.

### 2.1.3.1 Metal Induced Gap States (MIGS)

In 1965, Heine [6] proposed that metal induced gap states (MIGS) would replace any intrinsic electron states in the semiconductor band gap, which may be present on a free semiconductor surface, when a metal is deposited on that surface.

The MIGS are associated with the electrons from the metal that tunnel into the forbidden gap of the semiconductor. The wave functions of the electrons decay exponentially into the semiconductor leaving tails that penetrate the semiconductor up to a depth of a few Ångströms. These wavefunctions are associated with a continuum of interface states.

If there is a sufficiently large density of such extrinsic states ( $\sim 10^{14}$  states  $\text{cm}^{-2}$   $\text{eV}^{-1}$ ) [1], they will replace the intrinsic surface states and pin the Fermi level in the same way as described by Bardeen. Cohen and co-workers have conducted theoretical studies of MIGS for interfaces between Al and a number of semiconductors including Si, ZnSe and GaAs. For the case of Si, well into the semiconductor the density of states reflected that of bulk silicon and the band gap was well defined. Well into the metal, the density of states were free electron like with states occupied up to the Fermi level. At the interface however, extra states were seen in the band gap around  $E_f$  extending into the semiconductor for a few atomic layers [7-9]. Yndurain [10] and Tejedor, Flores and Louis [11] have shown that the MIGS at the interface can be derived from a decrease in the density of states in the valence and conduction bands of the semiconductor. This results in a continuum of states within the energy gap with a charge neutrality level at the midpoint of the band gap. Tersoff stated that this neutral level must lie at or near to the energy  $E_B$ , defined as the energy where the MIGS states cross over from being valence band type to conduction band type. He agreed with Tejedor, Flores and Louis that this should occur near to the centre of the band gap [10] and the Fermi level should be pinned close to the charge neutrality level, as in the Bardeen theory. This theory suggests that the barrier height is independent of the metal deposited, however Tersoff has adapted his theory to account for a weak dependence on the metal that varies the pinning position around the mid point of the band gap [13].

The fundamental concept of the MIGS model is therefore that the metal can induce Bardeen like states in the energy gap that pin the Fermi level. This model is supported by experimental evidence for thick metal overlayers on III-IV semiconductors

[14], although it cannot account for Fermi level shifts observed at sub-monolayer coverage's (i.e. when the overlayer is not completely of a metallic nature and hence the wavefunction in the metal is not completely defined).

### 2.1.3.2 The Unified Defect Model (UDM)

Spicer *et al.* [15] have proposed the Unified Defect Model (UDM) to account for Fermi level shifts observed by XPS that were apparent at sub-monolayer metal coverages that were considered too small to be accounted for by the MIGS model. The central assumption in the UDM is that defects or vacancies are generated in the semiconductor crystal lattice close to the interface upon metal deposition. These defects can perturb the intrinsic surface states to form discontinuous bands of sufficient density to pin the Fermi level in a similar nature to that described by the Bardeen model.

Spicer *et al.* observed interface states at energy levels of 0.75eV and 0.5eV above the valence band in GaAs(100) that were attributed to missing As acceptor sites and missing Ga donor sites respectively [15,16]. In order to pin the Fermi level at clean or low metal coverages it has been estimated that defect densities of the order of  $\sim 10^{12} \text{eV}^{-1} \text{cm}^{-2}$  are required. This density increases to  $\sim 10^{14} \text{eV}^{-1} \text{cm}^{-2}$  for pinning when the metal coverage is very large [17].

The UDM successfully accounts for Fermi level pinning at submonolayer coverages, unlike the MIGS model. However the model has been founded on the use of SXPS to measure Fermi level shifts and resulting barrier heights formed at metal-semiconductor interfaces. Since SXPS is fundamentally a surface sensitive technique, it is only possible to probe Fermi level shifts for very thin metal coverages, hence barrier height measurements of this kind are prone to inaccuracy as the Schottky barrier may not be fully formed at such low coverages.

### 2.1.3.3 Chemical reactions

In the case of all the models discussed so far in this chapter, it has been assumed that the interfaces between the metal and the semiconductor are atomically abrupt. Even in the case of the UDM, where defects are induced by the metal, the defects are confined to the interfacial region. In reality however abrupt interfaces are relatively rare

occurrences with experimental studies indicating that semiconductor and metal species can diffuse and intermix resulting in interfaces that are complicated and non-abrupt. The extent of intermixing species may be varied, and can protract several monolayers into either the metal or semiconductor [18]. The models discussed in the following section assume that the chemical reactions, which occur during interface formation, are sufficiently large to produce a sizeable interface region where the chemical and electronic characteristics are different to those in the bulk of the metal or semiconductor.

(i) The effective work function model

When chemical reactions occur between the metal and semiconductor it may be possible that an interfacial layer is formed containing species from both the semiconductor and metal. The species involved may be in a variety of mixed alloy phases each with their own distinct work functions.

In the effective work function model, Woodall and Freeouf [19] proposed that the Schottky-Mott model described in equation 2.1 can be modified by replacing the metal work function  $\phi_m$  with an effective work function  $\phi_{eff}$  and hence the barrier height can be given as,

$$\phi_b = \phi_{eff} - \chi_s \quad [2.5]$$

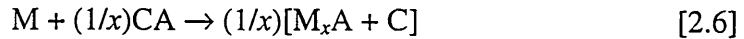
Here  $\phi_{eff}$  corresponds to the weighted average of the different work functions present in the interfacial region. It has been suggested by Woodall and Freeouf [19] that for III-V semiconductors, the interfacial reacted layer is group V rich (ie. As rich) with clusters of As forming the intimate contact with the semiconductor. The effective work function is therefore that of elemental As and not the metal. This model has gained good experimental support particularly for Au contacts to III-V and II-VI compounds [20]. It is highly likely that the degree of species intermixing at a metal semiconductor interface may account for variations in barrier heights observed for metal-semiconductor contacts achieved under differing surface preparation and metallisation techniques.

(ii) Heats of formation

The reactions occurring at metal-semiconductor interfaces will be reliant on

certain thermodynamic criteria.

Brillson [21] has reported a relationship between the barrier height and the heat of formation for the metal-semiconductor system. It has been proposed that a metal, M, undergoes a reaction with a compound semiconductor, CA, (C = cation, A = anion) such that,



The heat of reaction  $\Delta H_R$  can then be calculated from the heats of formation of the compound semiconductor and the most stable metal anion product  $M_xA$ . Reactions will take place if the reaction at the metal-semiconductor interface is exothermic (i.e.  $\Delta H_R < 0$ ). The value of  $\Delta H_R$  was established experimentally by Brillson with the use of electron energy loss spectroscopy (EELS) for numerous semiconductors. Variations of  $\phi_b$  with  $\Delta H_R$  indicated a sharp transition about a critical heat of reaction with the more reactive metals producing lower barrier heights. Brillson suggested that the redistribution of charge at the metal semiconductor interface due to the change in chemical environment accounted for the pinning of the Fermi level.

However although bulk thermodynamic aspects can be related to interfacial reactions, attempts to correlate Schottky barrier heights with thermodynamic properties have proved unsuccessful.

(iii) The effect of the temperature of metallisation on the barrier height

In further work by Brillson and co-workers, it was observed that metallisation of a semiconductor surface at low temperature produced barrier heights that varied linearly with the metal work function corresponding to the Schottky-Mott model described in section 2.1 [22,23]. They deduced that chemically induced defects accounted for Fermi level pinning observed on MBE grown GaAs(100) surfaces. Brillson proposed that low temperature metallisation would inhibit these chemical reactions, and hence defect induced Fermi level pinning, leading to barriers consistent with the Schottky-Mott limit. The barrier heights observed by Brillson were obtained at 100K on decapped MBE grown GaAs(100) using SXPS and confirmed by internal photoemission.

These results were subsequently contradicted by Wilks *et al.* [24] who established that metallisation at 80K on atomically clean MBE *as grown* GaAs(100)

surfaces did not show any correlation with the Schottky-Mott model, but rather followed the model postulated by Bardeen. The barrier height measurements here were obtained by conventional current-voltage techniques.

The difference in the results obtained for these two studies was attributed to discrepancies in the surface preparation and the measurement techniques used in each experiment.

## 2.2 Summary

### 2.2.1 Schottky barrier formation

In summary there have been numerous models proposed to account for the potential barrier formed when a metal comes into contact with a semiconductor. While each model discussed in this chapter has had experimental corroboration, no singular model can be completely applied to all the data obtained thus far. The original Schottky-Mott model fails to account for a wide spread in barrier heights observed for metals on semiconductors, and in practice the magnitude of  $\phi_b$  is governed by variations on the Bardeen model whereby interface states are introduced into the forbidden gap. The introduction of quantum mechanical or defect related interface states by the deposition of a metal, results in the pinning of the Fermi level and hence  $\phi_b$ . It is also possible for chemical reactions and inter-diffusion to adapt the Fermi level pinning position. It is highly likely therefore that a number of processes contribute to the electronic structure of the interface, and that a viable “universal” model does not exist.

## 2.3 References

- [1] E.H. Rhoderick and R.H. Williams, "Metal-Semiconductor Contacts", Clarendon Press, Oxford (1988) and references therein.
- [2] A.G. Milnes and D.L. Feucht, "Hetero-junctions and metal semiconductor junctions", (1972).
- [3] W. Schottky, *Naturwissenschaften*, **26**, 843 (1938).
- [4] N.F. Mott, *Proc. Cambr. Phil. Soc.* **34**, 568 (1938).
- [5] J. Bardeen, *Phys. Rev.* **71**, 717 (1947).
- [6] V. Heine, *Phys. Rev.* **A138**, 1689 (1965).
- [7] S.G. Louie and M.L. Cohen, *Phys. Rev.* **B13**, 4172 (1976).
- [8] S.G. Louie, J. R. Chelikowsky and M.L. Cohen, *Phys. Rev.* **B15**, 2145 (1977).
- [9] J. Ihm, S.G. Louie and M.L. Cohen, *Phys. Rev.* **B18**, 4172 (1978).
- [10] F. Yndurain, *J. Phys. C: Solid-St. Phys.* **4**, 2849 (1971).
- [11] C. Tejedor, F. Flores and E. Louis, *J. Phys. C: Solid-St. Phys.* **10**, 2163 (1977).
- [12] J. Tersoff, *Phys. Rev. Lett.* **52**, 465, (1984).
- [13] J. Tersoff, *Phys. Rev. B*, **32**, 6968 (1985).
- [14] O.F. Sankley, R.E. Allen and J.D. Dow, *J. Vac. Sci. Technol.*, **B1**, 1162, (1985).
- [15] W.E. Spicer, I. Lindau, P. Skeath, C. -Y. Su and P. Chye, *Phys. Rev. Lett.* **44**, 420 (1980).
- [16] W.E. Spicer, I. Lindau, P. Skeath and C. -Y. Su, *J. Vac. Sci. Technol.* **17**, 1019, (1980a).
- [17] A. Zur, T.C. McGill and D.L. Smith, *Phys. Rev. B*, **28**, 2060 (1983).
- [18] L.J. Brillson, C.F. Bucker, A.D. Katnani, N.G. Stoffel, R. Daniels and G. Margaritondo, *Physics and Chemistry of Semiconductor Interfaces Conference, Asilomar, Calif.*, (1982).
- [19] J.M. Woodall and J.L. Freeouf, *J. Vac. Sci. Technol.*, **21**, 564 (1982).
- [20] R. Ludeke, T.-C. Chiang and D.E. Eastman, *J. Vac. Sci. Technol.*, **21**, 599, (1982).
- [21] L.J. Brillson, *Phys. Rev. Lett.* **40**, 260 (1978).
- [22] R.E. Vitturo, S. Chang, J.L. Shaw, L.J. Brillson, P.D. Kirchner and J.M. Woodall, *J. Vac. Sci. Technol.* **B7**, 1007 (1989).

- [23] S. Chang, J.L. Shaw, R.E. Vitturo, L.J. Brillson, P.D. Kirchner and J.M. Woodall, *J. Vac. Sci. Technol.* **A8**, 3803 (1990).
- [24] S.P. Wilks, J.I. Morris, D.A. Woolf and R.H. Williams, *J. Vac Sci. Technol.* **B9(4)**, 2118 (1991).

# Chapter 3

## Theory of experimental techniques

### 3.0 Introduction

In this chapter the theory supporting the experimental techniques used to investigate the formation of both In and Au interfaces with  $\text{In}_{0.53}\text{Ga}_{0.47}\text{As}(100)$  and  $\text{In}_{0.52}\text{Al}_{0.48}\text{As}(100)$  are discussed.

SXPS has been the main experimental technique utilised during the course of this research. The non-destructive and surface sensitive nature of the photoemission process lends itself to the study of the chemical, electrical and structural nature of metal-semiconductor interfaces. XPS was also utilised for preliminary decapping studies; hence the fundamental principles of photoemission form the main part of this chapter.

LEED, TEM and MBE were also employed to characterise and grow the samples respectively; these techniques have also been described in lesser detail. Finally, the Schottky barrier heights formed at the metal-semiconductor interfaces examined in this study are measured by the photoemission technique, and correlated with values of  $\phi_b$  measured by the I-V technique. Hence the relevant theory behind Schottky barrier measurement is also described in this chapter.

### 3.1 The Photoemission process

Photoemission theory has been developed from Einstein's original work on the photoelectric effect [1]. Photoemission is the emission of electron from a solid as a result of the absorption of photons. The electrons are emitted from the surface if the incident photons have an energy ( $h\nu$ ) that is greater than the binding energy ( $E_b$ ) of the electron plus the work function ( $\phi$ ) of the solid. The subsequent kinetic energy of the emitted photoelectron is given by the following equation,

$$E_k = h\nu - E_b - \phi \quad [3.1]$$



“soft XPS” or SXPS and is discussed in chapter 4.1. The EDC obtained (see figure 3.1) reflects the density of occupied states in the solid. However, the EDC is not a direct representation of the density of states as there also exists a large featureless background to low kinetic energy which is characteristic of emitted electrons that have undergone inelastic scattering and lost energy during propagation through the solid to the surface [3]. Electrons that have been emitted from the comparatively narrow core levels and the broad valence band without loss of energy produce sharp discrete peaks in the EDC.

The sharp core level photoemission peaks can be used to identify specific atoms near the surface of the solid, as each element has its own set of discrete core level binding energies [4,5]. It is for this reason that XPS is occasionally known as ESCA (electron spectroscopy for chemical analysis) as the chemical composition of the material near the surface can be identified.

More importantly studying the changes in peak positions and hence binding energies of the core levels can give information on chemical, electrical and structural changes at the surface of the solid [6]. In order to observe these changes accurately, it is necessary to establish a reference energy level, usually the Fermi level. In a typical semiconductor, the Fermi level lies somewhere within the forbidden energy gap where usually no states exist. Thus there will be no detectable emission from which the Fermi levels position may be ascertained. In a metal however, the Fermi level can be easily determined as it is found at the maximum of the occupied states. It is usually the case therefore to measure a spectrum for a metal in electrical contact with the semiconductor. The energy of electrons at the Fermi edge of the metal will be at the same energy as the Fermi level in the semiconductor and the position of the Fermi level in the forbidden gap can be determined by referring it to the energy of the semiconductor valence band maximum.

Photoemission is a powerful tool in the non-destructive analysis of surfaces and interfaces. It is surface and chemically sensitive and provides information on the atomic bonding of species present in a material.

### **3.2 Photoemission theory**

There are many models that have been proposed to describe the photoemission process, the most accurate ones being those that describe it as a single quantum mechanical event, from the absorption of a photon through to the emission and detection

of the photoelectron [3,7,8]. These theories however are extremely intricate, and for the purpose of explaining the photoemission process and the phenomena observed in the photoemission data presented here, a far simpler model, The Three Step Model, is discussed [9,10]. This model ignores many body effects such as electron-electron interactions and inelastic scattering and focuses on the elastically scattered electrons.

### 3.2.1 The three step model

The Three Step Model describes the photoemission process in three stages, which are all dependent on the initial electron energy ( $E$ ) and the energy of the incident photons ( $h\nu$ ). These stages are:

- (i) Photoexcitation of the electron  $P(E, h\nu)$
- (ii) Propagation through the solid  $T(E, h\nu)$
- (iii) Escape from the solid surface into vacuum  $D(E, h\nu)$

The intensity of the resulting photocurrent  $I(E, h\nu)$  is given by the relation,

$$I(E, h\nu) = P(E, h\nu)T(E, h\nu)D(E, h\nu) \quad [3.2]$$

#### (i) Step one: Photoexcitation

If the photoemission process is considered for each individual particle one can use the independent particle approximation whereby the unperturbed system is described by the Hamiltonian energy operator,

$$\hat{H}_o = \frac{\hat{p}^2}{2m} + V(\mathbf{r}) \quad [3.3]$$

where  $p$  is the momentum operator,  $m$  is the mass of the electron and  $V(\mathbf{r})$  is the self consistent screening potential energy operator; which accounts for the effects of the other electrons on the independent electron as well as surface effects.

If this system is subsequently perturbed by the absorption of a photon, the introduction of an electromagnetic wave of vector potential  $\mathbf{A}$  will change the

momentum operator such that it becomes [11],

$$\hat{p} + \frac{e}{c} \mathbf{A} \quad [3.4]$$

And the new perturbed Hamiltonian can be written as,

$$\hat{H} = \frac{1}{2m} \left[ \hat{p} + \frac{e}{c} \mathbf{A} \right]^2 + V(\mathbf{r}) \quad [3.5]$$

If this equation is expanded we see that,

$$\hat{H} = \frac{p^2}{2m} + V(\mathbf{r}) + \frac{e}{2mc} (\hat{p} \cdot \mathbf{A} + \mathbf{A} \cdot p) + \frac{e^2 \mathbf{A}^2}{2mc^2} \quad [3.6]$$

And hence substituting equation 3.3 gives,

$$\hat{H} = \hat{H}_o + \hat{W} \quad [3.7]$$

where  $W$  is the electron-radiation interaction Hamiltonian. By applying the dipole approximation [12], only linear terms in  $\mathbf{A}$  apply and hence the electron-radiation interaction Hamiltonian can be written as,

$$\hat{W} = \frac{e}{2mc} (\hat{p} \cdot \mathbf{A} + \mathbf{A} \cdot \hat{p}) \quad [3.8]$$

The transition rate between an initial state  $|\psi_i\rangle$  and the final state  $|\psi_f\rangle$  in relation to an electron-phonon interaction can be given by the Fermi “Golden Rule” expression [12] such that,

$$P_{fi} = \frac{2\pi}{\hbar} |\langle \psi_f | \hat{W} | \psi_i \rangle|^2 \delta(E_f - E_i - h\nu) \quad [3.9]$$

where  $\psi_i$  and  $\psi_f$  are the initial state and final state wavefunctions, having energies  $E_i$  and  $E_f$ , respectively. The  $\delta$ -term ensures that there is energy conservation between  $h\nu$  and the transition energy ( $E_f - E_i$ ). The resulting photocurrent is given by the equation,

$$P(E, h\nu) = \frac{2\pi}{\hbar} \sum_i \left| \langle \psi_f | \hat{W} | \psi_i \rangle \right|^2 \delta(E_f - E_i - h\nu) \quad [3.10]$$

The summing over all initial states is an approximation, with a more accurate summation being one that incorporates all final states as well. However for a large density of final states, the modulation of the photocurrent will be negligible. Only for low final state energies ( $\leq 20$  eV) does this final state density become significant to the observed photocurrent and hence for XPS and SXPS experiments this effect will be trivial resulting in the photocurrent being characteristic of the initial density of states.

**(ii) Step two: Propagation of the electron through the solid**

Once the electrons have been excited due to the absorption of a photon, they must make their way to the surface of the solid where they will be emitted and detected. On route to the surface, it is highly likely that the electrons will be scattered and hence the resulting photocurrent will be modified. The propagation probability  $T(E, h\nu)$  can be expressed in terms of the inelastic mean free path of the electron  $\lambda(E)$ , which is defined as the average distance an electron with energy  $E$  can travel through a solid before being inelastically scattered. If one considers the number of electrons ( $N_0$ ) that are photoexcited at a distance  $x$  from the surface, then the number of electrons ( $N$ ) that actually reach the surface without losing any energy is given by the equation,

$$N = N_0 \exp\left(\frac{-x}{\lambda(E)}\right) \quad [3.11]$$

Hence the propagation probability can be written as [3],

$$T(E, h\nu) = \exp\left(\frac{-x}{\lambda(E)}\right) \quad [3.12]$$

If the penetration depth ( $x$ ) of the photon is assumed to be much larger than  $\lambda$ , then the above equation is thought to be a constant.

**(iii) Step three: Electron escape from the solid**

Once the electrons have propagated to the surface of the solid, they must possess enough energy to escape into vacuum. The electrons must have a component of momentum normal to the surface and enough energy to overcome the work function of the solid. Therefore the probability of escape from the solid  $D(E)$ , may be described simply as zero when the electrons do not possess enough energy to escape and one when they do such that,

$$D(E) = 0 \quad \text{when } E_{\text{norm}} - E_{\text{vac}} < \phi \quad [3.13]$$

$$D(E) = 1 \quad \text{when } E_{\text{norm}} - E_{\text{vac}} \geq \phi \quad [3.14]$$

where  $E_{\text{norm}}$  is the component of final state energy normal to the surface and  $E_{\text{vac}}$  is the vacuum level of the solid.

The final expression for the photocurrent can be written as a product of the three steps described previously, whereby,

$$I(E, h\nu) = \frac{2\pi}{\hbar} \sum_i \left| \langle \psi_f | \hat{W} | \psi_i \rangle \right|^2 \delta(E_f - E_i - h\nu) \exp\left(\frac{-x}{\lambda(E)}\right) D(E) \quad [3.15]$$

The Three Step Model is relatively basic as it neglects many body effects. However, it is useful for interpreting the EDC's obtained by the photoemission technique used in this work.

**3.3 Photo-ionisation cross section**

The probability of a transition per unit time for excitation of a single photoelectron from the core level of interest due to an incident photon flux of  $1\text{cm}^{-2}\text{s}^{-1}$  is given as the photo-ionisation cross section ( $\sigma$ ) and is related to the matrix element  $|\langle \psi_f | W | \psi_i \rangle|$  discussed in section 3.2. The intensity of the transition between the initial state and the final state is determined by the cross section and since the final state

energy depends on the energy of the incident photon beam,  $\sigma$  will also vary with the photon energy [4]. The resulting intensity of a given core level emission peak will vary with photon energy and the majority of core level emission peaks encounter a minimum in  $\sigma$  at certain photon energies known as a Cooper minimum [13]. Experimentally observed values of  $\sigma$  for individual core levels have been collected and tabulated as a function of photon energy by Yeh and Lindau [4]. These tables are of great use when performing experiments using a synchrotron radiation source as it is possible to maximise the emission intensity of the core level being studied by tuning the photon energy to exhibit the maximum possible cross section. However, this can result in a loss of surface sensitivity and hence a compromise between surface sensitivity and cross section usually needs to be found.

### **3.4 Surface sensitivity**

#### **3.4.1 Electron scattering and inelastic mean free path (IMFP)**

As the excited photoelectrons propagate through the solid towards the surface, they can be scattered either elastically or inelastically by scattering centres within the solid. If an electron is elastically scattered it suffers no loss in energy but can experience a change in direction and upon detection will provide information on the energy state of the core level it was emitted from. Inelastically scattered electrons undergo a loss of energy and may also experience a change in direction. Typically electrons may lose up to several eV due to inelastic scattering, however scattering by phonons results in a loss of energy of only a few meV and is negligible compared to the resolution of the spectrometer. Electrons that do encounter inelastic scattering may do so on a random number of occasions and hence may lose a significant amount of energy on route to the surface. Should the electrons still have enough energy to escape from the solid surface when they arrive, they will have a kinetic energy significantly different to that of the elastically scattered electrons and will contribute in a random way to the featureless background to lower kinetic energy on the EDC. Inelastic scattering occurs due to the creation of electron-hole pairs or by the generation of plasmons, which involve a collective oscillation of conduction, valence or shallow core level electrons. The plasmon loss features are not random and result in peaks at roughly 10 eV to the lower kinetic energy side of the unscattered elastic emission peak.

The mean free path ( $\lambda$ ) of an electron is defined as the average distance that an electron of energy  $E$ , can travel through the solid before being inelastically scattered [14]. The value of  $\lambda$  for electron in a solid is greatly dependent on the kinetic energy of the electron and the relationship between the two is shown in figure 3.2 [6]. The shape of the curve is determined by the formation of electron-hole pairs and plasmons typically in the energy range 20-100 eV. At low energies (below the plasmon energy) electron scattering is dictated by single-particle electron excitations involving valence electrons and the ionisation of core levels. The associated cross sections of these processes are small compared to other processes and hence the mean free path for such collisions is about two orders of magnitude greater than for plasmon scattering [15].

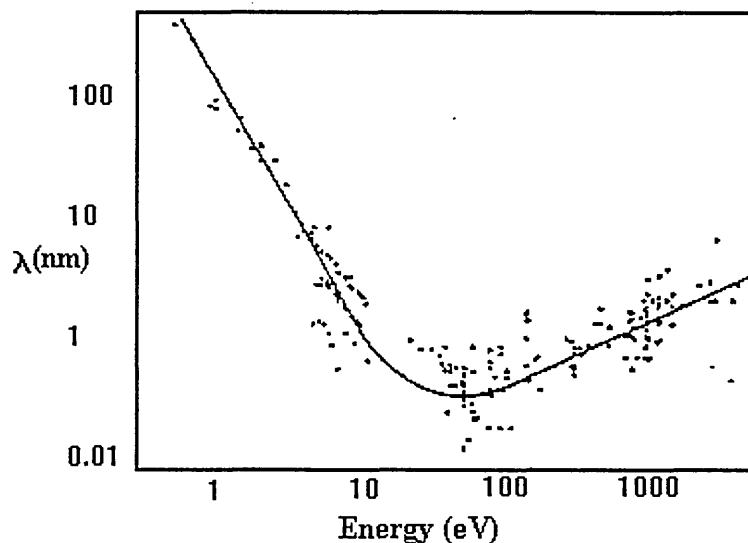


Fig 3.2: The dependence of attenuation length  $\lambda$  on the emitted electron energy for elements [6]

At energies above the plasmon energy, the plasmon scattering cross section rises sharply and hence the probability of inelastic scattering increases. This reduces the mean free path to about a few Å. When  $\lambda$  becomes this small, electrons emerging from the surface without loss of energy must have originated from within the first few monolayers of the solid. It is this aspect of photoemission that makes it a surface sensitive technique. As the energy of the electrons increases above  $\sim 100$  eV, the MFP increases. This is due to the fact that the electrons have a greater velocity and hence are not influenced as much by scattering centres. Typically a mean free path of  $\lambda \approx 5 \text{ \AA}$  can be achieved for electrons with a kinetic energy of around 40 eV. The surface sensitivity

can be altered by changing the photon energy and hence the kinetic energy (see equation 3.1) using a tuneable synchrotron radiation source.

### 3.4.2 Effective escape depth: Changing the angle of detection

It was discussed in section 3.4 that the photo-ionisation cross section varies with photon energy. This fact can cause problems when comparing emission intensities of bulk and surface sensitive spectra as the probability of photoelectron emission will change with changing photon energy. However, altering the angle of detection of the emitted photoelectrons may also increase surface sensitivity [6]. If we consider electrons escaping at an angle  $\theta$  from the normal to the surface as shown in figure 3.3, those electrons travelling a distance  $\lambda$  through the solid will have come from a depth normal to the surface given by,

$$d = \lambda \cos\theta \quad [3.16]$$

In normal emission the detector is placed  $90^\circ$  to the surface (i.e.  $0^\circ$  from normal) and hence electrons detected will have travelled from within a distance  $d = \lambda$  from the surface. If the angle of detection is changed to  $60^\circ$  from normal, the effective distance the electrons have travelled is given as  $d = \lambda/2$ , hence halving the effective escape depth and increasing surface sensitivity.

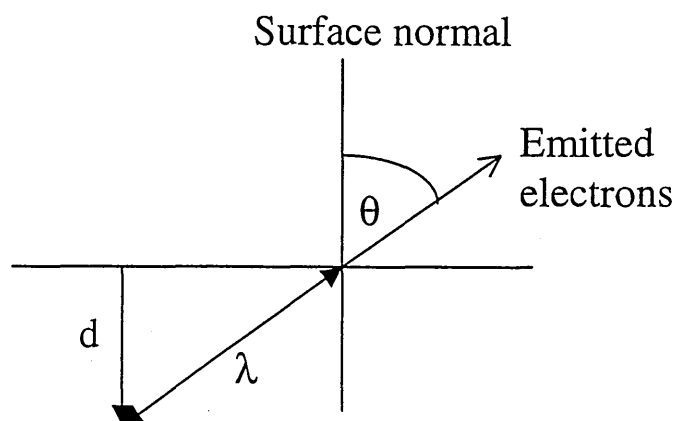


Figure 3.3: Surface sensitivity enhancement by variation of the angle of detection of the emitted electrons.

### **3.4.3 Photoelectron diffraction**

Changing the angle of electron detection (i.e. rotating the sample in the surface plane) can produce variations in the observed core level intensity. This is known as photoelectron diffraction, and is due to interference (destructive and constructive) between the various coherent components of the same photoelectron wavefunctions.

## **3.5 Core level analysis**

The binding energy of a particular core level peak is dependent on the chemical and electrical environment encountered by the emitting atom. If a change in environment of the emitting atom occurs, the binding energy of the core level emission peak will also change, with the difference in energy being described as a shift.

For example the controlled deposition of a metallic species onto a semiconductor surface may induce shifts in the binding energy positions of the semiconductor core level peaks. These shifts can be due to surface structural, chemical or electronic changes in the surface region as mentioned in chapter 2, with the total binding energy shift being a convolution of the various shifts. It is important that these shifts are distinguished from one another and hence the analysis of core level spectra is necessary in order to utilise photoemission as a technique to study solid surfaces and interfaces. The phenomena that give rise to such binding energy shifts are discussed in the following four subsections.

### **3.5.1 Structural or surface related shifts**

The properties of a surface differ from those in the bulk of a material due to the fact that at a surface, the bulk periodicity is abruptly terminated. The atoms at the surface therefore relax or reconstruct in order to minimise the surface energy and hence the binding energies of electrons emitted from atoms on or near the surface may be different to those emitted from bulk atoms. It is likely, therefore, that the observed emission from a given core level will be made up of a number of surface components and a bulk component. The relative intensities of these components will depend on the inelastic mean free path. An example of a core level consisting of bulk and surface

components is shown in figure 3.4. It can be seen that three components contribute to the overall EDC.

### **3.5.2 Chemical shifts**

When a metal is deposited onto a III-V semiconductor it is possible that a chemical reaction will occur between the metal and species from the semiconductor [16]. Atoms that are involved in the reaction process will have their chemical environment modified and the redistribution of valence charge that occurs during bonding is identified in the EDC by a shift in the binding energy of the core levels. The transfer of charge may also be affected by the electronegativities of the different elements [17] consequently altering the electronic properties of the reacted species.

### **3.5.3 Relaxation**

Following photoemission from an atom that initially consisted of  $N$  electrons, the remaining  $N-1$  electrons will relax to screen the hole that has been created from the nucleus. The effect of this relaxation will be a modification in the energy of the emitted electron and hence an apparent change in its binding energy.

### **3.5.4 Band bending**

When the position of the Fermi level shifts in a semiconductor due to the presence of surface states or the deposition of metals onto the surface, the resulting shift is known as band bending. This is an electronic effect and occurs due to the transfer of charge at the surface or interface as described in chapter 2. This band bending induces a change in the Fermi level position at the surface compared to its position relative to the valence and conduction band edges in the bulk. The band bending occurs within a region known as the depletion region. This depletion region is usually much larger than the sampling depth of the photoemission technique and hence all core level electrons that are detected will have been subjected to band bending with a subsequent shift in the core level peaks in the EDC. It is therefore possible to observe the development of the Schottky barrier during the initial stages of metal-semiconductor interface formation.

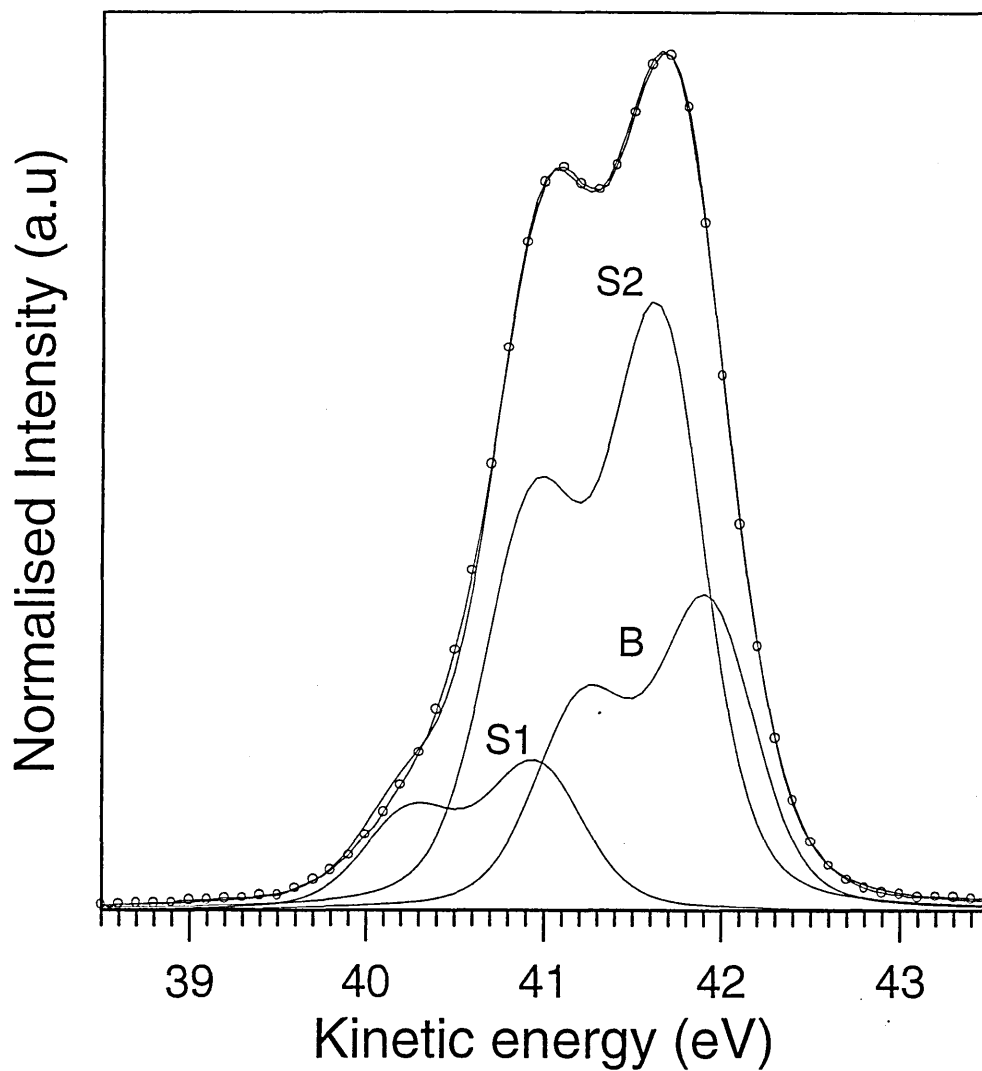


Figure 3.4: A surface sensitive As3d core level photoelectron peak obtained from clean (3×1) reconstructed  $\text{In}_{0.52}\text{Al}_{0.48}\text{As}(100)$  at a photon energy of 87eV. Open circles denote the raw data. The overall fit (given by the black line) is made up of three separate components. B is related to As in the bulk of the material, and S1 and S2 are surface components related to predominantly Al bonded As sites and predominantly In bonded As sites, respectively.

In order to determine accurately the extent of the core level shifts, an energy reference point must be used. In most photoemission studies it is common practise to measure the Fermi level of the system (in electrical contact with the sample) in order to obtain an exact position for the Fermi level [5]. This is easily achieved by scanning the Fermi edge of a metal, usually gold. The high density of states at the Fermi level in a metal ensures that emission from this region will be distinct and hence the Fermi level is easy to measure. Unfortunately this is not the case for a semiconductor, where the Fermi level often lies within the forbidden energy gap [5]. In this case it is more productive to determine the valence band maximum (VBM) and this is found at the cut off point of the valence band signal and the background signal. By subtracting the valence band maximum from the Fermi level position (both measured at the same photon energy) it is possible to determine the clean surface pinning position of the Fermi level within the band gap. The barrier height formed at metal-semiconductor interfaces (for low metal coverages) can therefore be estimated by adding the additional band bending due to metal deposition to the Fermi level pinning position.

### **3.5.5 Surface photovoltages**

During photoemission experiments, photovoltaic band flattening may occur due to the formation of electron-hole pairs in the depletion region. In low doped samples, this will give rise to shifts in the photoelectron peaks, and makes band bending measurements difficult [18]. This problem can be overcome by doing experiments on heavily doped material. The thin depletion layer in the more heavily doped material allows for a tunnelling current, which is sufficient to cancel the photovoltage, thus making band bending measurements possible.

### **3.5.6 Lineshape broadening effects**

In some cases it may be hard to identify small core level shifts due to the existence of peak broadening effects. The peak broadening is usually described as the full width at half maximum height (FWHM) of the photoelectron peak  $\Delta E$  and is a convolution of several contributions such that [6],

$$\Delta E = (\Delta E_n^2 + \Delta E_p^2 + \Delta E_a^2)^{1/2} \quad [3.0]$$

where  $\Delta E_n$  is the natural or inherent linewidth of the core level,  $\Delta E_p$  is the width of the photon source and  $\Delta E_a$  is the analyser resolution.

The natural linewidth of the core level (i.e. the range in KE of the emitted photoelectrons) is due to the uncertainty in the lifetime of the ion state remaining after photoemission [6]. The broadening due to a synchrotron radiation source is affected by the beamline optics, and is usually in the range of 0.1-0.6 eV. The broadening due to the analyser is dependent on the analyser pass energy and this is discussed in chapter 4.

### 3.5.7 Core level intensities and overlayer growth

Up until now this chapter has dealt with the analysis of the core levels to detect surface induced, chemical and band bending shifts. These are all attributed to changes in the binding energy of the core level peaks. In addition to these shifts the intensity of core level peaks can provide information on the growth mode of a deposited metal overlayer. As the metal is deposited onto the semiconductor surface, the photoemission signal from the core levels within the semiconductor will be attenuated due to inelastic scattering in the growing overlayer.

If the metal grows in a layer by layer mode of growth, the substrate core level intensity will attenuate as governed by the equation [19],

$$I = I_o \exp\left(\frac{-d}{\lambda}\right) \quad [3.17]$$

where  $I_o$  is the clean surface core level emission intensity,  $d$  is the thickness of the metal overlayer and  $\lambda$  is the mean free path of electrons in the overlayer. Deviation from this exponential decay indicates either a non-uniform or clustering growth mode or inter-diffusion of substrate and overlayer species. Hence it is possible to determine the growth mode of the metal overlayer by plotting the intensity of the attenuated signal as a function of metal overlayer thickness.

The three types of growth mode possible for a layer on a substrate are layer by layer (Franck van der Merwe mode), islanding (Volmer-Weber mode) and layer by layer followed by islanding (Stranski-Krastanov mode) and are illustrated in figure 3.5.

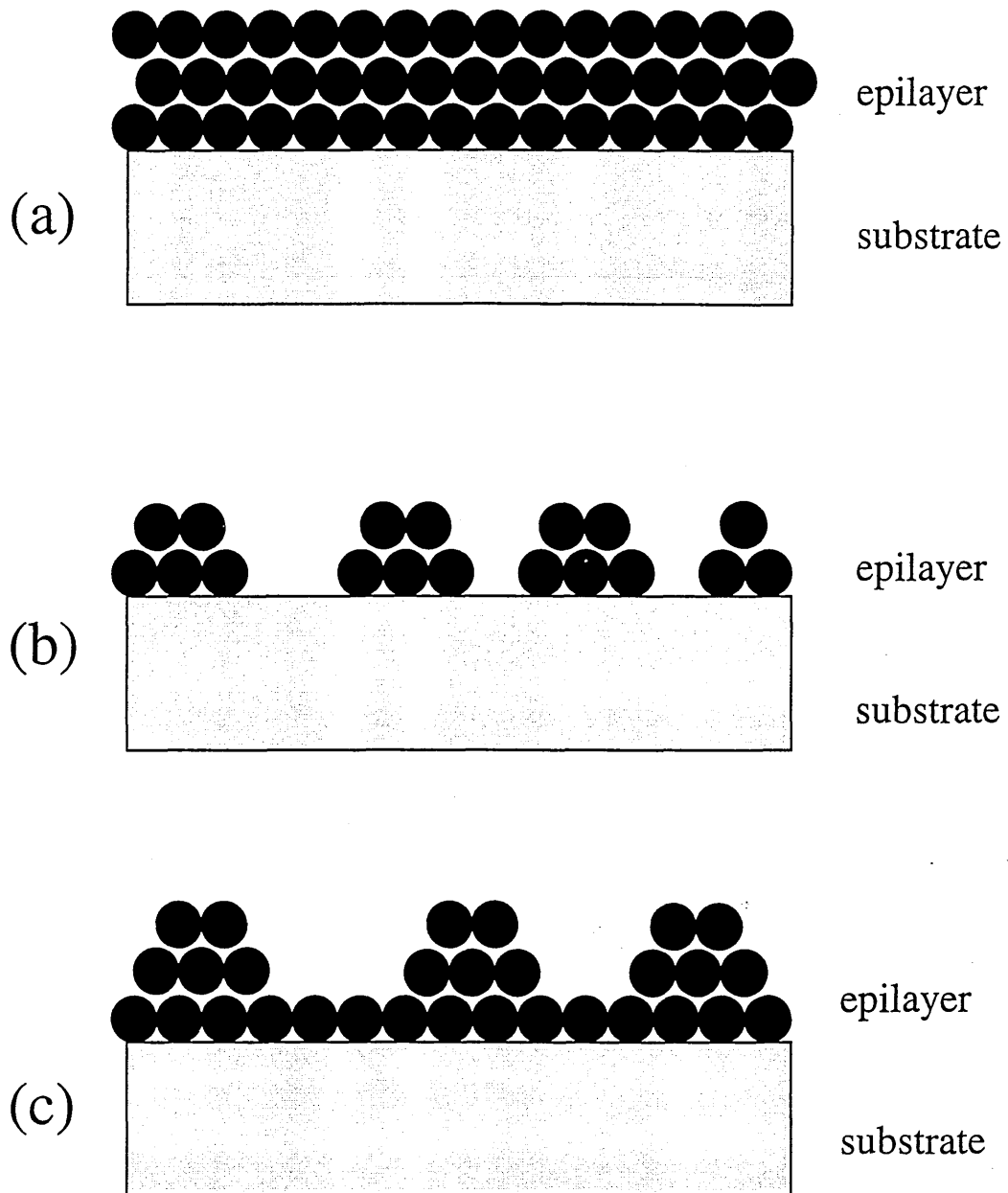


Figure 3.5: Schematic diagram of the three different types of growth mode. (a) layer-by-layer, (b) islanding and (c) layer-by-layer plus islanding.

### 3.5.8 Spin orbit splitting

Many core level peaks split into doublets due to the coupling of the orbital and spin angular momenta of the electrons. Only core levels with an angular quantum momentum number  $\ell > 0$  will exhibit doublets and hence core levels such as 1s, 2s and 3s will be singlets. The outcome of coupling is the new total angular momentum given by,

$$j = \ell + s \quad [3.18]$$

where  $\ell$  is the orbital angular momentum and  $s$  is the spin quantum number ( $\pm 1/2$ ) [20].

It is evident therefore that electrons with a total angular momentum of  $j = \ell + 1/2$  will have a different energy to those with  $j = \ell - 1/2$ . Electrons with  $j = \ell + 1/2$  are shifted to higher binding energy than those with  $j = \ell - 1/2$ . The resulting difference in energy is known as the spin orbit splitting. The relative intensities of the photoemission peaks in a doublet are given by the ratio of their respective degeneracies ( $2j + 1$ ) as shown below,

$$R = \frac{2(\ell - s) + 1}{2(\ell + s) + 1} \quad [3.19]$$

Hence for the d core levels where  $\ell = 2$ , the ratio of the 3/2 spin component to the 5/2 spin orbit component is 2:3.

### 3.5.9 Asymmetric metal core levels

The discussion so far in this chapter has concentrated on the analysis of emission from core levels in general. However the core level emission spectra will be different for a metal compared to a semiconductor. The high density of states at a metal Fermi level compared to a semiconductor results in increased electron scattering and a subsequent energy loss for those electrons emitted from the material. This has the effect of producing increased emission intensity at lower kinetic energies, which is observed as a tail to low kinetic energy side of the core level peak in the EDC.

### 3.5.10 Deconvolution of core level spectra

It has been discussed in this chapter that photoemission spectra can provide information on binding energy shifts and chemical interactions that occur during the formation of an interface. In order to interpret the reactions and shifts that take place, it is necessary to separate the raw photoemission data into its bulk, surface and reacted components. This can be done using a curve fitting routine on a computer. A mathematical technique developed by A.A. Cafolla, incorporating the conjugate gradient [21] and Levenberg-Marquardt [22] curve fitting methods was used to generate the basic shape of a single core level, and then the curve fitting routine performed a least squares minimisation to produce the best fit. A number of types of function have been used to fit core level spectra, the two most common being Lorentzian or Gaussian functions. The Lorentzian function is the natural linewidth of the core hole lifetime and is given by the equation,

$$L(E) = \frac{1}{1 + 4 \left( \frac{E - E_L}{\Gamma_L} \right)^2} \quad [3.20]$$

Where  $E_L$  is the energy centroid of the peak and  $\Gamma_L$  is the full width at half maximum (FWHM) of the peak.

The Gaussian function is governed by instrumental and other factors such as phonon broadening, and is given by the equation,

$$G(E) = \exp \left[ -4 \ln 2 \left( \frac{E - E_G}{\Gamma_G} \right)^2 \right] \quad [3.21]$$

Where  $E_G$  is the centroid of the peak and  $\Gamma_G$  is the full width at half maximum (FWHM) of the peak.

In the fitting routine used in this thesis, a Voigt function was employed which is a convolution of a Lorentzian function and a Gaussian function [23]. The Voigt function can be modified by changing various parameters such as the Lorentzian or Gaussian broadening, the spin orbit splitting of the core level, the intensity of individual components or the kinetic energy peak position of the components. Prior to any fit a

suitable background must be removed. Inaccurate removal of the background can lead to discrepancies in peak intensities and positions and hence distort quantitative data analysis. The removal of the background must take into account the contribution made by secondary processes such as satellites and asymmetries. In general, there are two types of background subtraction. The first is a simple linear background, which is removed by taking a straight line between the first and last set of points in the spectrum. This method is useful when the signal to noise ratio is large. The second method is the removal of a non-linear background either in the form of a polynomial or derived from the method described by Shirley [24].

Once a suitable background has been removed, the fitting can begin. The clean surface spectrum is fitted with an estimate first, with the intention that the overall spectrum is fitted with the least number of components necessary. Each individual component has a number of parameters that contribute to its lineshape. These are  $L(E)$ ,  $G(E)$ , the spin orbit splitting (SOSP) of the core level being probed and their relative intensities, the peak position and the peak intensity. Values of  $L(E)$ , SOSP and relative spin orbit peak intensities can be found in the literature and are shown in sections 6.1.3 and 7.1.3 for InGaAs and InAlAs related components respectively. These values were kept fixed during the fitting routine, as they are inherent of the core levels being probed. The fit of the overall spectrum is then iteratively refined using the least squares method, and the quality of the fit is gauged by the Chi-squared ( $\chi^2$ ) value. In comparing different fits of the same spectra, the fit with the lowest  $\chi^2$  value is usually best, with a value of  $\chi^2$  in the range  $10^{-5}$  -  $10^{-4}$  units. Once a clean surface has been fitted, the spectrum from the next incremental metal deposition should be fitted, starting with the same components as the clean surface fit. This procedure is then repeated for subsequent spectra. If the same components do not satisfy the lineshape of the new spectrum, it may be the case that new components need to be added, or others taken away. However it must be noted that although a fit may have a low  $\chi^2$  value, and look alright, in order to be of any use at all, the fit must make chemical and spectroscopic sense in the context of the metal-semiconductor material system being studied.

### **3.6 Low energy electron diffraction**

The surface structure of a solid can be investigated by LEED. A broad beam of monoenergetic electrons, with energy typically in the range 20-200 eV, is incident normally on the sample surface. The surface layer of atoms diffracts the beam of

electrons in the same way that a grating diffracts light. The backscattered low energy electrons constructively interfere to form the diffraction pattern, which is observed on a fluorescent screen. The interpretation of the diffraction pattern is that it is a direct map of the reciprocal lattice of the surface [25]. The LEED technique is extremely surface sensitive due to the fact that the low energy electrons have a short inelastic mean free path ( $\lambda$  is comparable to the interatomic spacing) and hence electrons contributing to the diffraction pattern will have been diffracted from the surface region. Furthermore the elastic backscattering cross section of low energy electrons is very large [26] and hence diffraction from successive atomic planes below the surface will contribute little to the diffraction pattern.

LEED is regularly utilised to determine the reconstructions of semiconductor surface. The most common form of notation for describing surface reconstructions was proposed by Wood [27] whereby the unit cell is described in the form ( $m \times n$ ), indicating that the surface cell has lattice vectors  $m$  and  $n$  times that of the underlying bulk. Any surface that possesses order will produce a LEED pattern unlike a disordered or amorphous surface where no LEED pattern will be observed. It is for this reason that LEED was employed during the course of this research, as the change from a disordered amorphous As cap to a clean ( $3 \times 1$ ) reconstructed surface during the decapping procedure could be easily identified from the LEED pattern.

### 3.7 Transmission electron microscopy

Transmission electron microscopy can be used for the structural characterisation of metal-semiconductor interfaces. In the technique of TEM electrons are emitted by a hot tungsten wire and accelerated through a potential difference of  $\sim 50$ - $200$  kV resulting in fast electrons ( $\lambda \sim 5$ - $2.5 \times 10^{-12}$  m). Three lenses as shown in figure 3.6 control the beam of electrons. The condenser lens produces a nearly parallel beam that is incident on a very thin sample. The sample must be very thin so that the electrons do not lose energy as they pass through it. The transmitted electrons are collected at the objective lens of the microscope and a magnified image is produced which acts as the object for the projector lens. This lens magnifies the image even further, and projects the final image onto a fluorescent screen or photographic plate. In a TEM micrograph contrast between adjacent areas is produced because the electrons are scattered by differing amounts in areas with differing lattice parameters. Under certain conditions a diffraction

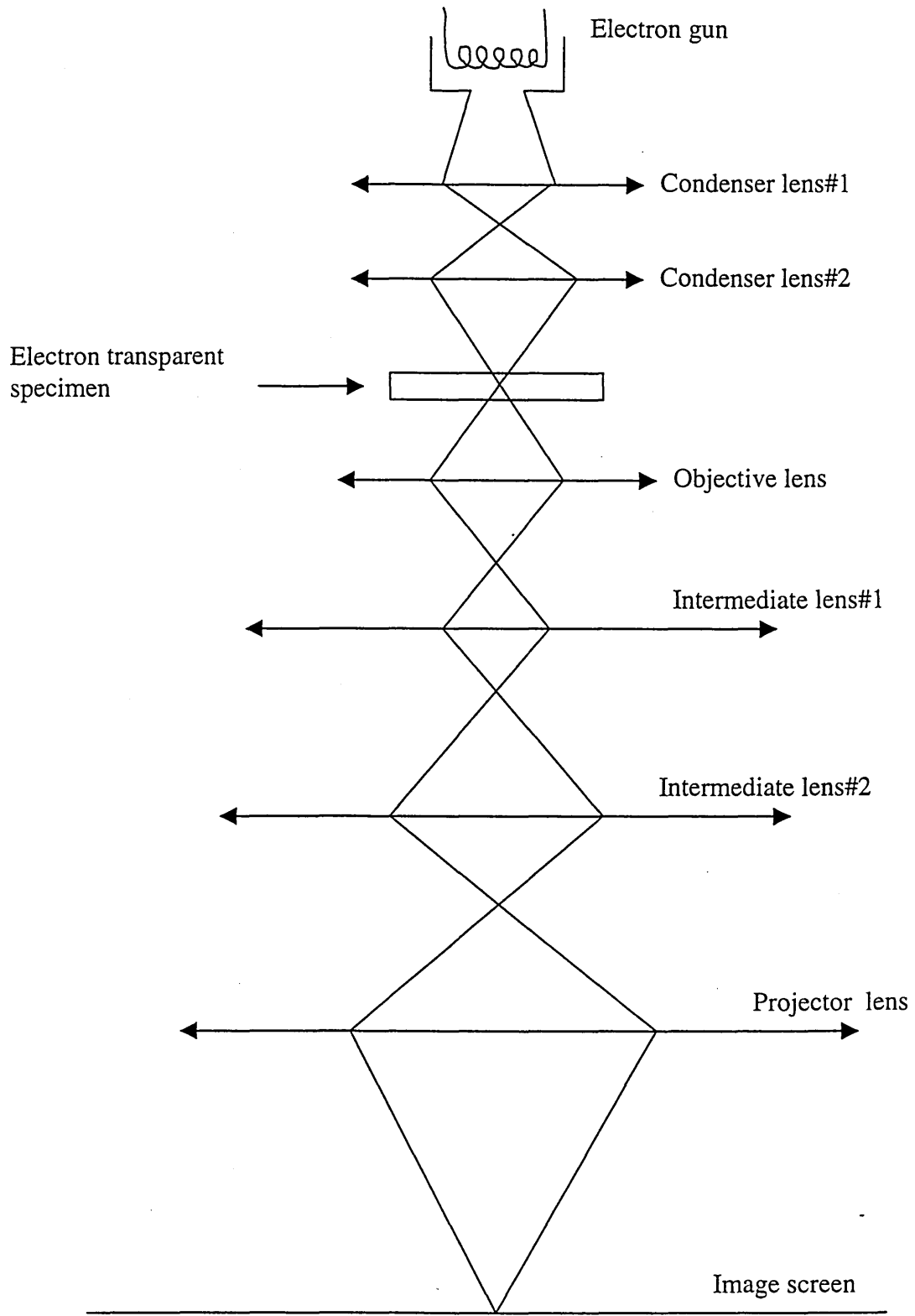


Figure 3.6: Ray diagram of the main components of a transmission electron microscope (TEM)

pattern may be taken from a specific area of the sample, known as selected area electron diffraction (SAED), and is formed at the back focal plane of the objective lens. The system must be maintained at a high vacuum of  $\sim 10^{-7}$  mbar.

The resolution of the system is essentially defined as the smallest separation of two points in an object that can be distinctly reproduced in the image. The limit of resolution can be given as [28],

$$(\Delta_r) = 1.22f\lambda/D \quad [3.22]$$

where  $\lambda$  is the de Broglie wavelength of the electrons,  $f$  is the focal length of the lens and  $D$  is the lens aperture diameter. Hence a reduction in the wavelength of the electrons will result in better resolution for a system with fixed dimensions. The de Broglie wavelength can be given as,

$$\lambda = \frac{h}{\sqrt{2mE}} \quad [3.23]$$

hence an increase in the energy of the electrons ( $E$ ) will result in a reduction in the wavelength of the electrons. Increasing the applied potential difference can therefore enhance the resolution in a TEM. A typical resolving power of a TEM is  $\sim 0.5$  nm while the best attain  $< 0.2$  nm [29].

### 3.8 Molecular beam epitaxy (MBE)

The basis of this growth technique is that epitaxial layers are grown by impinging thermal beams of molecules or atoms on a heated substrate (usually between  $\sim 520^\circ\text{C}$  and  $600^\circ\text{C}$ ) under ultra high vacuum (UHV) conditions. The substrate is usually chosen so that it is lattice matched to the material being grown. This allows the highest quality of crystal to grow on the substrate. In the particular case of compound semiconductors, separate cells for each of the component elements are needed to provide the atoms required for growth. Knudsen cells are used as the source of the molecular beams, and in effect they are heated enclosures, in which the elements required for growth are contained. The elevated temperature ensures a high vapour pressure, which forces the molecular beam out of an aperture, which is directed towards the substrate. A schematic of the MBE process is shown in figure 3.7.

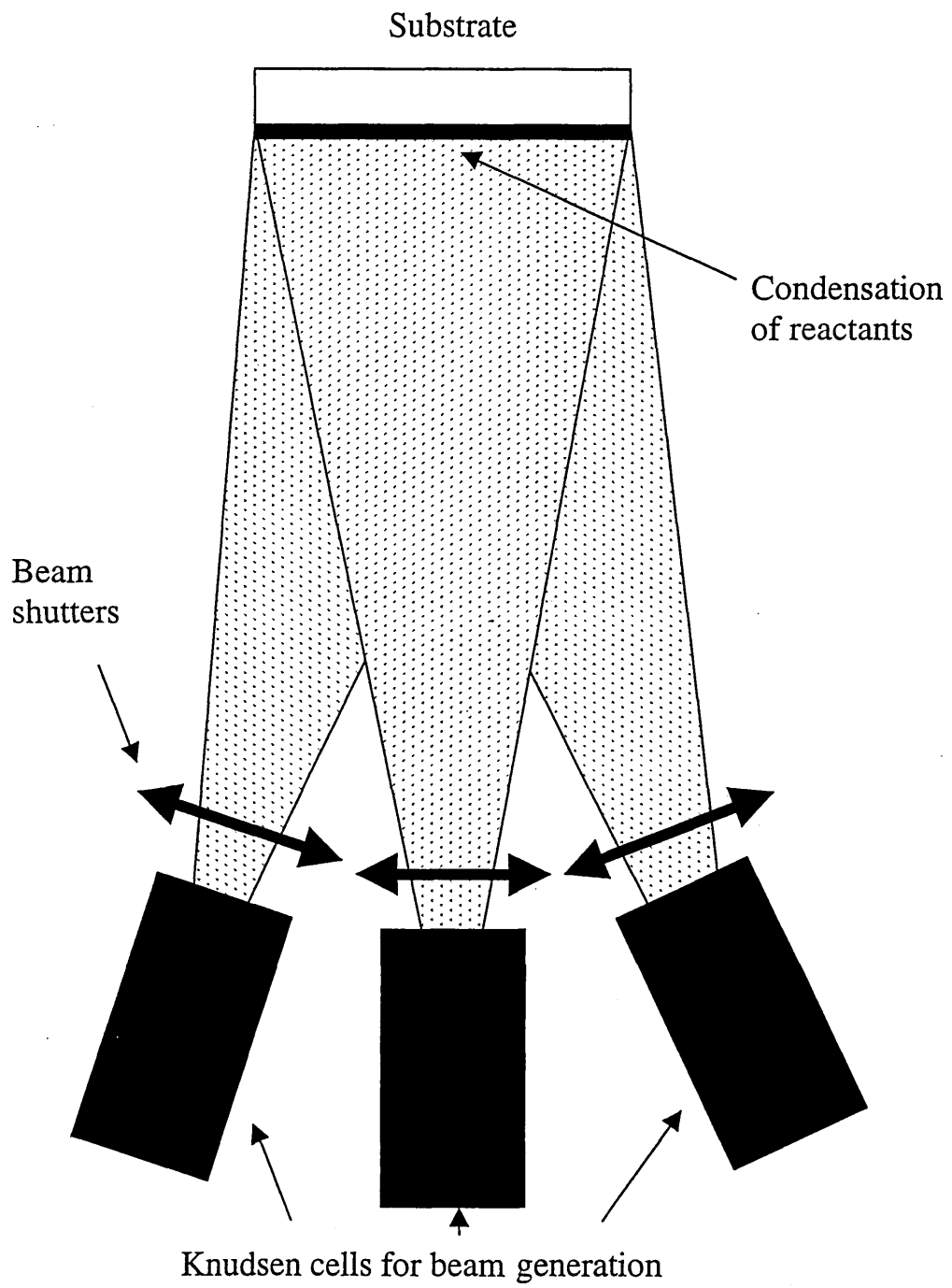


Figure 3.7: A schematic of the MBE growth process

The growth of multi-atom compounds such as  $\text{In}_x\text{Ga}_{1-x}\text{As}$  and  $\text{In}_y\text{Al}_{1-y}\text{As}$  can be difficult, and care must be taken to ensure that each of the sources is at the correct temperature for the respective molecular beams to form a stoichiometric solid. For the case of  $\text{In}_x\text{Ga}_{1-x}\text{As}$  and  $\text{In}_y\text{Al}_{1-y}\text{As}$ , As atoms will only stick to a group III surface, hence the rate limiting step is controlled by the arrival rate of the group III atoms. Therefore high quality epitaxial growth will take place if the group V/group III molecular beam flux ratio is above a certain value, which is a function of substrate temperature and surface orientation giving an “As stabilised “ surface structure [30]. The use of UHV means that atomic or molecular collisions are not important and the molecular beams are controlled by the cell temperature and mechanical shutters. UHV conditions also allow the use of reflection high energy electron diffraction (RHEED) to monitor the crystal structure throughout the growth procedure. In general the doping of epitaxial layers presents no real complications providing the elements concerned have a high sticking coefficient to the growth surface [31].

### 3.9 Measurement of the Schottky barrier height

The four most commonly applied methods of barrier height measurement are: -

1. I-V (current-voltage) characteristics.
2. C-V (capacitance-voltage) measurements.
3. Photoelectric measurements.
4. Photoemission studies.

In this thesis, Schottky barriers that have been previously measured by the I-V technique will be compared with values of  $\phi_b$  obtained by photoemission measurements. Hence in this section, a brief description of barrier height measurement by the photoemission technique is discussed.

#### 3.9.1 Photoemission measurements

The theory of photoemission is described in section 3.2. To obtain the barrier height, it is necessary to establish the position of the Fermi level,  $E_f$ , with respect to the valence band edge at the surface,  $E_{vs}$ . This is achieved by measuring an energy spectrum for a metal in electrical contact with the semiconductor; often the emission from the

metallic sample holder is used. Electrons emerging with the highest kinetic energies will originate from the Fermi level of the metal, which will be exactly the same as the Fermi level of the semiconductor. Hence the Fermi energy,  $E_f$ , may be established, allowing the barrier height to be found from the difference in the maximum energies of the photoelectrons from the metal and the semiconductor, respectively, using the equation,

$$\phi_b = E_g - (E_f - E_{vs}) \quad [3.24]$$

where  $E_g$  is the known energy gap of the semiconductor [5].

For metal coverages of more than a few Ångströms, photoemission from the metal overlayer tends to conceal that from the substrate and hence the accurate determination of  $E_f - E_{vs}$  becomes difficult. Photoelectron spectroscopy is therefore only suitable for measuring barrier heights for ultra-low metal coverages. In the cases where band bending occurs, changes in the binding energy of bulk components are monitored in order to determine the barrier height as described in section 3.6. However, the other binding energy shifts mentioned in chapter 3 can complicate the interpretation of the data, and hence the accuracy of Schottky barrier height determination by photoemission is perhaps at best  $\pm 0.1$  eV [5].

### 3.10 References

- [1] A. Einstein, *Ann. Physik*, **17**, 132 (1905).
- [2] T. Koopmans, *Physica*, **1**, 104 (1933).
- [3] C.S. Fadley in "Electron Spectroscopy: Theory, Techniques and Applications, Vol. 2", edited by C.R. Brundle and A.D. Baker, Academic Press (1978).
- [4] J.J. Yeh and I. Lindau, *Atomic Data and Nuclear Tables*, **32**,1 (1985).
- [5] E.H. Rhoderick and R.H. Williams, "Metal-Semiconductor Contacts", Clarendon Press, Oxford (1988) and references therein.
- [6] "Practical Surface Analysis, 2<sup>nd</sup> Edition, Volume 1 Auger and x-ray Photoelectron Spectroscopy", edited by D. Briggs and M.P. Seah, John Wiley and Sons (1990).
- [7] P.J. Feibelman and D.E. Eastman, *Phys. Rev. B*, **10**, 4932 (1974).
- [8] G.D. Mahan, *Phys. Rev. B*, **10**, 4392 (1970).
- [9] B. Feuerbacher and R.F. Willis, *J. Phys. C: Solid St. Phys.* **9**, 169 (1976).
- [10] C.N. Berglund and W.E. Spicer, *Phys. Rev.* **136**, (4A), A1030 (1964).
- [11] E.W. Plummer and W. Eberhardt, *Advances in Chemical Physics*, **49**, 533 (1982).
- [12] C. Cohen-Tannoudji, B. Dui and F. Laloë, "Quantum Mechanics, Vol. 2", J. Wiley & Sons (1977).
- [13] J.W. Cooper, *Phys. Rev.* **128**, 681 (1962).
- [14] M.P. Seah and W.A. Dench, *Surface and Interface Analysis*, **1**, 2 (1979).
- [15] D.P. Woodruff and T.A. Delchar, "Modern Techniques of Surface Science", Cambridge University Press (1990).
- [16] L.J. Brillson, *J. Vac. Sci. Technol.* **15** (4), 1378-1383 (1978).
- [17] W.A. Harrison, "Electronic Structure and Properties of Solids", W.H. Freeman and Co. (1980)
- [18] C. J. Spindt, M. Yamada, P. L. Meissner, K. E. Miyano, A. Herrera, W. E. Spicer and A. J. Arko, *J. Vac. Sci. Technol.* **B9** (4), 2090 (1991).
- [19] R. Ludeke, *Surf. Sci.* **132**, 143 (1983).
- [20] R.D. Rusk, "Introduction to Atomic and Nuclear Physics", Meredith Publications (1964)
- [21] W.H. Press, B.P. Flannery, S.A. Teukolsky and W.T. Vetterling, "Numerical Recipes in Fortran", Cambridge University Press (1986).

- [22] D.W. Marquardt, *J. Soc. Ind. Appl. Math.* **11**, 431 (1963).
- [23] J.J. Joyce, M. Del Guidice and J.H. Weaver, *J. Electron. Spec. Rel. Phen.* **49**, 31 (1989)
- [24] D.A. Shirley, *Phys. Rev. B*, **5**, 5, 4709 (1972).
- [25] M. Prutton, "Surface Physics, 2<sup>nd</sup> Edition", Oxford University Press (1983).
- [26] J.B. Pendry, "Low Energy Electron diffraction", Academic Press, London (1974).
- [27] E.A. Wood, *J. Appl. Phys.* **35**, 1306 (1964).
- [28] E. Hecht, "Optics, 2<sup>nd</sup> Edition", Addison-Wesley Publishing Company (1987).
- [29] H. Benson, "University Physics", John Wiley & Sons (1991)
- [30] "The Technology and Physics of Molecular Beam Epitaxy", edited by E.H.C Parker, Plenum Press, London and New York, (1985) and references therein.
- [31] D.V. Morgan and K. Board, "An introduction to Semiconductor Microtechnology", John Wiley & Sons (1983).

separated from the chamber by a valve and a crosspiece (to allow the transfer arm to be pumped down) for transferring samples to and from the chamber without losing UHV.

#### 4.1.4 Sample preparation

All  $\text{In}_{0.53}\text{Ga}_{0.47}\text{As}(100)$  and  $\text{In}_{0.52}\text{Al}_{0.48}\text{As}(100)$  samples were grown at the University of Wales, College of Cardiff using a VG Semicon V80H molecular beam epitaxy (MBE) system. Epi-ready 2-inch diameter  $\text{InP}(100)$   $n^+$ , S- doped substrates were cleaved into quarters and In bonded to Mo platters. The  $\text{In}_{0.53}\text{Ga}_{0.47}\text{As}(100)$  and  $\text{In}_{0.52}\text{Al}_{0.48}\text{As}(100)$  layers were grown at  $500^\circ\text{C}$ . The III to group V flux ratio was set to the minimum necessary to maintain an  $\text{As}_4$  stabilised,  $(2\times 1)$  surface reconstruction, observed by reflection high energy electron diffraction (RHEED). The samples were doped with Si to yield a carrier density of  $n \approx 2\times 10^{18} \text{ cm}^{-3}$ . All epilayers were  $1\mu\text{m}$  thick, grown at a rate of approximately  $1\mu\text{m h}^{-1}$ . At termination of growth, on cooling in an  $\text{As}_4$  flux, the surface reconstruction observed by RHEED transformed from a  $(2\times 1)$  to a  $(3\times 1)$  symmetry at which point the  $\text{As}_4$  flux was shuttered and cooled. The substrate was then further cooled, under UHV conditions, to less than  $-30^\circ\text{C}$  over a period of at least nine hours. No RHEED reconstructions were observed at substrate temperatures below  $150^\circ\text{C}$ . This was probably due to the condensation of ambient  $\text{As}_4$  from the growth chamber onto the sample surface. Below a substrate temperature of  $-30^\circ\text{C}$  the  $\text{As}_4$  source was reheated and opened to generate an  $\text{As}_4$  flux ( $\approx 10^{-5}$  mbar) on to the sample surface for approximately one hour until the initially mirror like surface became opaque. Following As deposition the samples were allowed to warm up slowly to room temperature over a period of one hour. The samples were then removed from the MBE system and de-mounted from the Mo blocks by heating to  $160^\circ\text{C}$  to melt the indium solder. The capped samples were then stored in a low vacuum chamber ( $\sim 1$  mbar) before transportation to the surface analysis chamber at Daresbury.

Once at the Daresbury SRS, the samples were cleaved into pieces of approximately 1cm by 0.5cm. The samples were then mounted onto a molybdenum spade with In solder as shown in figure 4.5. The spade was then admitted to the analysis chamber via a magnetic transfer arm that was pumped down to  $\sim 10^{-8}$  mbar before opening the valve to the chamber. The sample spade was then placed in the manipulator using a pincer wobble stick.

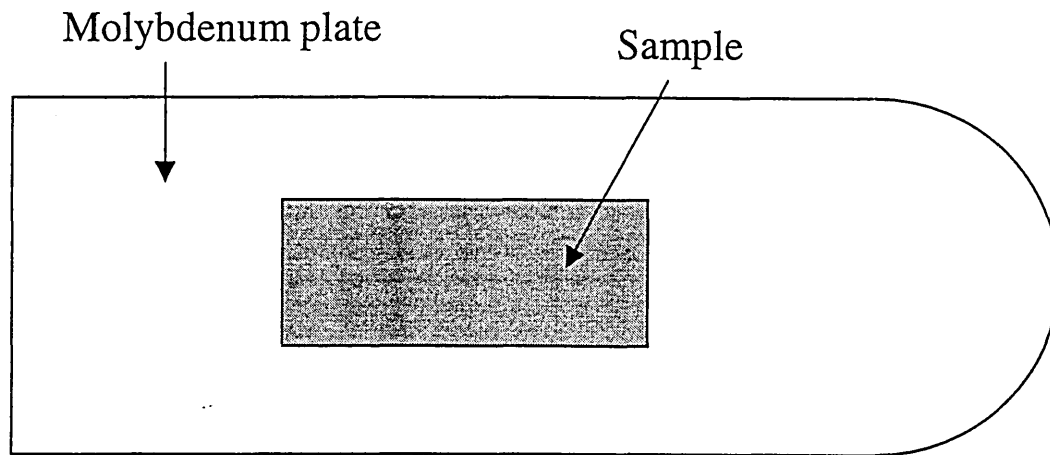


Figure 4.5: Sample spade used at Daresbury laboratory for mounting  $\text{In}_{0.53}\text{Ga}_{0.47}\text{As}(100)$  and  $\text{In}_{0.52}\text{Al}_{0.48}\text{As}(100)$  samples.

The sample was decapped at  $350^\circ\text{C}$  in the manipulator by way of an e-beam heater directly behind the sample spade, which was in thermal contact with the sample. The thermocouple attached to the manipulator lagged behind the actual temperature of the sample and so a calibration curve was produced for emission current versus sample temperature using an IR pyrometer. The accuracy of the temperature measurement using this technique is estimated to be  $\pm 25^\circ\text{C}$ . The atomically clean  $(3\times 1)$  reconstructed surfaces were achieved by further annealing at  $390^\circ$  and monitored using the LEED facility in the chamber. Once a clean  $(3\times 1)$  reconstructed surface had been achieved, photoemission studies of metal-semiconductor interface formation could begin.

#### 4.1.5 Metal evaporation sources

Resistive heating was employed for the thermal evaporation of both the indium and gold metals. 5N purity metal was wound around a thoroughly outgassed coil of tungsten wire. The metals melted on to the wire by passing a current through the tungsten filament. Increasing the filament current produced a steady flux of evaporant species, which was directed onto the sample by a collimating tube. Each source was thoroughly outgassed prior to evaporation of metal onto the clean semiconductor surface. A schematic of the evaporation source is shown in figure 4.6. The thickness ( $d_s$ )

of the metal deposited on to the sample, was measured by an Intellemetrics quartz crystal monitor and is given by the equation [5],

$$d_s = \left( \frac{r_2}{r_1} \right)^2 d_q \quad [4.1]$$

where  $r_1$  is the distance between the sample and the source,  $r_2$  is the distance between the monitor and the source and  $d_q$  is the thickness measured by the quartz crystal monitor. In the experiments performed on beamline 4.1, the value  $(r_2 / r_1)^2$  was  $\sim 0.04$ . The overlayer was initially deposited at a flux rate of  $\sim 0.02$  nm/s in small thickness steps. This flux rate increased to  $\sim 0.05$  nm/s for larger deposition thickness', thus allowing characterisation of interface formation at sub-monolayer, monolayer and thick metallic coverages.

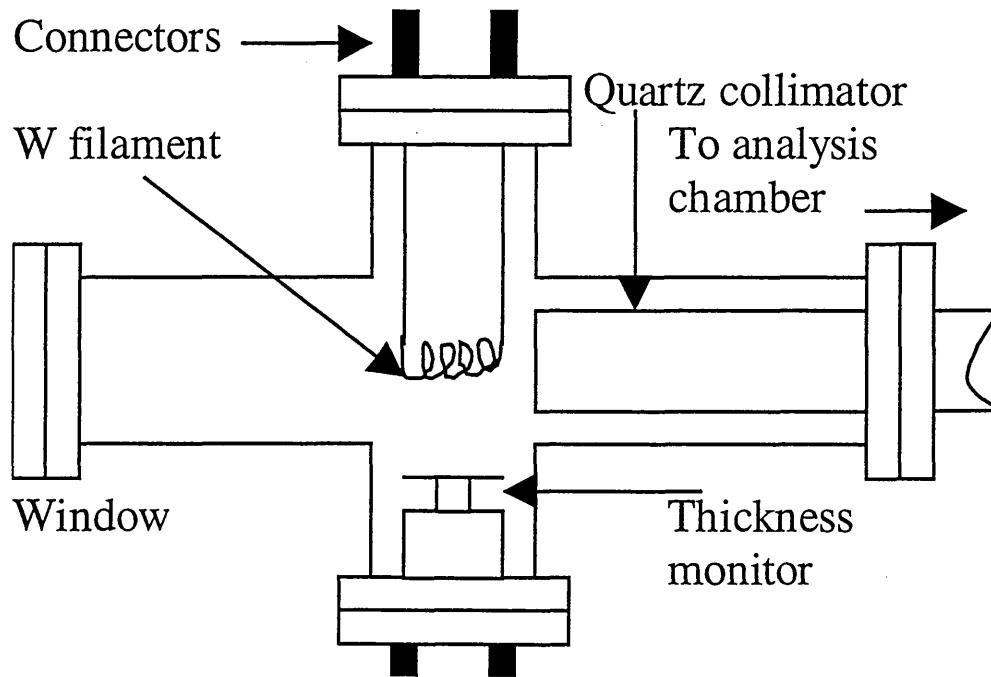


Figure 4.6: Schematic of the evaporation sources used on beamline 4.1

#### 4.1.6 The Scienta SES energy analyser

The photoelectrons emitted from the sample surface are detected by a Scienta SES 200 analyser. This is a relatively new analyser, which is based on the concentric hemispherical analyser (CHA) described by Rivière [6]. The basic form of a CHA is illustrated in figure 4.7 and consists of two concentric hemispheres of radius  $R_1$  and  $R_2$ . A potential difference is applied between the two hemispheres which results in only electrons of a selected energy known as the pass energy ( $E_p$ ) entering via the two hemispheres to the detector array of channel plates.

An electrostatic field is set up within the two plates by applying potentials  $-V_1$  and  $-V_2$  to the inner and outer plates, respectively, with  $V_1$  positive compared to  $V_2$ . An electrostatic lens focuses the photoelectrons so that they can pass through the entrance slit (width  $w$ ) on the Herzog plate. The median equipotential surface between the two hemispheres has a radius  $R_0$  and the entrance and exit slits are centred on this surface. The potential  $-V_0$  along the equipotential surface is given by [6],

$$V_0 = \frac{V_1 R_1 + V_2 R_2}{2R_0} \quad [4.2]$$

The Herzog plate retards or accelerates the electrons to the pass energy and the electrons travel in a circular orbit of radius  $R_0$  through the hemispheres to the exit slit where they are detected. The relationship between analyser pass energy ( $E_p$ ) and the potential difference ( $\Delta V$ ) across the hemispheres is given by [6],

$$e\Delta V = E_p \left( \frac{R_2}{R_1} + \frac{R_1}{R_2} \right) \quad [4.3]$$

If the pass energy is kept constant during an experiment, the voltage on the Herzog plate must be scanned in order to obtain an EDC. For example, to scan an energy range of 35-45 eV with a pass energy of 20 eV, the retard voltage would have to vary from 15-25 eV in accordance with the equation [7],

$$E_k = E_p + eV_r \quad [4.4]$$

In this case the EDC's are acquired in constant analyser energy (CAE) mode and the resolution of the spectra is kept constant for all core levels since the detected electrons all have the same energy,  $E_p$ . The resolution of a CHA is given by [8],

$$\frac{\Delta E}{E_p} = \frac{w}{2R_0} + \frac{\alpha^2}{4} \quad [4.5]$$

Here,  $w$  is the entrance slit width,  $R_0$  is the radius of the electrons circumventing the hemispheres and  $\alpha$  is the acceptance angle of the analyser. From equation 4.5 it can be seen that the resolution of the analyser can be improved by either reducing the pass energy or the slit width. However, a reduction in the slit width will also reduce the intensity of detected photoelectrons, and hence a compromise between resolution and intensity must be found.

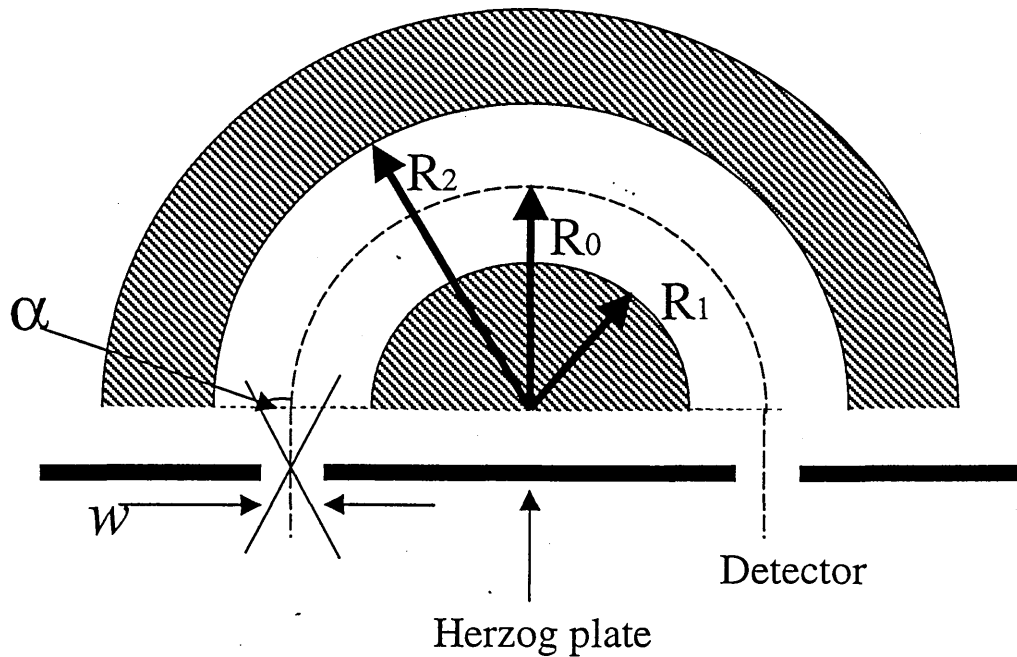


Figure 4.7: A schematic diagram of the Scienta SES 200 Concentric Hemispherical Analyser used on beamline 4.1.

The Scienta analyser detector system consists of a CCD camera, a phosphorous screen and two micro-channel plates (MCP's) which increase the resolution and the number of electrons detected. The CCD camera which detects the number and kinetic energy of the electrons is situated behind the phosphorous screen attached to the micro-channel plates as shown in figure 4.8. The photoelectrons that have circumvented the hemispheres hit the MCP's and produce an electron distribution curve. The MCP pair multiplies each incoming photoelectron  $\sim 10^7$  times by generating a cascade of electrons in a similar way to conventional channeltrons and this electron pulse is accelerated to the phosphor screen where it produces a light flash. The CCD camera detects this flash, and the position of the light flash is a unique function of the kinetic energy by which the corresponding electron was emitted [9]. The video signal from the camera is attached to the detector electronics and a microprocessor, which obtains the data. The signal is recorded as a function of intensity against kinetic energy and the data is stored on a PC where it can be changed into ASCII format. Once in ASCII format, the data can be analysed using TCFIT, a curve fitting program devised and developed by A. A. Cafolla [10], details of which are described in chapter 3.

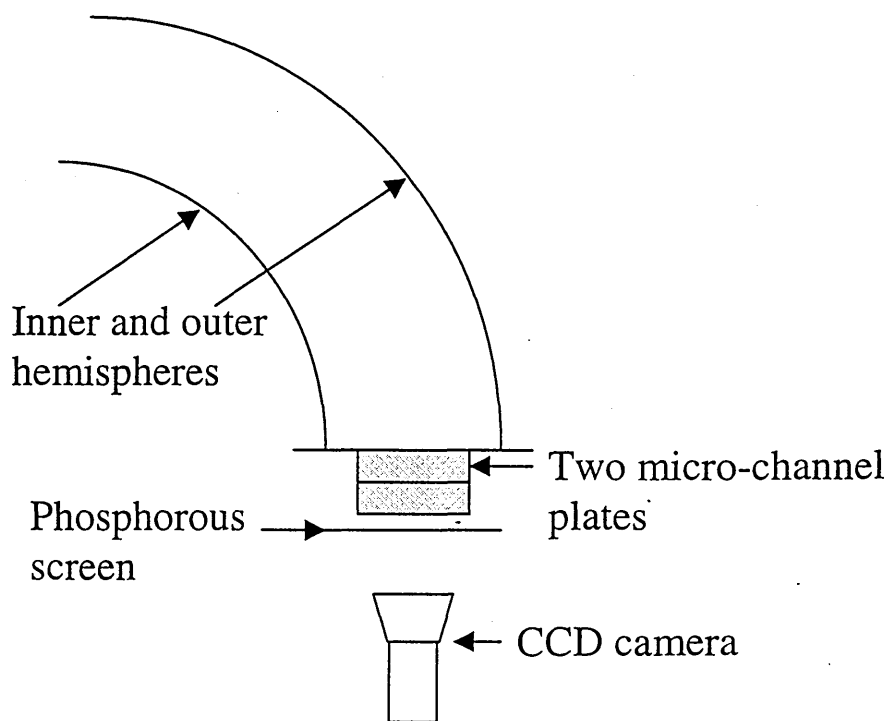


Figure 4.8: A schematic of the Scienta analyser detection system [9]

### 4.1.7 LEED apparatus

The LEED system at Daresbury is made up of an electron gun, four concentric spherical grids and a fluorescent screen and is shown schematically in figure 4.9. The electron gun produces a collimated beam of monoenergetic electrons with an energy range of  $\sim 20\text{-}400$  eV which is fired at the sample, and subsequently backscattered towards the grids. The earthed sample was positioned at the centre of curvature of the grids and G1, G2 and G3 are held at earth to inhibit the formation of electric fields that would interfere with the backscattered electrons [11]. A negative potential is placed on the retard grid with respect to earth. The potential is directly linked to the energy of the electron beam, and is set so that only elastically backscattered electrons can pass through to the fluorescent screen. The screen is applied with a large positive voltage ( $\sim 7$  kV) which accelerates the electrons towards it. The diffracted beams reach the screen, emitting light and producing spots on the screen. Hence the diffraction pattern can be observed, and recorded onto film with the use of a camera.

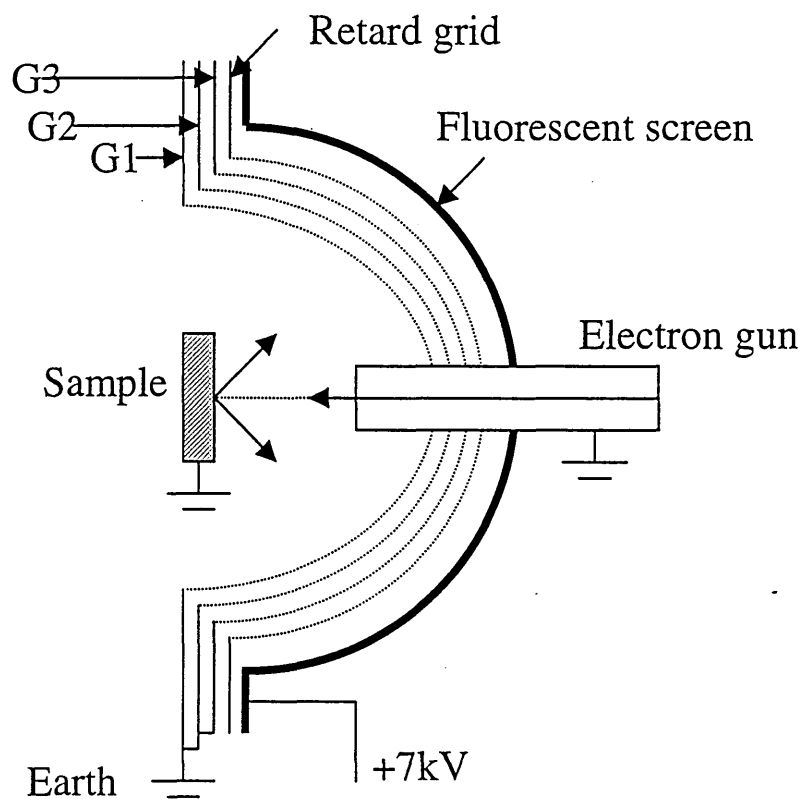


Figure 4.9: A schematic of the LEED system at Daresbury

## 4.2 The Sheffield Hallam Microlab

The VG microlab at Sheffield Hallam University contains a number of surface science analysis techniques including XPS, Auger Electron Spectroscopy (AES) and Secondary Ion Mass Spectroscopy (SIMS). However, for the sole purpose of a preliminary decapping study, only XPS was utilised.

The UHV system was comprised of an XPS/AES analysis chamber, a SIMS chamber and a sample heating/evaporation chamber which were all interconnected via a transfer chamber as shown schematically in figure 4.10. The heating chamber was isolated from the transfer chamber using a gate valve. The samples were introduced to the system via a load lock chamber connected to the transfer chamber in order to maintain vacuum and were subsequently transferred to the XPS analysis chamber by a combination of railway tracks and wobblesticks. The sample was transferred to the heating chamber via a magnetic transfer arm and wobblesticks. The load lock chamber was rough pumped by a rotary pump to  $\sim 5 \times 10^{-3}$  mbar. The analysis and transfer chambers were individually pumped by liquid nitrogen trapped oil diffusion pumps to  $\sim 1 \times 10^{-10}$  mbar and the sample heating/evaporation chamber was maintained at  $\sim 5 \times 10^{-10}$  mbar using a turbo pump.

### 4.2.1 Sample mounting and heater stage

The samples used for decapping studies in the microlab were prepared in exactly the same way and from the same wafer as those in the SXPS experiments described in section 4.1.4. The samples were mounted on to thin silicon heater strips with In solder in order to produce a good thermal contact. The silicon strips were then mounted on to specially designed heater stubs that allowed resistive heating of the silicon strip (see figure 4.11). The stub casing acts as an earth contact and the isolated screw passing through the body of the stub acts as the other electrical contact. The sample was heated by passing electric current through the silicon strip. The relationship between applied current and sample temperature was calibrated by way of an IR pyrometer with an additional reference point at the melting point of In ( $156^\circ\text{C}$ ). A typical calibration curve is shown in figure 4.12 with the accuracy of the temperature measurement using this technique estimated to be  $\pm 25^\circ\text{C}$ .

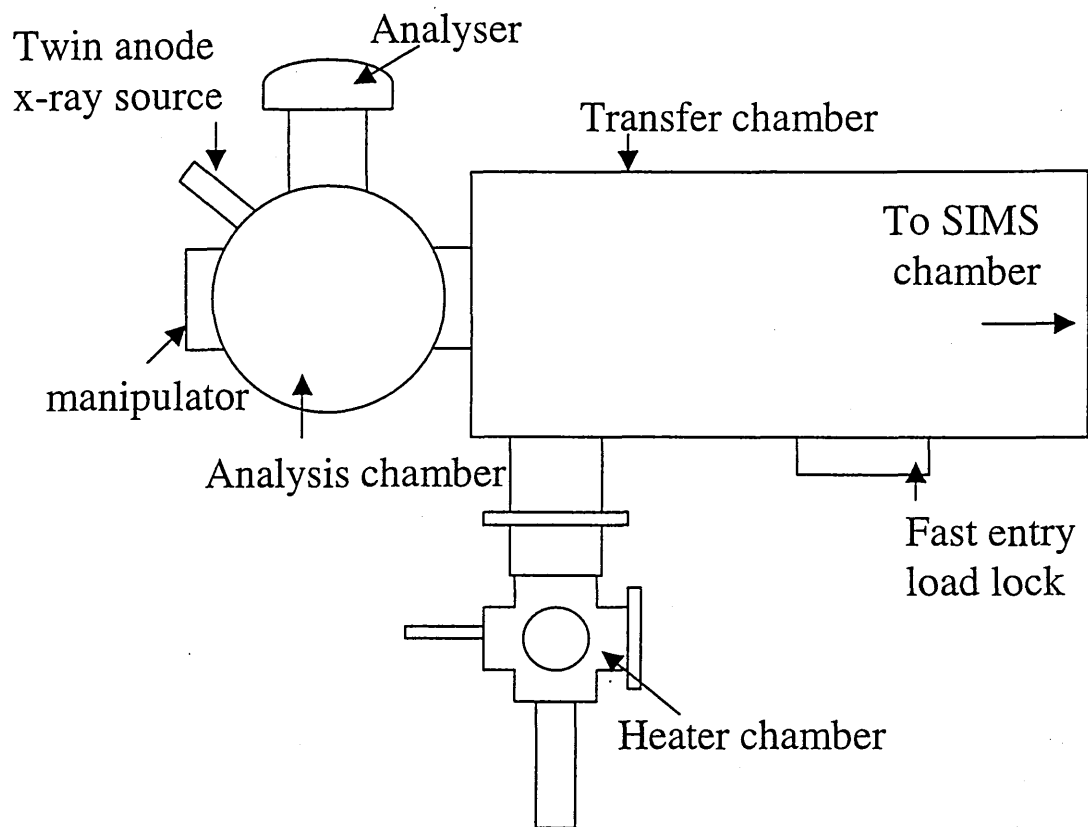


Figure 4.10: A plan view schematic of the VG microlab system at Sheffield Hallam University.

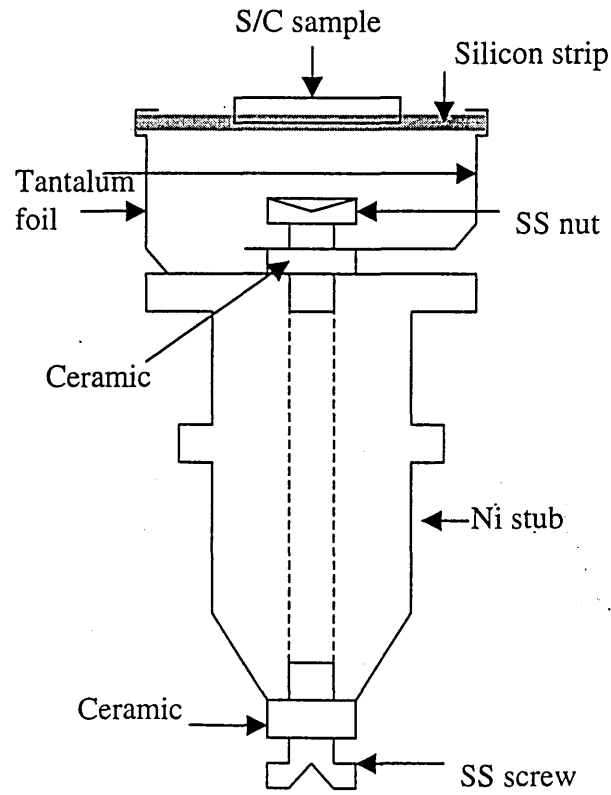


Figure 4.11: The heater stub designed for As decapping experiments.

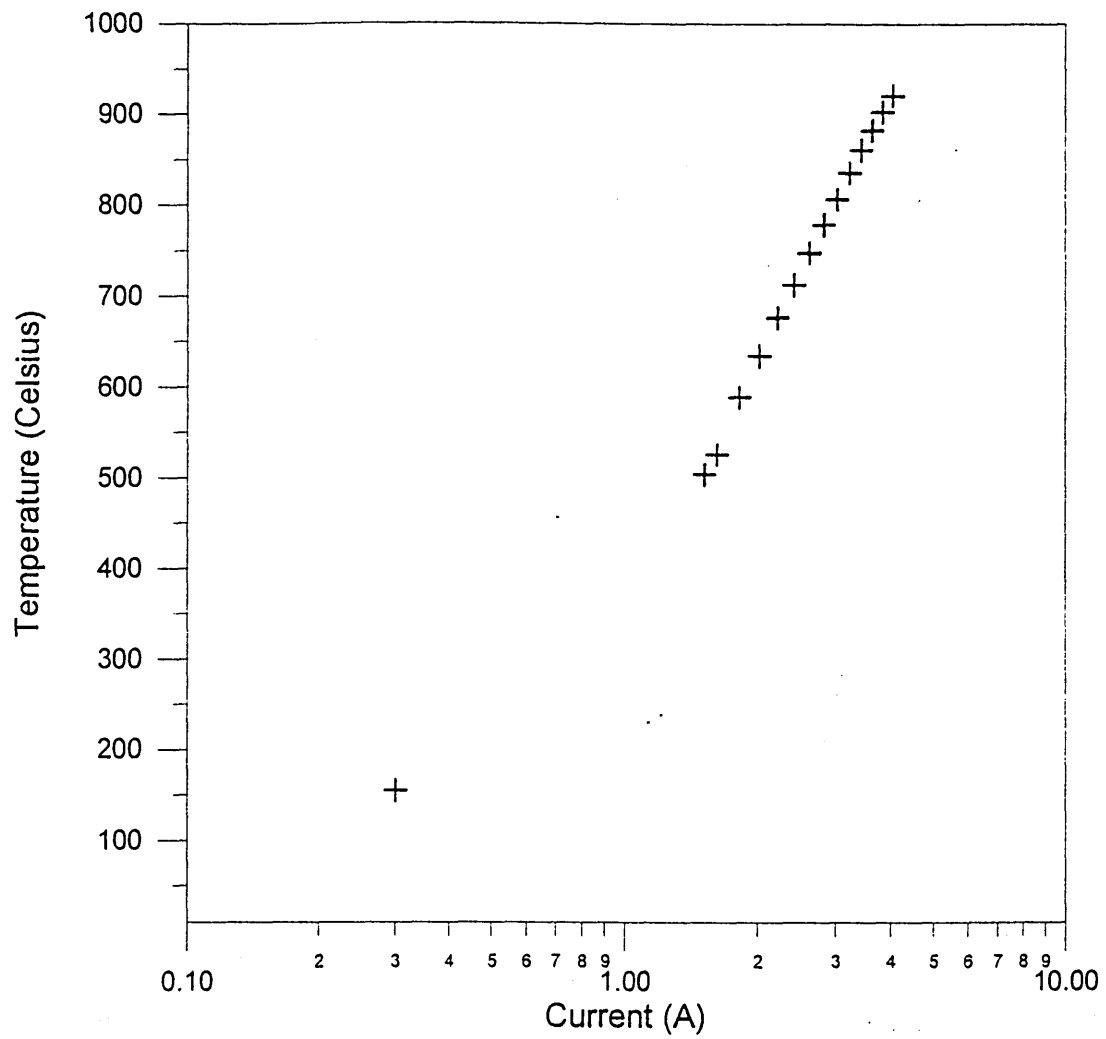


Figure 4.12: Calibration curve of applied current versus temperature for the silicon heater stub used at Sheffield Hallam University.

The sample heating stage with external electrical contacts was attached to a manipulator that allowed horizontal orientation and 360° rotation. In order to heat the sample, current was passed through the silicon strip on the heater stub via the external contacts. The sample was rotated to face the viewport window so that the temperature could be measured with an IR pyrometer and the condition of the As cap could be observed by the eye.

#### **4.2.2 The Microlab X-ray sources**

The microlab analysis chamber was equipped with a twin anode x-ray source capable of producing Al K $\alpha$ (1486.6 eV) and Mg K $\alpha$  radiation. The source was operated at an accelerating voltage of ~15 kV and a 20 mA target current. The x-rays passed through a thin (~1  $\mu$ m) Al window separating the x-ray source from the chamber. This window protects the sample from contamination from the source and also reduces the amount of background radiation (Bremsstrahlung). The sample surface was uniformly irradiated with a low flux of x-rays over an area corresponding to the size of the sample (~1 cm<sup>2</sup>). The natural linewidth (FWHM) of the Al K $\alpha$  and Mg K $\alpha$  sources were 0.85 eV and 0.7 eV, respectively.

#### **4.2.3 The Microlab energy analyser**

The energy analyser used in the microlab was a concentric hemispherical analyser (CHA) which has been described in section 4.1.6. The detector system however was slightly different from the Scienta SES analyser. The detector array consisted of five channeltrons. The analyser was used in CAE mode where the retardation of the electrons is varied while the pass energy remains constant ensuring a constant energy resolution during a scan. The data was acquired by a DEC PDP 11/53 microcomputer which was linked to the CHA. This microcomputer varied the lens voltage, the retard voltage, the channeltron voltages and the voltages to both hemispheres whilst sampling the ratemeter signal in order to produce a digitised energy distribution curve which was subsequently stored on disc for future analysis.

### 4.3 The Transmission electron microscope and sample preparation

The TEM observations were carried out on a Hitachi H800-NA electron microscope operating at 200 keV at Barcelona University. Samples were viewed in plan view and cross section to provide complimentary information on the mode of growth of the metal overlayers and the nature of the metal-semiconductor interface that had been formed. Peiró [12] and Romano et al. [13] have carried out detailed reports of TEM sample preparation and hence only a brief description of sample preparation is presented here.

Cross sectional samples were produced by cutting the metallised samples resulting from the experiments at Daresbury into thin strips and then bonding them together metal overlayer to metal overlayer as in figure 4.13. The samples were then attached to silicon strips in order to produce a “sandwich” (figure 4.13) for stability during the polishing process. The sandwiches were then subjected to a mechanical flat polish, reducing them to a thickness of 50  $\mu\text{m}$  and subsequently a mechanical concave polish to 25-30  $\mu\text{m}$ . Once at this thickness the sample was mounted on to a copper ring of 3.05 mm diameter with the sample centred over a 600  $\mu\text{m}$  diameter hole in the middle of the ring (figure 4.14). The sample was then transferred to a Gatan ion milling machine where it was  $\text{Ar}^+$  etched until it became perforated. During ion milling, a low energy (4 keV), low intensity (0.15 mA) ion beam was used and the sample was held in a liquid nitrogen cooled stage in order to prevent both the evaporation of phosphorous from the InP substrate and the production of In islands. Planar view samples were prepared in a similar way, details of which have also been described elsewhere [12,13]. Once the samples had been ion milled to a stage where they were transparent, they could be transferred to the electron microscope for SAED and TEM studies.

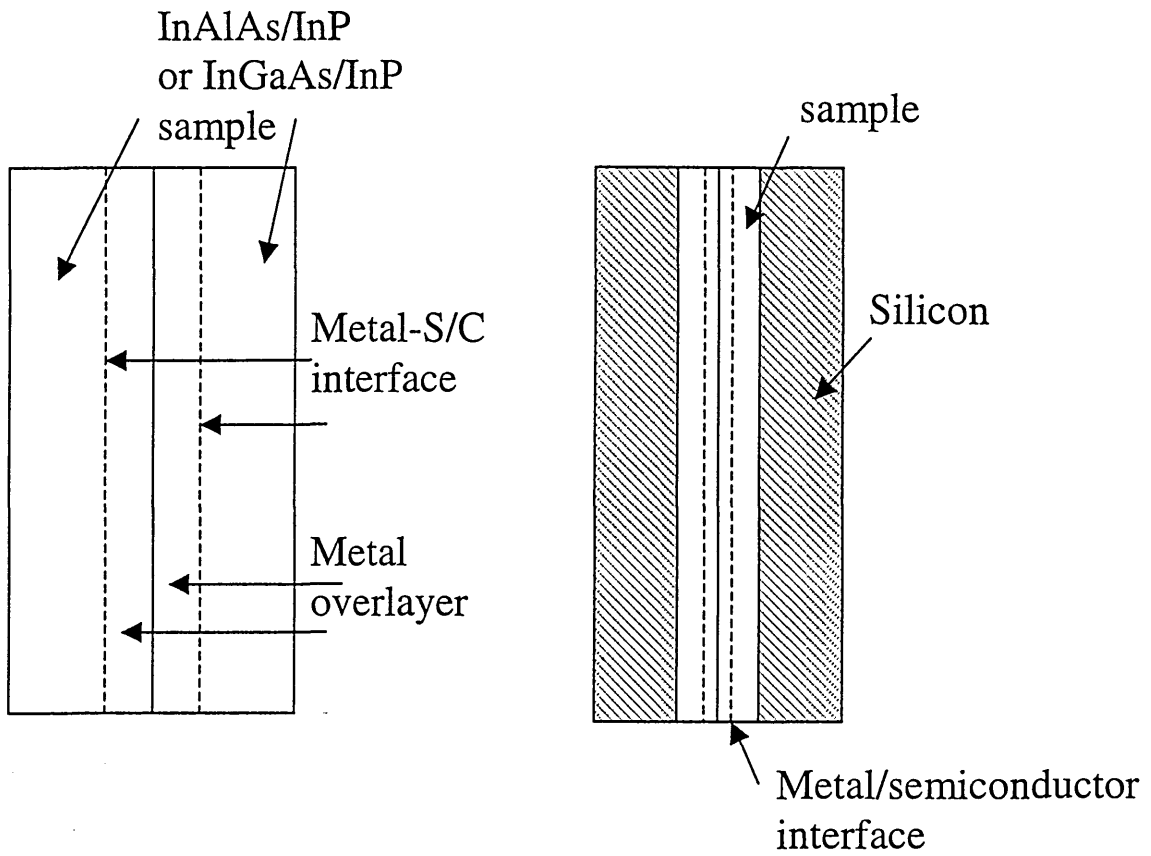


Figure 4.13: The production of Silicon/semiconductor sample “sandwiches” for TEM studies.

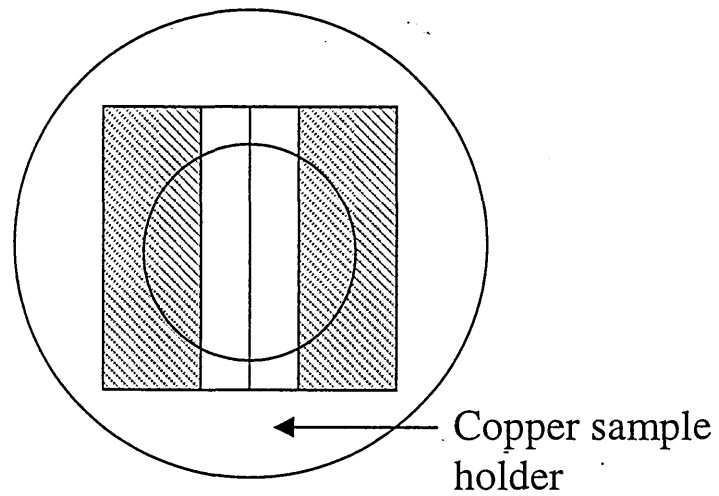


Figure 4.14: TEM sample mounted and centred on a copper ring for ion milling and TEM purposes.

#### 4.4 References

- [1] W. Hayes, *Contemp. Phys.*, **13**, 441 (1972)
- [2] C.T. Chen, *Nuc. Instr. Meth. Phys. Res.*, **A256**, 595 (1987)
- [3] V.R. Dhanak, A.W. Robinson, G. van der Laan and G. Thornton, *Rev. Sci. Instrum.* **63**, 1342 (1992)
- [4] "Practical Surface Analysis, 2<sup>nd</sup> Edition, Volume 1 Auger and x-ray Photoelectron Spectroscopy", edited by D. Briggs and M.P. Seah, John Wiley and Sons (1990)
- [5] J.W. Cairns, PhD Thesis, University of Wales (1991)
- [6] J.C. Rivière, in "Practical Surface Analysis, 2<sup>nd</sup> Edition, Volume 1 Auger and x-ray Photoelectron Spectroscopy", edited by D. Briggs and M.P. Seah, John Wiley and Sons (1990)
- [7] P.R Dunstan, PhD Thesis, University of Wales, College of Cardiff (1998).
- [8] A.B. Christie, in "Methods of Surface Analysis", edited by J.M. Walls, published by Cambridge University Press (1986)
- [9] Operating instructions for the Scienta SES 200 Analyser manufactured by Scienta.
- [10] A. A. Cafolla, *Surf. Sci.* **402-404**, 561-565 (1998).
- [11] D.P. Woodruff and T.A. Delchar, "Modern Techniques of Surface Science", Cambridge University Press (1986)
- [12] F. Peiró, PhD Thesis, Barcelona (1993)
- [13] A. Romano, J. Vanhellefont, H. Hender and J.R. Morante, *Ultramicroscopy* **31**, 183 (1989)

# Chapter 5

## Arsenic decapping of the $\text{In}_{0.53}\text{Ga}_{0.47}\text{As}$ surface

### 5.0 Introduction

The motivation for this study, as discussed in chapter 1 was the observation by Clark *et al.* that In contacts to intimate  $\text{In}_{0.53}\text{Ga}_{0.47}\text{As}(100)$  formed under cryogenic deposition conditions produced improved rectification compared to diodes formed at room temperature by conventional methods [1].

In chapters 6 & 7 the nature of the interfaces between two metals, In and Au, with the semiconductor materials  $\text{In}_{0.53}\text{Ga}_{0.47}\text{As}$  and  $\text{In}_{0.52}\text{Al}_{0.48}\text{As}$  and the reactions occurring during their formation are probed using SXPS. In the work carried out by Clark *et al.* discussed previously, the intimate interfaces were formed by metallisation of “*as grown*”  $\text{In}_{0.53}\text{Ga}_{0.47}\text{As}$  surfaces by transferring the samples from the MBE reactor straight after growth under UHV conditions to an integrated metallisation chamber. Hence the clean semiconductor surfaces were not subjected to air exposure prior to the diodes being formed.

Characterisation of such interfaces by SXPS necessitates air exposure and hence potential contamination, as the samples need to be transferred from the MBE reactor to the synchrotron radiation facility, in air. To be consistent with the work carried out by Clark *et al.*, the clean “*as grown*” (3×1) reconstructed surface upon which the diodes were formed, needs to be reproduced in the SXPS chamber. The method utilised in this work therefore was to form a protective As “cap” on the surfaces, after growth, in the MBE reactor. The samples could then be transferred through air to the surface analysis chamber at Daresbury. Details of the As capping procedure are described in section 4.1.4 Once in the SXPS chamber, the cap can be thermally desorbed leaving behind a surface that closely replicates that of the “*as grown*” surface.

Numerous studies have taken place to assess the validity of the As capping technique for comparison with “*as grown*” surfaces of a variety of semiconductor materials [2-4]. Extensive XPS and LEED studies have been carried out by Lau *et al.* [3] and Clark [4,5] on the decapping of MBE grown  $\text{In}_{0.53}\text{Ga}_{0.47}\text{As}$  and  $\text{In}_{0.52}\text{Al}_{0.48}\text{As}$  respectively. The results presented indicate that within the limits of the investigation

techniques employed, As capping/decapping is a viable method of preserving and regenerating clean surfaces that closely replicate those obtained straight after growth. In the following chapter a preliminary decapping study is presented, undertaken in the Microlab at Sheffield Hallam University on As capped  $\text{In}_{0.53}\text{Ga}_{0.47}\text{As}$  samples, to define an As-decapping process technology prior to undertaking experiments at the Daresbury synchrotron radiation laboratory.  $\text{In}_{0.53}\text{Ga}_{0.47}\text{As}$  samples were selected for study, as investigations of  $\text{In}_{0.52}\text{Al}_{0.48}\text{As}$  decapping using the same techniques have been described elsewhere [4,5]. A LEED facility is currently not available at Sheffield Hallam University; therefore LEED patterns obtained at Daresbury of the decapped surfaces are described in chapter 6.

## 5.1 Arsenic cap sublimation

The removal of the As cap was carried out in the Microlab surface analysis chamber at Sheffield Hallam University described in chapter 4. The capped samples were cleaved into pieces of approximately  $0.5\text{ cm} \times 1\text{ cm}$  size and mounted onto a  $1\text{ cm} \times 1.5\text{ cm}$  thoroughly outgassed piece of silicon wafer with In solder. The silicon was then placed in a Ta foil heater stub. The sample was heated by the passage of current through the silicon wafer, via the electrical connections on a manipulator stage in the UHV chamber. The relationship between temperature and applied current for the silicon heater stub (figure 4.12) was calibrated by the use of an IR pyrometer (Si emissivity  $\sim 0.3$ ) with an additional reference to the melting point of In ( $156^\circ\text{C}$ ).

The As cap was removed by annealing the sample at temperatures rising incrementally from room temperature to  $550^\circ\text{C}$  for fifteen minutes at each step. On completion of each annealing stage, the sample was allowed to cool to room temperature and subsequently transferred *in-situ* to the analysis chamber for XPS measurements. The  $\text{In}4d$ ,  $\text{Ga}3d$ ,  $\text{As}2p_{3/2}$ ,  $\text{Ga}2p_{3/2}$ ,  $\text{In}3d_{3/2}$ ,  $\text{C}1s$  and  $\text{O}1s$  core levels were probed using an unmonochromated  $\text{AlK}_\alpha$  ( $h\nu = 1486.6\text{ eV}$ ) excitation source. No evidence of C was detected at any stage while the  $\text{O}1s$  peak was only evident until an annealing temperature of  $\sim 300^\circ\text{C}$  was reached. This indicates that the  $\text{O}1s$  signal was a consequence of the oxidised surface of the As cap. In conjunction with measurements taken with the detector in normal emission position, spectra were also obtained with the detector position at  $60^\circ$  emission in order to halve the effective electron escape depth normal to the surface and hence become more surface sensitive (see section 3.5.2).

### 5.1.1 Core level photoemission

Figure 5.1 shows the stacked normalised As $2p_{3/2}$  spectra (a) before annealing and (b-d) after anneals at 300°C, 350°C and 390°C respectively. Before annealing, two peaks are clearly evident in the As $2p_{3/2}$  spectra. The peak at 1323.5 eV is attributed to elemental As from the As cap, while the peak at 1326.5 is associated with oxidised As on the surface of the amorphous As cap. In the decapping study of As capped In $_{0.52}$ Al $_{0.48}$ As carried out by Clark *et al.*, similar spectra were obtained for As capped samples prior to annealing [4]. Following annealing at 300°C (figure 5.1(b)), the peak related to oxidised As on the surface of the capping layer is no longer evident, indicating the desorption of the surface arsenic oxide. The resulting lineshape is characteristic of emission entirely from the elemental cap at 1323.5 eV. The removal of the As cap occurs at a temperature of ~350°C and was noted by an increase in the chamber pressure from  $\sim 4 \times 10^{-10}$  to  $1 \times 10^{-8}$  mbar as the As was desorbed. Fig 5.1 (c) outlines the change in the As $2p_{3/2}$  lineshape after annealing at 350°C. The peak has shifted by  $\sim 0.7$  eV to lower binding energy and is characteristic of emission from As covalently bonded in the In $_{0.53}$ Ga $_{0.47}$ As [3]. Further annealing to 390°C (figure 5.1 (d)) and up to a maximum of 550°C resulted in no significant change in the lineshape or peak position of the As $2p_{3/2}$  peak.

The intensity ratio between the emission from the In3d and As $2p_{3/2}$  peaks as a function of increasing annealing temperature is shown in figure 5.2. At a temperature up to  $\sim 325^\circ\text{C}$ , the amount of As signal is large compared to In and is characteristic of an excess of As on the surface due to the As cap. Increased annealing up to and after 350°C induces an increased In emission intensity compared to that from the As $2p_{3/2}$  core level and concurs with the observed cap removal at 350°C. A similar increase in the In3d/As $2p_{3/2}$  ratio at temperatures higher than that for cap removal was observed by Clark *et al.* and was attributed to desorption of As from the surface to produce a surface that was rich in group III species. It is highly probable that a similar effect is being seen here with As preferentially desorbed from the In $_{0.52}$ Ga $_{0.48}$ As surface with increasing temperature.

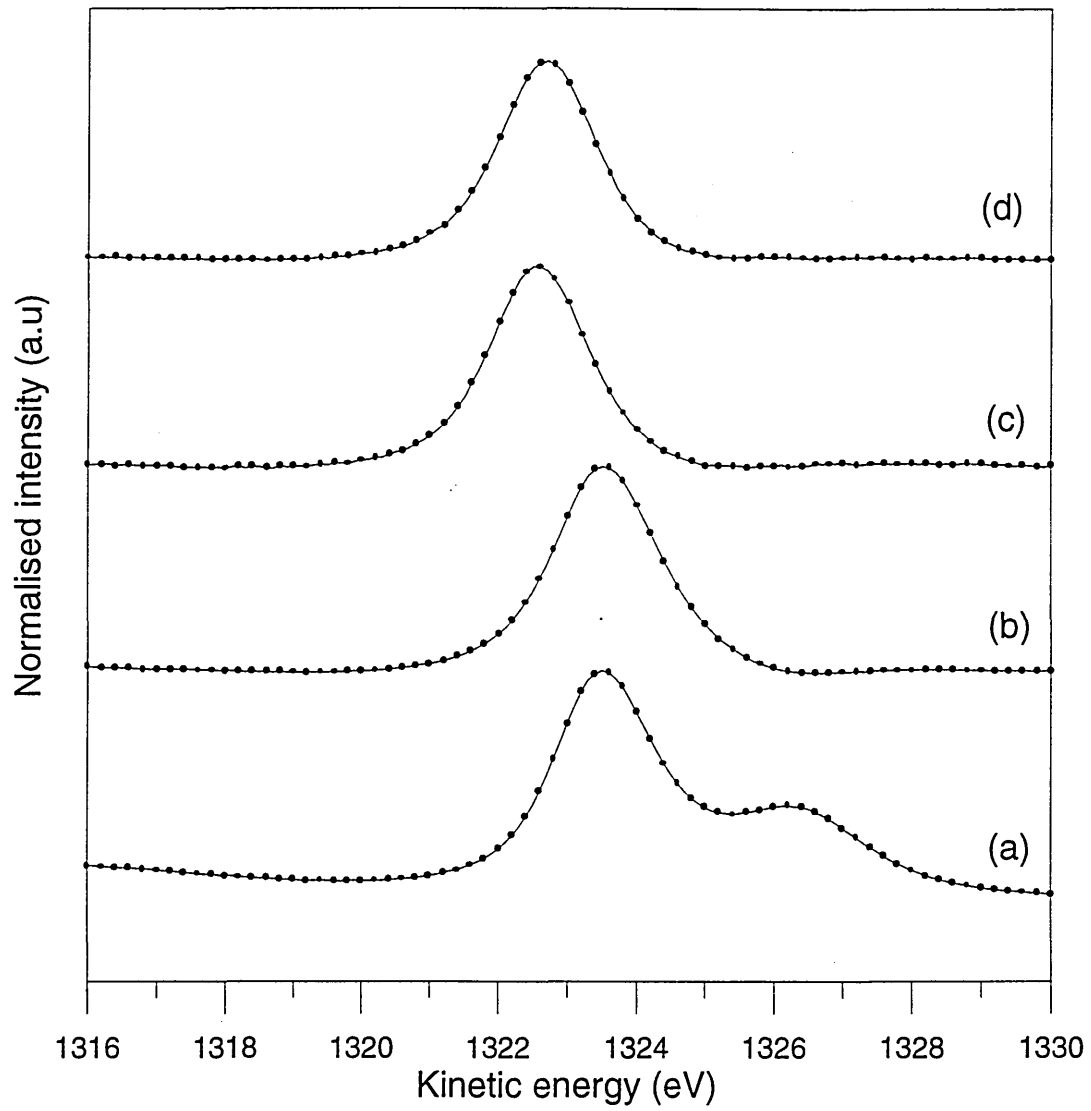


Figure 5.1: Stacked and normalised As<sub>2p<sub>3/2</sub></sub> core level spectra acquired from As capped In<sub>0.52</sub>Ga<sub>0.48</sub>As on InP(100) (a) prior to annealing, and annealed at (b) 300°C, (c) 350°C and (d) 390°C.

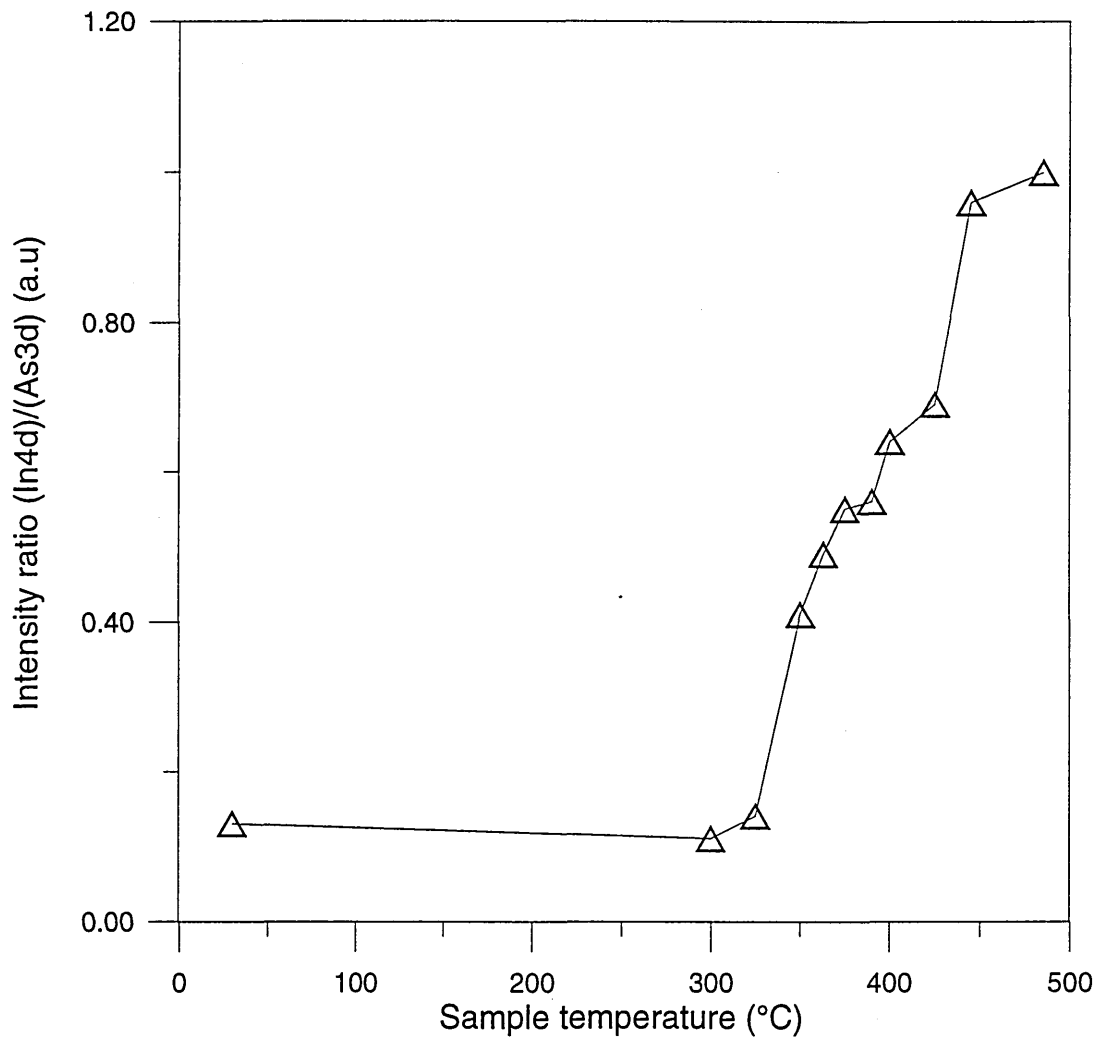


Figure 5.2: Intensity ratio between the In3d and As2p<sub>3/2</sub> core levels from an As capped In<sub>0.53</sub>Ga<sub>0.47</sub>As sample as a function of increasing annealing temperature. The lines drawn are intended to be a guide to the eye.

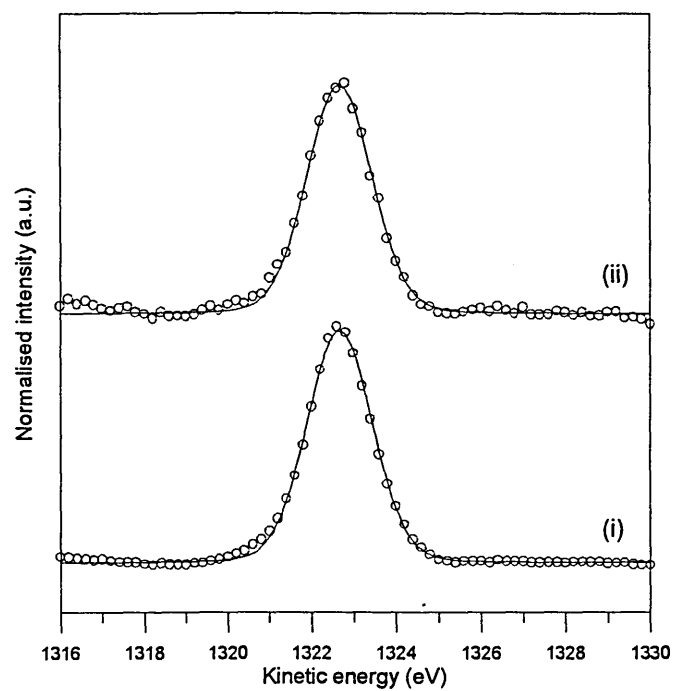
### 5.1.2 Clean surface stoichiometry

Figures 5.3 and 5.4 present As $2p_{3/2}$  and In $4d$ /Ga $3d$  photoemission spectra taken from In $_{0.53}$ Ga $_{0.47}$ As(100) annealed at 390°C and 420°C. The spectra have been acquired at (i) normal emission and (ii) at an emission angle of 60° to the surface normal. The lineshape and binding energy position of the As $2p_{3/2}$ , In $4d$  and Ga $3d$  core levels does not change significantly as a result of changing the annealing temperature or increasing the surface sensitivity. This indicates that within the resolution of the XPS technique, there is a similar chemical environment at the surface of the material compared to the bulk for the two annealing temperatures. However, closer inspection of the In $4d$  and Ga $3d$  core level spectra (figure 5.4) indicates that the surface stoichiometry is different to that in the bulk of the material.

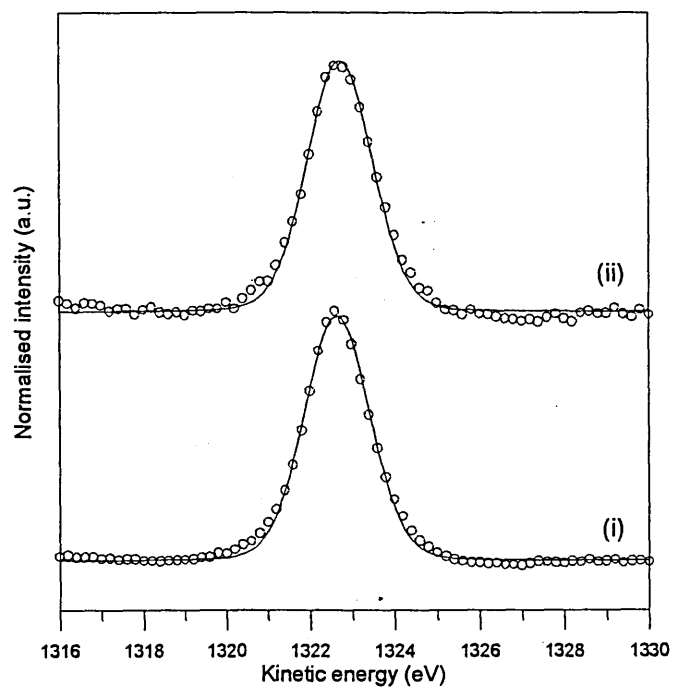
Taking into account first the surface annealed to 390°C, it can be seen that the intensity of the In $4d$  signal compared to the Ga $3d$  signal increases as the attenuation length is halved. In an XPS study on the growth of As stabilised In $_{0.53}$ Ga $_{0.47}$ As(100) by Grenet *et al.* a similar increase in the In content with respect to the Ga content was observed on “as grown” MBE In $_{0.53}$ Ga $_{0.47}$ As(100) surfaces [6]. This phenomenon was interpreted as the surface segregation of In to form an InAs surface layer. Since the samples used in these experiments were grown at a similar temperature, by MBE, it is highly likely that In surface segregation is a consequence of MBE growth producing an In rich surface in comparison to Ga, with the possibility of the formation of an InAs rich surface layer. These observations concur with theoretical studies of the growth of In $_x$ Ga $_{1-x}$ As(100) [7].

Similar characteristics were observed for the surface annealed at 420°C. However returning to the intensity ratio between In and As as a function of temperature in figure 5.2, it can be seen that the As intensity decreases with respect to In as the annealing temperature is increased. Since the maximum congruent evaporation temperature of InAs is 380°C (see table 6.3) it is probable that the decrease in As content compared to that of In is a result of the desorption of As from the In $_{0.53}$ Ga $_{0.47}$ As(100) surface leaving a surface that is abundant in group III species.

Clark proposed a simple model to describe the (3×1) and (4×1) surfaces obtained on In $_{0.52}$ Al $_{0.48}$ As(100) whereby the (3×1) surface is comprised of two distinct zones these being an As-stabilised, In rich (Al deficient) layer ~ 20-50 Å thick on top of bulk In $_{0.52}$ Al $_{0.48}$ As(100). Similarly the (4×1) surface comprises of a group III (predominately



(a)



(b)

Figure 5.3: As $2p_{3/2}$  core level emission spectra from an As decapped In $_{0.53}$ Ga $_{0.47}$ As(100) sample annealed at (a) 390°C and (b) 420°C. Spectra were obtained using an AlK $_{\alpha}$  source at (i) normal emission and (ii) 60° from normal emission.

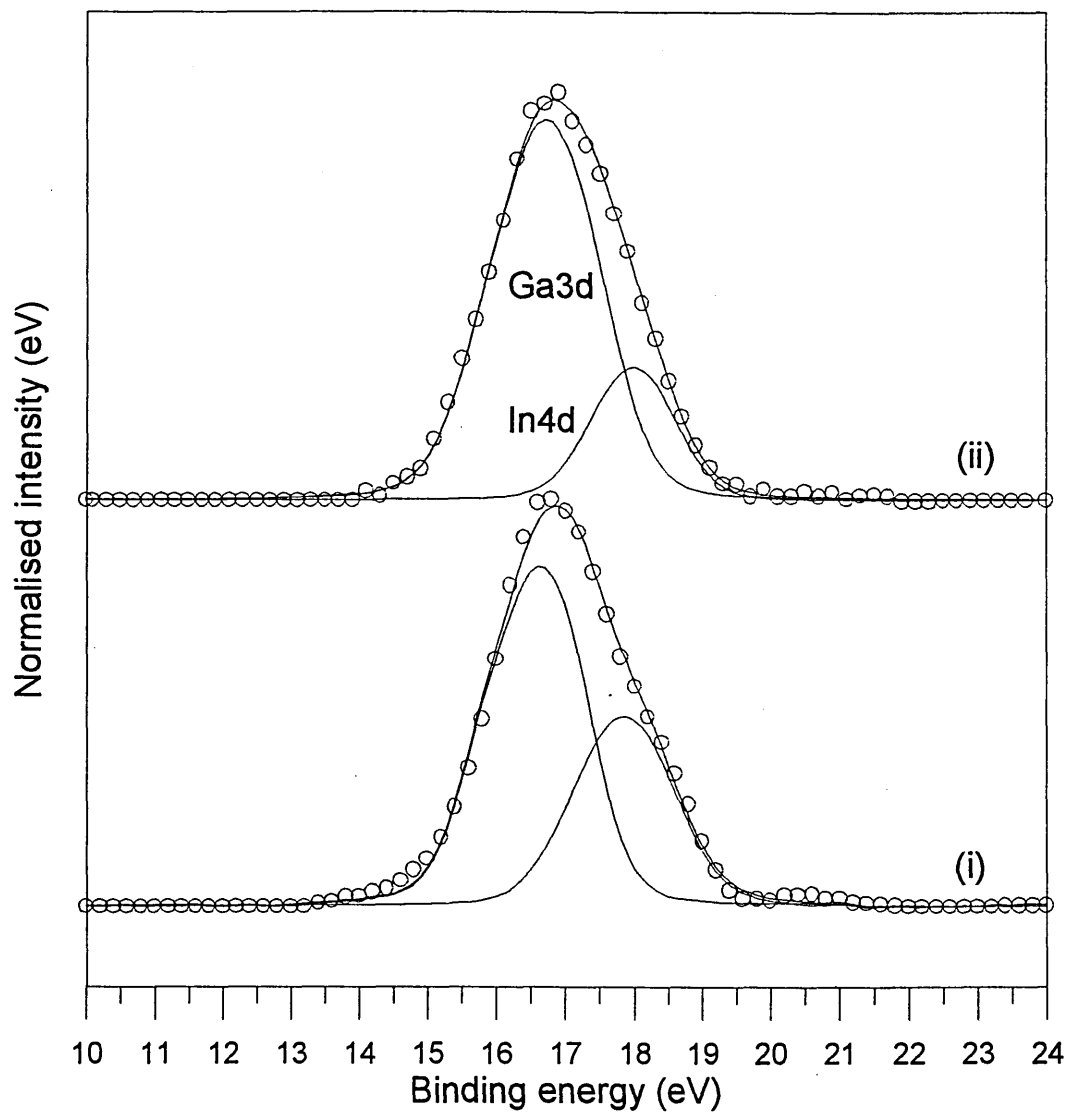


Figure 5.4: In4d and Ga3d core level XPS emission spectra from an As decapped  $\text{In}_{0.53}\text{Ga}_{0.47}\text{As}(100)$  sample annealed at  $390^\circ\text{C}$ . Spectra were obtained using an  $\text{AlK}_\alpha$  source at (i) normal emission and (ii)  $60^\circ$  from normal emission.

In) stabilised Al deficient layer over bulk  $\text{In}_{0.52}\text{Al}_{0.48}\text{As}(100)$  [5]. In the In surface segregation study carried out by Grenet *et al.* on MBE grown  $\text{In}_{0.52}\text{Al}_{0.48}\text{As}(100)$  and  $\text{In}_{0.53}\text{Ga}_{0.47}\text{As}(100)$  it was proposed that the phenomenon of In surface segregation was more profound for the  $\text{In}_{0.52}\text{Al}_{0.48}\text{As}(100)$  case than for the  $\text{In}_{0.53}\text{Ga}_{0.47}\text{As}(100)$  case. This was thought to be due to the difference between group III atom mobility on the surface during the growth process.

From the results presented here therefore, it seems that the  $\text{In}_{0.53}\text{Ga}_{0.47}\text{As}(100)$  samples exhibit In surface segregation, with a possible model for the surface obtained by annealing the sample to  $390^\circ\text{C}$  being an As stabilised, In rich (Ga deficient) layer of less than a few monolayers thickness, surmounting bulk  $\text{In}_{0.53}\text{Ga}_{0.47}\text{As}(100)$ . The surface annealed to  $420^\circ\text{C}$  can be considered as a predominantly group III stabilised surface layer over bulk  $\text{In}_{0.53}\text{Ga}_{0.47}\text{As}(100)$ .

## 5.2 Summary

In chapter 5 a decapping study of As capped  $\text{In}_{0.53}\text{Ga}_{0.47}\text{As}(100)$  has been undertaken on the microlab at Sheffield Hallam University has been described. This work was carried out prior to experiments at the Daresbury Synchrotron Radiation Laboratory to determine the temperature at which the amorphous As cap is desorbed. Following the procedure adopted in the literature, the sample was annealed in various stages for 15 minutes at a time. The As oxide on the surface of the As cap was removed at about  $300^\circ\text{C}$  and the removal of the elemental As cap was achieved by annealing the sample above  $350^\circ\text{C}$ . The clean surface achieved on the full desorption of the As cap was free of O and C contamination.

The sample was further annealed to  $390^\circ\text{C}$  and  $420^\circ\text{C}$  in order to detect any changes in surface stoichiometry with increasing annealing temperature. The relative abundance of As on the  $\text{In}_{0.53}\text{Ga}_{0.47}\text{As}(100)$  surface decreased as the annealing temperature increased, indicating the preferential desorption of As from the surface with increasing temperature. The intensity ratio between In and Ga at the sample surface was greater than that observed in the bulk of the material. This phenomenon is likely to be due to the surface segregation of In during the MBE growth process.

Subsequent LEED studies performed at Daresbury showed that As capped  $\text{In}_{0.53}\text{Ga}_{0.47}\text{As}(100)$  samples annealed at  $390^\circ\text{C}$  exhibited a  $(3\times 1)$  surface reconstruction

(replicating that observed after MBE growth). Similar samples annealed at 420°C and above exhibited a (4×1) reconstruction, characteristic of a group III rich surface [4].

### 5.3 References

- [1] S.A. Clark, S.P. Wilks, A. Kestle, D.I. Westwood and M. Elliott, *Surf. Sci.* **352-354**, 850 (1996).
- [2] R.W. Bernstein, A. Borg, H. Husby, B.-O. Fimland and J.K. Grepstad, *Appl. Surf. Sci.* **56-58**, 74 (1992).
- [3] W.M. Lau, R.N.S. Sodhi, S. Jin, S. Ingrey, N. Puetz and A. SpringThorpe, *J. Appl. Phys.* **67 (2)** (1990).
- [4] S.A. Clark, C.J. Dunscombe, D.A. Woolf, S.P. Wilks and R.H. Williams, *J. Vac. Sci. Technol. B* **12(2)** 551 (1994).
- [5] S.A. Clark, PhD Thesis, University of Wales, College Cardiff (1995).
- [6] G. Grenet, E. Bergignat, M. Gendry, M. Lapeyrade and G. Hollinger, *Surf. Sci.* **352-354**, 734 (1996).
- [7] J.Tersoff, *Phys. Rev. Lett.* **77(10)** 2017 (1996).

## Chapter 6

### Metal-In<sub>0.53</sub>Ga<sub>0.47</sub>As(100) interfaces formed as a function of temperature

#### 6.0 Introduction

Recent studies of metal-In<sub>0.53</sub>Ga<sub>0.47</sub>As/InP(100) interfaces by Clark *et al.* have indicated the potential to select barrier heights for this particular materials system by a combination of surface preparation and cryogenic processing. Current-Voltage (I-V) characteristics of In and Au contacts to the idealised case of the atomically clean (3×1) reconstructed (100) surface of MBE grown In<sub>0.53</sub>Ga<sub>0.47</sub>As, have shown that In diodes produced an increase in the Schottky barrier height when the diodes were formed at low temperature ( $\phi_b = 0.45$  eV) compared to room temperature ( $\phi_b = 0.25$  eV). Conversely, Au deposition resulted in diodes that were Ohmic for both low and room temperature formation [1]. The I-V technique is a useful tool for determining the size of the potential barrier formed at a metal-semiconductor interface, and can also predict the mechanisms that dominate electron transport across the interface. However, to fully characterise the nature of the interfaces and the reactions occurring during their formation, requires the use of spectroscopic and microscopic techniques. In this chapter the formation of In and Au interfaces with In<sub>0.53</sub>Ga<sub>0.47</sub>As(100) are examined using SXPS and TEM.

In order to be consistent with the experiments by Clark *et al.* discussed previously, the clean '*as grown*' surfaces upon which the diodes were formed need to be achieved in the surface analysis chamber. It is well understood that As capped samples can be transferred through air between an MBE reactor and a surface analysis chamber without significant damage to the sample surface [2-4]; a near replica of the clean '*as grown*' surface being achieved upon thermal desorption of the As cap under UHV in the analysis chamber. It is possible however that some surface damage may occur during the decapping procedure, and a technique such as Scanning Tunnelling Microscopy (STM) must be utilised in order to fully assess the validity of the decapping technique. The As capping technique was used in this work and the characterisation of the resulting surface by STM will be the subject of future work.

In this chapter the clean In<sub>0.53</sub>Ga<sub>0.47</sub>As(100) surface achieved after cap removal is characterised by SXPS, and the subsequent formation of In-In<sub>0.53</sub>Ga<sub>0.47</sub>As(100) and Au-In<sub>0.53</sub>Ga<sub>0.47</sub>As(100) interfaces are probed.

To date little work has been reported on the reactions occurring between metals and  $\text{In}_{0.53}\text{Ga}_{0.47}\text{As}(100)$ . As a consequence, the results presented here are compared to work on the similar binary III-V semiconductor GaAs and the ternary III-V  $\text{In}_{0.52}\text{Al}_{0.48}\text{As}$ .

## 6.1 Photoemission studies

### 6.1.1 Introduction

High resolution SXPS was used to study the In- and Au- $\text{In}_{0.53}\text{Ga}_{0.47}\text{As}(100)$  interfaces using the synchrotron radiation source on beamline 4.1 at the Daresbury Laboratory. Details of the experimental apparatus have been discussed in chapter 4. In order to obtain surface sensitive spectra, one has to take into account the escape depth of the emitted photoelectrons as a function of their energy. Consultation of the universal curve shown in figure 3.2 shows that for ultimate surface sensitivity an escape depth of  $\sim 4\text{-}5 \text{ \AA}$  (K.E.  $\sim 40 \text{ eV}$ ) is required [5]. Therefore, using equation 3.1 the As3d core level spectra were acquired using photon energies ( $h\nu$ ) of 87 eV and 119 eV in order to attain maximum and somewhat less surface sensitive spectra respectively. The Ga3d and In4d core level spectra were likewise acquired at  $h\nu = 63 \text{ eV}$  and 119 eV respectively. The respective core levels were chosen to exhibit the maximum photoionisation cross section for the photon energy used. The core levels and their respective parameters are shown in table 6.1.

	As3d		Ga3d		In4d	
$E_B$ (eV)	42.0		19.0		17.7	
$h\nu$ (eV)	87	119	63	119	63	119
KE (eV)	40.0	72.0	39.0	95.0	40.3	96.3
$\lambda$ ( $\text{\AA}$ )	$\sim 4$	$\sim 8$	$\sim 4$	$\sim 8$	$\sim 4$	$\sim 8$
$\sigma$ (Mb)	$\sim 5$	$\sim 7$	$\sim 4$	$\sim 7$	$\sim 17$	$\sim 1$

Table 6.1: A table of useful parameters associated with the photon energies required for examination of the respective core levels in this study [5,6].

### 6.1.1 Experimental details

The n-type  $\text{In}_{0.53}\text{Ga}_{0.47}\text{As}(100)$  samples were grown by molecular beam epitaxy (MBE) and doped with Si to yield a carrier density of  $n \approx 2 \times 10^{18} \text{ cm}^{-3}$ . In order to protect the surface from contamination the samples were “capped” *in-situ* with a thick layer of amorphous arsenic as described in section 4.2.4. The samples were then transferred, in air, to an ultra high vacuum (UHV) chamber equipped with a Scienta SES 200 analyser for surface analysis on beamline 4.1 of the Daresbury Synchrotron Radiation Laboratory. The samples were loaded into a manipulator/continuous flow liquid nitrogen cryostat capable of cooling the sample to 125K. The capped  $\text{In}_{0.53}\text{Ga}_{0.47}\text{As}(100)$  samples were annealed to a temperature of  $\sim 350^\circ\text{C}$  for around 5-10 minutes, to remove the protective cap. The sample temperature was monitored using an IR pyrometer (emissivity  $\sim 0.7$ ), and the desorbed As present in the chamber by a quadrupole mass spectrometer. In addition, upon removal of the As cap at  $\sim 350^\circ\text{C}$ , an increase in the chamber pressure from  $2 \times 10^{-10}$  to  $2 \times 10^{-9}$  mbar was observed. Following further annealing up to  $\sim 380^\circ\text{C}$ , examination of the clean decapped  $\text{In}_{0.53}\text{Ga}_{0.47}\text{As}(100)$  surface by LEED revealed a  $(3 \times 1)$  surface reconstruction replicating that observed by RHEED following MBE growth. High purity In and Au metals were evaporated from thoroughly out-gassed tantalum filaments onto decapped samples held at room temperature (RT  $\sim 294\text{K}$ ) and low temperature (LT  $\sim 125\text{K}$ ). The metals were deposited at a rate of  $0.01 \text{ nms}^{-1}$  as measured by a quartz crystal monitor. For both RT and LT samples, a total of  $70\text{\AA}$  In and  $140\text{\AA}$  Au were deposited in increments ranging from  $0.5\text{\AA}$  to  $90\text{\AA}$ . On production of the clean surface, and following subsequent depositions, the samples were analysed by SXPS.

### 6.1.3 The clean $(3 \times 1)$ reconstructed $\text{In}_{0.53}\text{Ga}_{0.47}\text{As}(100)$ surface

The As3d and In4d/Ga3d photoemission spectra for a clean  $(3 \times 1)$  reconstructed  $\text{In}_{0.53}\text{Ga}_{0.47}\text{As}(100)$  surface are shown in figures 6.1 and 6.2 respectively. The As3d, Ga3d and In4d core levels were fitted using the curve fitting routine described in chapter 3. An appropriate linear background was subtracted from all core level spectra, and the peak intensities were normalised to unity in order to distinguish changes in core level lineshape. The fixed parameter values obtained from the relevant literature [7-9], for individual core levels are shown in table 6.2, and the aim throughout the fitting

procedure was to use the minimum number of components to produce a good fit. The peak intensity, peak positions and gaussians were allowed to vary.

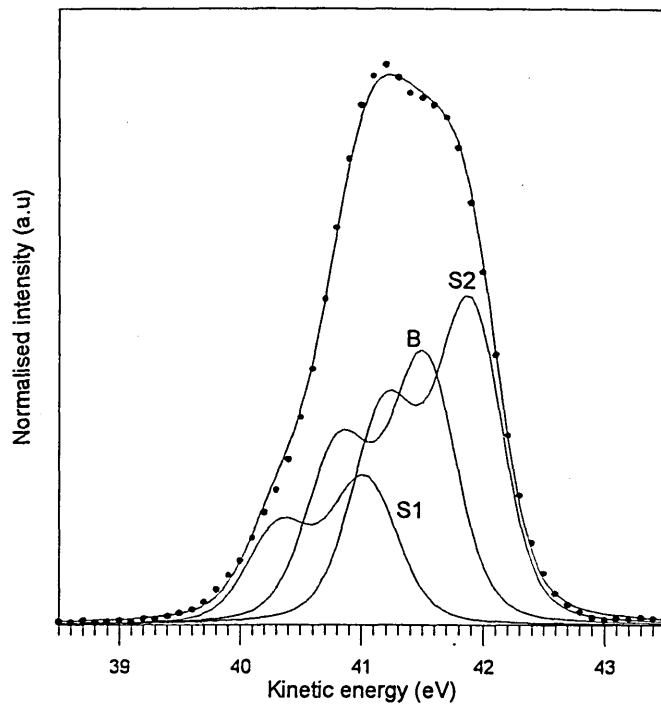
Core level	Lorentzian FWHM (eV)	Spin Orbit Splitting (eV)	Relative Intensity of Spin Orbit Split
As3d	0.170	0.695	0.67
Ga3d	0.155	0.450	0.67
In4d	0.250	0.870	0.67

Table 6.2: Table of fixed parameters used to fit the core level spectra obtained from clean (3×1) reconstructed  $\text{In}_{0.53}\text{Ga}_{0.47}\text{As}(100)$  [7-9].

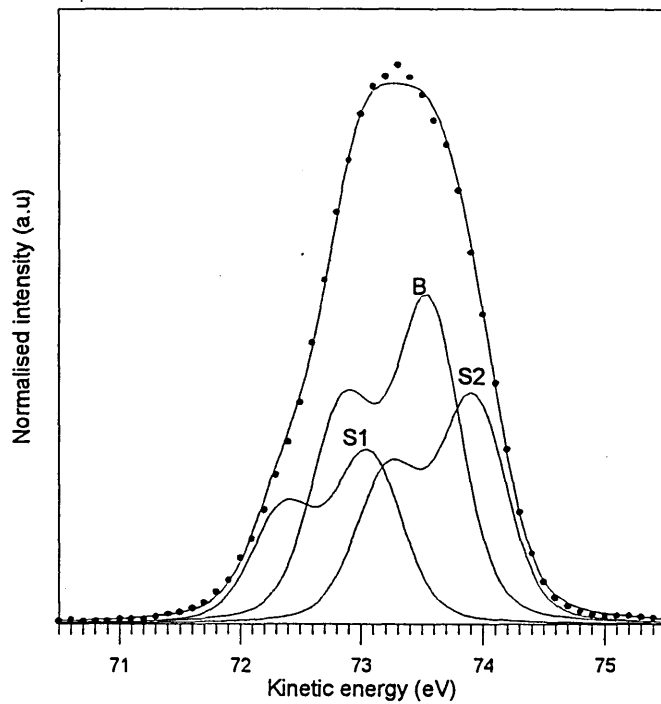
(i) *As3d Core level spectra*

Figure 6.1 shows the curve fitted As3d core level probed using photon energies of (a)  $h\nu = 87$  eV and (b)  $h\nu = 119$  eV, for maximum and somewhat less surface sensitive spectra respectively.

Considering the less surface (“bulk”) sensitive case first (Fig. 6.1(b)), the arsenic rich (3×1) reconstructed  $\text{In}_{0.53}\text{Ga}_{0.47}\text{As}(100)$  surface was fitted with three components marked S1, S2 and B, separated by  $\Delta E_k = 0.43$  eV (S1-B) and  $\Delta E_k = 0.40$  eV (B-S2). Comparison with the more surface sensitive spectra, in which the energy positions respective to each other are the same, shows that the bulk component B decreases in intensity as the surface sensitivity is increased (Fig. 6.1(a)). The component B is therefore thought to be related to emission from As in the bulk of the material. S1 and S2 are attributed to As surface components. It is also noted that component S2 increases while S1 remains virtually the same. XPS studies of As rich  $\text{In}_{0.53}\text{Ga}_{0.47}\text{As}$  on  $\text{InP}(100)$  [10] have shown that In segregates to the surface, producing an InAs surface layer. Therefore it is proposed that the increased component S2 is related to predominantly In bonded As sites at the surface while S1 is attributed to predominantly Ga bonded As sites.



(a)



(b)

Figure 6.1: As3d core level spectra from the clean (3×1) reconstructed  $\text{In}_{0.53}\text{Ga}_{0.47}\text{As}(100)$  surface. The spectra were obtained using photon energies of (a) 87 eV and (b) 119 eV.

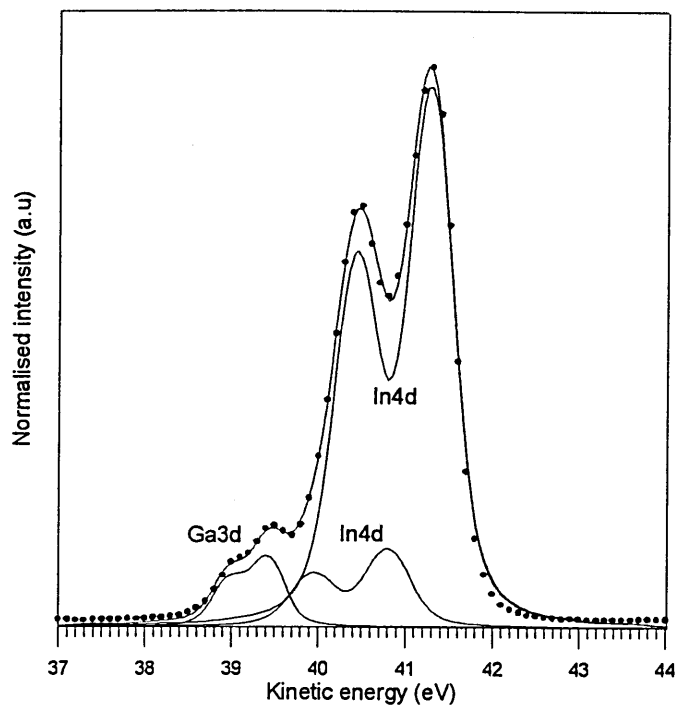
(ii) *In4d/Ga3d core level spectra*

In figures 6.2 a & b the In4d and Ga3d core level spectra are shown. Both these core levels were obtained using photon energies of (a)  $h\nu = 63$  eV and (b)  $h\nu = 119$  eV, for maximum and somewhat less surface sensitive spectra respectively. In figure 6.2(a) the raw data is fitted with a single Ga3d component and two In4d components. The Ga3d component to lower kinetic energy has a much lower intensity than the In4d core levels to higher kinetic energy. This is because the photo-ionisation cross section for In4d is larger than that of the Ga3d core level, at the particular photon energy used (see Table 6.1). It can be seen that at the higher photon energy (Figure 6.2 (b)) where  $h\nu = 119$  eV the Ga3d intensity increases significantly compared to the In4d core level due to the fact that the Ga3d now has the greater cross section.

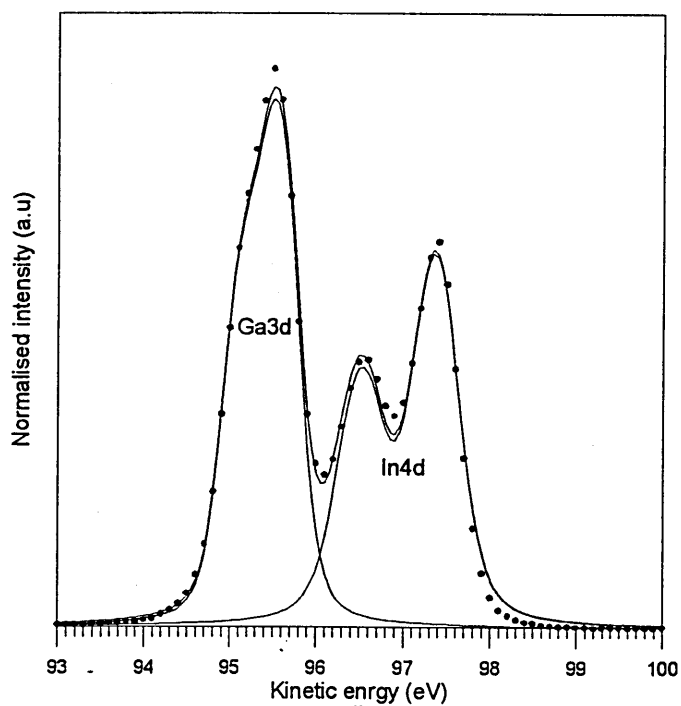
The Ga3d component is attributed to Ga bonded to surface As. No other Ga3d components could be resolved due to the small ionisation cross section. In the XPS study of As terminated  $\text{In}_{0.53}\text{Ga}_{0.47}\text{As}(100)$  by Grenet *et al.* discussed previously, the In4d lineshape was fitted with two components. A surface component found at higher binding energy than the bulk component was associated with In atoms bonded to surface As atoms in an InAs rich surface layer. The results shown here tend to agree with these findings. A surface component (S) to lower kinetic energy (higher binding energy) than a bulk (B) component is again observed and likewise attributed to In atoms bonded to As surface atoms, and concurs with the results obtained from the As3d core level. Comparison with the spectrum obtained at  $h\nu = 119$  eV reveals little in the way of bulk population of either In or Ga due to the change in respective core level photo-ionisation cross sections at the increased photon energy. However, in the XPS study of the decapping of  $\text{In}_{0.53}\text{Ga}_{0.47}\text{As}(100)$  described in Chapter 5, the effect of the ionisation cross section was negated by varying the angle of detection of the emitted electrons as described in chapter 3. Here it was found that nearer the clean  $(3\times 1)$  reconstructed  $\text{In}_{0.53}\text{Ga}_{0.47}\text{As}(100)$  surface the In/Ga ratio increased in comparison to that in the bulk of the material.

(iii) *Summary*

The clean  $(3\times 1)$  reconstructed  $\text{In}_{0.53}\text{Ga}_{0.47}\text{As}(100)$  surface has been studied using soft X-ray photoelectron spectroscopy. Examination of the As3d, Ga3d and In4d core



(a)



(b)

Figure 6.2: In4d/Ga3d core level spectra from the clean  $(3 \times 1)$  reconstructed  $\text{In}_{0.53}\text{Ga}_{0.47}\text{As}(100)$  surface. The spectra were obtained using photon energies of (a) 63 eV and (b) 119 eV.

levels indicate a surface that is predominantly In rich with respect to Ga with the likelihood of an InAs surface layer.

The change in stoichiometry from a (3×1) to a (4×1) reconstruction due to annealing is not a straightforward step function, but more likely a gradual transition. Although great care was taken to reproduce the conditions for decapping of the In<sub>0.53</sub>Ga<sub>0.47</sub>As(100) samples, it is likely that the same decapping temperature was not achieved every time. It is possible that the uncertainty in sample temperature may be as much as ± 25K. Hence it is probable that the clean surface core level spectra for each deposition experiment will be similar, rather than identical.

#### 6.1.4 In-In<sub>0.53</sub>Ga<sub>0.47</sub>As(100) interface formation

##### (i) Substrate core level attenuation

The growth mode of the metal overlayer can be determined by the attenuation of the intensity of the core level signal from atoms in the original substrate material. The core level intensity is given by the area under the photoelectron peak after an appropriate removal of the secondary electron background. The normalised integrated emission intensities from the As3d core level are shown as a function of overlayer thickness for both room temperature and low temperature In deposition, in figure 6.3. For the case of low temperature deposition, the intensity of the As3d signal exhibits an exponential attenuation up to the first ~5Å of In deposition, indicating an initial layer by layer mode of growth [11]. Deviation from this exponential attenuation occurs after 5Å of In has been deposited and is indicative of the formation of In islands as the overlayer develops [11]. For room temperature In deposition however, there is no evidence of laminar growth, as the attenuation of the core level signal is significantly reduced. In a photoemission study of In-GaAs(100) interface formation, Spindt *et al.* have reported a growth morphology that involves the competition between chemisorption of In atoms on the GaAs surface and In clusters [8,9]. Conversely SXPS studies of In-GaAs(100) interfaces formed at room and low temperature (120K) by Mao *et al.* have shown the growth mode to be two dimensional followed by clustering with increased In clustering at room temperature [7]. It is highly likely that a similar effect to that reported by Mao *et al.* is being observed here.

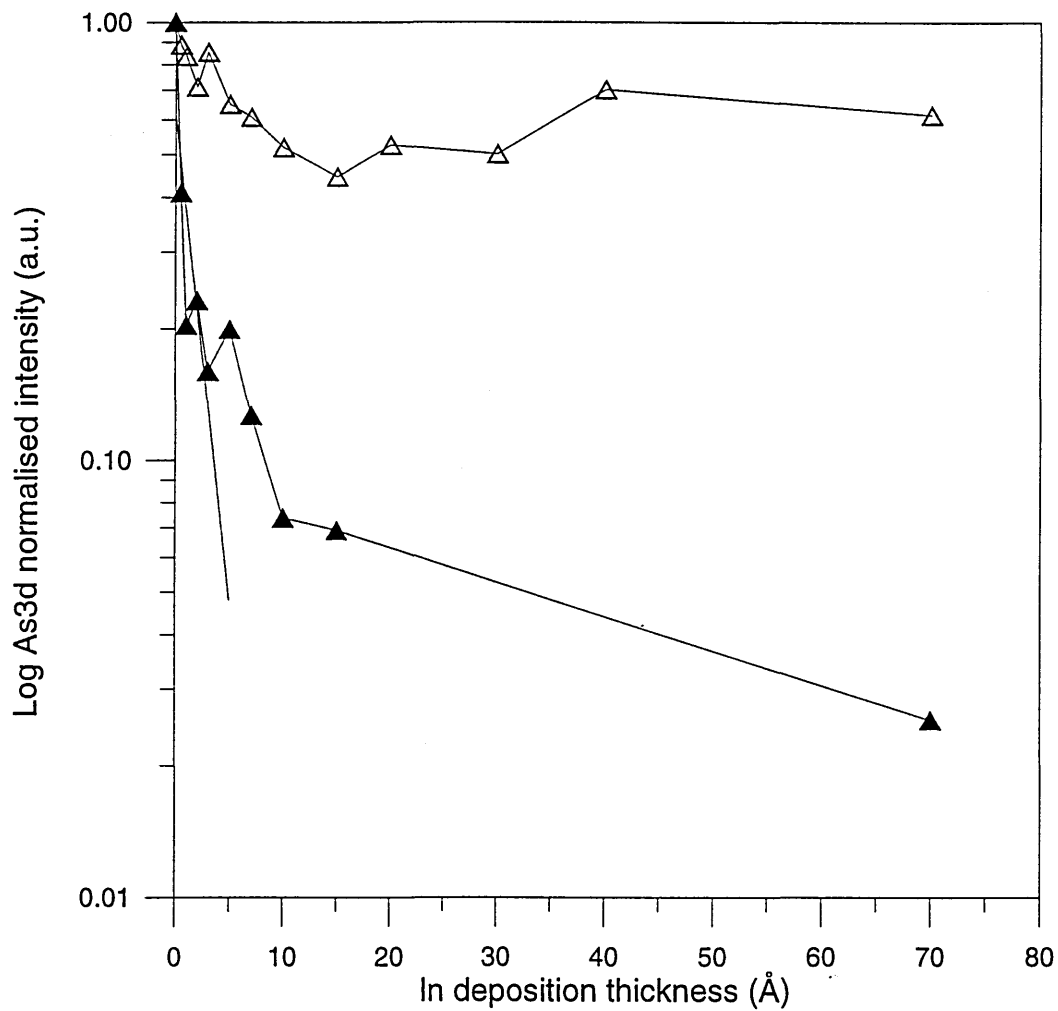


Figure 6.3 As3d core level emission intensity ( $I/I_0$ ), plotted as a function of In coverage on decapped  $\text{In}_{0.53}\text{Ga}_{0.47}\text{As}(100)$ , obtained at an excitation energy of 87 eV. The open triangles denote In deposition at 294K (RT), the closed triangles denote deposition at 125K (LT).

One possible reason for an increased core level attenuation could be a reduced surface mobility of In adatoms at low temperature. At room temperature, an indium atom landing on the surface will diffuse across the surface until it is captured either by an indium cluster, or an adsorption site on the  $\text{In}_{0.53}\text{Ga}_{0.47}\text{As}(100)$  surface [8]. It may be the case that at low temperatures, the In atoms arriving at the surface do not have enough energy to move around and find their preferred positions. The reduced surface mobility would have the effect of modifying the order of the growing In overlayer by reducing the grain size of the growing In film and tending towards a more amorphous growth mode. Hence a core-level attenuation corresponding to that of layer by layer overlayer growth could be expected.

It is unlikely however, that In cluster formation can completely account for the reduced attenuation of the As3d core level signal at room temperature. At an In coverage as high as  $70\text{\AA}$ , the As3d signal intensity has only reduced to 70% of the original clean surface value. Photoemission studies of In- $\text{In}_{0.52}\text{Al}_{0.48}\text{As}(100)$  interfaces formed at room temperature have reported a similar truncated As core level intensity attenuation. In this case, it was believed that the As from the  $\text{In}_{0.52}\text{Al}_{0.48}\text{As}(100)$  substrate out-diffused into the In metal overlayer [12]. The results obtained here for In- $\text{In}_{0.53}\text{Ga}_{0.47}\text{As}(100)$  seem to concur with these observations. Similarly Cao *et al.* have shown that In deposition on GaAs(110) at room temperature and above can lead to a chemically reacted interface resulting in an InAs interfacial layer [13]. However no such reaction was resolved for deposition at lower temperatures. It is possible that the process of out-diffusion is temperature dependent. Therefore it may be that the rapid attenuation of the As3d core level at low temperature metallisation is due to an inhibition of the out-diffusion of As from the  $\text{In}_{0.53}\text{Ga}_{0.47}\text{As}(100)$  substrate.

The apparent out-diffusion of As into the In overlayer at room temperature limits any prediction of the growth mode at this temperature to the attenuation of the In4d and Ga3d core levels. As In is both a substrate species and the metal overlayer, there will be contributions to the total In core level emission intensity  $I_d$  from both the substrate  $I_s$  and the overlayer  $I_l$ . The Ga3d core level signal is overwhelmed by the growing In4d signal after as little as  $3\text{\AA}$  In deposition. This is due to the fact that the In4d and Ga3d core levels are less than 1 eV apart, and that the Ga3d cross-section ( $\sigma = \sim 4 \text{ Mb}$ ) is less than that of the In4d core level ( $\sigma = \sim 17 \text{ Mb}$ ) at the photon energy used [6]. The low cross section of the Ga3d core level combined with the relatively low Ga composition at

the surface compared to In prevents an accurate assessment of the growth mode from Ga emission attenuation.

However the total In core level intensity is given by [14],

$$I_d = I_s + I_l \quad [6.1]$$

where,

$$I_s = I_c \exp(-d/\lambda) \quad [6.2]$$

and

$$I_l = I_f [1 - \exp(-d/\lambda)] \quad [6.3]$$

In these equations,  $I_c$  and  $I_f$  represent the In core level emission intensities from the clean surface before any In is deposited and for very thick ( $\gg \lambda$ ) In overlayer coverages, respectively. Here  $d$  is the layer thickness and  $\lambda$  is the attenuation length of photoelectrons travelling through the In overlayer.

By combining these two equations, the following expression can be obtained,

$$(I_f - I_d)/(I_f - I_c) = \exp(-d/\lambda) \quad [6.4]$$

Figure 6.4 shows the left hand side of this relationship plotted against In overlayer thickness for both room and low temperature deposition. For room temperature In deposition at no point is there any evidence of exponential decay, confirming the lack of laminar growth and therefore a predominantly clustering mode of growth. However when the deposition temperature is reduced, a more exponential attenuation is observed. This concurs with the apparent laminar growth observed for As3d attenuation.

(ii) *As3d core level emission*

From the attenuation of the As3d core level as a function of In overlayer thickness, there is evidence of As out-diffusion at room temperature, but not at low temperature. Figure 6.5 details the change in As3d core level lineshape as a function of In overlayer coverage at low temperature. The individual spectra are curve fitted using the parameters discussed in section 6.1.3. Three components S1, S2 and B were

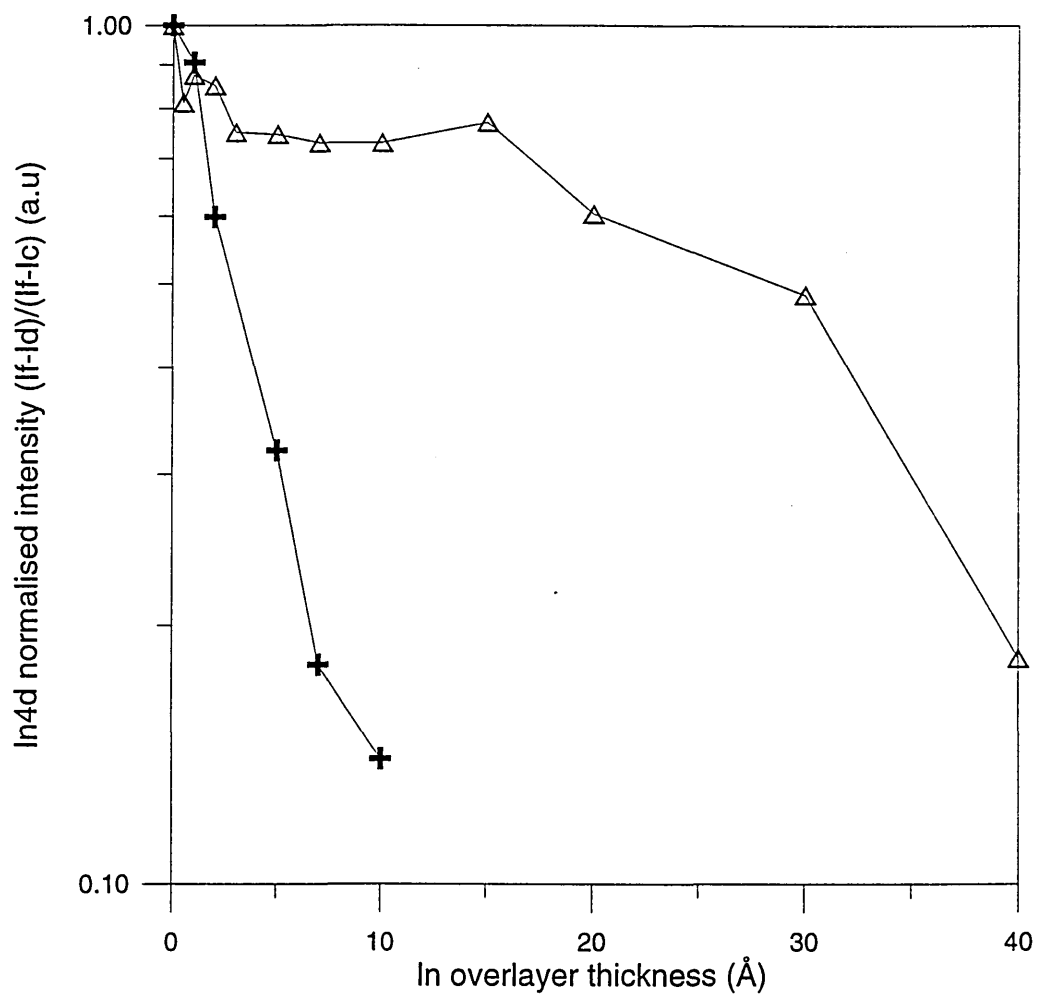


Figure 6.4 In4d core level emission intensity  $(I_f - I_d)/(I_f - I_c)$ , plotted as a function of In coverage on decapped  $\text{In}_{0.53}\text{Ga}_{0.47}\text{As}(100)$ , obtained at an excitation energy of 63 eV. The open triangles denote In deposition at 294K (RT), the crosses denote deposition at 125K (LT).

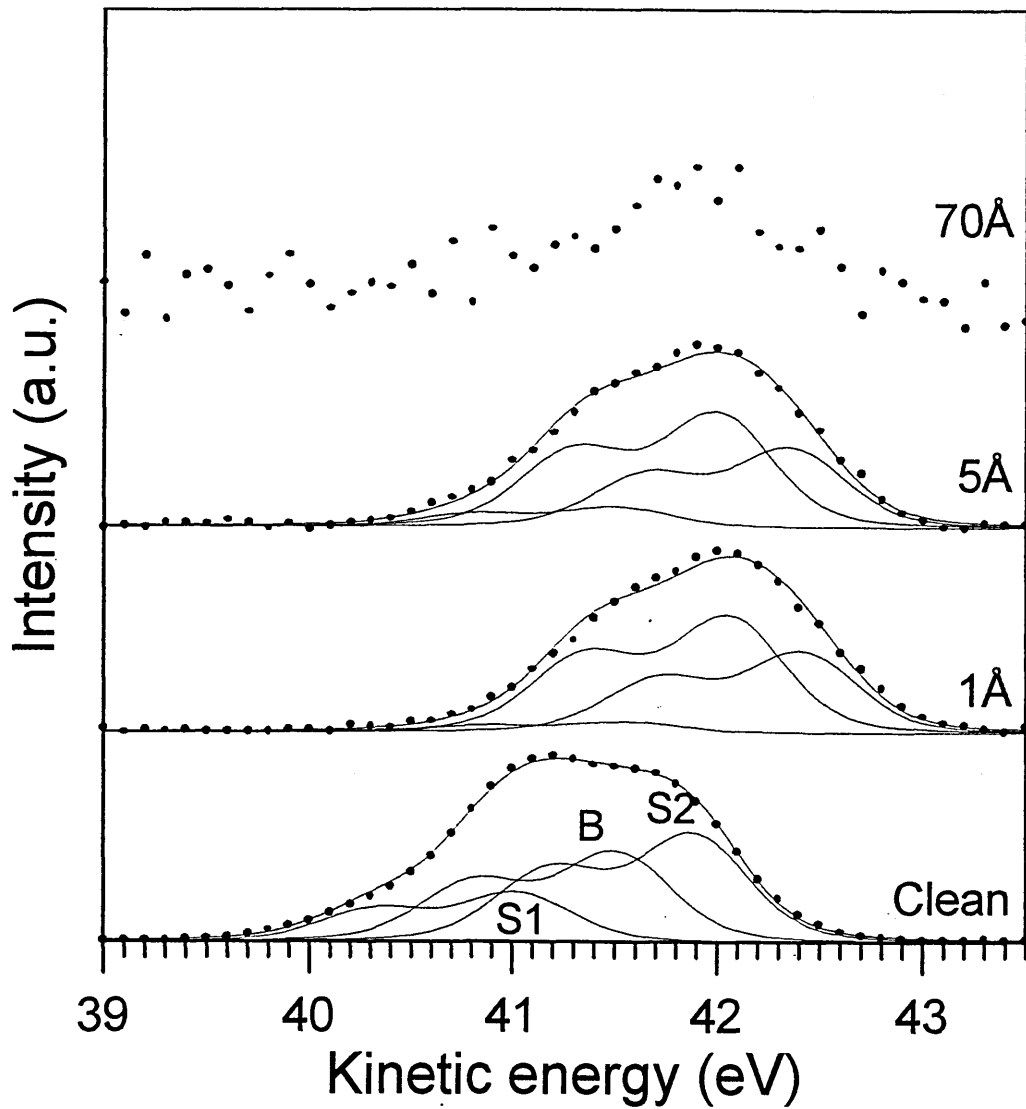


Figure 6.5: Evolution of the As3d core level spectra ( $h\nu = 87$  eV), with increasing In coverage on decapped  $(3\times 1)$  reconstructed  $\text{In}_{0.53}\text{Ga}_{0.47}\text{As}(100)$ , deposited at 125K (LT). The peaks have been synthesised with three components, S1, S2 and B, shown along with the overall fit as continuous lines.

necessary to accurately fit the experimental line shape of the clean  $\text{In}_{0.53}\text{Ga}_{0.47}\text{As}(100)$  surface. The components and their respective binding energy positions are identical to those described in section 6.1.3.

As the In metal is deposited, all three components are attenuated at similar rates, and at high In coverages the spectra is noisy and of low intensity. No interfacial reactions were resolved indicating the metal-semiconductor interface formed at low temperature is relatively abrupt and unreacted.

For In deposition at room temperature shown in figure 6.6, the clean surface is extremely similar to that observed at low temperature. In contrast though, the evolution of the As3d core level components differ immensely. As in the low temperature case, S1 and B are attenuated as the In overlayer develops. However the component S2, related to In bonded As sites, increases as the In metal is deposited. Furthermore, at high In coverages, this component solely accounts for the As3d lineshape. This observation concurs with the notion that As diffuses from the  $\text{In}_{0.53}\text{Ga}_{0.47}\text{As}(100)$  substrate into the In overlayer forming an InAs interfacial region in the same way as described by Cao *et al.* for In/GaAs(110) interfaces. In Cao's study the source of As for InAs formation was unclear as it is energetically unfavourable to break GaAs bonds in favour of InAs (see table 6.3). The excess As was thought to have diffused from the bulk of the GaAs material. In the study presented here, it is highly likely that the excess As comes from the In/As rich surface region.

Binary semiconductor compound	Congruent evaporation temperature (°C)	Bond energy (eV)
InAs	380	1.41
GaAs	650	1.59
AlAs	850	1.98

Table 6.3: A table of congruent evaporation temperatures and bond energies for the binary compounds, which make up the ternary semiconductors  $\text{In}_{0.53}\text{Ga}_{0.47}\text{As}(100)$  and  $\text{In}_{0.52}\text{Al}_{0.48}\text{As}(100)$  [10,15].

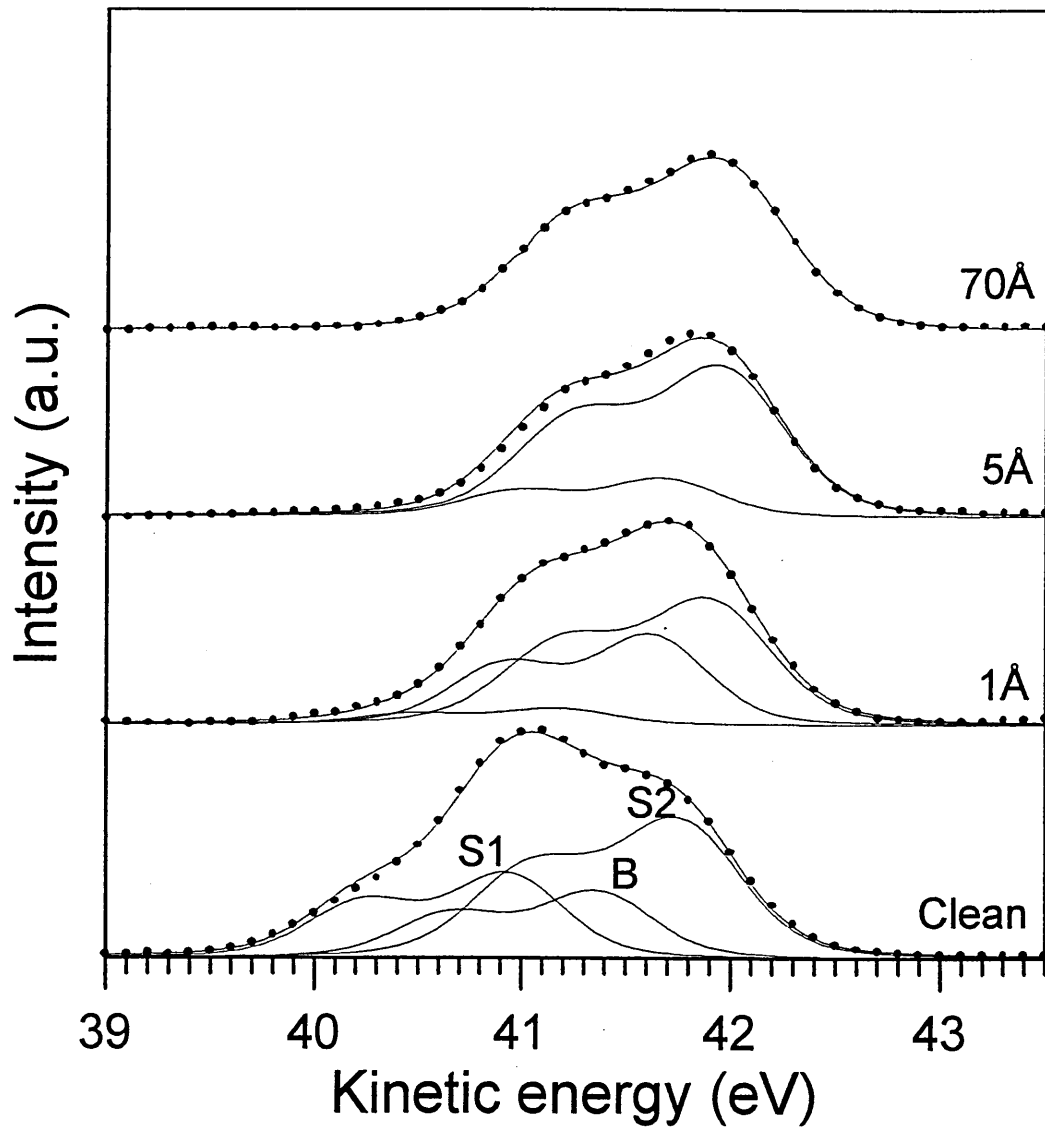


Figure 6.6: Evolution of the As3d core level spectra ( $h\nu = 87$  eV), with increasing In coverage on decapped  $(3 \times 1)$  reconstructed  $\text{In}_{0.53}\text{Ga}_{0.47}\text{As}(100)$ , deposited at 294K (RT). The peaks have been synthesised with three components, S1, S2 and B, shown along with the overall fit as continuous lines.

The evolution of the In4d and Ga3d core level emission spectra as a function of In overlayer coverage are shown in figures 6.7 and 6.8 for low temperature and room temperature In deposition, respectively. The spectra were obtained at a photon energy of  $h\nu = 63$  eV.

Figure 6.7 shows the case of low temperature deposition. The clean surface is fitted with similar components to those described in section 6.1.3. The Ga3d component is rapidly attenuated during the first  $\sim 5\text{\AA}$  of In deposition. The In4d surface and bulk components are also attenuated during this time, and after  $\sim 5\text{\AA}$  a third component developing at a higher kinetic energy is observed. With successive In depositions, this component increases at the expense of the two original clean surface components, and for the highest In coverage, this new component solely accounts for the In4d lineshape. The lineshape at the highest In coverage is narrower than that of the original clean surface components, and there is a degree of asymmetry apparent. Unfortunately it was not possible to fit this component as the facility to account for asymmetries was not available. However from the raw data alone, an asymmetry is clearly evident.

A higher density of states in a metal near the Fermi level compared with a semiconductor results in increased electron scattering and a subsequent energy loss for those electrons leaving the material, producing increased emission intensity at lower kinetic energies. The narrow lineshape and asymmetry are characteristic of emission from a metallic phase. The evolution of the In4d core level at LT from the clean surface to high In coverages is therefore thought to be the result of a transition of emission from In covalently bonded in the semiconductor to In in the metal overlayer.

The evolution of the In4d/Ga3d core level spectra following room temperature deposition is again however strikingly different. Figure 6.8 outlines the change in lineshape of the In4d/Ga3d core level spectra as a function of increasing In overlayer thickness at room temperature. The clean surface is again fitted with similar components to those described in section 6.1.3. In the early stages of In overlayer growth (up to  $\sim 2\text{\AA}$ ), a small Ga component is resolved to higher kinetic energy than the clean surface component. In the work carried out by Mao *et al.* on In/GaAs(100) interfaces, a similar component was observed and was attributed to metallic Ga formed by the freeing of Ga upon In reaction with the substrate. It is possible that a similar reaction is taking place here, whereby the As is released from its bonds with Ga in order

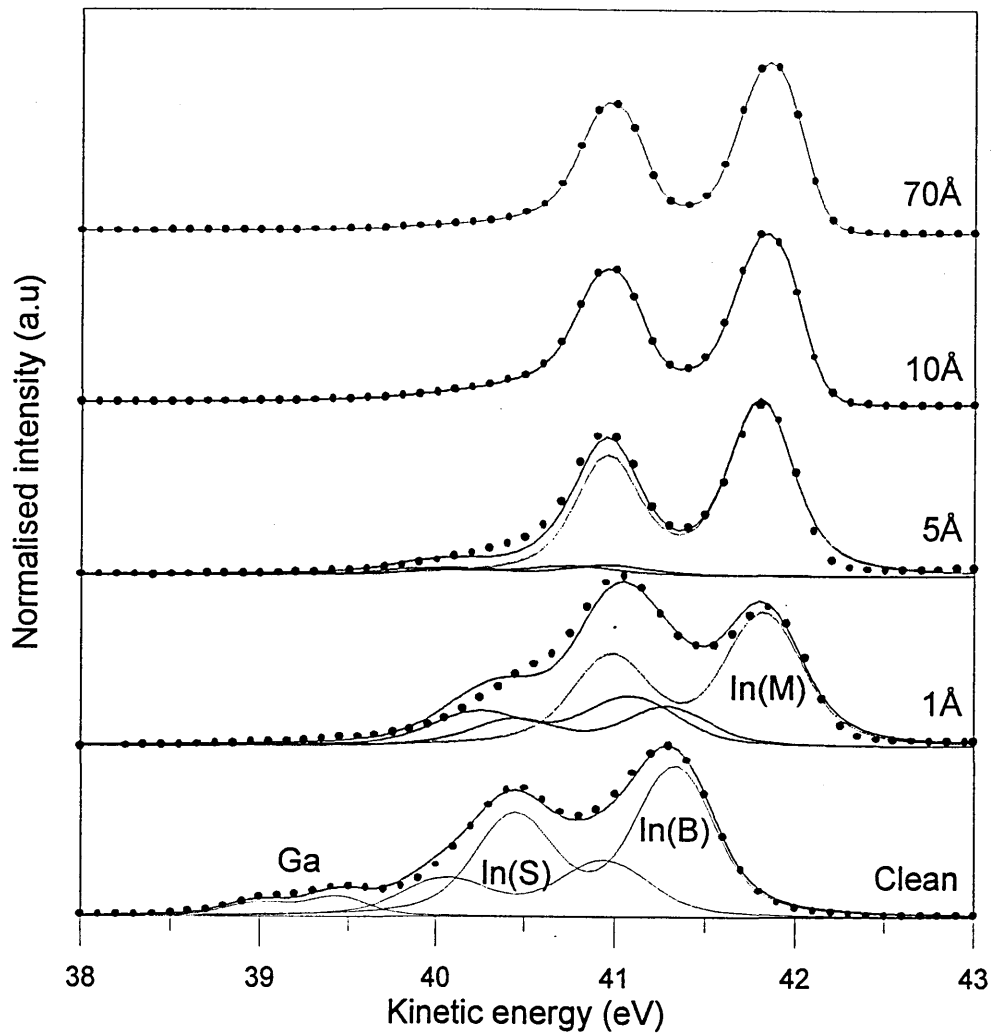


Figure 6.7: Evolution of the In<sub>4d</sub>/Ga<sub>3d</sub> core level spectra ( $h\nu = 63$  eV), with increasing In coverage on decapped (3×1) reconstructed In<sub>0.53</sub>Ga<sub>0.47</sub>As(100), deposited at 125K (LT). Areas where the fits are aesthetically poor are due to the fact that it was not possible to fit the component related to emission from the metallic In with an asymmetrical lineshape. The fits are therefore shown purely to establish the emergence of a new metallic In component In(M).

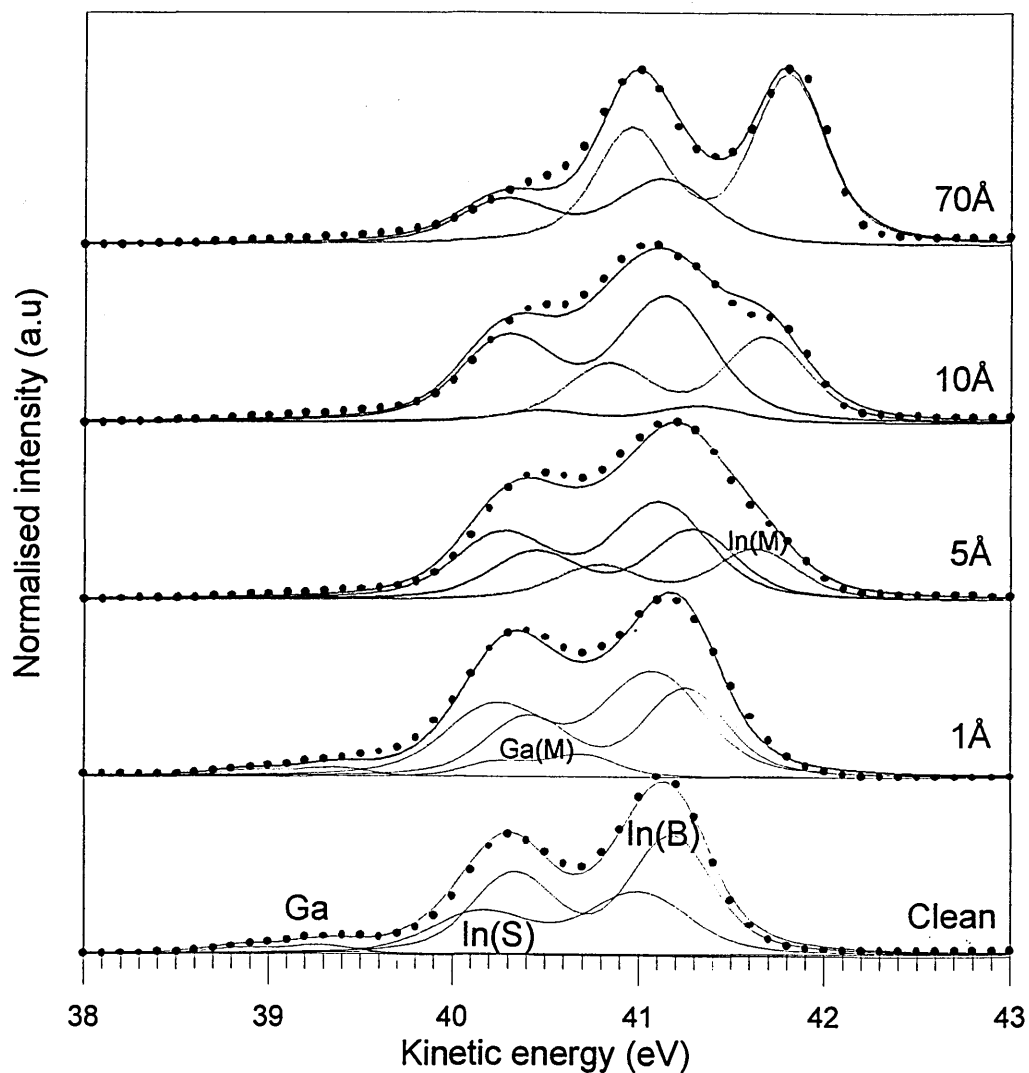
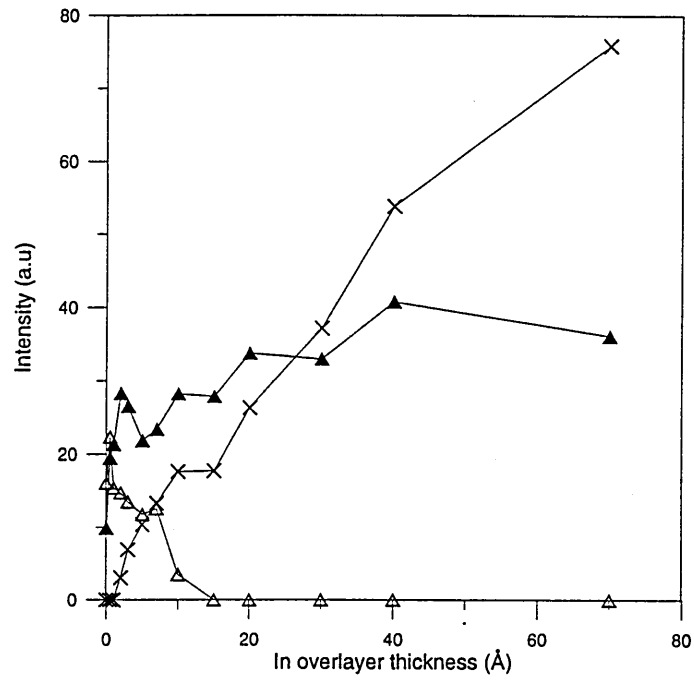


Figure 6.8: Evolution of the In<sub>4d</sub>/Ga<sub>3d</sub> core level spectra ( $h\nu = 63$  eV), with increasing In coverage on decapped (3×1) reconstructed In<sub>0.53</sub>Ga<sub>0.47</sub>As(100), deposited at 294K(RT). Areas where the fits are aesthetically poor are due to the fact that it was not possible to fit the component related to emission from the metallic In with an asymmetrical lineshape. The fits are therefore shown purely to establish the emergence of the new components Ga(M) and In(M).

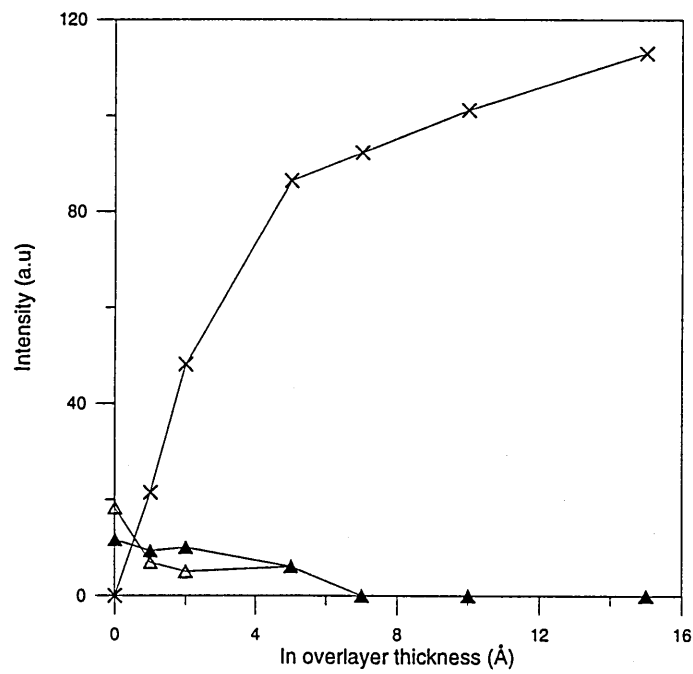
to form an In/As compound in the growing In overlayer, thus leaving behind free Ga. The component related to In bonded As sites increases in intensity with respect to the bulk In component at these coverages, indicating further that As is out diffusing into the In overlayer and forming InAs. After about 3Å of In have been deposited, a third In component arises to higher kinetic energy (lower binding energy). This component continues to increase as the In is deposited, subsequently burying both the metallic Ga and the bulk In components. The difference in energy (~0.6-0.7 eV) between the clean surface components and the component to higher kinetic energy coupled with its energy position at high In coverages, indicate that this growing component is again a feature of metallic In as seen in the low temperature case. However at the highest In coverage, this metallic In component does not completely dominate the In4d lineshape, and there is still a considerable signal from the InAs related component. It is evident that as the metallic signal increases, the overall fit of the lineshape deteriorates. This is a consequence of being unable to account for the assymetry observed from a metallic signal. However the fits have been shown to establish the fact that there are quite clearly two components that make up the observed lineshape for high In coverages at room temperature compared to just one at low temperature. This result can be seen more clearly in figure 6.9, where the intensity of the In4d bulk, surface and metallic components are shown as a function of In overlayer thickness for (a) room temperature and (b) low temperature deposition. It is quite clear that for the room temperature case, both the InAs related surface component and the metallic component increase in intensity as the In overlayer is deposited while the bulk intensity is attenuated. However in the low temperature case, both the bulk and surface intensities diminish in conjunction with a rapidly increasing metallic component intensity.

(iv) *Band bending*

The band bending induced when a metal and semiconductor come into contact can be determined from the rigid shift of the bulk derived As3d core level component. The effect of surface photovoltages have been negated by using highly doped ( $n^+$ )  $\text{In}_{0.53}\text{Ga}_{0.47}\text{As}(100)$  samples [16]. The change in the bulk As3d peak position as a function of In overlayer coverage is shown for room temperature and low temperature deposition in figure 6.10. Room temperature deposition of In produces a shift in the bulk As3d peak of  $(0.3 \pm 0.1)$  eV, while low temperature deposition produces a  $(0.5 \pm$



(a)



(b)

Figure 6.9: Plots of the intensities of the In4d components with increasing In overlayer coverage at (a) Room temperature and (b) Low temperature. Closed triangles denote the In4d surface component, open triangles denote the bulk component and crosses denote the metallic In4d component.

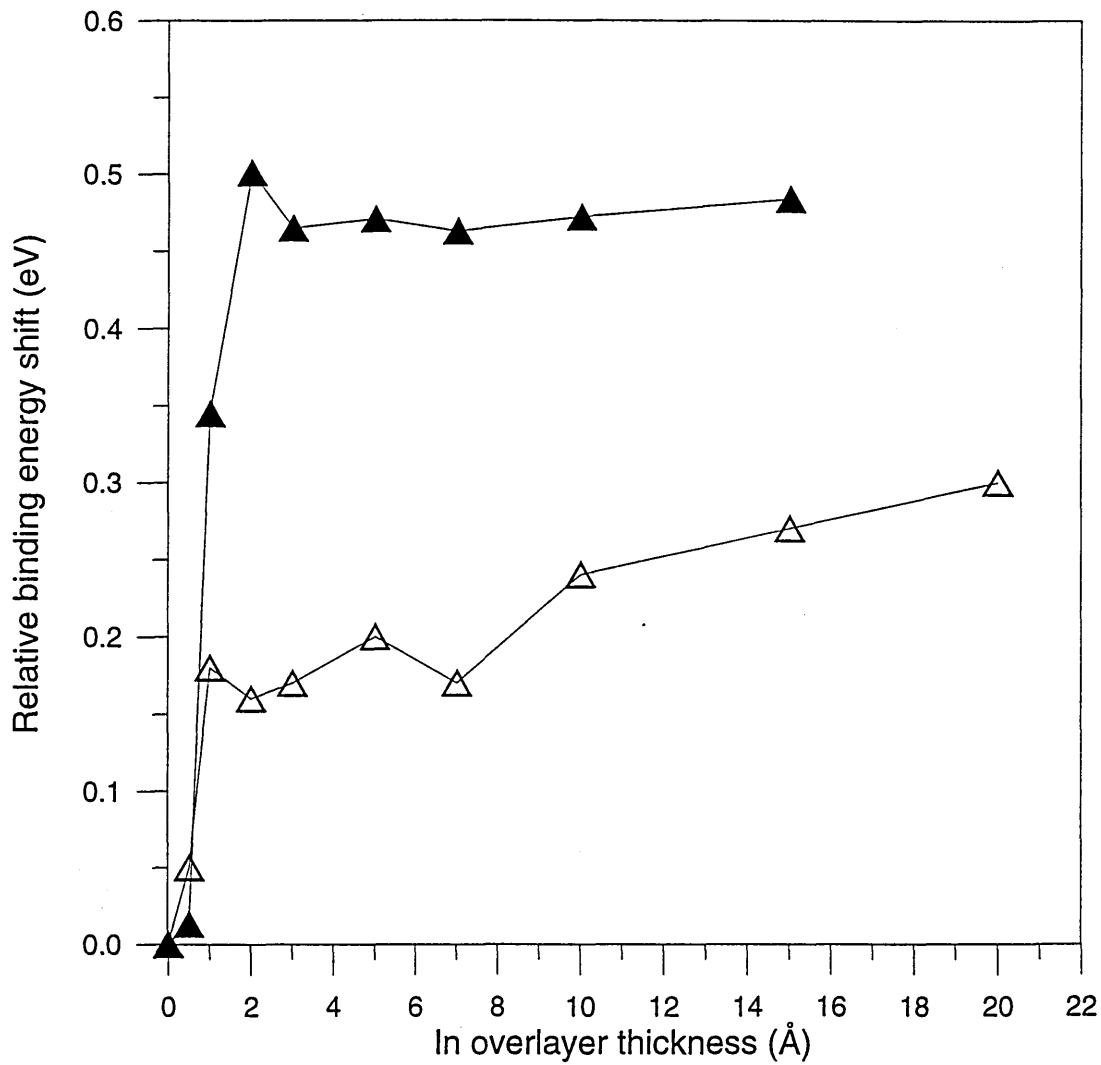


Figure 6.10: A plot of the band bending observed for the In-In<sub>0.53</sub>Ga<sub>0.47</sub>As(100) interface as a function of increasing In coverage. The band bending is determined from the relative binding energy shift in the As3d core level bulk component. The open triangles denote In deposition at 294K (RT), the closed triangles denote deposition at 125K (LT).

0.1) eV shift. Both these values are in good agreement with the barrier heights observed for In diodes formed at these temperatures using the I-V technique [1].

(v) *Valence band spectra*

The valence band spectra were recorded at a photon energy of 87 eV and are shown as a function of In overlayer thickness in figures 6.11 and 6.12 for low temperature and room temperature depositions respectively. Low temperature In deposition induces a change in structure of the clean  $\text{In}_{0.53}\text{Ga}_{0.47}\text{As}(100)$  derived states, indicating a transition from emission from the semiconductor surface to emission from a different material. After about 3Å In has been deposited, the valence band begins to show a prominent Fermi edge indicative of metallic emission. This feature becomes more prominent as the In overlayer thickness is increased and concurs with the notion that at low temperature the overlayer is metallic as discussed previously. The shift from the valence band maximum on the clean surface to the Fermi edge is about the order of 0.7-0.8 eV. The  $\text{In}_{0.53}\text{Ga}_{0.47}\text{As}(100)$  material used in this study was  $n^+$  type, implying that the Fermi level is close to the conduction band. Since the semiconductor sample and Fermi edge reference point are electrically connected, the two Fermi levels should be at the same energy position. Taking these two factors into account, the band gap of the semiconductor can be assumed to be the difference between the valence band maximum and the Fermi edge. The band gap of  $\text{In}_{0.53}\text{Ga}_{0.47}\text{As}$  is  $\sim 0.7$  eV, in good agreement with the value of shift observed.

For room temperature In deposition no significant change in valence band structure was observed from clean surface to final In thickness. This indicates that emission could still be seen from the substrate or that the overlayer is of a similar nature to that of the initial clean surface. Both these are the case as we have seen that there is increased clustering at room temperature, and there is As out-diffusion from the predominantly In/As rich surface to form In/As in the In overlayer. However at 1Å thickness of In, the valence band spectrum is different from the other spectra, and resembles that observed at low temperature. The signal to noise ratio for this spectrum is also significantly better than the other spectra, and hence it is likely that somewhere, a mistake has been made here, rendering this spectrum unreliable. There is again a shift of  $\sim 0.7-0.8$  eV between the clean surface valence band maximum and the valence band maximum at high In coverages. It is well understood that Ohmic contacts are readily

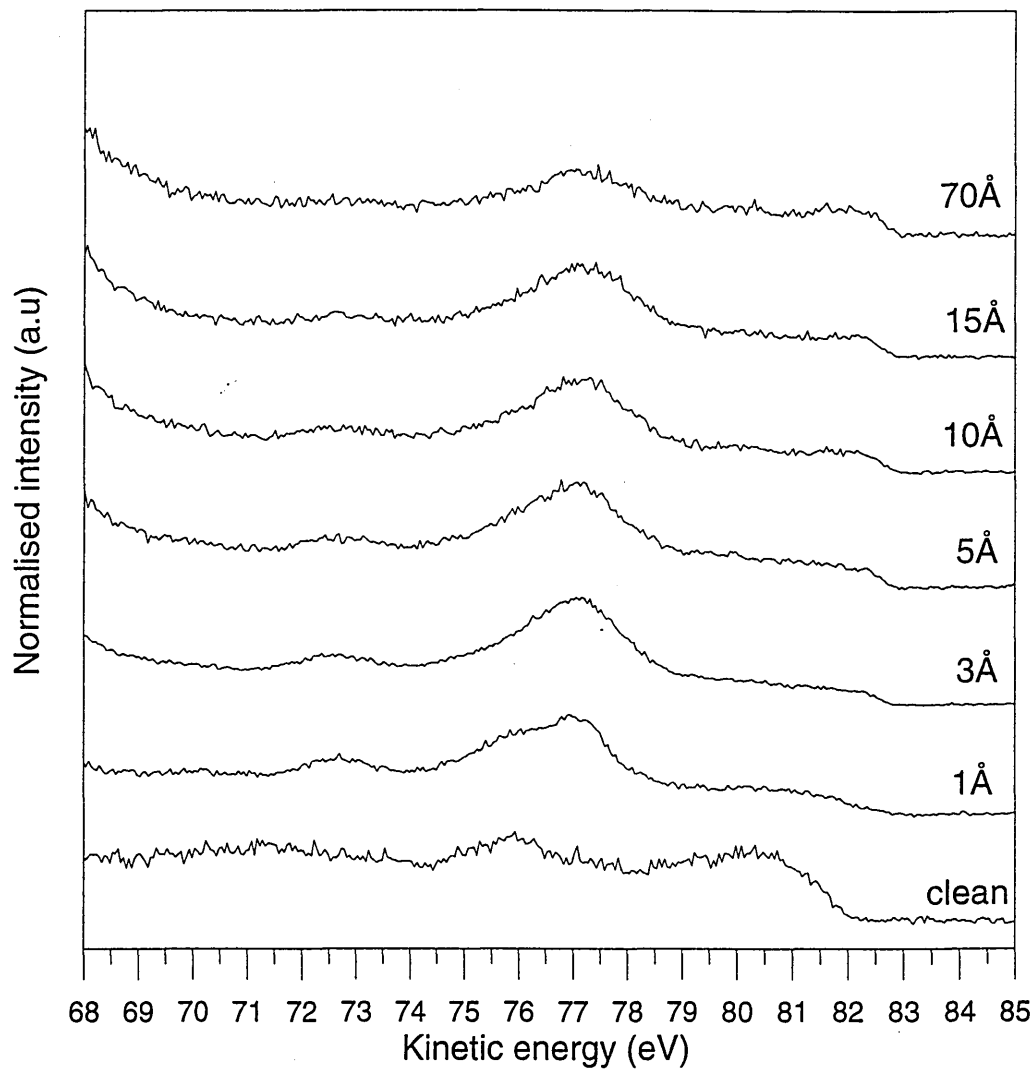


Figure 6.11: A stack plot of the valence band spectra as a function of increasing In overlayer coverage deposited at low temperature. The spectra were obtained using a photon energy of,  $h\nu = 87$  eV.

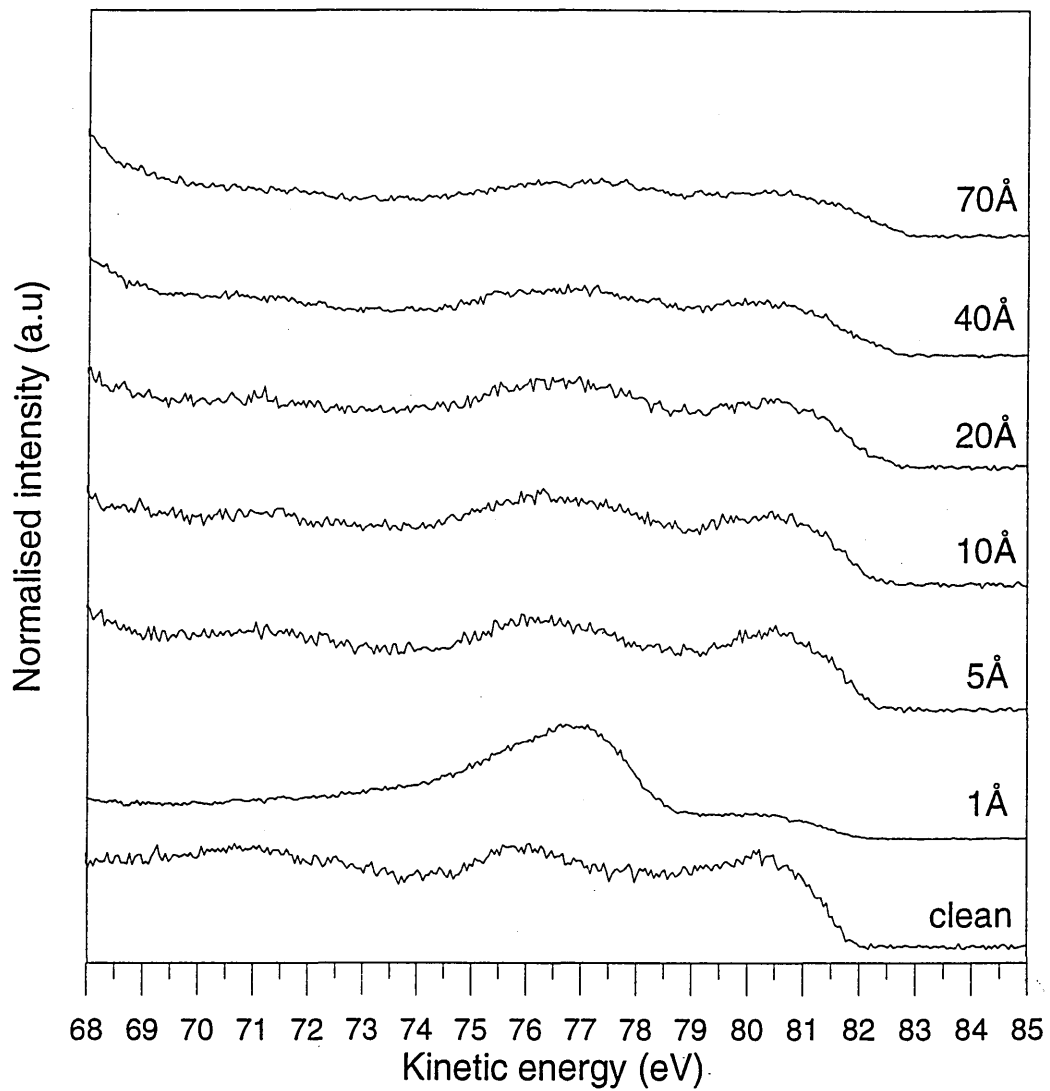


Figure 6.12: A stack plot of the valence band spectra as a function of increasing In overlayer coverage deposited at room temperature. The spectra were obtained using a photon energy of,  $h\nu = 87$  eV.

formed on n-InAs as the Fermi level is located in the conduction band [17]. The overlayer is highly likely to consist of a mixture of In metal and InAs, therefore we can again say that the shift is of the order of the band gap.

### 6.1.5 Au-In<sub>0.53</sub>Ga<sub>0.47</sub>As(100) interface formation

#### (i) *Substrate core level attenuation*

The growth mode of the Au overlayer can be determined by the attenuation of the As3d, Ga3d and In4d core signals as a function of Au overlayer thickness. In figure 6.13 the normalised integrated emission intensities from the As3d core level as a function of Au overlayer deposition at room and low temperature are shown. In the low temperature case, the As3d core level intensity has an exponential attenuation for the first ~15Å of Au deposition. Deviation from an exponential attenuation occurs after 15Å Au have been deposited, and is indicative of a layer by layer followed by clustering mode of growth. As in the case of In deposition, the attenuation at room temperature is significantly reduced, suggesting either increased clustering or the possibility of As out-diffusion. In a soft x-ray photoemission study of Au/GaAs(100) interfaces formed at room and low temperatures, Mao *et al.* reported a similarly reduced attenuation of the As signal at room temperature. In this particular case, the reduced attenuation was attributed to increased clustering of the Au overlayer as opposed to the out-diffusion of As into the metal overlayer [7]. However other reports of Au-GaAs(100) interface formation have suggested that an Au/Ga alloy is formed resulting in the out-diffusion of As to segregate near the surface [9,18]. It may be possible that a similar effect occurs for the Au-In<sub>0.53</sub>Ga<sub>0.47</sub>As(100) system, whereby the formation of either Au/Ga or Au/In alloys result in the out-diffusion of As into the metal overlayer.

If substantial clustering at room temperature were to be the sole cause of the reduced attenuation, it would be correct to assume that the In4d and Ga3d core level intensities would show similar behaviour; this however is not the case. Figures 6.14(a) & (b) show the attenuation of the As3d, Ga3d and In4d core level intensities for room temperature Au deposition and low temperature Au deposition respectively. Figure 6.14(a) indicates a much reduced attenuation of the As signal at room temperature compared to that of the In and Ga. All three components attenuate at similar rates up until a coverage of about 7 Å. After 7 Å Au deposition, the As3d signal has a much

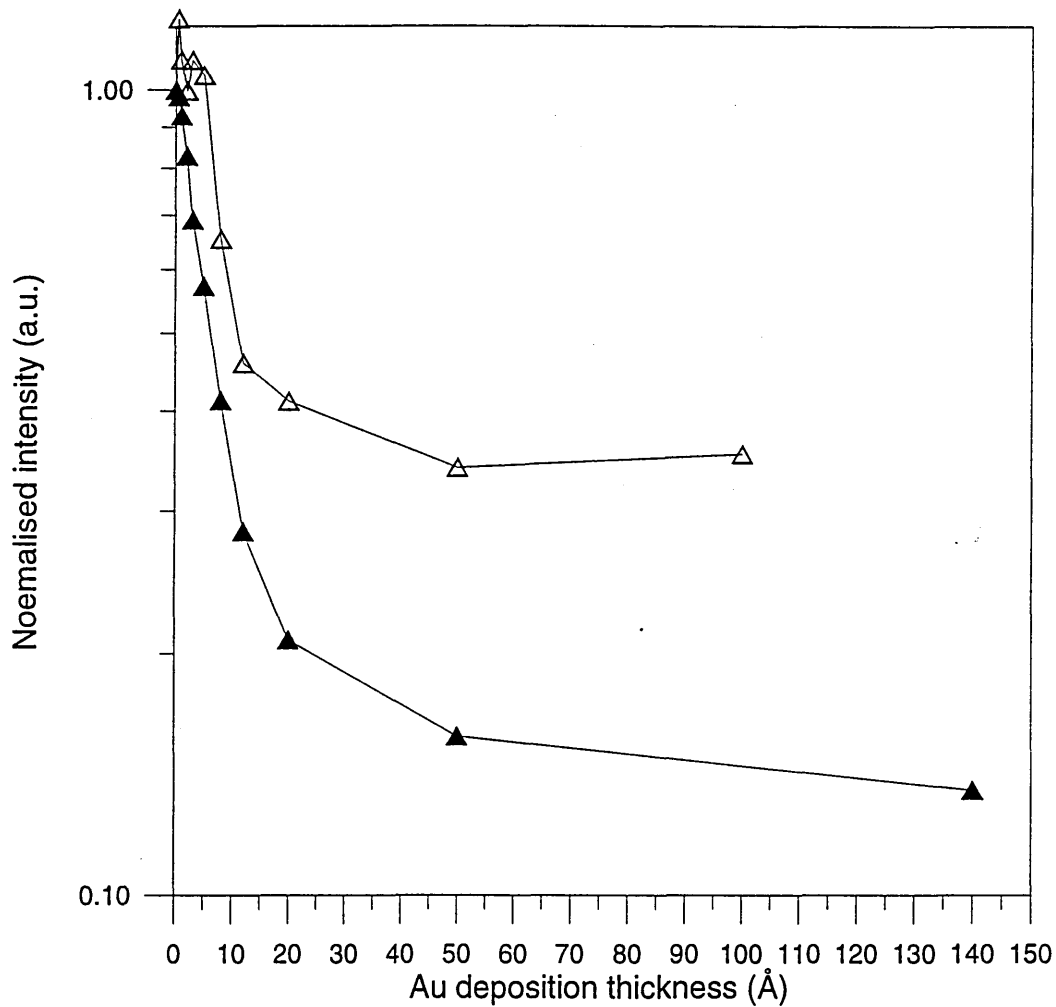


Figure 6.13: As3d core level emission intensity ( $I/I_0$ ), plotted as a function of Au coverage on decapped  $\text{In}_{0.53}\text{Ga}_{0.47}\text{As}(100)$ , obtained at an excitation energy of 87 eV. The open triangles denote Au deposition at 294K (RT), the closed triangles denote deposition at 125K (LT).

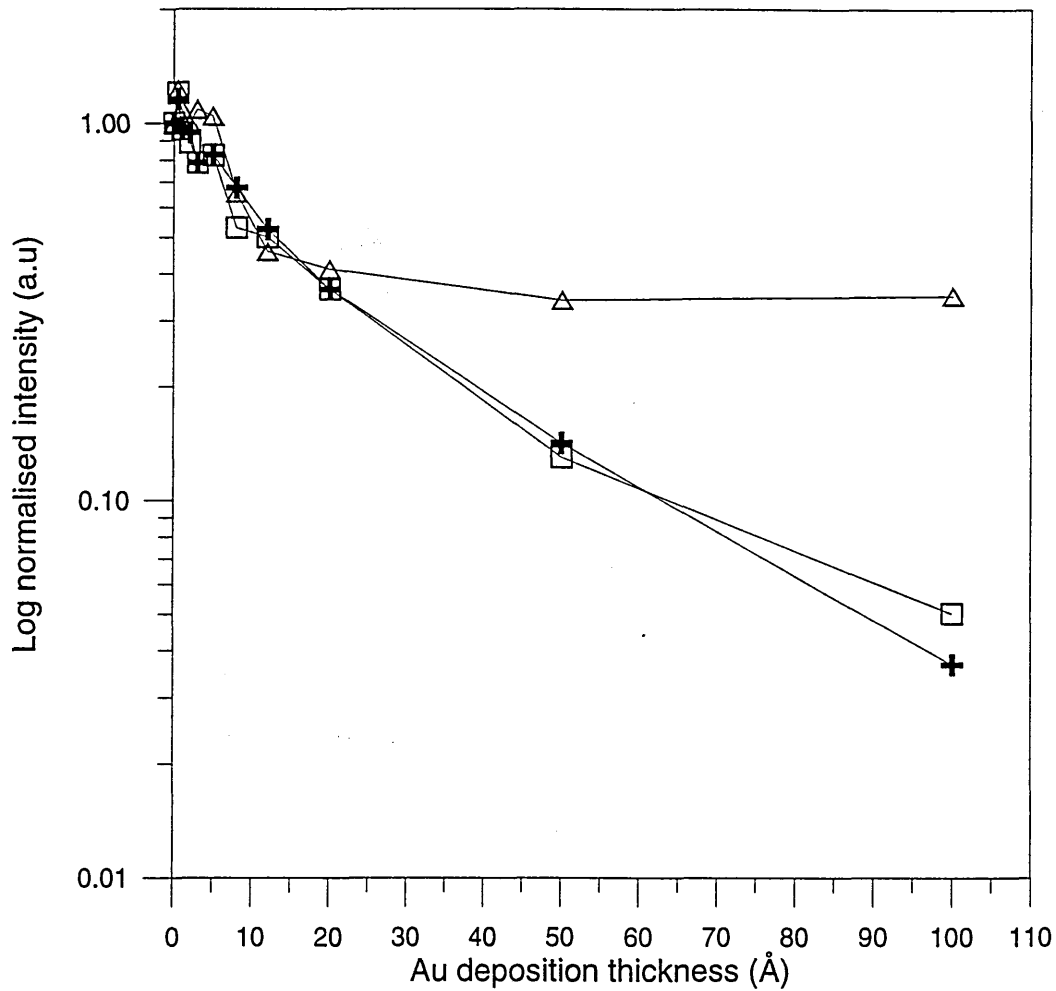


Figure 6.14(a): As3d, In4d and Ga3d core level emission intensity ( $I/I_0$ ), plotted as a function of Au deposited on decapped  $\text{In}_{0.53}\text{Ga}_{0.47}\text{As}(100)$  at room temperature. Open triangles denote emission from the As3d core level, squares denote emission from the In4d core level and crosses denote emission from the Ga3d core level.

more truncated attenuation than either the In4d or Ga3d signals, and at high Au coverages the signal has only reduced to 35% of its original clean surface value; in comparison to ~5% for both the In and Ga signals. It can be seen then that as in the case of In/InGaAs interface formation at room temperature, As out-diffuses from the InGaAs substrate into the growing metal overlayer. It has already been mentioned that the attenuation of the In and Ga core level signals can be interpreted as a layer by layer followed by clustering mode of growth. However the presence of a signal from the In and Ga core levels at large coverages may also be a consequence of the formation of Au/Ga and Au/In alloys in the interfacial region. From the data obtained it is difficult to determine which interpretation is most prevalent, and the likelihood is, that a combination of both effects is being observed.

The attenuation of the core level signals with increasing Au deposition at low temperature (figure 6.14(b)) is however somewhat different. All three core level signals are attenuated at similar rates in the early stages of Au deposition, continuing up to ~15Å. By taking a line of best fit in this region, and applying the equation,

$$I/I_0 = \exp(-d/\lambda) \quad [6.5]$$

values of  $\lambda \approx 7-8\text{\AA}$  can be calculated for electrons emitted from the As3d, In4d and Ga3d core levels. This is in good agreement with the estimated attenuation length of ~5Å and is indicative of laminar growth in this region [11]. After 15Å of Au deposition all three core level signals deviate from an exponential attenuation which is indicative of the onset of metal clustering. However as in the room temperature case, the As3d signal has a much slower attenuation, indicating that once again As out-diffuses into the metal overlayer. The increased attenuation of the In and Ga core level signals at low temperature may be determined as either a more laminar growth mode or the inhibition of alloy formation due to the reduced temperature.

In summary, low temperature Au deposition results in a layer by layer followed by islanding mode of growth, accompanied by As out-diffusion into the growing Au overlayer. Room temperature Au deposition also results in As out-diffusion with increased metal clustering and the possibility of Au/Ga and Au/In alloy formation.

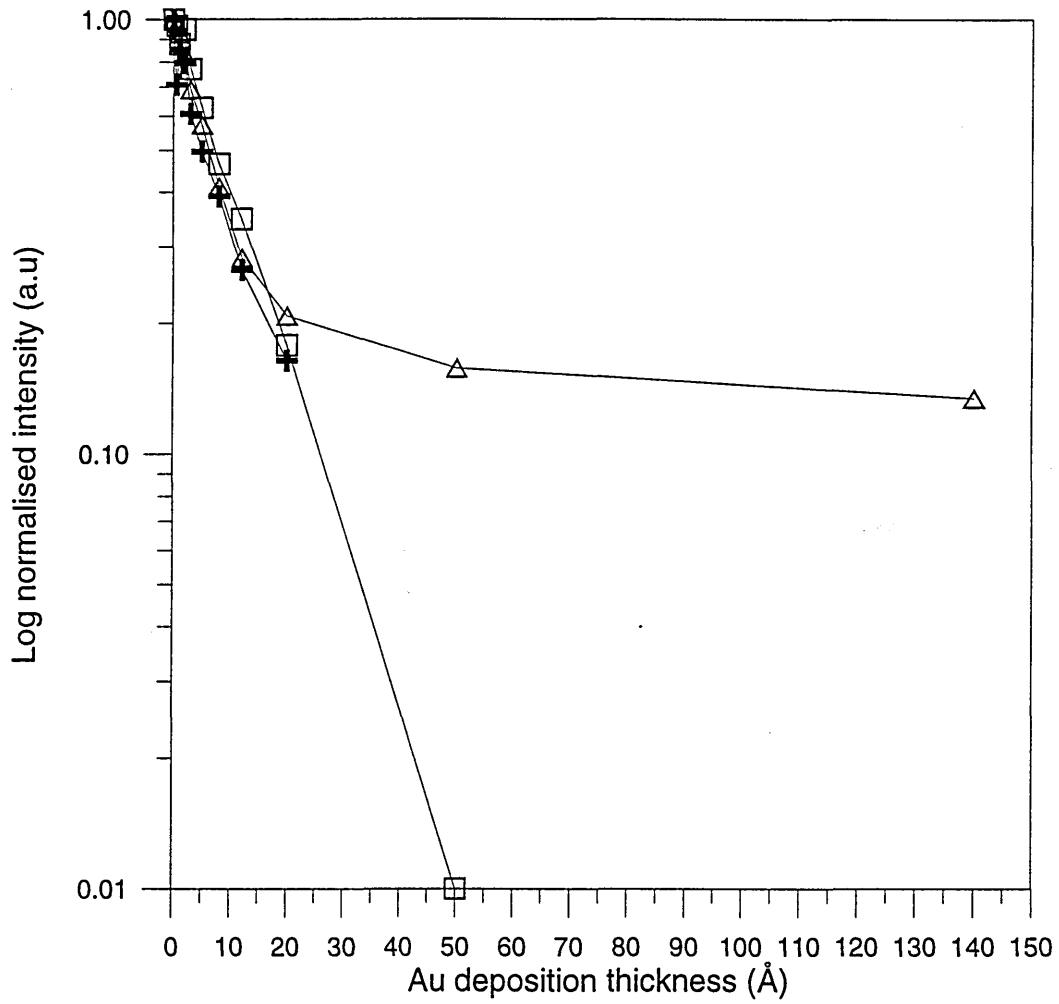


Figure 6.14(b): As3d, In4d and Ga3d core level emission intensity ( $I/I_0$ ), plotted as a function of Au deposited on decapped  $\text{In}_{0.53}\text{Ga}_{0.47}\text{As}(100)$  at low temperature. Open triangles denote emission from the As3d core level, squares denote emission from the In4d core level and crosses denote emission from the Ga3d core level.

(ii) *Au overlayer growth*

The intensity of core level emission ( $I$ ) from a laminar overlayer is given by,

$$I = I_f [1 - \exp(-d/\lambda)] \quad [6.6]$$

Where  $d$  is the overlayer thickness,  $\lambda$  is the attenuation length and  $I_f$  is the intensity at very large ( $d \gg \lambda$ ) overlayer coverages. Rearranging this equation gives us an expression in terms of  $(-d/\lambda)$  as shown below,

$$(I_f - I)/I_f = \exp(-d/\lambda) \quad [6.7]$$

Figure 6.15 shows a plot of the left hand side of this equation as a function of Au overlayer thickness for deposition at both room and low temperature. As was the case for the attenuation of the substrate core levels, the attenuation at room temperature deviates from the exponential after  $\sim 5\text{\AA}$  Au has been deposited. Similarly the attenuation at low temperature deviates from the exponential after  $\sim 10\text{\AA}$  Au has been deposited, confirming that greater clustering occurs during the formation of the Au overlayer at room temperature.

(iii) *As3d core level emission*

Figures 6.16 and 6.17 outline the change in shape of the As3d lineshape as a function of Au overlayer coverage, for low temperature and room temperature deposition respectively. The spectra were obtained using a photon energy of  $h\nu = 87$  eV. The clean surface is fitted with three components S1, S2 and B, similar to those described in section 6.1.3, with S1 related to Ga bonded As sites, S2 related to In bonded As sites and B emanating from As in the bulk of the material. The intensity of the In/As related component for both room temperature and low temperature deposition is reduced compared to clean surface in the case of In deposition. This is thought to be a consequence of discrepancies in the decapping temperatures for individual experiments.

After  $1\text{\AA}$  Au deposition, the In/As related surface component is attenuated further and a new reacted component S3, in a similar energy position becomes evident. By  $5\text{\AA}$  Au deposition, this reacted component has increased significantly at the expense

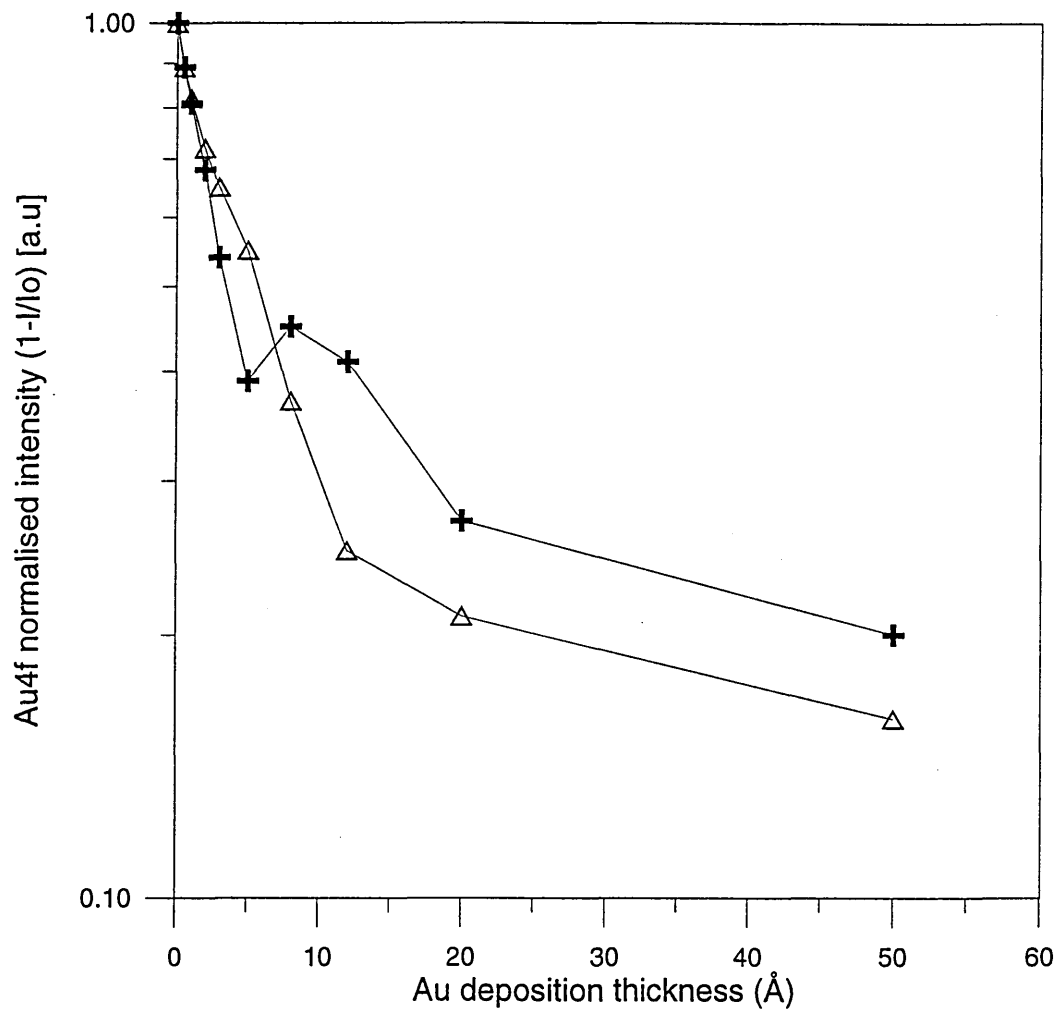


Figure 6.15: Au4f core level emission intensity in the form  $(1-I/I_f)$ , plotted as a function of Au deposited on decapped  $\text{In}_{0.53}\text{Ga}_{0.47}\text{As}(100)$  at room and low temperature. Open triangles denote Au deposition at low temperature, while the crosses denote Au deposition at room temperature.

of component S2, and at high Au coverages completely dominates the As3d core level lineshape. Comparison with the room temperature deposition case outlines a similar evolution of the As3d lineshape. A reacted component S3 again arises at the expense of component S2 after 1Å of Au is deposited, and continues to grow with increasing Au coverage. However at the highest Au coverages there is still a significant signal from the bulk component and component S1. This is in good agreement with the results obtained from the core level attenuation, whereby increased Au clustering would expose more of the underlying substrate and hence lead to an increased signal from the substrate components at room temperature compared to low temperature.

Both the low temperature and room temperature stack plots tend to compound the observation that As out-diffuses from the  $\text{In}_{0.53}\text{Ga}_{0.47}\text{As}(100)$  substrate into the Au overlayer irrespective of interface formation temperature. Numerous studies of Au/GaAs interface formation have shown that Ga out-diffuses from the GaAs to either form an Au-Ga alloy [9,19,20] or to segregate on the Au surface [18,21,22]. In the soft x-ray photoemission study by Mao *et al.* discussed previously, it has been suggested that room temperature Au deposition results in Ga surface segregating on Au while low temperature Au deposition indicates Ga diluted in Au [7]. The results presented here do not concur with these observations. In the present study, the substrate is ternary semiconductor material with In and Ga as the two contributing group III species. The clean surface characterisation indicated that the clean (3×1) reconstructed  $\text{In}_{0.53}\text{Ga}_{0.47}\text{As}(100)$  surface is predominantly In rich in comparison to Ga. Furthermore table 6.3 shows that the bond energies of In-As and Ga-As are 1.41 and 1.59 eV respectively. Hence it is highly likely that in contrast to the Au/GaAs case, As rather than Ga out-diffuses with the As emanating from the predominantly In/As rich surface region.

Comparison of the As3d lineshape at high Au coverages with that of emission from the elemental amorphous cap for both room and low temperature deposition indicates that As is not present in an elemental form, and is therefore attributed to As in a Au/As compound.

(iv) *In4d/Ga3d core level emission*

The evolution of the In4d and Ga3d core level spectra are shown as a function of Au overlayer coverage in figures 6.18 and 6.19 for low and room temperature

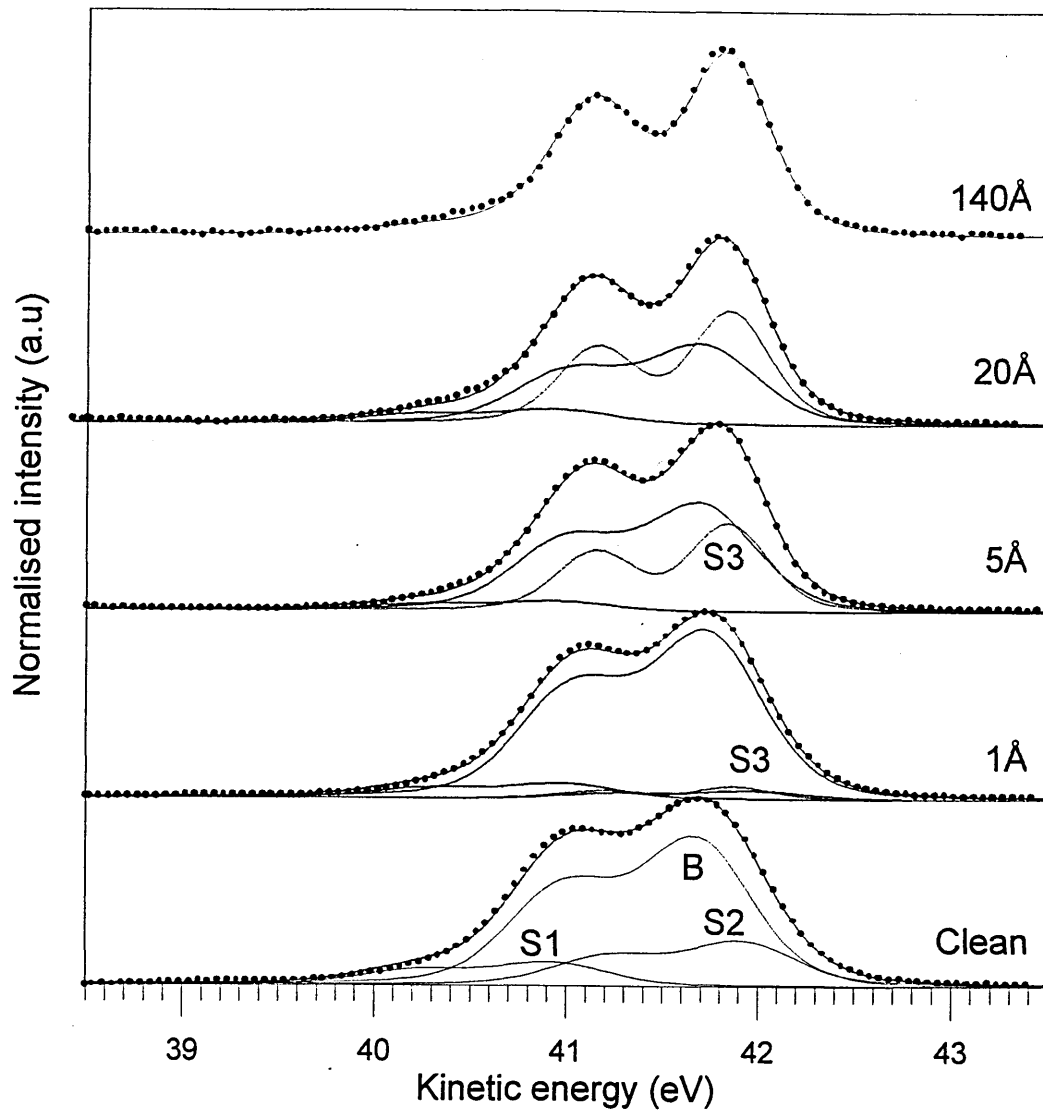


Figure 6.16: Evolution of the As3d core level spectra ( $h\nu = 87$  eV), with increasing Au coverage on decapped  $(3 \times 1)$  reconstructed  $\text{In}_{0.53}\text{Ga}_{0.47}\text{As}(100)$ , deposited at 125K (LT). The peaks have been synthesised with three components, S1, S2, S3 and B, shown along with the overall fit as continuous lines.

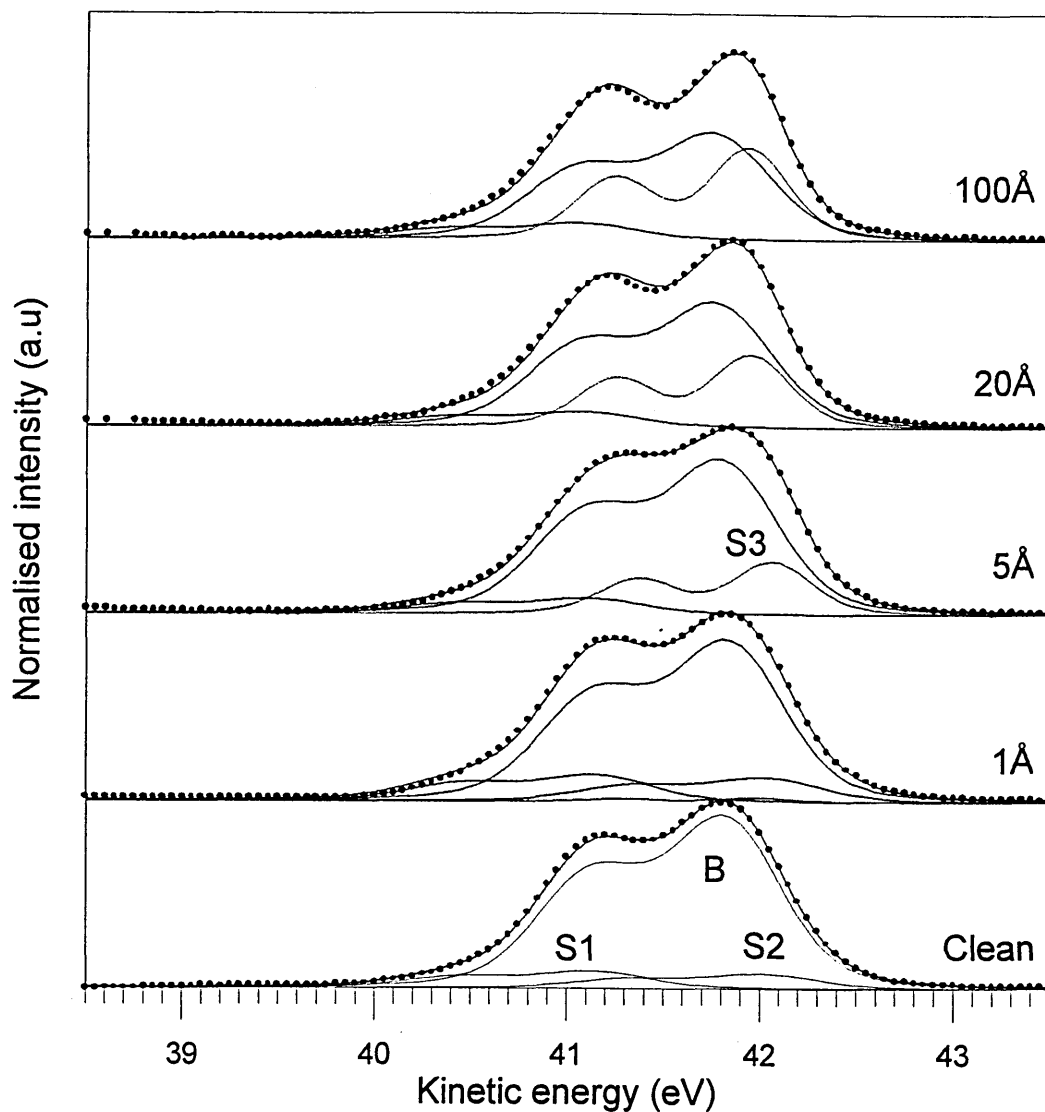


Figure 6.17: Evolution of the As3d core level spectra ( $h\nu = 87$  eV), with increasing Au coverage on decapped (3×1) reconstructed  $\text{In}_{0.53}\text{Ga}_{0.47}\text{As}(100)$ , deposited at 294K (RT). The peaks have been synthesised with three components, S1, S2, S3 and B, shown along with the overall fit as continuous lines.

deposition respectively. The spectra were acquired with a photon energy of 63 eV and the clean surface is fitted with similar components to those described in section 6.1.3. As was observed in the As3d clean surface, the component related to In bonded As sites in the In/As rich surface is smaller than for the In/  $\text{In}_{0.53}\text{Ga}_{0.47}\text{As}(100)$  experiment.

As the Au is deposited at low temperature (figure 6.18), the surface In4d component reduces in intensity in comparison to the Ga3d signal and the bulk In signal. By 5Å of Au deposition, the surface component has almost completely been attenuated; however there is still a significant signal from the Ga3d core level. This is in contrast to the case of In deposition on  $\text{In}_{0.53}\text{Ga}_{0.47}\text{As}(100)$  where the Ga3d signal attenuated rapidly as the In/As related surface component increased. This reduction of the In/As surface component was also observed in the As3d spectra discussed previously. It is therefore suggested that in the early stages of Au deposition on  $\text{In}_{0.53}\text{Ga}_{0.47}\text{As}(100)$ , As is released from the weaker In/As bonds (1.41 eV) at the surface to diffuse into the metal overlayer. After deposition of 20 Å Au, only emission from the bulk In4d signal is evident, as the Ga3d emission is not resolved. The lineshape is slightly narrower than for the clean surface, and the component has shifted by  $\sim 0.7$  eV to higher kinetic energy. A similar shift was seen in the In/ $\text{In}_{0.53}\text{Ga}_{0.47}\text{As}(100)$  experiment, and was attributed to emission from metallic In in the growing In overlayer. In the case presented here this theory can be dismissed; as In is not the overlayer species involved. It is probable however that as the Au overlayer becomes thicker, the As will diffuse from the surface leaving behind an interface environment containing excess In. It is conceivable therefore that the In4d emission will begin to resemble that of metallic In, hence the change in energy position and the narrowing of the lineshape. It may also be possible that the Au diffuses into the In rich environment, producing an Au/In alloy hence producing an In core level signal of metallic characteristics. At high Au coverages, the core level signal has been completely attenuated indicating a reasonably thick quasi-laminar Au overlayer. Upon warming the sample to room temperature, a significant In4d bulk signal is again observed. It will be shown later that this signal is similar to that observed for a similar Au deposition thickness at room temperature. It may be possible that as the sample warms up, the Au overlayer begins to cluster leaving areas where the substrate signal can be detected. It may also be the case that In diffuses into the Au overlayer upon warming of the sample. Similarly Au may dissolve into the substrate to form an Au/In/Ga alloy. However from the results obtained here, the source of this increased In signal remains an open question.

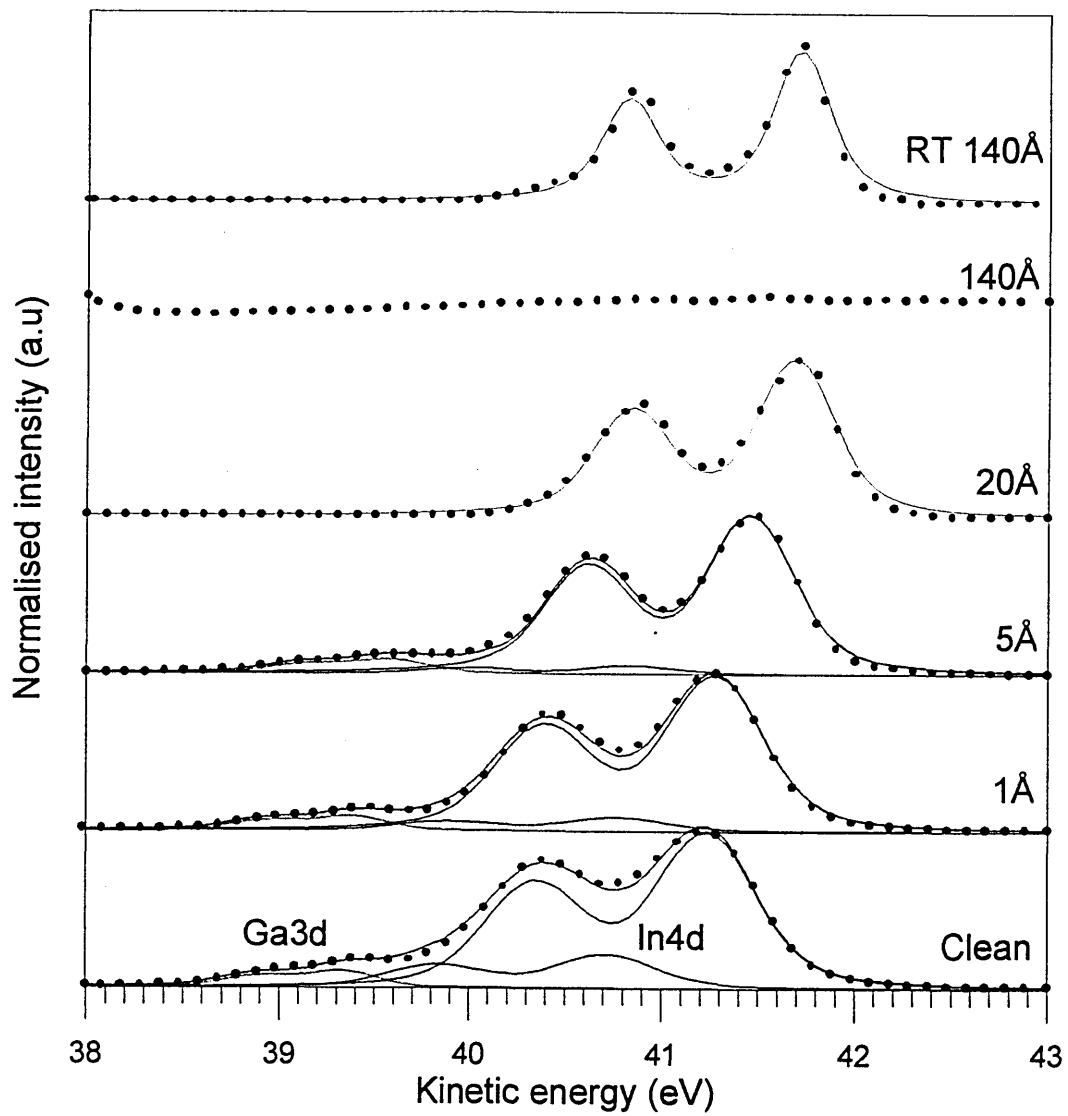


Figure 6.18: Evolution of the In4d/Ga3d core level spectra ( $h\nu = 63$  eV), with increasing Au coverage on decapped  $(3\times 1)$  reconstructed  $\text{In}_{0.53}\text{Ga}_{0.47}\text{As}(100)$ , deposited at 125K (LT).

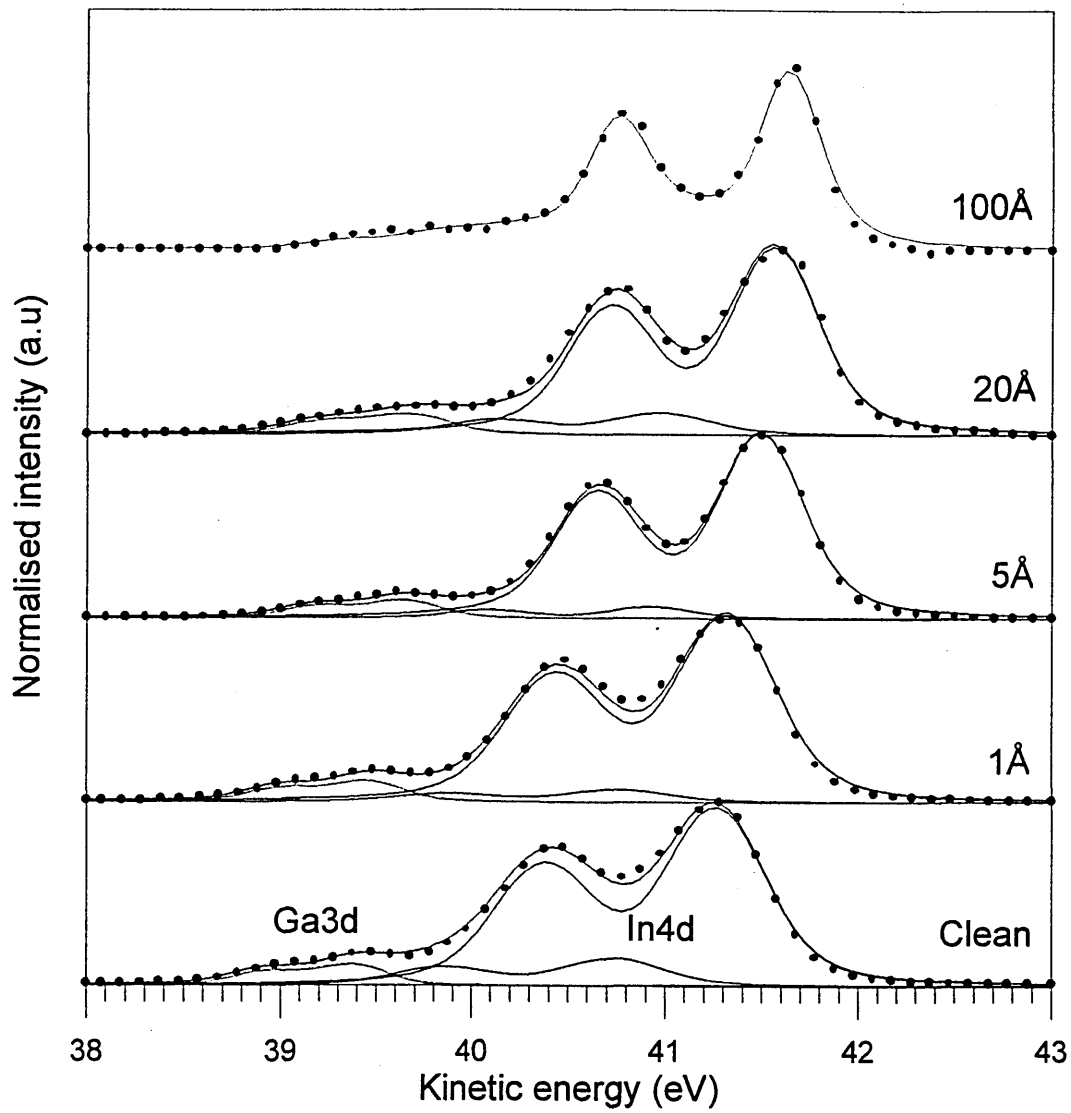


Figure 6.19: Evolution of the In4d/Ga3d core level spectra ( $h\nu = 63$  eV), with increasing Au coverage on decapped (3x1) reconstructed In<sub>0.53</sub>Ga<sub>0.47</sub>As(100), deposited at 294K (RT).

For room temperature deposition of Au as shown in figure 6.19, the evolution of the core levels is very similar to that observed during low temperature metallisation. As the Au is deposited, the surface In4d component is again reduced indicating the loss of As from the In/As rich surface. After 5Å Au deposition the core level spectra is similar to that obtained at low temperature. However after 20Å Au has been deposited there is still a signal from all three clean surface components, corresponding to emission from either the underlying substrate due to overlayer clustering or the formation of Au/In/Ga alloy. At the highest Au coverages, a single In4d component whose lineshape is narrower and has once again shifted to higher kinetic energy is evident. This lineshape is similar to that of the low temperature experiment after the sample was allowed to warm to room temperature, and is again attributed to emission from In in an interface environment that has excess In, which may be alloyed with Au.

(v) *Band bending*

The band bending at the metal/semiconductor interface is determined from the rigid shift of the bulk derived As3d core level component. Using highly doped (n+)  $\text{In}_{0.53}\text{Ga}_{0.47}\text{As}(100)$  samples has again negated the effect of surface photovoltages. The band bending observed for both room temperature and low temperature Au deposition was negligible (less than 0.1eV). This indicates that an Ohmic contact is formed at the Au- $\text{In}_{0.53}\text{Ga}_{0.47}\text{As}(100)$  interface for both room and low temperature formation, and is in good agreement with the Ohmic values of barrier heights measured for Au diodes on  $\text{In}_{0.53}\text{Ga}_{0.47}\text{As}(100)$  using the I-V technique [1].

(vi) *Valence band emission*

The evolution of the valence band as a consequence of low temperature and room temperature Au deposition is highlighted in figures 6.20(a) and (b) respectively. The stack plots show a strikingly similar trend in the evolution of the valence band, indicating that the same interface change is occurring irrespective of the Au deposition temperature. This is again in good agreement with the results already presented.

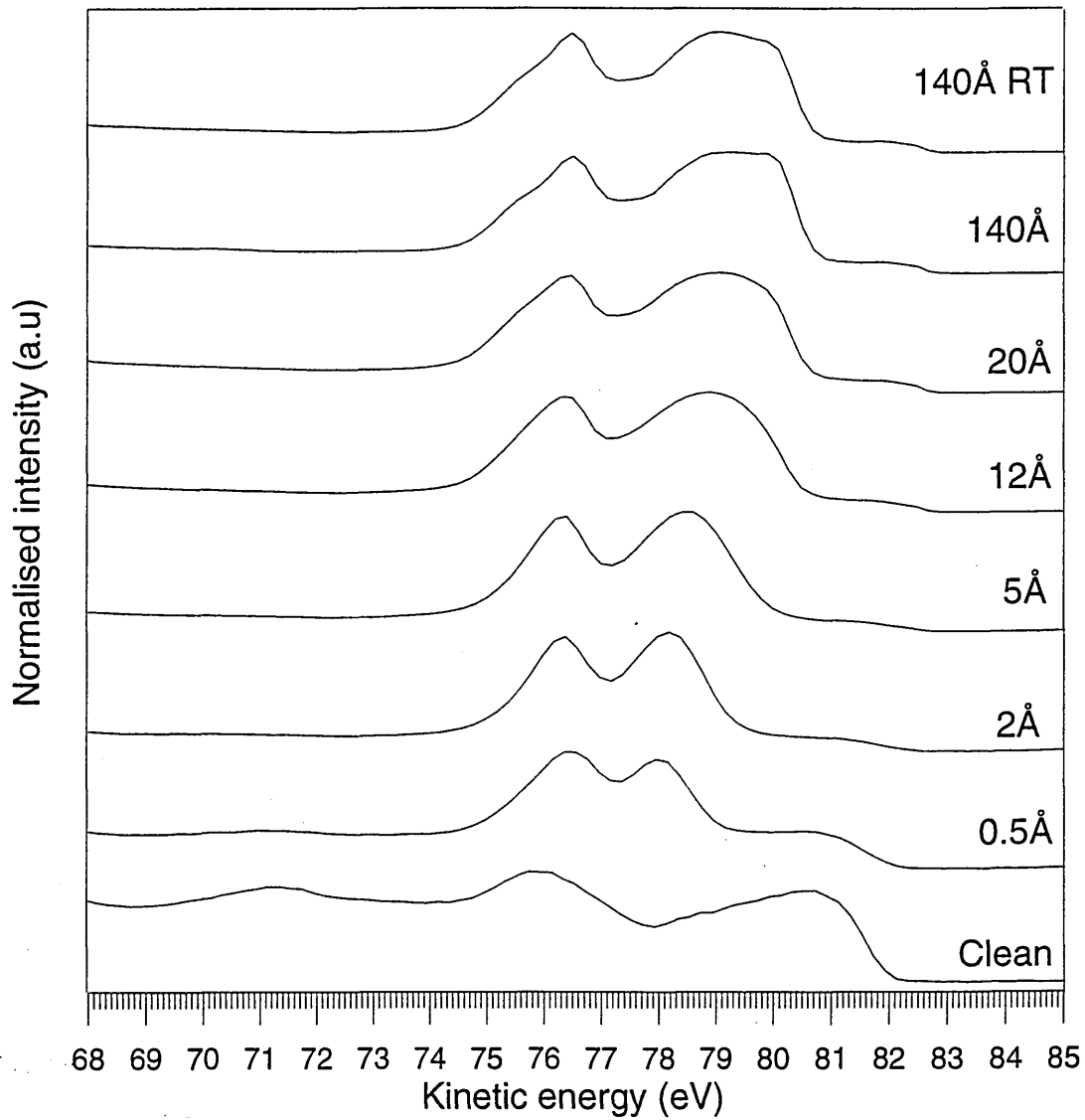


Figure 6.20(a): A stack plot of the valence band spectra as a function of increasing Au overlayer coverage deposited at low temperature onto decapped (3×1) reconstructed  $\text{In}_{0.53}\text{Ga}_{0.47}\text{As}(100)$ . The spectra were obtained using a photon energy of,  $h\nu = 87$  eV.

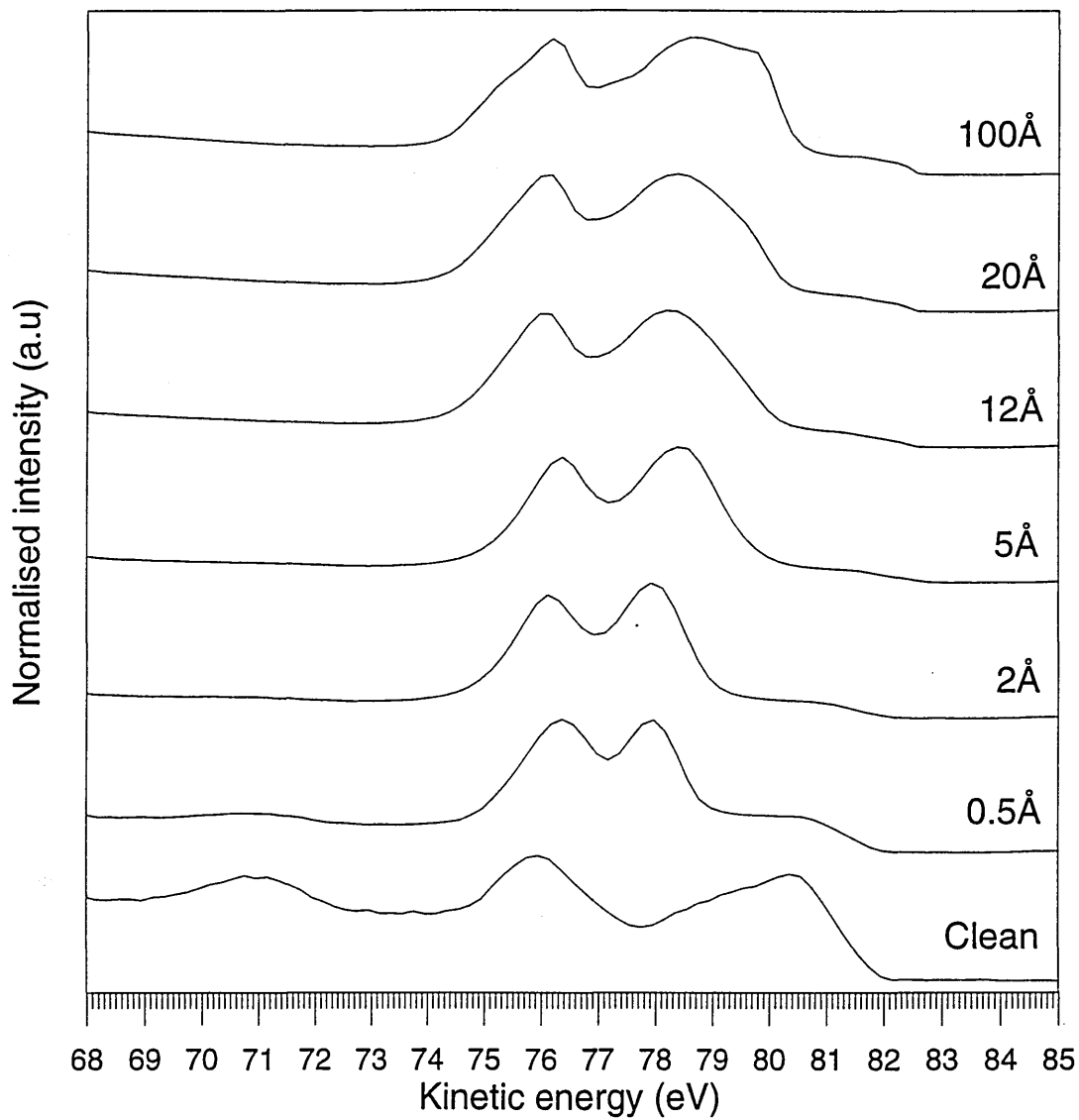


Figure 6.20(b): A stack plot of the valence band spectra as a function of increasing Au overlayer coverage deposited at room temperature onto decapped  $(3 \times 1)$  reconstructed  $\text{In}_{0.53}\text{Ga}_{0.47}\text{As}(100)$ . The spectra were obtained using a photon energy of,  $h\nu = 87$  eV.

## 6.2 Microscopy studies

### 6.2.1 Introduction

In this section, TEM and SAED have been utilised to provide structural information on the metal interfaces formed with  $\text{In}_{0.53}\text{Ga}_{0.47}\text{As}(100)$  at room and low temperatures. The experiments were performed in a Hitachi H800-NA electron microscope operating at 200 keV. The experimental equipment and sample preparation has been described in chapter 4.

Samples were observed in cross section to characterise the morphology of the metal overlayer, and in plan view to reveal the crystal structure of the overlayer. The extent of clustering and crystal grain size at the respective temperatures was monitored by sampling a constant area of sample.

### 6.2.2 The In- $\text{In}_{0.53}\text{Ga}_{0.47}\text{As}(100)$ interface

In figure 6.21(a) a micrograph of the cross section of the room temperature In- $\text{In}_{0.53}\text{Ga}_{0.47}\text{As}(100)$  interface is shown. The In layer thickness is very irregular, corresponding to metal overlayer clustering. Examination of the interface over a wider range showed that the distance between surface hillocks was not homogeneous, but varied between 130-430 nm. The glue used in sample preparation was evident on the In layer surface, suggesting that the layer fluctuations are not a consequence of thinning due to the ion etching. A micrograph of the low temperature In- $\text{In}_{0.53}\text{Ga}_{0.47}\text{As}(100)$  interface obtained under similar conditions is shown in figure 6.21(b). The In overlayer thickness is a lot more uniform, with this uniformity extending over a wide range. These results confirm that the interface formed at low temperature is more abrupt compared to the less well-defined room temperature interface, where InAs extends into the In overlayer.

In figures 6.22(a) & (b), SAED patterns of the metal overlayer formed at room temperature and low temperature are shown respectively. For a single crystal, the diffraction pattern would ideally consist of an ordered array of dots. However for crystallites in random relative orientations (i.e. grains), several of them may be in a reflecting position at any one time and hence a ring pattern will be formed with each ring associated with a particular set of planes. The SAED pattern from the In overlayer

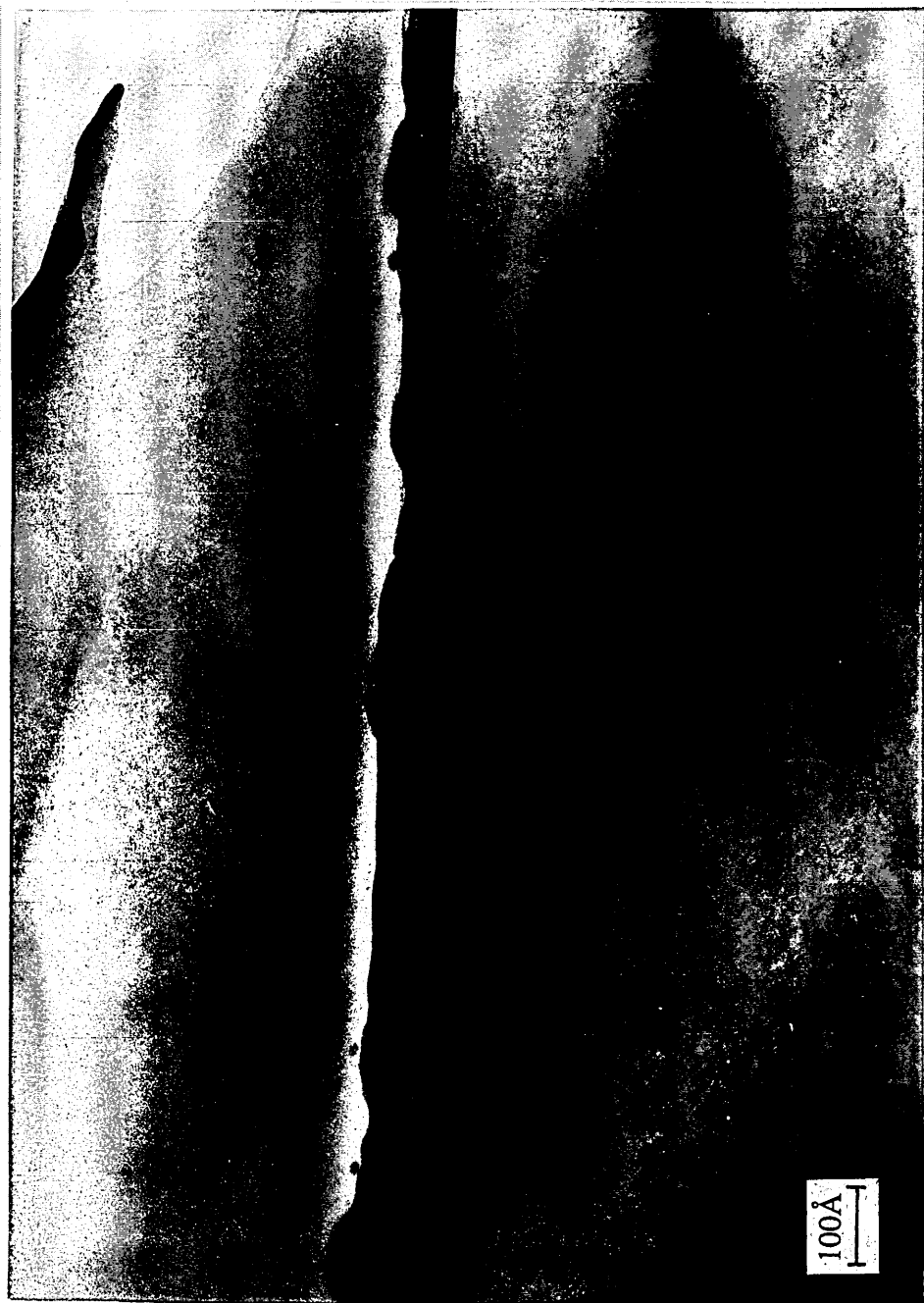


Figure 6.21 (a): A TEM cross sectional micrograph of the room temperature In-In<sub>0.53</sub>Ga<sub>0.47</sub>As(100) interface. The magnification used is 200,000 times.



Figure 6.21 (b): A TEM cross sectional micrograph of the low temperature In-In<sub>0.53</sub>Ga<sub>0.47</sub>As(100) interface.  
The magnification used is 300,000 times.

deposited at low temperature displays a more prominent ring pattern than from the In overlayer deposited at room temperature. This indicates that a greater number of random crystalline orientations are present in the low temperature In overlayer, supporting the notion that at low temperature a reduced grain size is achieved due to a reduction in surface mobility of the In adatoms.

### 6.2.3 The Au-In<sub>0.53</sub>Ga<sub>0.47</sub>As(100) interface

The results obtained for the formation of Au-In<sub>0.53</sub>Ga<sub>0.47</sub>As(100) interfaces at room and low temperature showed little difference in the overlayer growth mode, or crystal grain size as a function of temperature. This concurs with the results obtained by photoemission, indicating that the Au-In<sub>0.53</sub>Ga<sub>0.47</sub>As(100) interface system is relatively unaltered by changing the interface formation temperature.

## 6.3 Summary

### 6.3.1 The In-In<sub>0.53</sub>Ga<sub>0.47</sub>As(100) interface

The SXPS and TEM results presented here indicate that In metallisation at room temperature results in a predominantly three dimensional mode of growth accompanied by the out-diffusion of As from the In<sub>0.53</sub>Ga<sub>0.47</sub>As(100) substrate into the growing In metal overlayer, to produce an overlayer consisting of metallic In and InAs. Low temperature metallisation of In<sub>0.53</sub>Ga<sub>0.47</sub>As(100) tends to reduce clustering with an overlayer that appears to be laminar in growth for the first ~4-5 Å. No reacted components were observed in the As3d core level lineshape, and hence it is also thought that the use of low temperature inhibits As out-diffusion resulting in an overlayer consisting of entirely metallic In. The degree of band bending observed for both the room temperature ( $\phi_b \sim 0.3$  eV) and low temperature ( $\phi_b \sim 0.5$  eV) In deposition, is in good agreement with I-V measured values of Schottky barriers reported for In diodes formed under similar conditions on “as grown” In<sub>0.53</sub>Ga<sub>0.47</sub>As(100) surfaces [1]. It has been shown that the interface that exhibits As out-diffusion produces a lower Schottky barrier, indicating that the height of the Schottky barrier may be dependent on interface chemistry.

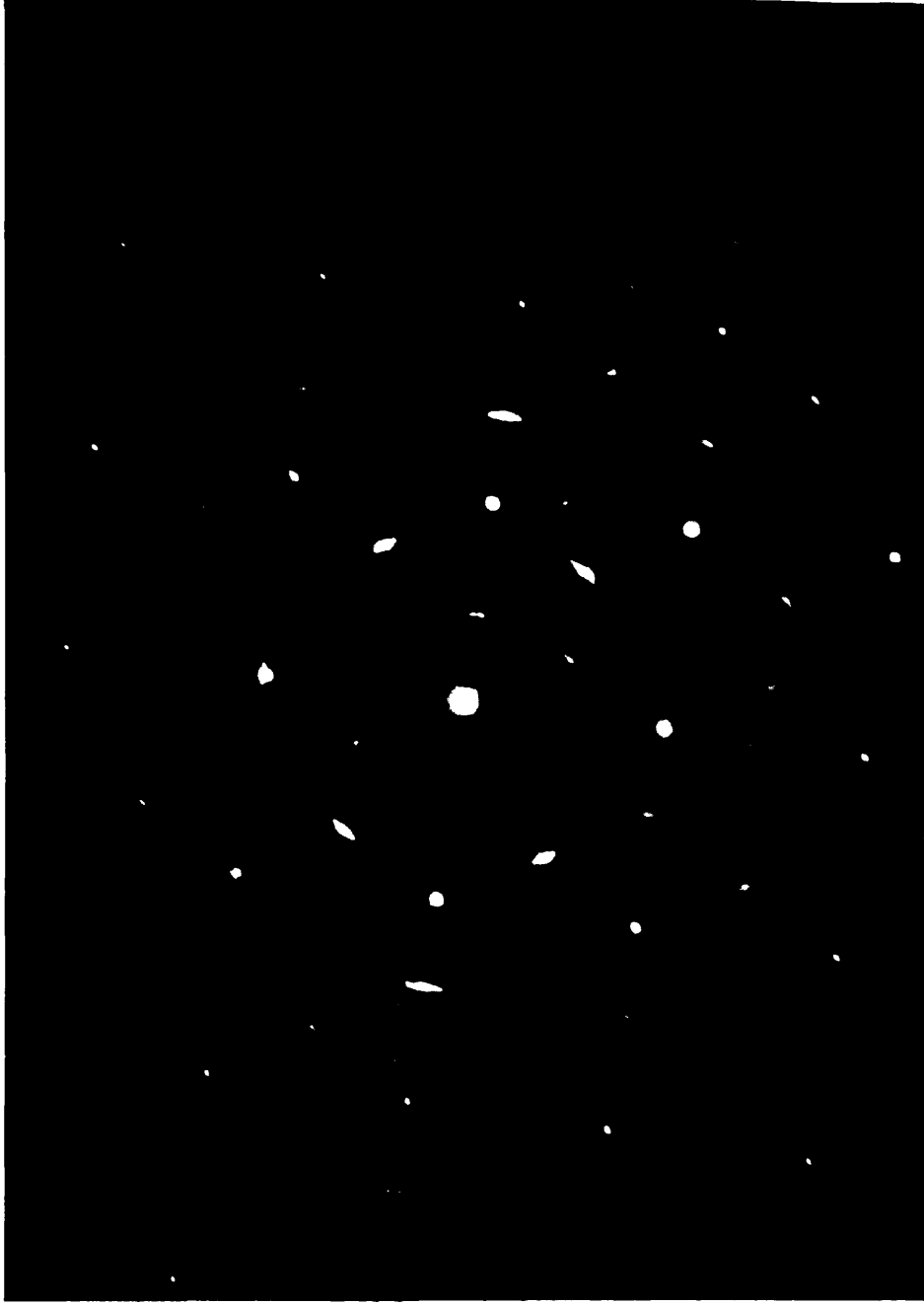


Figure 6.22 (a): An SAED pattern of the In overlayer deposited on  $\text{In}_{0.53}\text{Ga}_{0.47}\text{As}(100)$  at room temperature (295K).

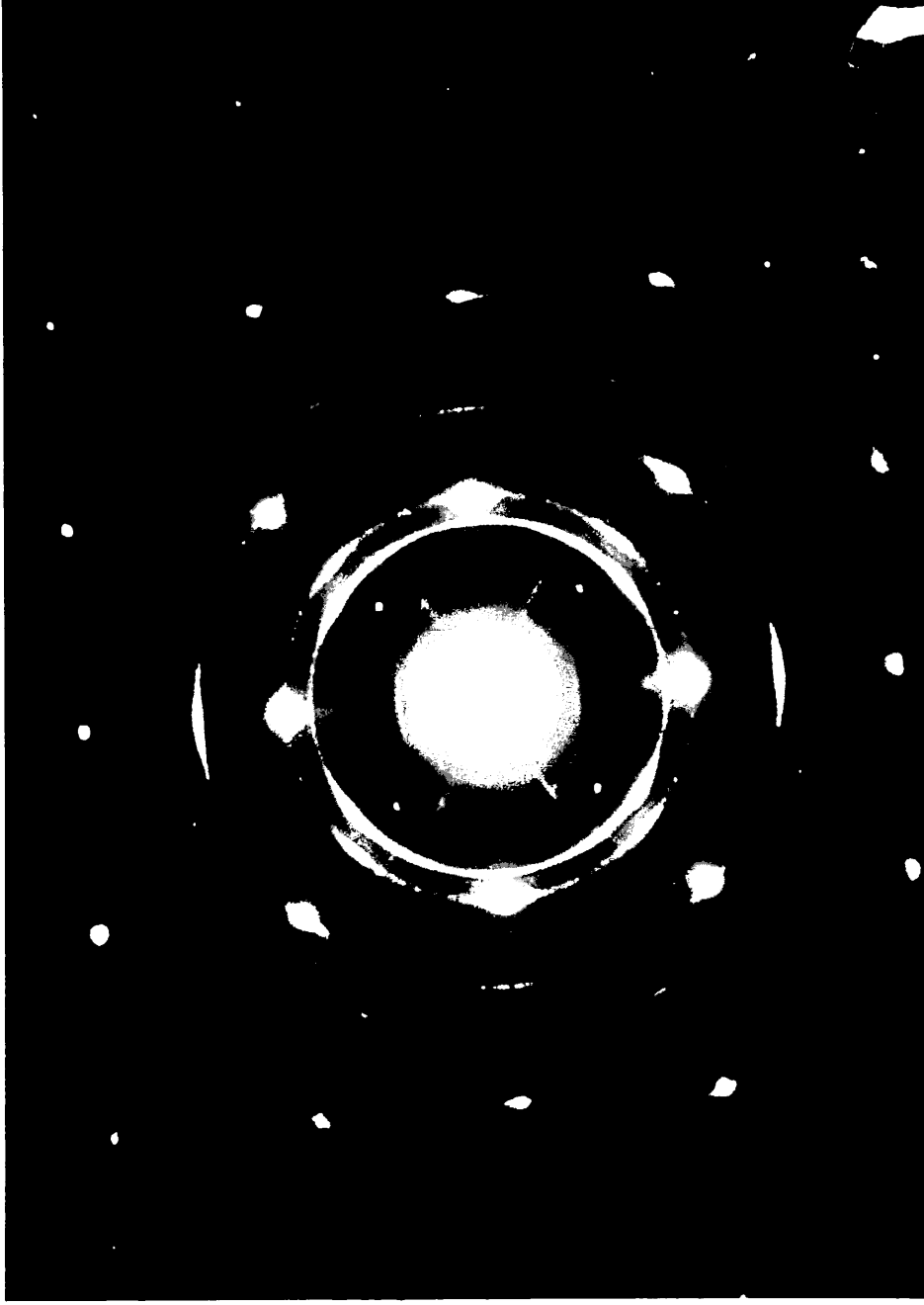


Figure 6.22 (b): An SAED pattern of the In overlayer deposited on  $\text{In}_{0.53}\text{Ga}_{0.47}\text{As}(100)$  at low temperature (125K).

### 6.3.2 The Au-In<sub>0.53</sub>Ga<sub>0.47</sub>As(100) interface

SXPS results of Au-In<sub>0.53</sub>Ga<sub>0.47</sub>As(100) interface formation at room temperature have indicated that the first  $\sim 7\text{\AA}$  of Au are deposited in a laminar fashion and that above this thickness the onset of clustering occurs together with the possibility of Au/In/Ga alloy formation. However, the attenuation of the As3d core level is much slower than that of the In4d and Ga3d core level attenuation, and hence As is again thought to out-diffuse into the metal overlayer. A reacted component was resolved in the evolution of the As3d core level spectra indicating the formation of an Au/As compound. Low temperature Au deposition seems to have little effect on the formation of the Au-In<sub>0.53</sub>Ga<sub>0.47</sub>As(100) interface other than to reduce metal clustering. The initial  $\sim 15\text{\AA}$  of Au are deposited with a layer by layer growth mode with islanding predominating above this thickness. The attenuation of the core level signals implied the out-diffusion of As which was confirmed by the presence of a reacted component in the As3d core level evolution, similar to that observed for Au deposition at room temperature. Hence in the case of the Au-In<sub>0.53</sub>Ga<sub>0.47</sub>As(100) system, low temperature deposition fails to inhibit As out-diffusion into the Au overlayer, but results in an overlayer that is somewhat more laminar in growth to that for room temperature overlayer deposition.

The band bending observed for both room and low temperature Au deposition was negligible, and hence the Schottky barriers formed at both interfaces were deemed "Ohmic". This is in good agreement with I-V measurements of Au diodes formed on "as grown" In<sub>0.53</sub>Ga<sub>0.47</sub>As(100) surfaces [1]. As in the case of In-In<sub>0.53</sub>Ga<sub>0.47</sub>As(100) interface formation, it is observed that interfaces that are perturbed, exhibit low Schottky barriers.

## 6.4 References

- [1] S.A. Clark, S.P. Wilks, A. Kestle, D.I. Westwood and M. Elliott, *Surf. Sci.* **352-354**, 850 (1996).
- [2] W. M. Lau, R. N. S. Sodhi, S. Jin, S. Ingrey, N. Puetz and A. SpringThorpe, *J. Appl. Phys.* **67(2)**, 768-773 (1990).
- [3] R.W. Bernstein, A. Borg, H. Husby, B. -O. Fimland and J.K. Grepstad, *Appl. Surf. Sci.* **56-58**, 74 (1992).
- [4] S.A. Clark, C.J. Dunscombe, D.A. Woolf, S.P. Wilks and R.H. Williams, *J. Vac. Sci. Technol. B* **12(2)** 551 (1994).
- [5] "Practical Surface Analysis, 2<sup>nd</sup> Edition, Volume 1 Auger and x-ray Photoelectron Spectroscopy", edited by D. Briggs and M.P. Seah, John Wiley and Sons (1990).
- [6] J.J. Yeh and I. Lindau, *Atomic Data and Nuclear Tables*, **32**,1 (1985).
- [7] D. Mao, M. Santos, M. Shayegan, A. Khan, G. Le Lay, Y. Hwu, G. Margaritondo, L.T. Flores and J.P. Harbison, *Phys. Rev. B*, **45**, 1273 (1992).
- [8] C.J. Spindt, R. Cao, K. E. Miyano, I. Lindau, W.E. Spicer and Y. -C. Pao, *J. Vac. Sci. Technol. B* **8 (4)**, 974-979 (1990).
- [9] C.J. Spindt, M. Yamada, P.L. Meissner, K.E. Miyano, T. Kendelewicz, A. Herrera-Gomez, W.E. Spicer and A.J. Arko, *Phys. Rev. B*, **45(19)**, 11108-11119 (1992)
- [10] G. Grenet, E. Bergignat, M. Gendry, M. Lapeyrade and G. Hollinger, *Surf. Sci.* **352-354**, 734 (1996).
- [11] R. Ludeke, *Surf. Sci.* **132**, 143-168 (1983).
- [12] S.A. Clark, S.P. Wilks, J. I. Morris, D.A. Woolf and R.H. Williams, *J. Appl. Phys.* **75**, 2481 (1994).
- [13] R. Cao, K.E. Miyano, I. Lindau and W.E. Spicer, *J. Vac. Sci. Technol. A* **8 (4)**, 3460-3465 (1990).
- [14] S. A. Clark, PhD Thesis, University of Wales, College of Cardiff (1995).
- [15] "The Technology and Physics of Molecular Beam Epitaxy", edited by E.H.C Parker, Plenum Press, London and New York, (1985) and references therein.
- [16] C.J. Spindt, M. Yamada, P.L. Meissner, K.E. Miyano, A. Herrera, W.E. Spicer and A.J. Arko, *J. Vac. Sci. Technol. B* **9 (4)**, 2090-2094 (1991).

- [17] L.J. Brillson, M.L. Slade, R.E. Vitturo, M.K. Kelly, W. Pache, G. Margaritondo, J.M. Woodall, P.D. Kirchner, G.D. Petit and S.L. Wright, *J. Vac. Sci. Technol.*, **B4**, 919 (1986).
- [18] F. Xu, Y. Shapira, D.M. Hill and J.H. Weaver, *Phys. Rev. B*, **35(14)**, 7414-7422 (1987).
- [19] W. G. Petro, T Kendelwicz, I. Lindau and W. E. Spicer, *Phys. Rev.* **B34**, 7089 (1986).
- [20] J.J. Joyce, M. Grioni, M. del Giudice, M.W. Ruckman, F. Boscherini and J.H. Weaver, *J. Vac. Sci. Technol.* **A5(4)**, 2019-2023 (1987).
- [21] M. Grioni, J.J. Joyce and J.H. Weaver, *J. Vac. Sci. Technol.* **A4**, 965 (1986).
- [22] P. W. Chye, I. Lindau, P. Pianetta, C. M. Garner, C. Y. Su and W. E. Spicer, *Phys. Rev.* **B18**, 5514 (1978).

# Chapter 7

## Metal- $\text{In}_{0.52}\text{Al}_{0.48}\text{As}(100)$ interfaces formed as a function of temperature

### 7.0 Introduction

Chapter 6 details a spectroscopic and microscopic study of the formation of In- and Au-interfaces with  $\text{In}_{0.53}\text{Ga}_{0.47}\text{As}(100)$  as a function of formation temperature. The motivation for the study was the observation that at a low deposition temperature, In produced Schottky contacts to  $\text{In}_{0.53}\text{Ga}_{0.47}\text{As}(100)$  that exhibited larger barrier heights than the virtually Ohmic barriers observed by conventional metallisation at room temperature.

The lattice matched ternary semiconductor  $\text{In}_{0.52}\text{Al}_{0.48}\text{As}(100)$  is frequently used in conjunction with  $\text{In}_{0.53}\text{Ga}_{0.47}\text{As}(100)$  for a variety of high speed and optoelectronic devices. Whereas  $\text{In}_{0.53}\text{Ga}_{0.47}\text{As}(100)$  diodes conventionally produce low barrier heights and are used for Ohmic contacts, metal contacts to  $\text{In}_{0.52}\text{Al}_{0.48}\text{As}(100)$  produce high barriers in the range 0.6 – 0.9 eV as shown in table 7.1 [1-6], making them ideal for Schottky contacts. This is in part due to the fact that  $\text{In}_{0.52}\text{Al}_{0.48}\text{As}(100)$  has a band gap ( $E_g \sim 1.45$  eV at RT)[7] that is larger than that of  $\text{In}_{0.53}\text{Ga}_{0.47}\text{As}(100)$  ( $E_g \sim 0.75$  eV at RT)[8].

It seems a logical progression to probe the initial stages of interface formation for  $\text{In}_{0.52}\text{Al}_{0.48}\text{As}(100)$  and the metals deposited in chapter 6. As well as information on the adaptation of interfacial reactions for the metal- $\text{In}_{0.52}\text{Al}_{0.48}\text{As}(100)$  system at low temperature, useful information can be gained in the understanding of the variation in barrier heights for metals on  $\text{In}_{0.52}\text{Al}_{0.48}\text{As}(100)$ . The idealised case of atomically clean  $\text{In}_{0.52}\text{Al}_{0.48}\text{As}(100)$  surfaces was again studied, this was achieved by utilising the As capping technique.

### 7.1 Photoemission studies

#### 7.1.1 Introduction

High resolution soft X-ray photoemission spectroscopy was used to study In- and Au- $\text{In}_{0.52}\text{Al}_{0.48}\text{As}(100)$  interfaces formed as a function of temperature using the

Metal	Growth method	Surface preparation	Barrier height (eV)		Ref
			I-V	C-V	
Au	MBE	Etched		0.84	1
Au	“	Intimate	0.82		2
In	“	“	0.91		2
Ag	“	“	0.78		2
Cu	“	“	0.82		2
Au	“	Etched	0.699		3
Al	“	“	0.56		3
Ti/Pt/Au	“	“	0.655		3
Au	MOCVD	“	0.60		4
Al	MBE	Intimate	0.80		5
Pt/Au	“	Etched	0.82		6

Table 7.1: Previously reported Schottky barrier heights measured by current-voltage (I-V) or capacitance-voltage (C-V) techniques, for a variety of metal contacts to n-type  $\text{In}_{0.52}\text{Al}_{0.48}\text{As}(100)$ .

synchrotron radiation source on beamline 4.1 at the Daresbury Laboratory. Details of the experimental apparatus have been discussed in chapter 4. The As3d core level spectra were acquired using photon energies ( $h\nu$ ) of 87 eV and 119 eV in order to attain maximum and somewhat less surface sensitive spectra, respectively. The In4d core level spectra were likewise acquired at  $h\nu = 63$  eV and 119 eV, respectively, and the Al2p core level spectra similarly at  $h\nu = 119$  eV and 147 eV, respectively. The core levels were chosen to exhibit the maximum photo-ionisation cross section for the photon energy used and are shown in table 7.2 below along with other important parameters. During metal deposition, the signal from the Al2p core level became noisy and in the case of Au deposition, completely overwhelmed by the Au5s core level signal. This made it difficult to accurately deconvolve the overall lineshape into individual components. Hence no Al2p spectra have been shown in this thesis. However, the overall intensity has been used for core level attenuation purposes where possible.

	As3d		Al2p		In4d	
$E_B$ (eV)	42		73		18	
$h\nu$ (eV)	87	119	119	147	63	119
KE (eV)	40	72	40	69	40	96
$\lambda$ (Å)	~4	~8	~4	~8	~4	~8
$\sigma$ (Mb)	~5	~7	~5	~4	~17	~1

Table 7.2: A table of useful parameters associated with the photon energies required for examination of the respective core levels studied in this chapter [9,10].

### 7.1.2 Experimental details

The n-type  $\text{In}_{0.52}\text{Al}_{0.48}\text{As}(100)$  samples were grown by MBE and doped with Si to yield a carrier density of  $n \approx 2 \times 10^{18} \text{ cm}^{-3}$ . In order to protect the surface from contamination, the samples were “capped” *in-situ* with a thick layer of amorphous arsenic as described in section 4.1.4. The samples were decapped following the same procedure described in section 6.1.2. Examination of the clean decapped  $\text{In}_{0.52}\text{Al}_{0.48}\text{As}(100)$  surface by LEED revealed a (3×1) surface reconstruction replicating

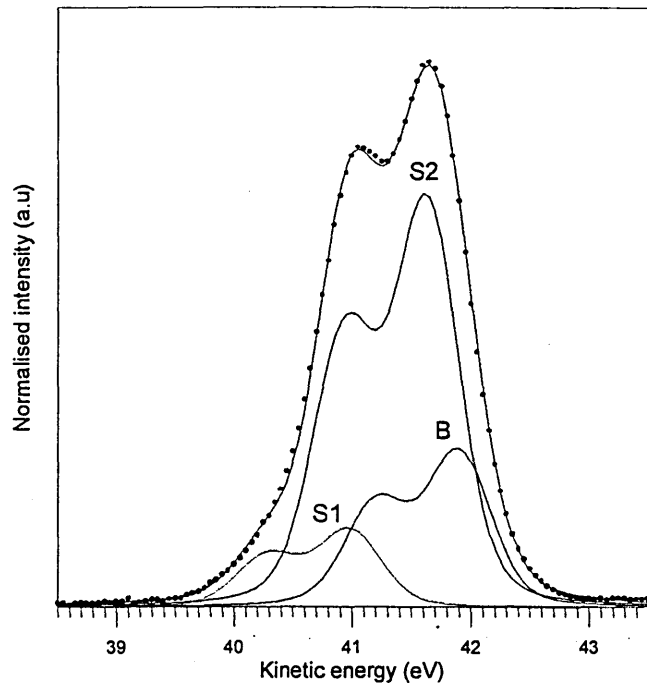
that observed by RHEED following MBE growth. High purity In and Au metal were independently evaporated from thoroughly out-gassed tantalum filaments on to decapped samples held at room temperature ( RT ~ 294K) and low temperature ( LT ~ 125K); the evaporations taking place at a chamber pressure of  $\sim 6 \times 10^{-10}$  mbar. The metals were deposited at a rate of  $0.01 \text{ nms}^{-1}$  as measured by a quartz crystal monitor. For RT and LT samples respectively, a total of 220Å In and 380Å Au were deposited in increments ranging from 0.5Å to 180Å. On production of the clean surface, and following the subsequent depositions, the samples were analysed by SXPS.

### 7.1.3 The clean (3 × 1) reconstructed $\text{In}_{0.52}\text{Al}_{0.48}\text{As}(100)$ surface

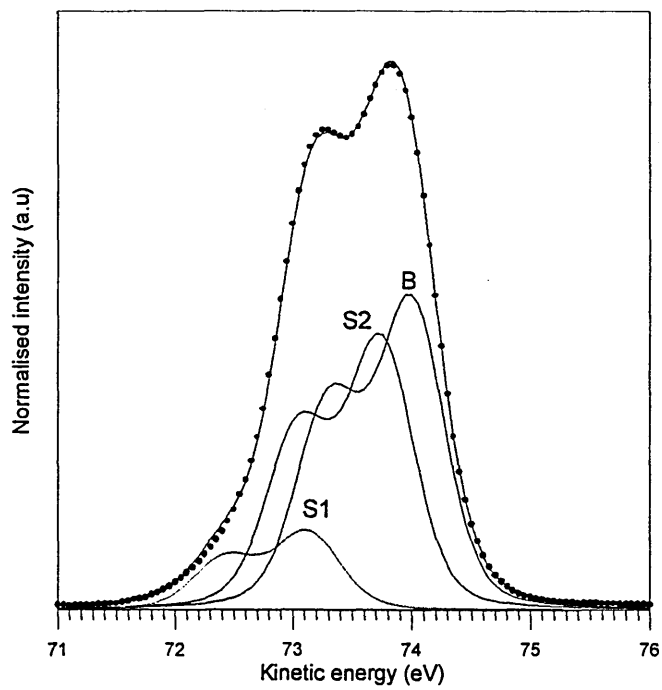
The As3d and In4d photoemission spectra for a clean (3×1) reconstructed  $\text{In}_{0.52}\text{Al}_{0.48}\text{As}(100)$  surface are shown in figures 7.1 and 7.2 respectively. The As3d and In4d core levels were fitted using the curve fitting routine described in chapter 3. An appropriate background was subtracted from all core level spectra, and the peak intensities were normalised to unity in order to distinguish changes in core level lineshape. The fixed parameter values for core level emission from the clean surface are shown in table 7.3, and the aim throughout the fitting procedure was to use the minimum number of components to produce a good fit. The peak intensity, peak positions and gaussian were allowed to vary for the clean surface.

Core level	Lorentzian FWHM (eV)	Spin Orbit Splitting (eV)	Relative Intensity of Spin Orbit Split
As3d	0.170	0.695	0.670
Al2p	0.100	0.400	0.500
In4d	0.250	0.870	0.670

Table 7.3: Table of fixed parameters used to fit the core level spectra obtained from clean (3×1) reconstructed  $\text{In}_{0.52}\text{Al}_{0.48}\text{As}(100)$  [11-14].



(a)



(b)

Figure 7.1: As3d core level spectra from the clean (3×1) reconstructed  $\text{In}_{0.52}\text{Al}_{0.48}\text{As}(100)$  surface. The spectra were obtained using a photon energy of (a) 87 eV and (b) 119 eV.

(i) *As3d core level spectra*

The surface sensitive As3d core-level spectrum from the clean, (3×1) reconstructed  $\text{In}_{0.52}\text{Al}_{0.48}\text{As}(100)$  surface is shown in Figure 7.1(a). Three components were necessary to fit the observed lineshape; these are marked S1, S2 and B and are separated by  $\Delta E_k = 0.92$  eV (S1-B) and  $\Delta E_k = 0.27$  eV (S2-B). Comparison of this surface sensitive spectrum ( $\lambda \sim 4\text{\AA}$ ) with similar though somewhat less surface sensitive emission obtained at  $h\nu = 119$  eV ( $\lambda \sim 8\text{\AA}$ ) as shown in figure 7.1(b), indicates that component B, which increases at reduced surface sensitivity, originates from As in the bulk  $\text{In}_{0.52}\text{Al}_{0.48}\text{As}(100)$ . As in the case of the  $\text{In}_{0.53}\text{Ga}_{0.47}\text{As}(100)$  clean surface described in section 6.1.3, S1 and S2 are thought to be derived from states on or near to the semiconductor surface. XPS studies of As decapping of  $\text{In}_{0.52}\text{Al}_{0.48}\text{As}(100)$  surfaces have shown that the (3×1) reconstructed As-stabilised surface consists of an InAs-rich surface layer with a subsurface AlAs-rich layer over stoichiometric bulk  $\text{In}_{0.52}\text{Al}_{0.48}\text{As}(100)$  [15]. Comparison of the surface sensitive As3d spectra in figure 7.1(a) indicates that component S2 is a consequence of emission from predominantly In-bonded As sites at the surface and that S1 relates to predominantly Al-bonded As sites in the subsurface region.

(ii) *In4d core level spectra*

The In4d core level spectra from the clean  $\text{In}_{0.52}\text{Al}_{0.48}\text{As}(100)$  surface obtained at photon energies of  $h\nu = 63$  eV and 119 eV are shown in figure 7.2(a) and (b) respectively. The experimental lineshapes have been accurately fitted with two components S and B. Similar components have been reported by Grenet *et al.* in XPS studies of clean  $\text{In}_{0.52}\text{Al}_{0.48}\text{As}(100)$  surfaces [16] and were also observed in the In4d lineshape on clean  $\text{In}_{0.53}\text{Ga}_{0.47}\text{As}(100)$  described in section 6.13. The component S corresponded to emission from an InAs surface layer and B was attributed to In in the bulk. This InAs layer was thought to result from the surface segregation of In during MBE growth of As-stabilised  $\text{In}_{0.52}\text{Al}_{0.48}\text{As}/\text{InP}(100)$ .

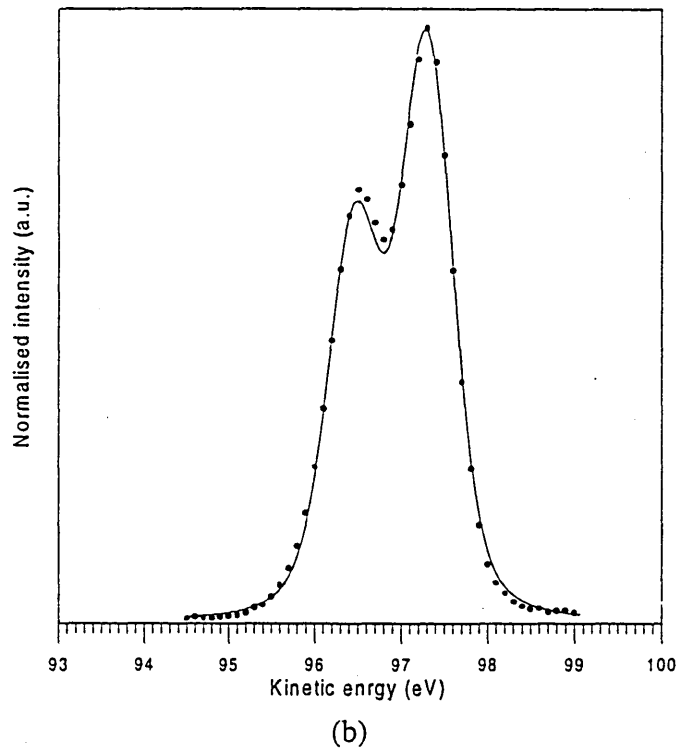
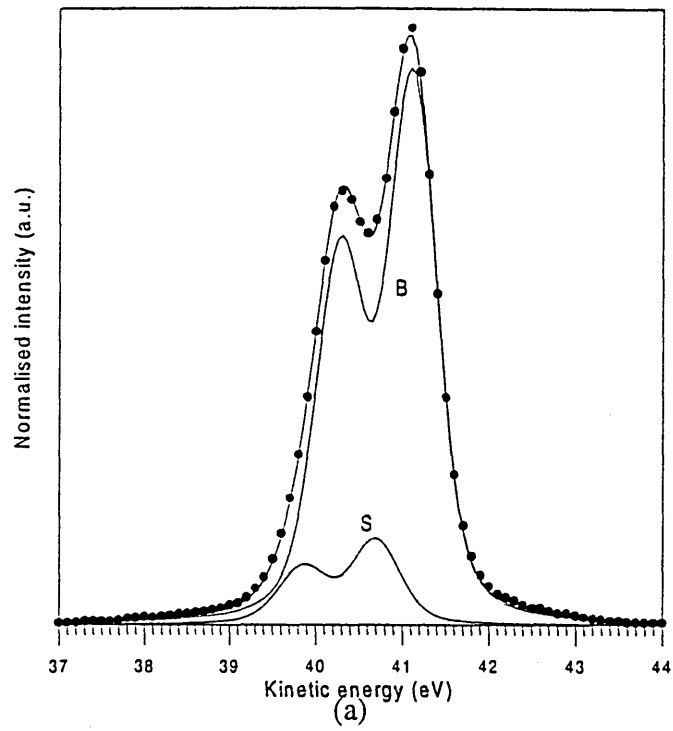


Figure 7.2: In4d core level spectra from the clean (3×1) reconstructed  $\text{In}_{0.52}\text{Al}_{0.48}\text{As}(100)$  surface. The spectra were obtained using a photon energy of (a) 63 eV and (b) 119 eV.

The clean (3×1) reconstructed  $\text{In}_{0.52}\text{Al}_{0.48}\text{As}(100)$  surface has been characterised using soft X-ray photoemission spectroscopy. Examination of the As3d and In4d core levels indicate a surface that is InAs rich due to the surface segregation of In during growth.

Once more it should be noted that slight variations in decapping temperature might alter the relative magnitude of the individual components in the clean surface spectra for the following experiments.

#### 7.1.4 In- $\text{In}_{0.52}\text{Al}_{0.48}\text{As}(100)$ interface formation

##### (i) *Substrate core level attenuation*

In figure 7.3 the normalised integrated emission intensities from the As3d and Al2p core levels are presented as a function of In overlayer thickness deposited at room and low temperatures. For room temperature deposition, deviation from an exponential attenuation ( $e^{-x/\lambda}$ ) for both core levels occurs after the first  $\sim 3\text{\AA}$  of In has been deposited. Using a least squares fit in the region 0-3 $\text{\AA}$ , the attenuation length of electrons travelling through the metal overlayer is calculated to be  $\sim 5\text{\AA}$ , indicative of an initial layer by layer followed by islanding mode of growth. These results tend to concur with the findings of Mao *et al.* who studied the In-GaAs(100) interface with XPS [12] rather than those of Spindt *et al.* where competition between chemisorption and clustering occurred during the formation of similar interfaces [13]. In direct contrast however, XPS studies of In-  $\text{In}_{0.52}\text{Al}_{0.48}\text{As}(100)$  interfaces by Clark *et al.* have reported a much steeper attenuation of the Al signal compared to that of the As signal. The reduced As attenuation was linked to the apparent out-diffusion of As into the metal overlayer, and its subsequent accumulation on the metal surface [17]. It appears that this is not the case here as both the As and Al core level intensities attenuate at similar rates.

Comparison of the attenuation of the core levels as a function of low temperature In deposition indicates a similar mode of growth to that observed at room temperature. On this occasion the attenuation deviates from an exponential after  $\sim 5\text{\AA}$  of In has been deposited, a line of best fit in this region showing  $\lambda \sim 4\text{\AA}$ . After 5 $\text{\AA}$  of In deposition at low temperature, the gradient of the core level intensities is steeper than

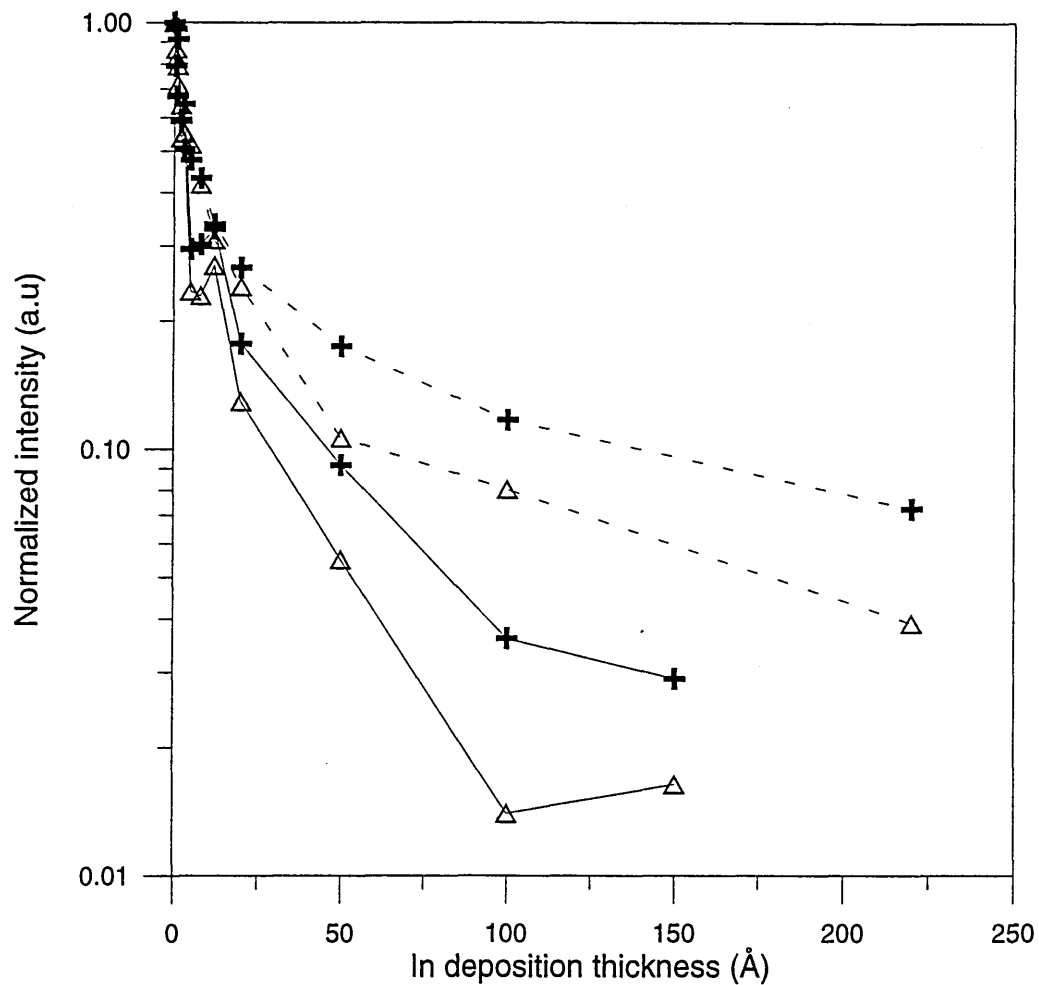


Figure 7.3: Core level emission intensity ( $I/I_0$ ) from the As3d and Al2p core levels, plotted as a function of In coverage on decapped  $\text{In}_{0.52}\text{Al}_{0.48}\text{As}(100)$ , obtained at an excitation energy of 87 eV. The dashed lines denote In deposition at 294K(RT), the full lines denote In deposition at 125K(LT). The crosses denote emission from the Al2p core level and the open triangles denote emission from the As3d core level.

for room temperature deposition. This is similar to the case of low temperature In deposition on  $\text{In}_{0.53}\text{Ga}_{0.47}\text{As}(100)$  described in section 6.1.4, and is likewise attributed to reduced In clustering and a reduced grain size at low temperature. However, it may be possible that the discrepancies between the core level intensities at room and low temperature are a consequence of the onset of interfacial interactions between the semiconductor and the overlayer, such as diffusion of In into the  $\text{In}_{0.52}\text{Al}_{0.48}\text{As}(100)$  to form an Al/In alloy or an In/As phase. It is highly likely therefore, that these reactions may occur more readily at room temperature, resulting in a slower attenuation of the core level signals.

(ii) *In overlayer growth*

As Indium is again a substrate species and the overlayer, the core level signal will have contributions from both the substrate and the overlayer. An expression for the total In core level intensity as a function of overlayer thickness is given by equation 6.4. The left hand side of the equation is plotted against overlayer thickness in figure 7.4, and it is evident that for both room and low temperature deposition there is a degree of exponential decay up to  $\sim 5\text{\AA}$  of In. Above this overlayer thickness, deviation from the exponential occurs, indicating a layer by layer followed by clustering mode of growth for both temperature depositions. This is in good agreement with the results obtained from the attenuation of the As3d and Al2p core levels.

(iii) *As3d core level emission*

Figure 7.5 outlines the evolution of the As3d core level lineshape as a function of In overlayer deposition at low temperature. The individual spectra are curve fitted using the parameters mentioned in section 7.1.3. For the clean surface, three components S1, S2 and B, similar to those mentioned in section 7.1.3, were necessary to accurately fit the experimental lineshape. The clean surface spectrum prior to cooling the sample to 125K was identical to that after the sample had been cooled.

As the In overlayer increases, all three components attenuate at similar rates and there is no change in the respective energy positions of the three components. However the three peaks simultaneously shift to higher kinetic energy during In deposition, indicating band bending and will be discussed later in this chapter. No reacted

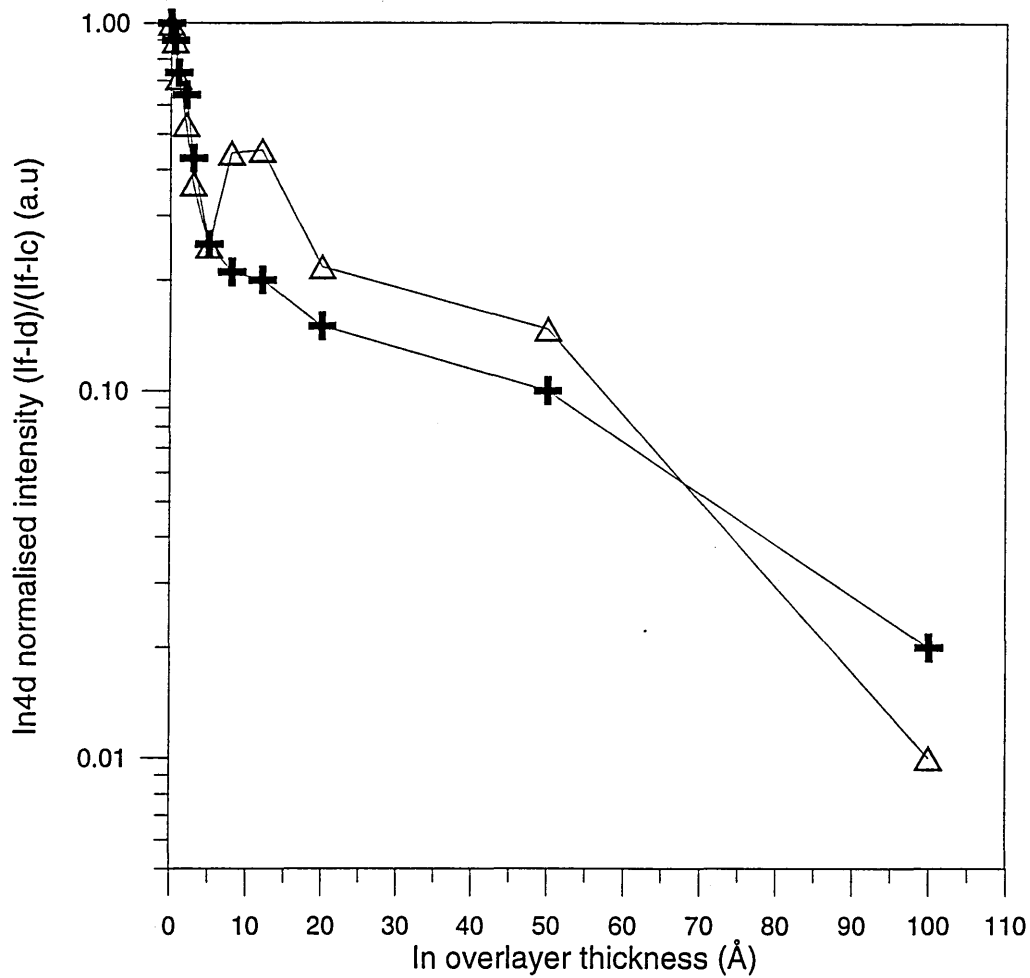


Figure 7.4: In4d core level emission intensity ( $I_f - I_d / I_f - I_c$ ), plotted as a function of In coverage on decapped  $\text{In}_{0.52}\text{Al}_{0.48}\text{As}(100)$ , obtained at an excitation energy of 63 eV. The crosses denote In deposition at 125K(LT) and the open triangles denote In deposition at 294K(RT).

components were resolved and this tends to suggest that the interface is not perturbed, and that it is relatively abrupt. This concurs with the results observed for In on  $\text{In}_{0.53}\text{Ga}_{0.47}\text{As}(100)$  described in Chapter 6, where low temperature In deposition restricted As out-diffusion to produce an abrupt interface. The evidence of an As3d signal at 50Å of In indicates that the In clusters have not coalesced into a continuous film of metallic In by this stage. However after 150Å of In has been deposited, hardly any signal is evident from the As3d core level and it is believed that at this point the In overlayer is of a metallic nature.

The evolution of the As3d core level lineshape for room temperature In deposition is shown in figure 7.6. The clean surface is again accounted for by three components S1, S2 and B, corresponding to those mentioned in section 7.13. There is a small difference in the relative intensities of the S1, S2 and B components, in comparison with the low temperature scans. Although the surface reconstructions observed were identical, these discrepancies are believed to be related to small inequalities in the decapping procedure. In the early stages of In deposition, the component S1 related to Al bonded As sites attenuates quite rapidly along with the bulk component. After 20Å of In has been deposited, only the component S2 related to In bonded As sites remains. In the previous chapter, room temperature deposition of In on  $\text{In}_{0.53}\text{Ga}_{0.47}\text{As}(100)$  resulted in As out-diffusing into the metal overlayer to form InAs. This does not appear to be the case here however, as at high In coverages (~ 100Å) there is relatively little signal from the As3d core level, and the attenuation of the As signal is comparable to that of Al. One interpretation of this could be that a signal from the component S2 is still evident from regions of the InAs rich surface which have been left virtually exposed in areas where clustering has left relatively little metal coverage. However in the low temperature case, where the attenuation of the core level signals suggest clustering is slightly less pronounced, all three components are evident at 20Å In.

In studies of Al/GaAs interfaces it has been observed that an AlAs interfacial layer is formed as the Al is deposited. This AlAs layer subsequently provides a barrier to the formation of additional AlAs by restricting the out-diffusion of As [18]. It is possible that a similar effect is being seen here, whereby the subsurface AlAs rich layer limits the out-diffusion to that of As already in the InAs rich surface layer. It may be the case therefore that at room temperature there is a limited amount of As out-diffusion, which contributes to the As3d signal. Furthermore, the bond energies of In-As, Ga-As

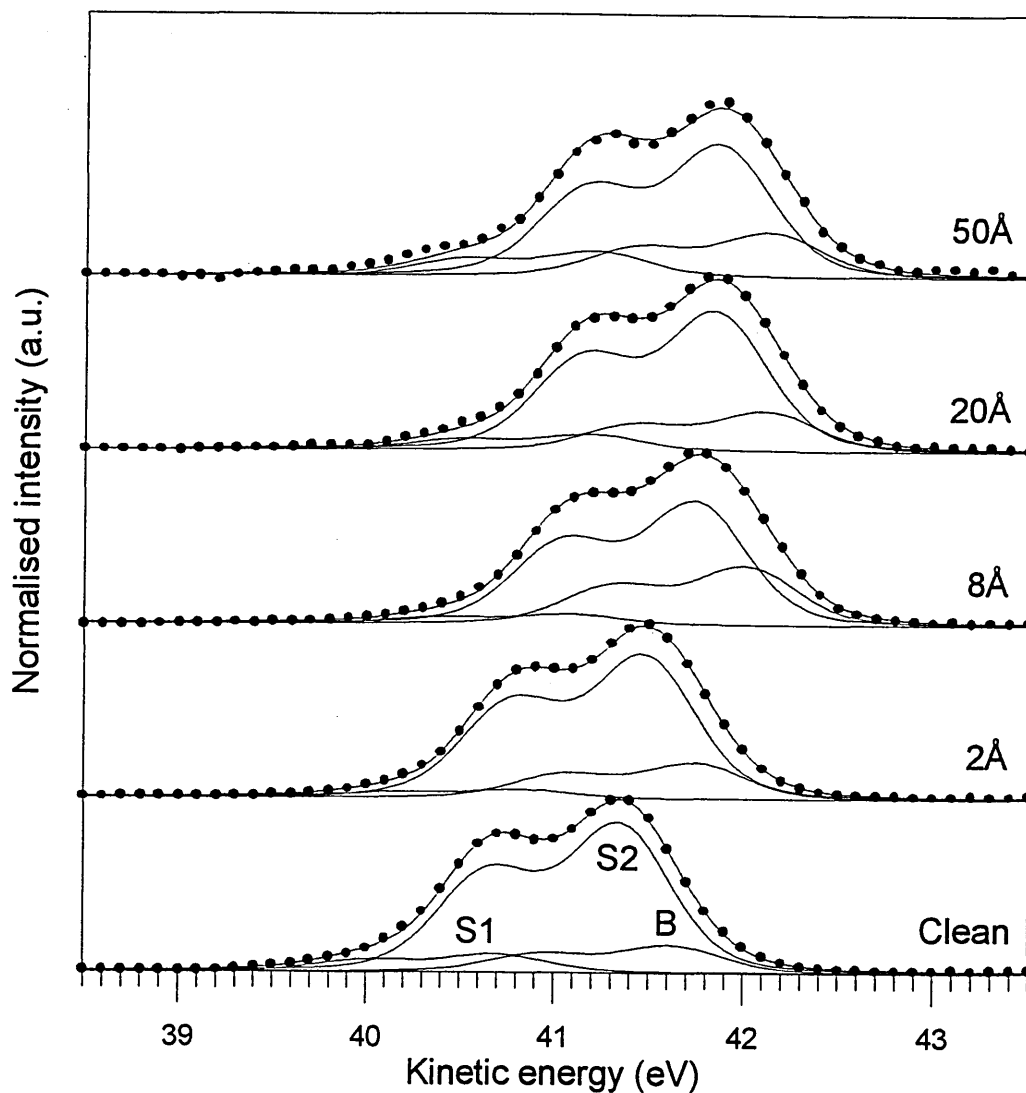


Figure 7.5: Evolution of the As3d core level spectra ( $h\nu = 87$  eV), with increasing In coverage on decapped  $(3 \times 1)$  reconstructed  $\text{In}_{0.52}\text{Al}_{0.48}\text{As}(100)$ , deposited at 125K (LT). The peaks have been synthesised with three components, S1, S2 and B, shown along with the overall fit as continuous lines.

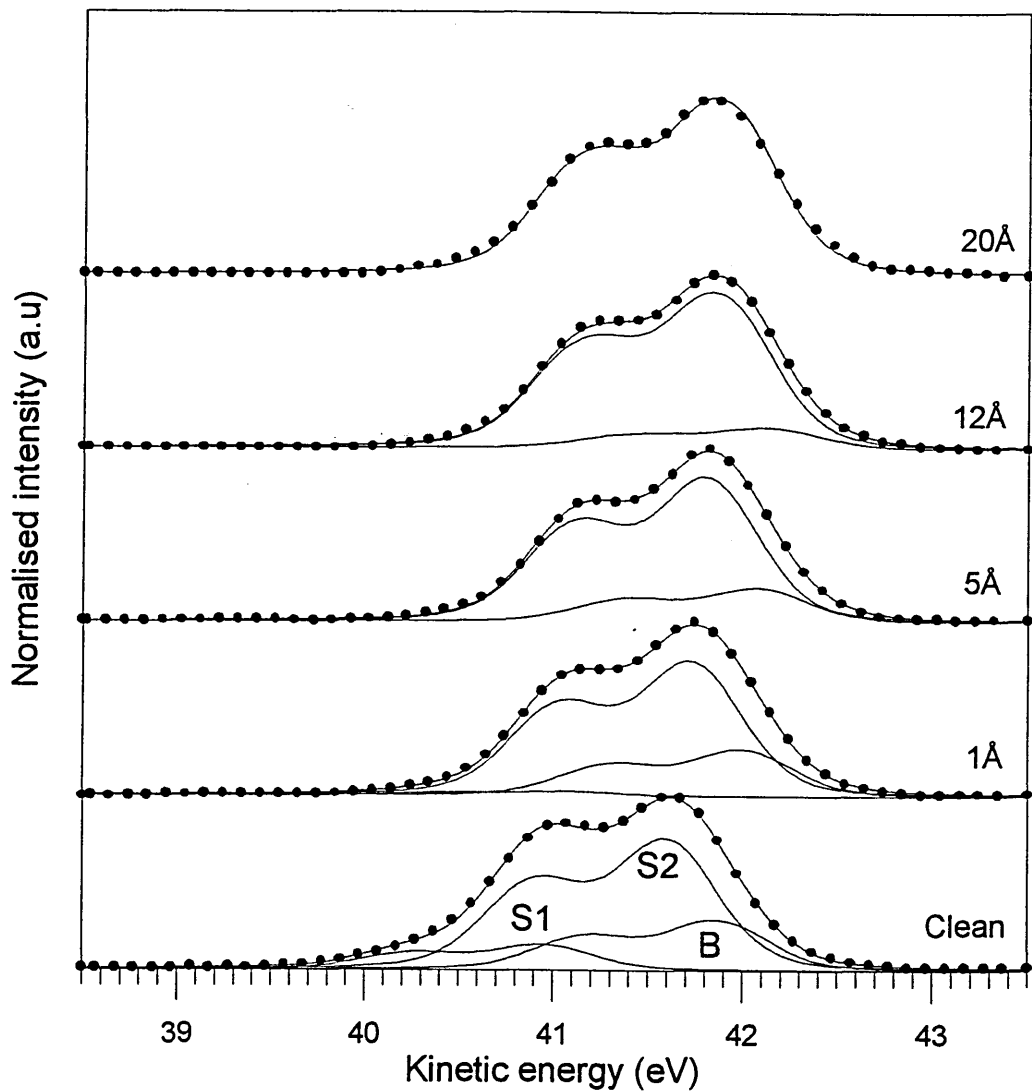


Figure 7.6: Evolution of the As3d core level spectra ( $h\nu = 87$  eV), with increasing In coverage on decapped  $(3\times 1)$  reconstructed  $\text{In}_{0.52}\text{Al}_{0.48}\text{As}(100)$ , deposited at 294K (RT). The peaks have been synthesised with three components, S1, S2 and B, shown along with the overall fit as continuous lines.

and Al-As are 1.41 eV, 1.59 eV and 1.98 eV respectively (see table 6.3). The energy difference between Ga-As and In-As bonds is therefore much smaller than between Al-As and In-As and hence one would expect As out-diffusion from the bulk of the material to be more likely for In deposition on the  $\text{In}_{0.53}\text{Ga}_{0.47}\text{As}(100)$  system than the  $\text{In}_{0.52}\text{Al}_{0.48}\text{As}(100)$  materials system.

The lack of significant interface diffusion or additional chemical reactions between substrate and overlayer species at either room or low temperature interface formation indicate that the In- $\text{In}_{0.52}\text{Al}_{0.48}\text{As}(100)$  interface is relatively abrupt.

(iv) *In4d core level emission*

Figures 7.7 and 7.8 detail the change in shape of the In4d core level emission as a function of increasing In overlayer thickness at low temperature and room temperature respectively. The spectra were obtained using a photon energy of  $h\nu = 63$  eV.

For the case of low temperature deposition (figure 7.7), the clean surface is fitted with a surface component S and a bulk component B similar to those described in section 7.1.3. In the early stages of In deposition a third component S2 appears to higher kinetic energy than the bulk component B; this new component has a similar lineshape to that of components S and B. With increasing In overlayer thickness, the intensity of S2 increases accompanied by a narrowing of its lineshape and components S and B are attenuated. There is a shift to higher kinetic energy of all three components. At the highest In coverages, S2 completely dominates the In4d lineshape, and a degree of asymmetry is evident. These observations are similar to those mentioned in chapter 6 for low temperature In deposition on  $\text{In}_{0.53}\text{Ga}_{0.47}\text{As}$  where the low deposition temperature produced a metallic overlayer with smaller grain sizes than at room temperature.

In a photoemission study of In on GaAs(110) by Cao *et al.*, low temperature In deposition resulted in a slow shift of the In4d peak to higher kinetic energy accompanied by a narrowing of the linewidth with increasing In coverage. This shift was associated with the transition of emission from isolated In atoms on the surface to emission from bulk metal, which is consistent with the evolution from very small clusters to larger ones [13,19]. It has been suggested that low temperature deposition reduces the surface mobility of the In atoms thus reducing clustering. It is therefore possible that in the early stages of deposition the component S2 originates from In

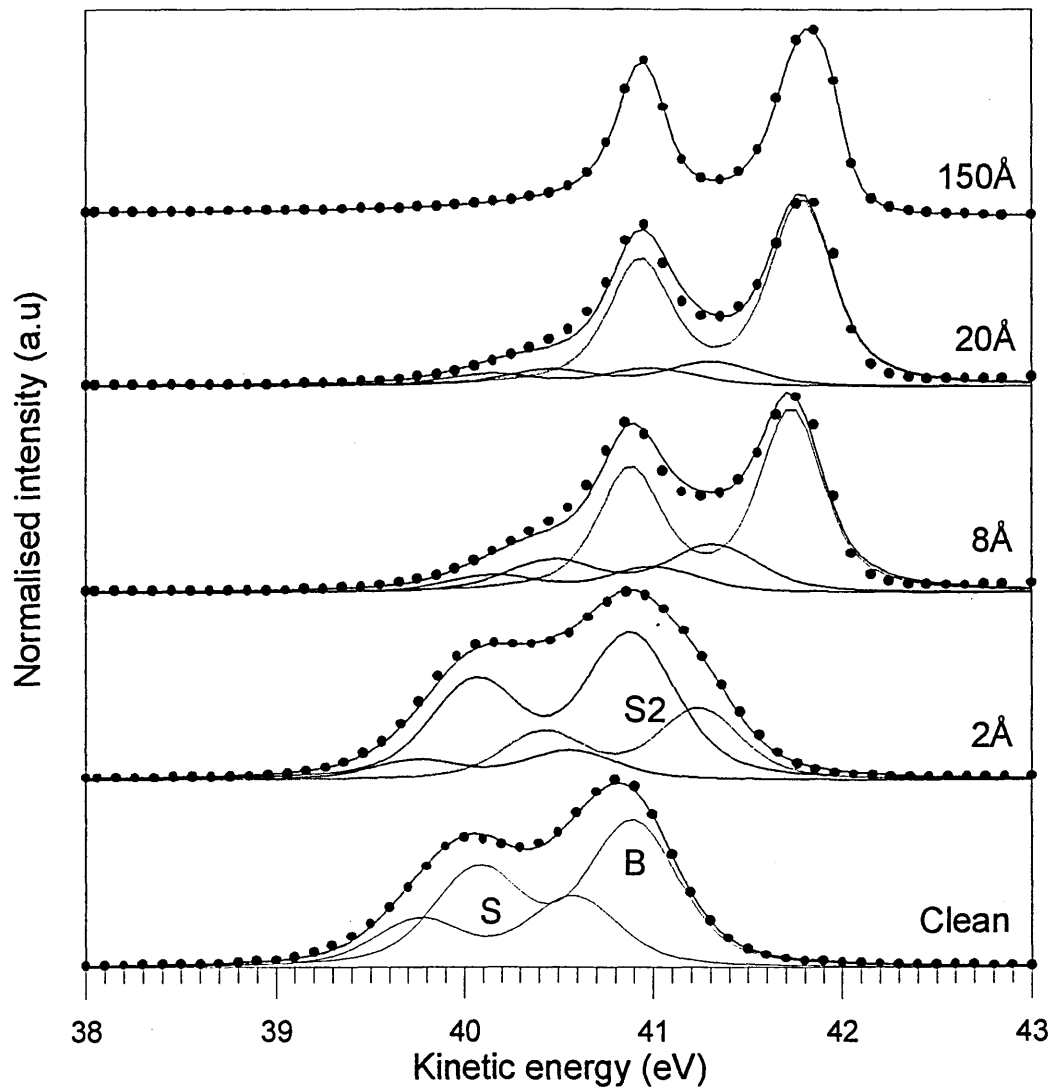


Figure 7.7: Evolution of the In<sub>4d</sub> core level spectra ( $h\nu = 63$  eV), with increasing In coverage on decapped (3×1) reconstructed In<sub>0.52</sub>Al<sub>0.48</sub>As(100), deposited at 125K (LT).

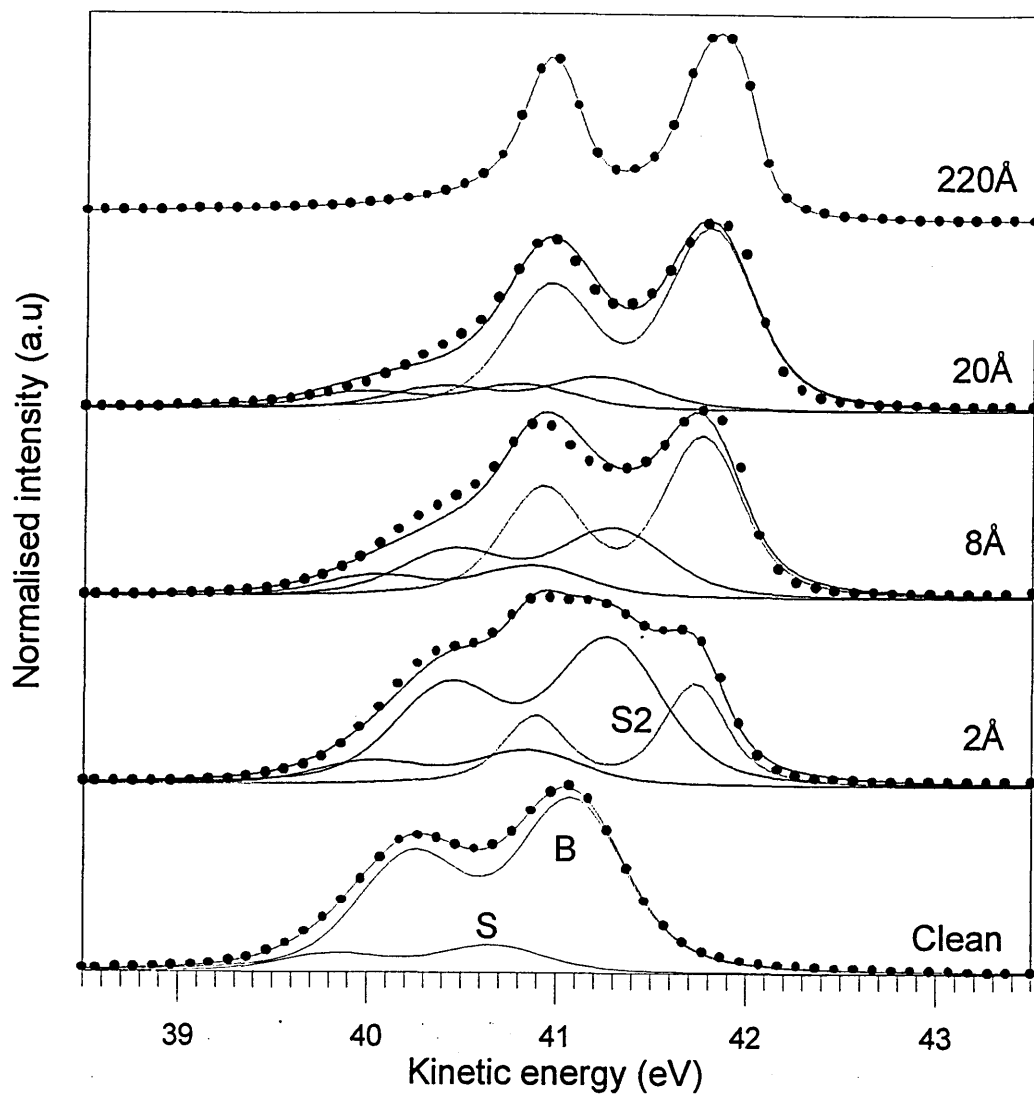


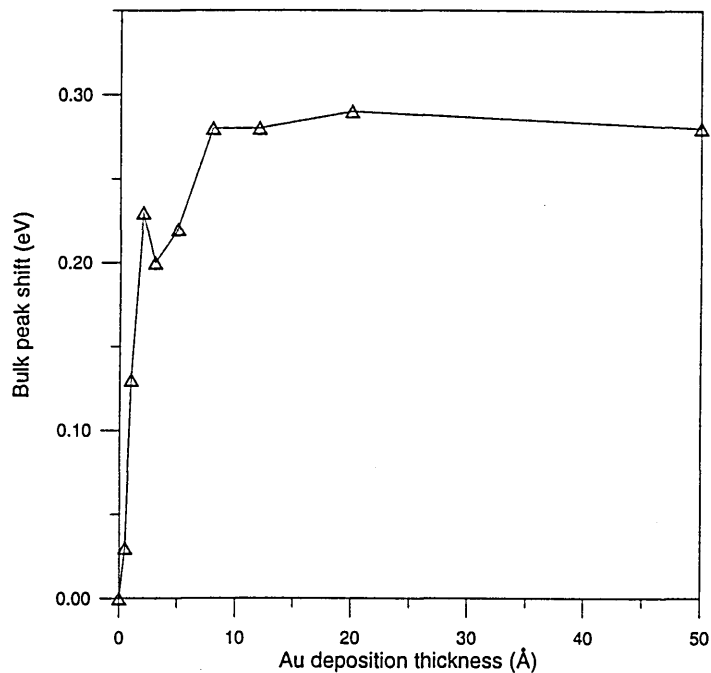
Figure 7.8: Evolution of the In4d core level spectra ( $h\nu = 63$  eV), with increasing In coverage on decapped  $(3 \times 1)$  reconstructed  $\text{In}_{0.52}\text{Al}_{0.48}\text{As}(100)$ , deposited at 294K (RT).

atoms which are likely to be isolated on the surface of the semiconductor. As the overlayer grows, the In atoms will begin to coalesce, producing a more metallic overlayer and hence emission with a narrower linewidth.

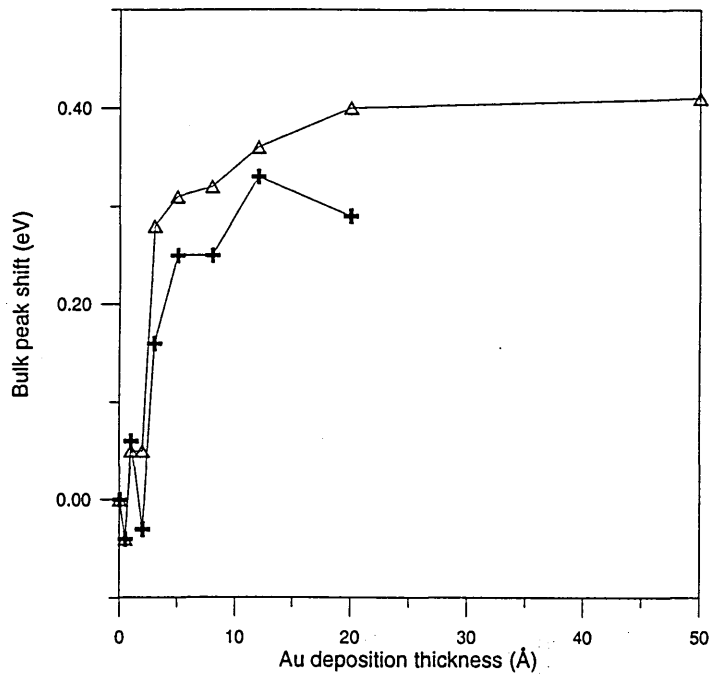
Room temperature deposition of In (figure 7.8) produces a slightly different evolution of the In4d lineshape. The clean surface is again fitted with two components S and B. Comparison with the low temperature clean surface (figure 7.7) indicates that the In/As related surface component S is smaller for the room temperature experiment, in concurrence with emission from the As3d core levels. As In is deposited, a component S2 similar to that observed at low temperature arises. However, the lineshape of this component is much narrower than at the corresponding overlayer thickness for low temperature deposition. Referring to the attenuation of the Al and As signals in figure 7.3, it is apparent that laminar growth occurs for the first few monolayers ( $\sim 5\text{\AA}$ ) of In growth at room temperature. It is likely then that this narrow lineshape is due to metallic emission indicative of a laminar growth mode where the In atoms arrange themselves in a more ordered array on the surface of the semiconductor. As in the low temperature case, the component S2 increases with a corresponding decrease in the components S and B as the In overlayer develops: there is no significant change in the lineshape of S2. At high In coverages, the experimental lineshape is once more accounted for solely by S2 and shows a degree of asymmetry.

(v) *Band bending*

The band bending induced when a metal and semiconductor come into contact can be determined from the rigid shift of the bulk derived core level components. The effect of surface photovoltages has been negated by using highly doped ( $n^+$ ) $\text{In}_{0.52}\text{Al}_{0.48}\text{As}$  samples. The change in the bulk As3d peak position as a function of In overlayer coverage is shown for room temperature and low temperature deposition in figure 7.9(a) and (b). Room temperature deposition of In produces a shift in the bulk As3d peak of  $(0.3 \pm 0.1)$  eV. The position of the Fermi level was determined from the Fermi edge of a thick gold layer deposited “*in-situ*”, on to a tantalum spade in electrical contact with the sample, prior to the experiment. Using a photon energy of 87 eV the Fermi level was located at 82.77 eV, whilst the valence band maximum for the clean  $\text{In}_{0.52}\text{Al}_{0.48}\text{As}(100)$  surface obtained at 87 eV was situated at 81.9 eV. The valence band maximum was therefore positioned 0.87 eV below the Fermi level of the system,



(a)



(b)

Figure 7.9: A plot of the band bending observed for the In-In<sub>0.52</sub>Al<sub>0.48</sub>As(100) interface as a function of increasing In coverage at (a) 294K(RT) and (b) 125K(LT). The band bending is determined from the relative binding energy shift in the As3d core level bulk component (denoted as open triangles) and Al2p core level bulk component (crosses).

indicating that the conduction band minimum is situated 0.58 eV above the Fermi level for clean  $\text{In}_{0.52}\text{Al}_{0.48}\text{As}(100)$  with a band gap of 1.45 eV. Hence the additional band bending at the surface of 0.3 eV produces a barrier height,  $\phi_b$ , obtained by SXPS of  $\sim 0.88 \pm 0.1$  eV for the room temperature In- $\text{In}_{0.52}\text{Al}_{0.48}\text{As}(100)$  interface. This result is in good agreement with barrier heights observed for intimate In- $\text{In}_{0.52}\text{Al}_{0.48}\text{As}(100)$  diodes measured by the I-V technique as shown in table 7.1 [2]. Low temperature deposition produces band bending of  $\sim 0.4 \pm 0.1$  eV. Following the same procedure as above, the conduction band was found to be 0.36 eV above the Fermi level. The barrier height obtained by SXPS for low temperature In- $\text{In}_{0.52}\text{Al}_{0.48}\text{As}(100)$  formation was therefore  $\sim 0.76 \pm 0.1$  eV. It is highly likely that in both deposition cases band bending occurs at the clean  $\text{In}_{0.52}\text{Al}_{0.48}\text{As}(100)$  surface following one or more of the models described in chapter 2 and that metal deposition adapts this pinning position further.

(vi) *Valence band emission*

The evolution of the emission from the valence band as a consequence of In deposition is presented in figures 7.10 (a) and (b) for room and low temperature In deposition respectively. Ultimately the stack plots show a similar trend in evolution for both deposition cases with a transition from states observed on the clean  $\text{In}_{0.52}\text{Al}_{0.48}\text{As}(100)$  surface to emission from the Fermi edge of a metallic overlayer. However at low temperature, there is a more pronounced Fermi edge at high In coverages.

The distribution of states at the Fermi level can be described by Fermi-Dirac statistics [20]. At absolute zero this distribution is a step function. At higher temperatures however, the range of energies of the levels occupied by electrons becomes wider producing a smoother less abrupt transition. It is highly likely therefore that the more pronounced nature of the Fermi edge at low temperature is a direct consequence of the reduction in substrate temperature.

Both stack plots tend to suggest a similar interface is formed for In on  $\text{In}_{0.52}\text{Al}_{0.48}\text{As}(100)$  regardless of the formation temperature.

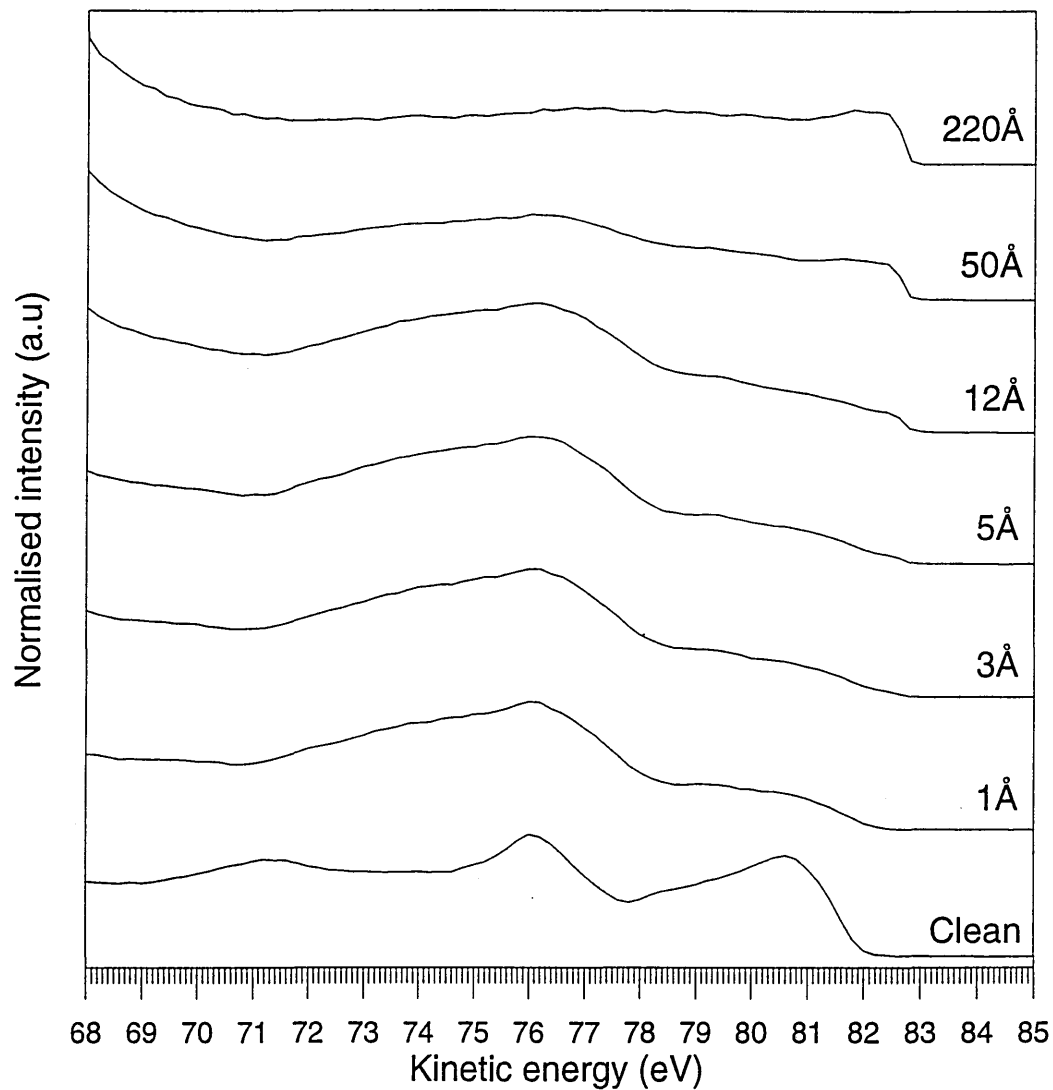


Figure 7.10a: A stack plot of the valence band spectra as a function of increasing In overlayer coverage deposited at 294K(RT). The spectra were obtained using a photon energy of,  $h\nu = 87$  eV.

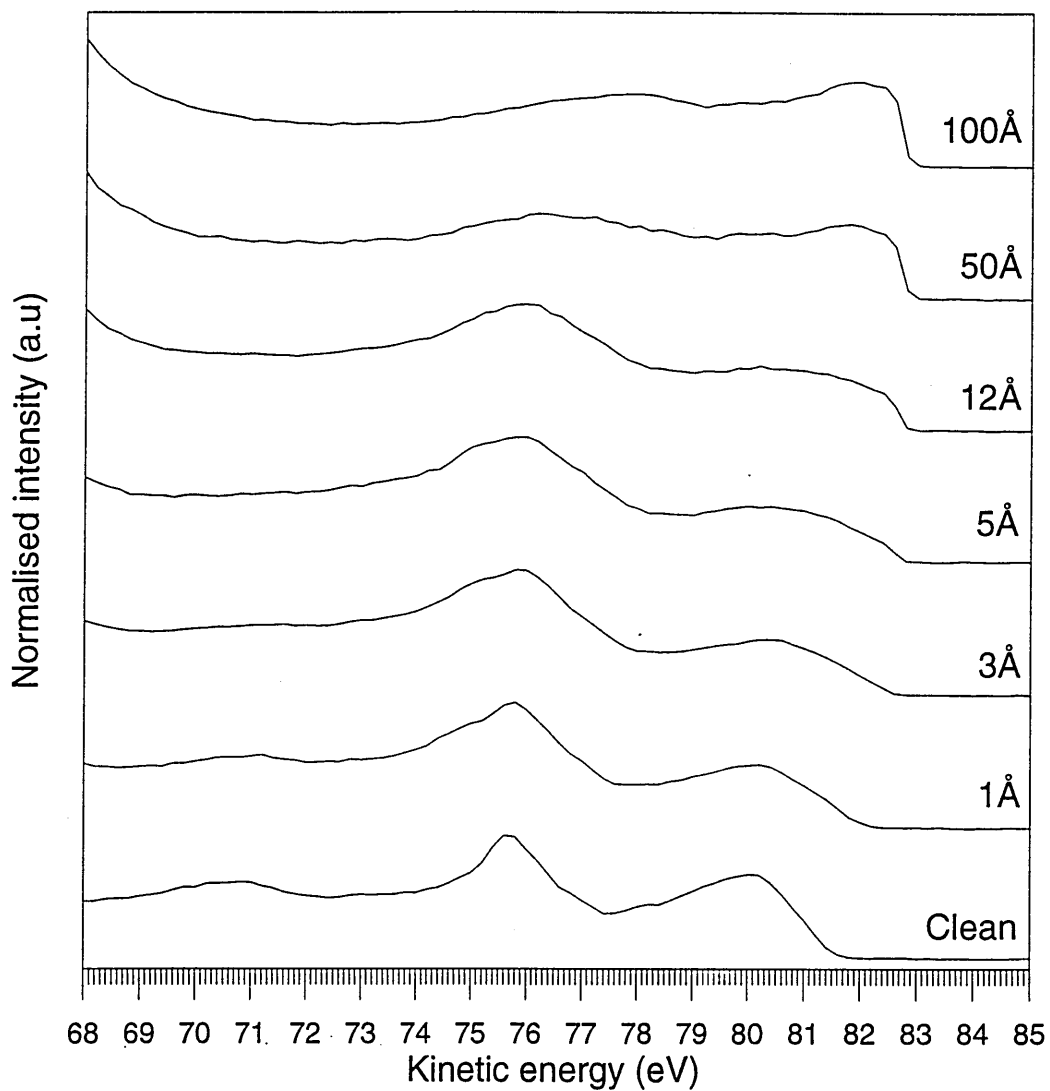


Figure 7.10b: A stack plot of the valence band spectra as a function of increasing In overlayer coverage deposited at 125K(LT). The spectra were obtained using a photon energy of,  $h\nu = 87$  eV.

### 7.1.5 Au-In<sub>0.52</sub>Al<sub>0.48</sub>As(100) interface formation

#### (i) Substrate core level attenuation

The normalised integrated emission intensities from the As3d, Al2p and In4d core levels are presented in figure 7.11 as a function of Au overlayer thickness deposited at room temperature. The Al2p and In4d signals deviate from an exponential attenuation after the first monolayer (~ 3-4Å) Au has been deposited, indicating that there is a degree of three-dimensional growth after the initial Au monolayer is deposited. Comparison of the Al2p core level attenuation at Au coverages greater than 4Å with the attenuation of the Al2p core level for similar In coverages (figure 7.3) shows an increased attenuation for Au deposition. It is deduced therefore that the extent of overlayer clustering is much more profound for In deposition than for Au deposition.

As observed in the previous chapter for Au-In<sub>0.53</sub>Ga<sub>0.47</sub>As(100) interfaces, the As3d core level signal exhibits a much reduced attenuation than the corresponding core level signals, and at large Au coverages has only reduced to 25% of the clean surface value. Similar behaviour has been reported by Clark *et al.* in XPS studies of intimate Au-In<sub>0.52</sub>Al<sub>0.48</sub>As(100) interfaces and was linked to the out-diffusion of As from the substrate to surface segregate on the Au overlayer [17]. Comparisons with the results presented in section 6.1.5 for Au-In<sub>0.53</sub>Ga<sub>0.47</sub>As(100) interfaces and work carried out by Bauer *et al.* on Au-AlAs(100) interfaces [21] further imply that As out-diffuses from the In<sub>0.52</sub>Al<sub>0.48</sub>As(100) into the Au overlayer to either segregate on the metal surface or form an Au/As compound.

The attenuation of the core levels as a function of low temperature Au deposition (figure 7.12) shows a strikingly similar mode of growth to that observed at room temperature. Deviation from an exponential attenuation of the Al2p and In4d core level intensities again occurs after about the first monolayer of Au is deposited, indicating a layer by layer followed by clustering mode of growth. As out diffusion is also evident with ~25% of the signal still observed at high Au coverages. Comparison of the Al2p and As3d core level attenuation at both room and low temperature (figure 7.13), indicates no significant deviation in the extent of either metal clustering or As out-diffusion for low temperature Au deposition compared to room temperature Au deposition.

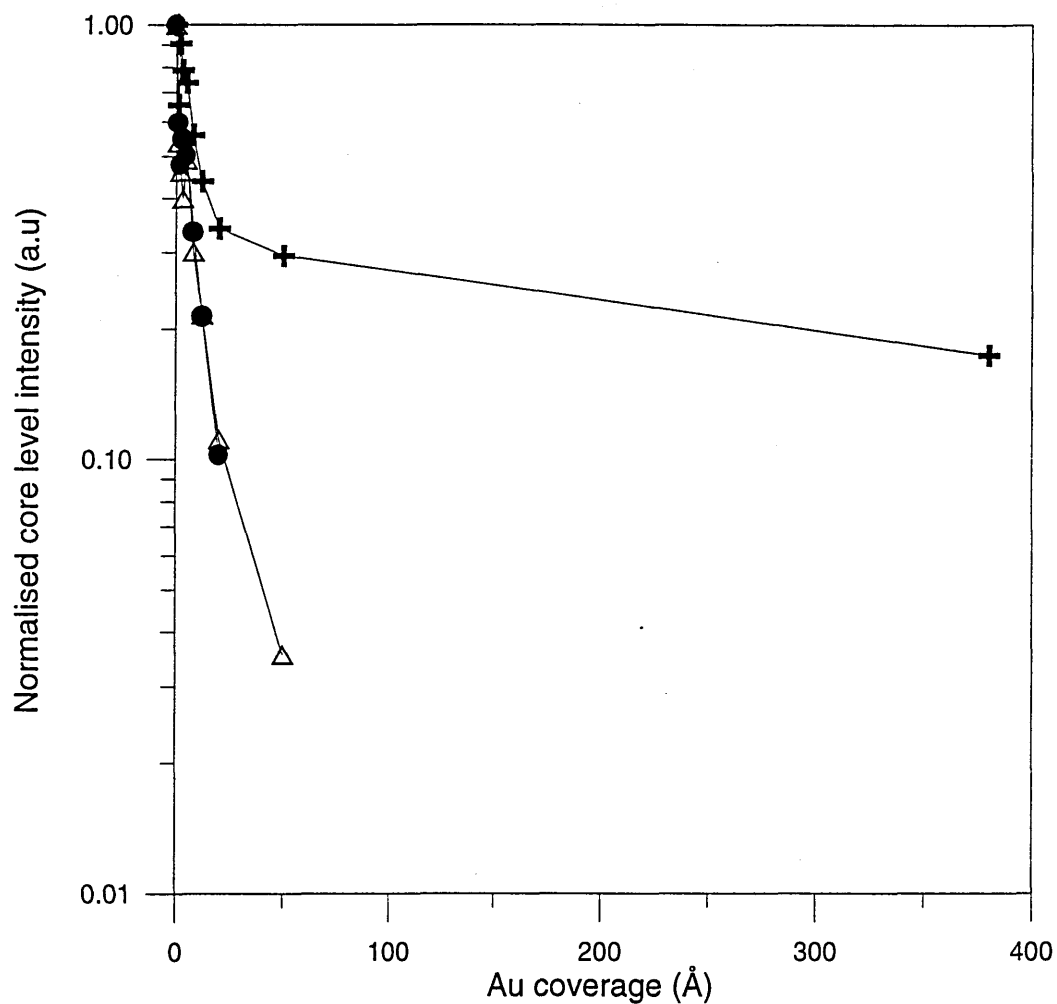


Figure 7.11: Core level emission intensity ( $I/I_0$ ) from the As3d, Al2p and In4d core levels, plotted as a function of Au coverage on decapped  $\text{In}_{0.52}\text{Al}_{0.48}\text{As}(100)$  at 294K (RT). The crosses denote emission from the As3d core level, the open triangles denote emission from the In4d core level and the circles denote emission from the Al2p core level.

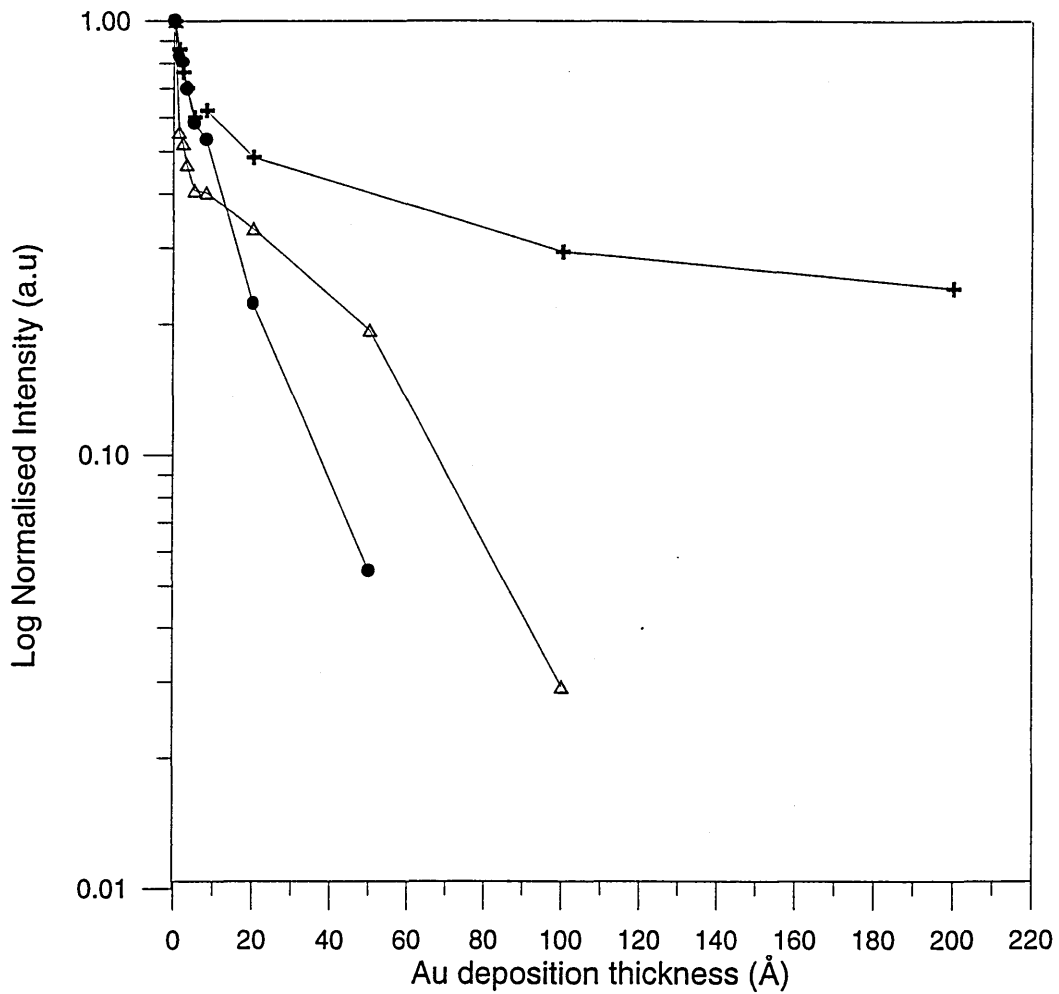


Figure 7.12: Core level emission intensity ( $I/I_0$ ) from the As3d, Al2p and In4d core levels, plotted as a function of Au coverage on decapped  $\text{In}_{0.52}\text{Al}_{0.48}\text{As}(100)$  at 125K (LT). The crosses denote emission from the As3d core level, the open triangles denote emission from the In4d core level and the circles denote emission from the Al2p core level.

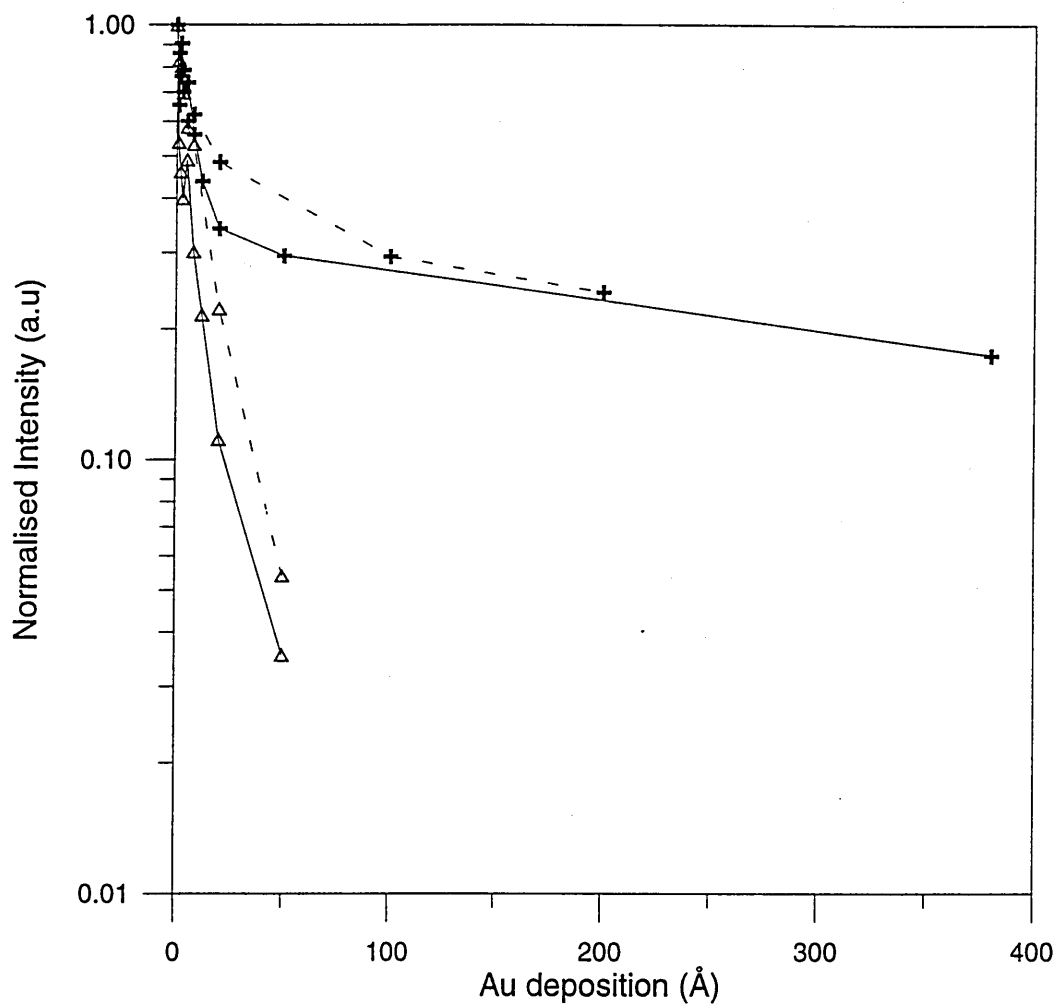


Figure 7.13: Core level emission intensity ( $I/I_0$ ) from the As3d and Al2p core levels, plotted as a function of Au coverage on decapped  $\text{In}_{0.52}\text{Al}_{0.48}\text{As}(100)$ . The dashed lines denote Au deposition at 294K(RT), the full lines denote Au deposition at 125K(LT). The crosses denote emission from the As3d core level and the open triangles denote emission from the Al2p core level.

(ii) *Au overlayer growth*

The relationship between overlayer core level intensity and the attenuation length can be obtained from equation 6.6 such that,

$$(I_f - I)/I_f = \exp(-d/\lambda) \quad [7.1]$$

Figure 7.14 shows the left hand side of this equation as a function of Au overlayer thickness ( $d$ ) for both room and low temperature. It can be seen that for room temperature deposition, the core level intensity deviates from an exponential attenuation after  $\sim 3-4\text{\AA}$ , concurring with the results obtained for substrate core level attenuation. Low temperature deposition again shows no significant change in the growth mode.

(iii) *As3d core level emission*

Figures 7.15 and 7.16 outline the change in shape of the As3d lineshape as a function of Au overlayer coverage, for room temperature and low temperature deposition respectively. The spectra were obtained using a photon energy of  $h\nu = 87$  eV. The clean surface is fitted with three components S1, S2 and B, similar to those described in section 7.1.3, with S1 related to Al bonded As sites, S2 related to In bonded As sites and B emanating from As in the bulk of the material.

After  $3\text{\AA}$  Au deposition at room temperature (figure 7.15), the bulk component B is attenuated and a reacted component S3 rises to slightly lower kinetic energy than component S2. As the Au overlayer develops the two components S2 and S1 related to surface In rich In-As and subsurface Al rich Al-As are also attenuated. In conjunction with this attenuation, the component S3 continues to grow and at high Au coverages totally dominates the As3d lineshape. Comparison with the low temperature deposition case reveals a strikingly similar evolution of the As3d lineshape. The bulk component B, S1 and S2 are again attenuated at the expense of the reacted component S3, and at high Au coverages the component completely accounts for the As3d lineshape.

Both the room temperature and low temperature stack plots indicate that As out-diffuses from the  $\text{In}_{0.52}\text{Al}_{0.48}\text{As}(100)$  substrate into the Au overlayer. XPS studies of Au- $\text{In}_{0.52}\text{Al}_{0.48}\text{As}(100)$  interface formation have indicated that a chemical reaction takes place between the Au and As forming an Au/As phase which segregates to the surface

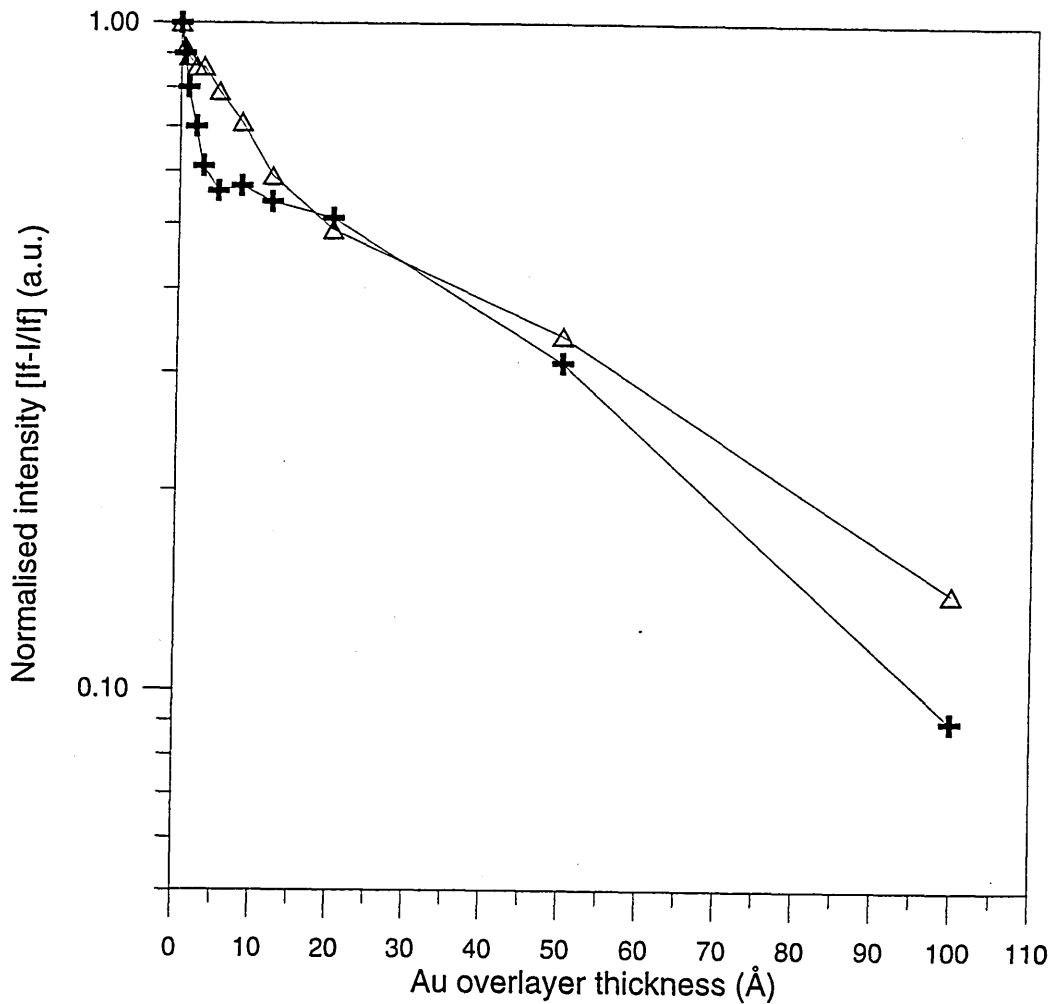


Figure 7.14: Au4f core level emission intensity ( $1 - I/I_f$ ), plotted as a function of Au coverage on decapped  $\text{In}_{0.52}\text{Al}_{0.48}\text{As}(100)$  at 294K(RT) and 125K(LT). The crosses denote Au deposition at 294K(RT), the open triangles denote Au deposition at 125K(LT).

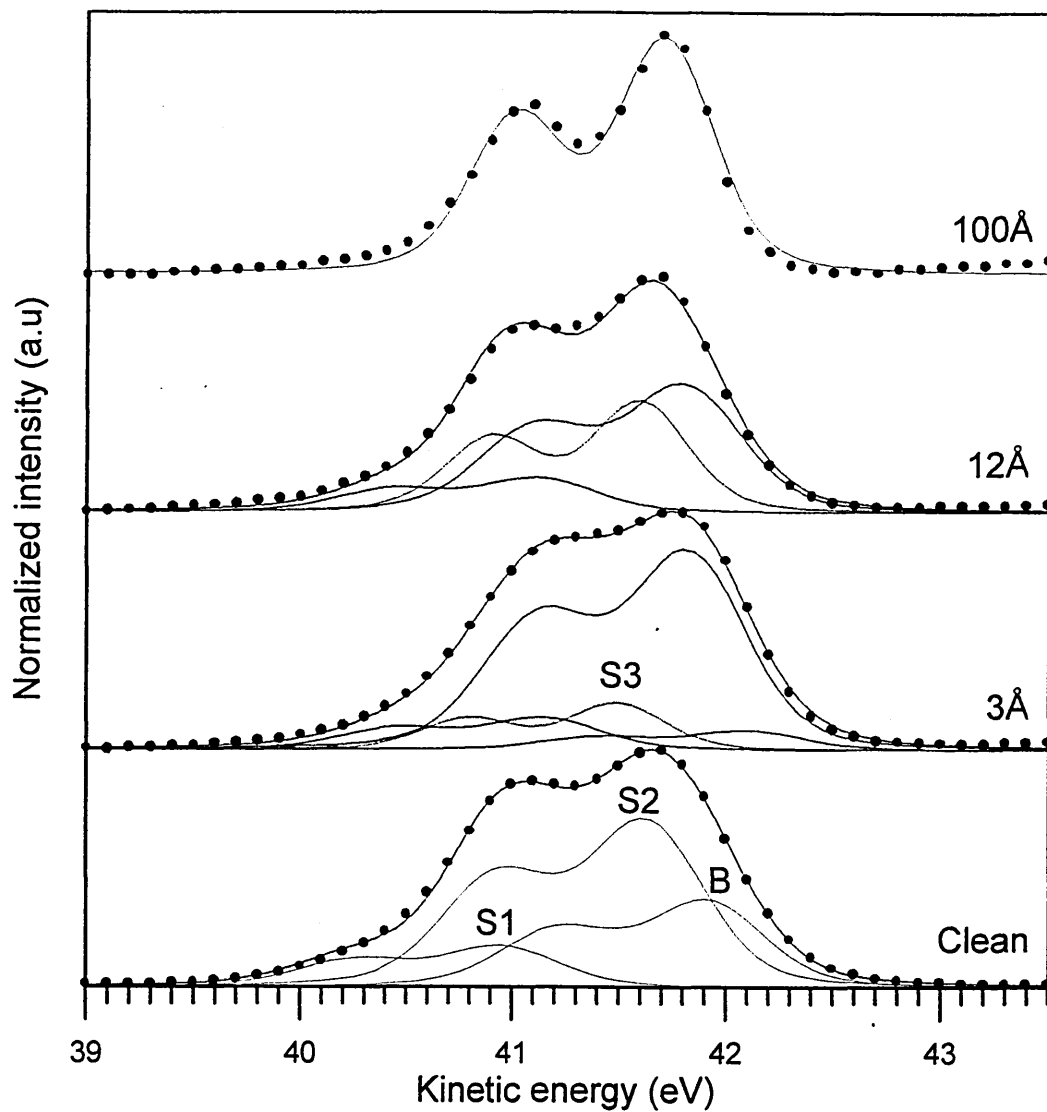


Figure 7.15: Evolution of the As3d core level spectra ( $h\nu = 87$  eV), with increasing Au coverage on decapped  $(3 \times 1)$  reconstructed  $\text{In}_{0.52}\text{Al}_{0.48}\text{As}(100)$  at 294K(RT). The peaks have been synthesised with four components, S1, S2, S3 and B, shown along with the overall fit as continuous lines.

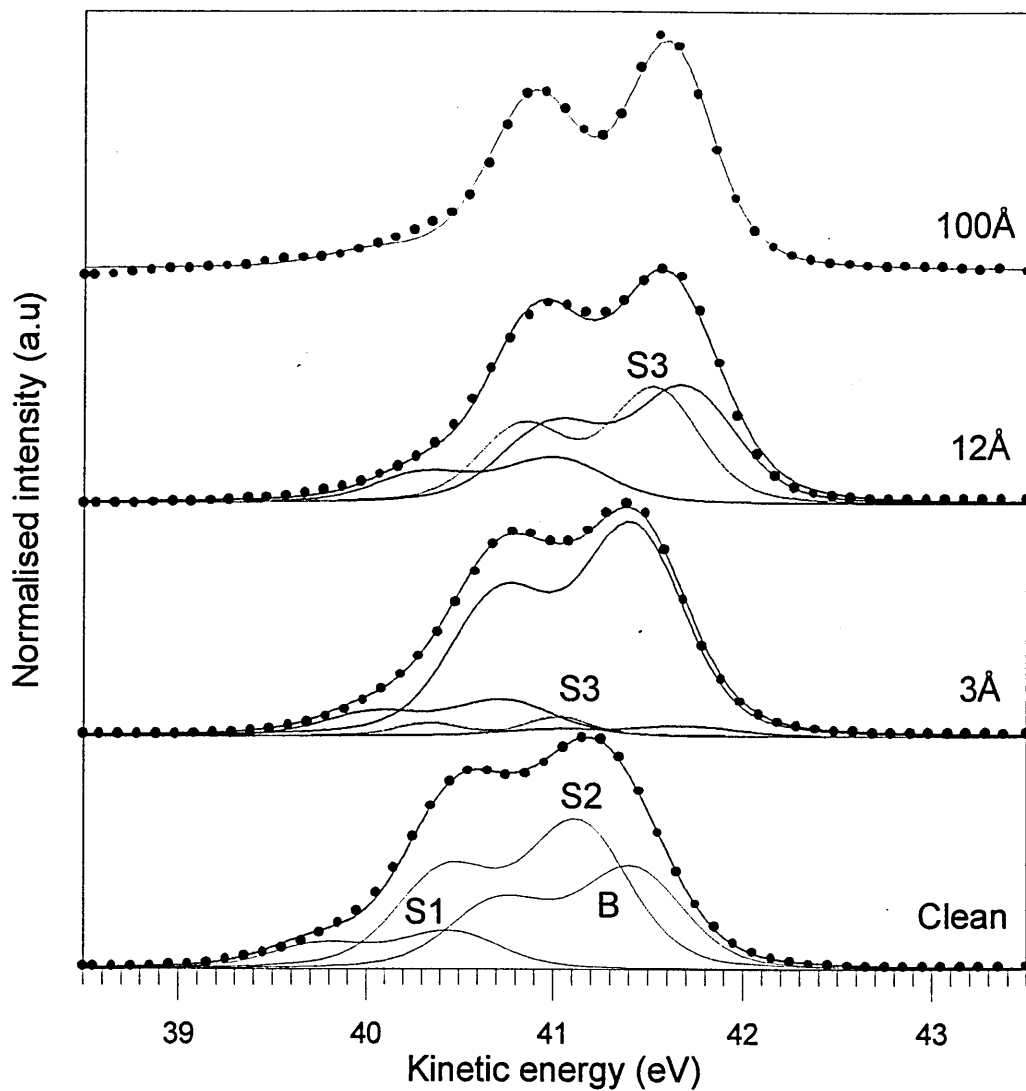


Figure 7.16: Evolution of the As<sub>3d</sub> core level spectra ( $h\nu = 87$  eV), with increasing Au coverage on decapped (3×1) reconstructed  $\text{In}_{0.52}\text{Al}_{0.48}\text{As}(100)$  at 125K(LT). The peaks have been synthesised with four components, S1, S2, S3 and B, shown along with the overall fit as continuous lines.

of the metal [22]. Similarly, studies of Au-In<sub>0.53</sub>Ga<sub>0.47</sub>As(100) interfaces described in section 6.1.5 produced interfaces that were reacted, with an Au/As compound thought to be present in the Au overlayer. The energy position of the high coverage reacted As component S3, with respect to the clean surface components in this study is very similar to that observed in section 6.1.5. It is highly probable therefore that an Au/As compound is once again formed for both room and low temperature Au deposition.

(iv) *In4d core level emission*

The evolution of the In4d core level spectra as a function of Au overlayer thickness are shown in figures 7.17 and 7.18 for low and room temperature Au deposition respectively. The spectra were acquired using a photon energy of 63 eV and the clean surfaces are fitted with two components S and B similar to those described in section 7.1.3.

Low temperature Au deposition results in a slow attenuation of the surface and bulk In4d components, S and B, as the overlayer is formed. As the overlayer develops, the components shift to higher kinetic energy by ~ 0.6 eV and at 20Å Au deposition the lineshape of the bulk component B has become narrower: a signal from the InAs surface component S is also still observed. At large Au coverages, only a small noisy signal can be detected, indicating that the metal overlayer clusters are beginning to coalesce into a more uniform film. As was the case for the core level attenuation and the As3d core level evolution, the evolution of the In4d core level spectra for the room temperature Au deposition case (figure 7.18) is again uncannily similar to the low temperature deposition case. Once again there is a slow attenuation of the two core levels with increasing Au coverage, accompanied by a shift of ~ 0.6 eV to higher kinetic energy. At 20Å Au, the lineshape of the bulk In4d peak has become narrower, and there is still evidence of the InAs component. At high Au coverages a small signal is again detected.

Comparison with the case of Au-In<sub>0.52</sub>Ga<sub>0.48</sub>As(100) interface formation discussed previously in chapter 6, shows that low temperature Au deposition resulted in a rapid attenuation of the surface InAs component whereas for room temperature Au deposition it was still evident at 20Å Au coverage. In both cases the attenuation of the InAs component was related to a combination of a reduced signal due to the growing Au overlayer, and the release of As from the InAs rich region to diffuse into the Au overlayer. The presence of the InAs component up to 20Å coverage of Au at room

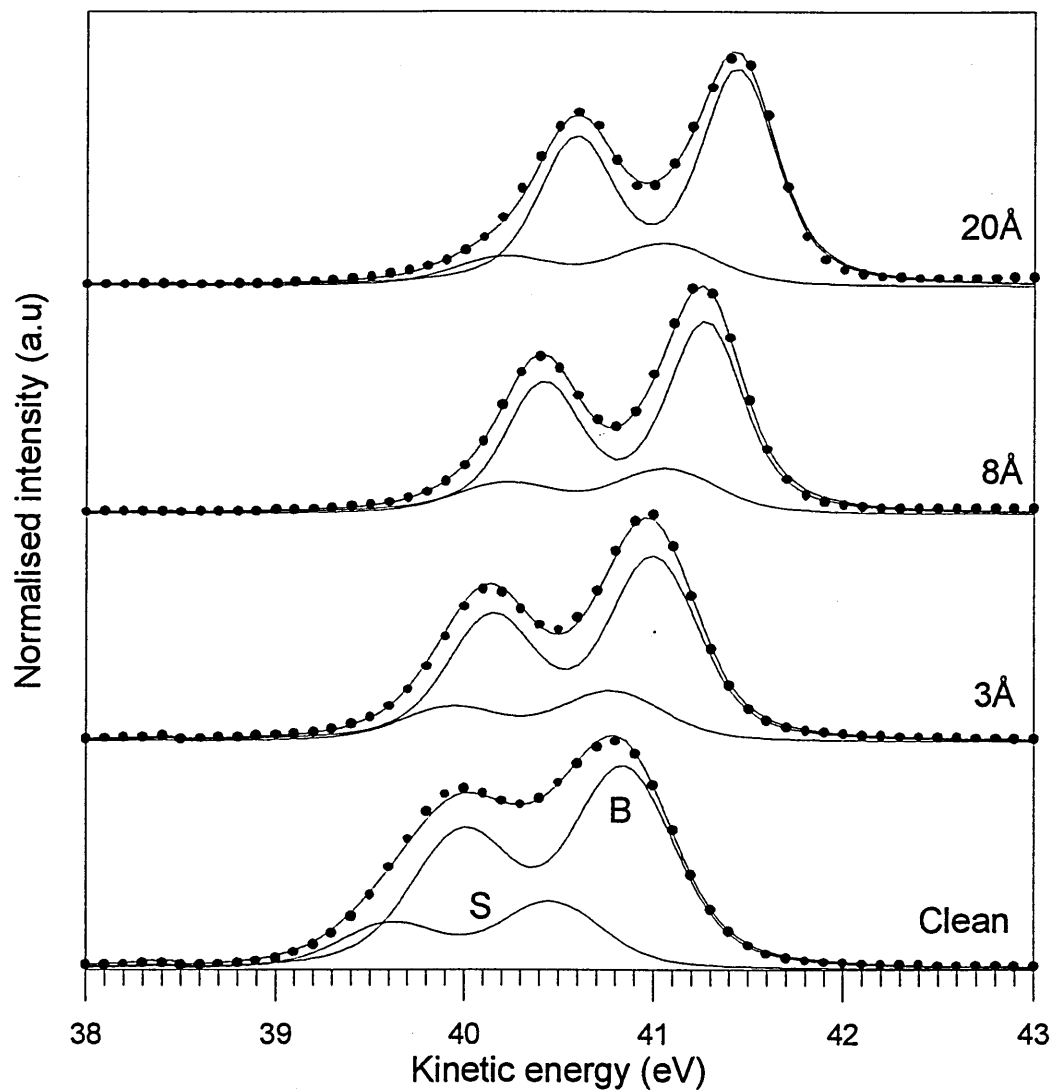


Figure 7.17: Evolution of the In4d core level spectra ( $h\nu = 63$  eV), with increasing Au coverage on decapped  $(3\times 1)$  reconstructed  $\text{In}_{0.52}\text{Al}_{0.48}\text{As}(100)$  at 125K(LT). The peaks have been synthesised with two components, S and B, shown along with the overall fit as continuous lines.

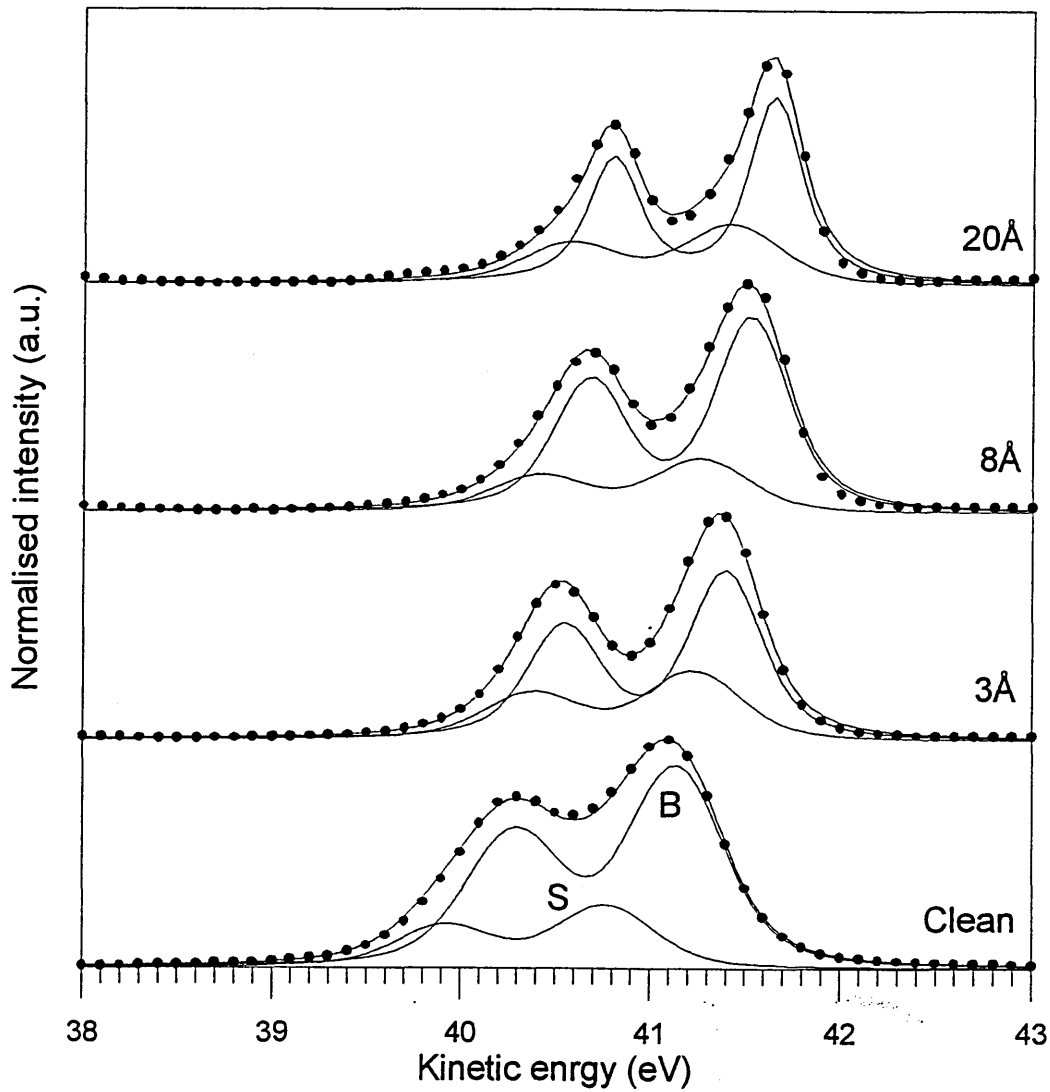


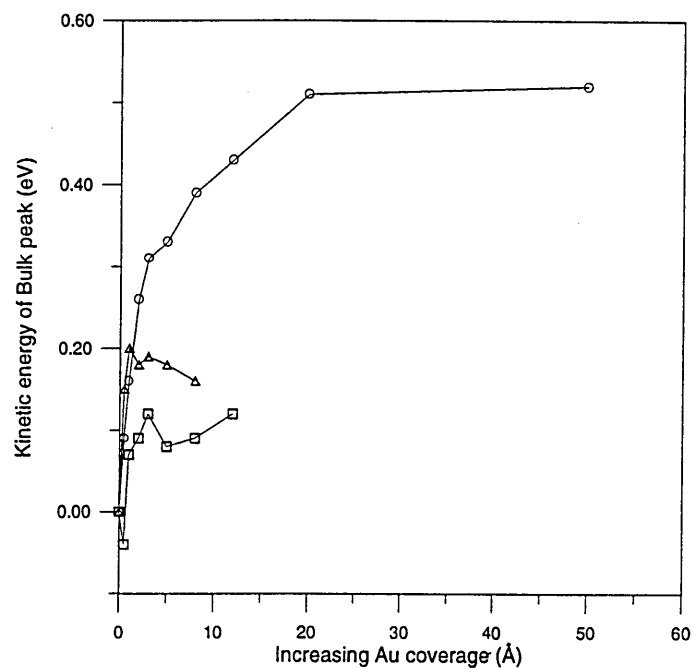
Figure 7.18: Evolution of the In4d core level spectra ( $h\nu = 63$  eV), with increasing Au coverage on decapped  $(3 \times 1)$  reconstructed  $\text{In}_{0.52}\text{Al}_{0.48}\text{As}(100)$  at 294K(RT). The peaks have been synthesised with two components, S and B, shown along with the overall fit as continuous lines.

temperature was thought to be a consequence of increased Au clustering. It is highly likely that a similar effect is being seen here for the Au-  $\text{In}_{0.52}\text{Al}_{0.48}\text{As}(100)$  interface. Referring back to the attenuation plots for room and low temperature deposition (figure 7.11), it was evident that there was no significant change in the Au overlayer growth mode with respect to formation temperature. Hence it is probable that the less laminar growth mode of the overlayer in comparison to the Au- $\text{In}_{0.52}\text{Ga}_{0.48}\text{As}(100)$  overlayer at low temperature accounts for the surface InAs component seen at coverages of  $20\text{\AA}$  Au for both deposition temperatures.

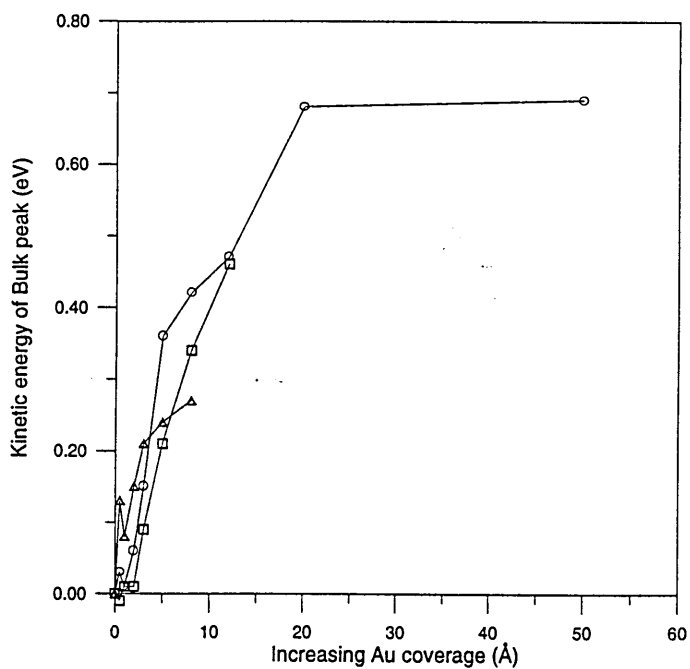
The narrowing of the bulk In4d lineshape and its consequent shift to high kinetic energy has also been observed for Au- $\text{In}_{0.52}\text{Ga}_{0.48}\text{As}(100)$  interface formation, and was attributed to emission from In in an interface environment devoid of As and with an abundance of In.

(v) *Band bending*

In the case of Au deposition on  $\text{In}_{0.52}\text{Al}_{0.48}\text{As}(100)$ , it is difficult to extract the bulk core level peaks, in particular the As3d bulk peak, due to the intermixing of species at the metal-semiconductor interface. This can make band bending measurements unreliable. For both deposition cases, the bulk As3d and Al2p core level components are attenuated after about  $12\text{\AA}$  of Au deposition. There is still a signal from the bulk In4d component at  $50\text{\AA}$ . However it is possible that this emission is a consequence of initially surface segregated In at the Au- $\text{In}_{0.52}\text{Al}_{0.48}\text{As}(100)$  interface, in an environment where there is an excess of In due to As out-diffusion. The measured change in the bulk As3d, Al2p and In4d peak positions as a function of Au overlayer coverage are shown for room temperature and low temperature deposition in figure 7.19 (a) and (b), respectively. Room temperature deposition of Au produces a shift in the bulk As3d and Al2p peak of  $\sim (0.15-0.2 \pm 0.1)$  eV, while the In4d peak shifts by about 0.5 eV. Low temperature deposition produces shifts of As3d  $\approx 0.25 \pm 0.1$  eV, Al2p  $\approx 0.5 \pm 0.1$  eV and In4d  $\approx 0.7 \pm 0.1$  eV. These values of band bending are inconsistent with each other with the variation in bulk peak energies likely to be a factor of the complex reacted interface that is formed when Au is deposited on  $\text{In}_{0.52}\text{Al}_{0.48}\text{As}(100)$ , as mentioned above. It is probable however that the actual band bending at the Au- $\text{In}_{0.52}\text{Al}_{0.48}\text{As}(100)$  interface is somewhere in between the maximum and minimum values of band bending observed. Since the In4d and As3d core levels have been severely modified due to As



(a)



(b)

Figure 7.19: The relative binding energy shifts of the As3d, In4d and Al2p core level bulk components as a function of increasing Au coverage onto decapped (3×1) reconstructed  $\text{In}_{0.52}\text{Al}_{0.48}\text{As}(100)$  at (a) 294K(RT) and (b) 125K(LT). The open triangles denote the As3d core level, the open squares denote the Al2p core level and the open circles denote the In4d core level.

out-diffusion from the surface InAs rich region, the Al<sub>2</sub>p bulk peak band bending shall be considered for the purpose of barrier height measurement by SXPS. It should be stressed again however, that this value is only intended as a guide and that the true value of band bending may differ from this slightly. The position of the Fermi level was determined from the Fermi edge of a thick gold layer deposited “*in-situ*”, on to a tantalum spade in electrical contact with the sample, prior to the experiment. Using a photon energy of 87 eV the Fermi level was located at 82.77 eV, whilst the valence band maximum for the room temperature clean In<sub>0.52</sub>Al<sub>0.48</sub>As(100) surface obtained using the same photon energy was found to be at 82 eV. The valence band was therefore positioned 0.77 eV below the Fermi level of the system and the conduction band minimum 0.68 eV above the Fermi level for clean In<sub>0.52</sub>Al<sub>0.48</sub>As(100). Hence the additional band bending at the surface of ~ 0.15 eV produces a barrier height obtained by SXPS of  $\sim 0.83 \pm 0.1$  eV for the room temperature Au-In<sub>0.52</sub>Al<sub>0.48</sub>As(100) interface. This result is in good agreement with barrier heights observed for intimate Au-In<sub>0.52</sub>Al<sub>0.48</sub>As(100) diodes measured by the I-V technique as shown in table 7.1 [2]. Low temperature deposition produces band bending of  $\sim 0.47 \pm 0.1$  eV. Following the same procedure as above, the conduction band was found to be 0.33 eV above the Fermi level. The barrier height obtained by SXPS for low temperature Au-In<sub>0.52</sub>Al<sub>0.48</sub>As(100) formation was therefore  $\sim 0.80 \pm 0.1$  eV. The relevance of these shifts in accordance to barrier height pinning is discussed in detail in chapter 8.

(vi) *Valence band emission*

Figures 7.20 (a) and (b) illustrate the evolution of the valence band spectra as a function of Au overlayer coverage for room temperature and low temperature deposition respectively. Both stack plots exhibit a similar evolution from the clean surface to high Au coverages. It is believed that in the temperature range studied, a similar interface is formed for Au deposition on In<sub>0.52</sub>Al<sub>0.48</sub>As(100), irrespective of deposition temperature. These results are in good agreement with those discussed previously for overlayer growth and core level emission.

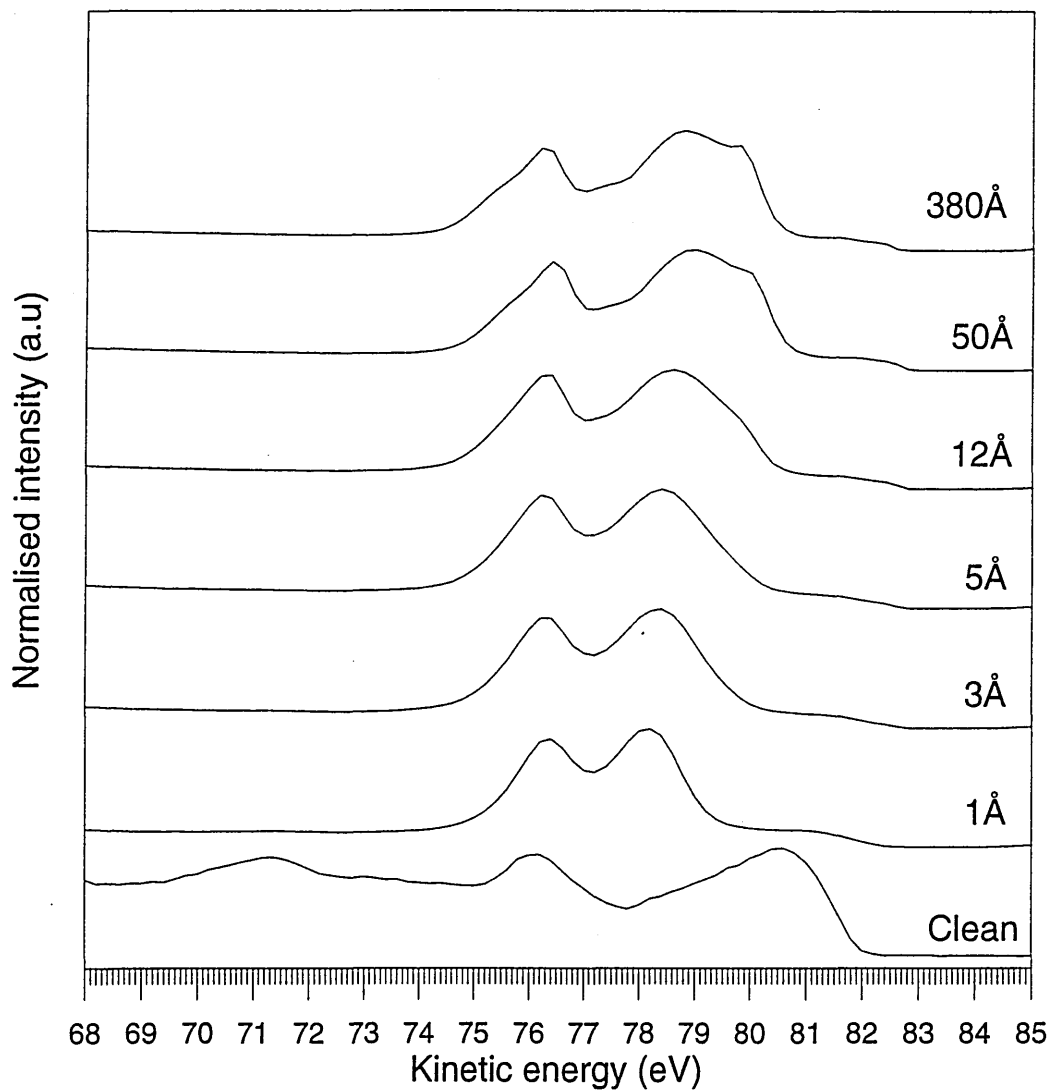


Figure 7.20a: A stack plot of the valence band spectra as a function of increasing Au coverage onto decapped (3×1) reconstructed  $\text{In}_{0.52}\text{Al}_{0.48}\text{As}(100)$  at 294K(RT). The spectra were obtained using a photon energy of,  $h\nu = 87$  eV.

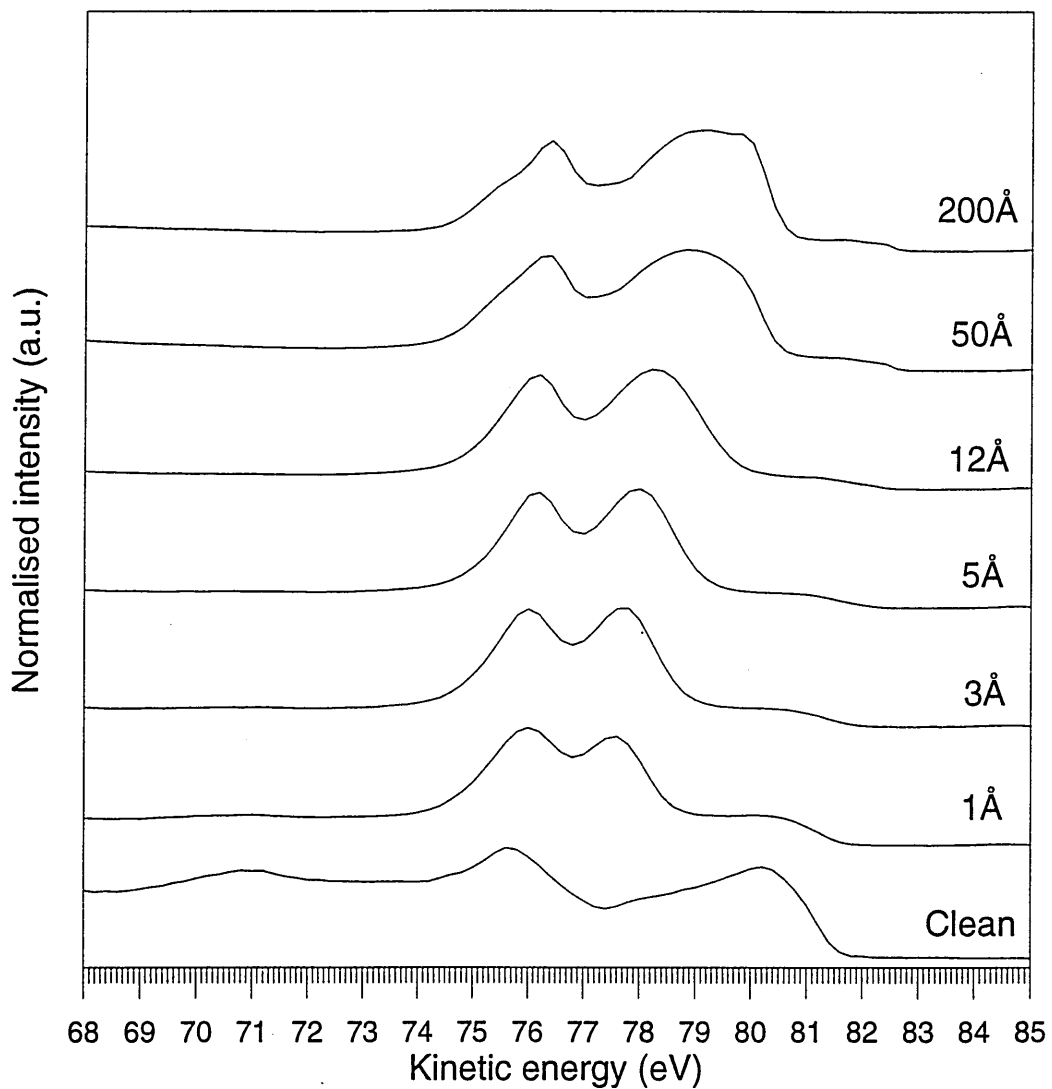


Figure 7.20b: A stack plot of the valence band spectra as a function of increasing Au coverage onto decapped (3×1) reconstructed  $\text{In}_{0.52}\text{Al}_{0.48}\text{As}(100)$  at 125K(LT). The spectra were obtained using a photon energy of,  $h\nu = 87$  eV.

## 7.2 Microscopy studies

### 7.2.1 Introduction

A structural characterisation of the interfaces formed at room and low temperature between the metals In and Au and  $\text{In}_{0.52}\text{Al}_{0.48}\text{As}(100)$  has been carried out by TEM and SAED.

The experiments were performed in a Hitachi H800-NA electron microscope operating at 200 keV. The preparation of the samples and the experimental equipment employed has been discussed previously in chapter 4.

The samples were observed in plan view to reveal the crystal structure of the metal overlayer. Cross section observations were carried out to clarify the plan view results and to characterise the morphology of the interfaces formed. The area of material sampled was kept the same for respective room temperature and low temperature comparison. This would enable us to confidently compare the extent of clustering and crystal grain size. Due to sample preparation difficulties and time restrictions, it was not possible to obtain good TEM results for the In-  $\text{In}_{0.52}\text{Al}_{0.48}\text{As}(100)$  interface.

### 7.2.2 The Au- $\text{In}_{0.52}\text{Al}_{0.48}\text{As}(100)$ interface

Figures 7.21 (a) and (b) show plan view micrographs of the Au overlayer on  $\text{In}_{0.52}\text{Al}_{0.48}\text{As}(100)$  for room and low temperature deposition respectively. Room temperature deposition (figure 7.21(a)) produces an overlayer with a larger grain size than for low temperature deposition (figure 7.21(b)). This is consistent with the notion that at low temperature the reduced surface mobility of the Au atoms arriving at the surface will produce an overlayer that is less ordered, and tends towards that of an amorphous nature.

Selected area diffraction patterns of the Au overlayer are shown for room and low temperature deposition in figures 7.22 (a) and (b) respectively. In figure 7.22(b), it can be seen that the diffraction pattern for low temperature Au deposition consists of a stronger set of rings than for that obtained from the overlayer deposited at room temperature (figure 7.22(a)). It is deduced therefore that in the case of low temperature deposition, a greater number of random crystalline orientations are present concurring



Figure 7.21 (a): A plan view micrograph of the Au overlayer deposited on  $\text{In}_{0.52}\text{Al}_{0.48}\text{As}(100)$  at room temperature (295K). The magnification used was 120,000 times.



Figure 7.21 (b): A plan view micrograph of the Au overlayer deposited on  $\text{In}_{0.52}\text{Al}_{0.48}\text{As}(100)$  at low temperature (125K). The magnification used was 120,000 times.

with concept that a reduced grain size is achieved by depositing Au at low temperature compared to room temperature.

TEM micrographs obtained from samples prepared in cross section indicated that the nature of the Au-In<sub>0.52</sub>Al<sub>0.48</sub>As(100) interface was virtually the same regardless of Au deposition temperature. In both deposition cases a band of white contrast is evident below the Au layer, indicating that the out-diffusion of substrate species could be occurring. This is in good agreement with the results obtained by photoemission spectroscopy.

### 7.3 Summary

#### 7.3.1 In-In<sub>0.52</sub>Al<sub>0.48</sub>As interface formation

SXPS studies of In deposition onto decapped In<sub>0.52</sub>Al<sub>0.48</sub>As(100) have shown that for evaporation at room temperature the initial monolayer ( $\sim 3\text{\AA}$ ) of In is of a laminar nature. Above this thickness, a three dimensional mode of growth dominates leading to the formation of In clusters. The attenuation of the As3d and Al2p core levels indicates that the out-diffusion of substrate species into the growing In overlayer does not take place.

No significant chemical reactions were resolved from the As3d core level evolution, however a shift in the bulk As3d core level energy of  $\sim 0.3$  eV was observed. The size of the resulting Schottky barrier formed at the In-In<sub>0.52</sub>Al<sub>0.48</sub>As(100) interface as determined by SXPS was found to be  $\sim 0.88 \pm 0.1$  eV, consistent with I-V measured values of  $\phi_b$  for In diodes formed on intimate In<sub>0.52</sub>Al<sub>0.48</sub>As(100) surfaces [2]. A larger shift was observed in the In4d core level energy and this was attributed to the transition of emission from covalently bonded In in the semiconductor to emission from the metallic In overlayer. The absence of chemically reacted components tends to suggest that the In-In<sub>0.52</sub>Al<sub>0.48</sub>As(100) interface is relatively abrupt.

Reducing the temperature of the substrate appears to have little effect on the formation of the In-In<sub>0.52</sub>Al<sub>0.48</sub>As(100) interface other than to reduce the effect of In overlayer clustering. It is thought that this may be a consequence of a reduction in the surface mobility of the In atoms as they arrive at the semiconductor surface. The barrier height obtained by SXPS was found to be  $\sim 0.76 \pm 0.1$  eV.

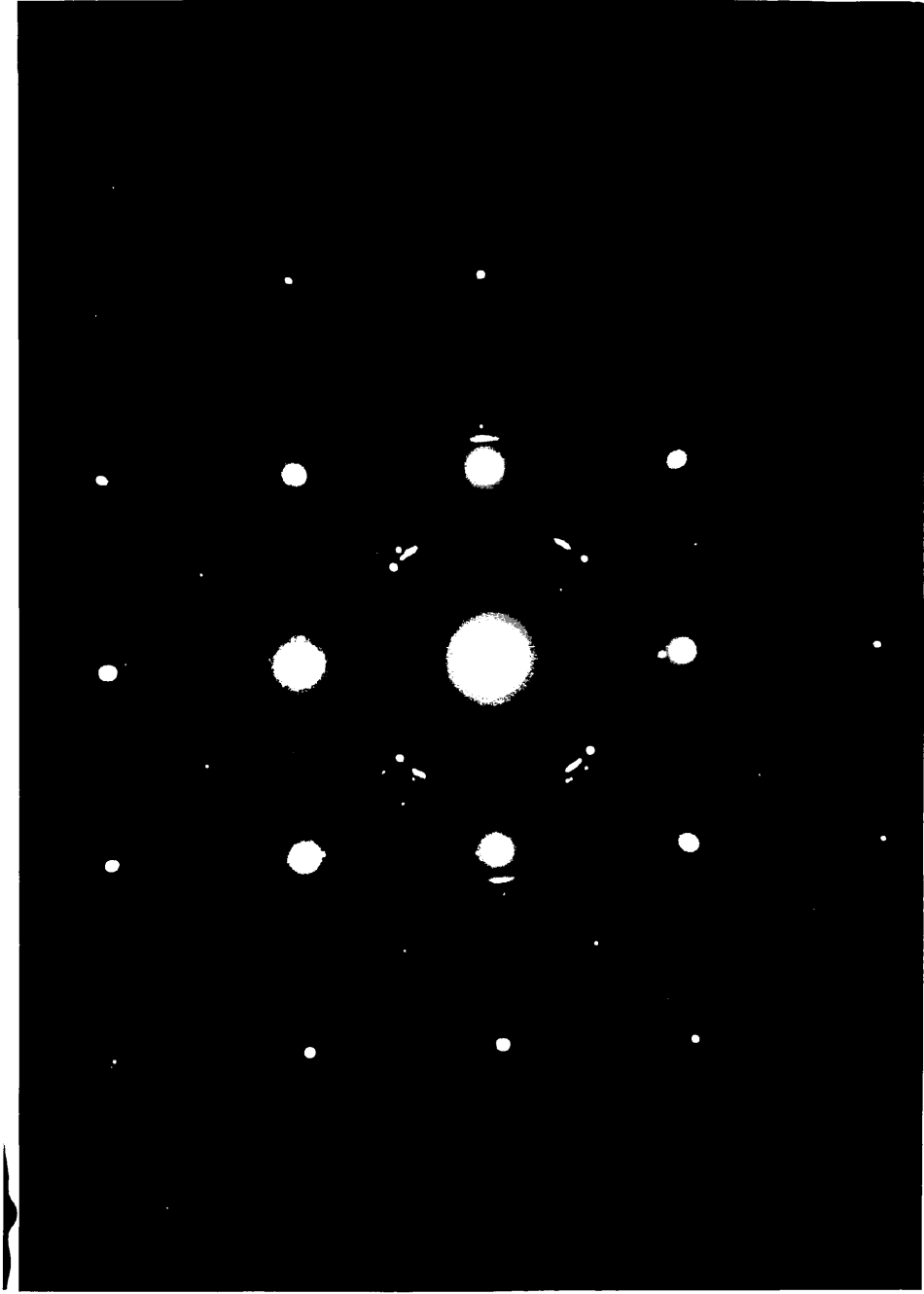


Figure 7.22 (a): A Selected Area Diffraction Pattern (SAED) of the Au overlayer deposited on In<sub>0.52</sub>Al<sub>0.48</sub>As(100) at room temperature (295K).

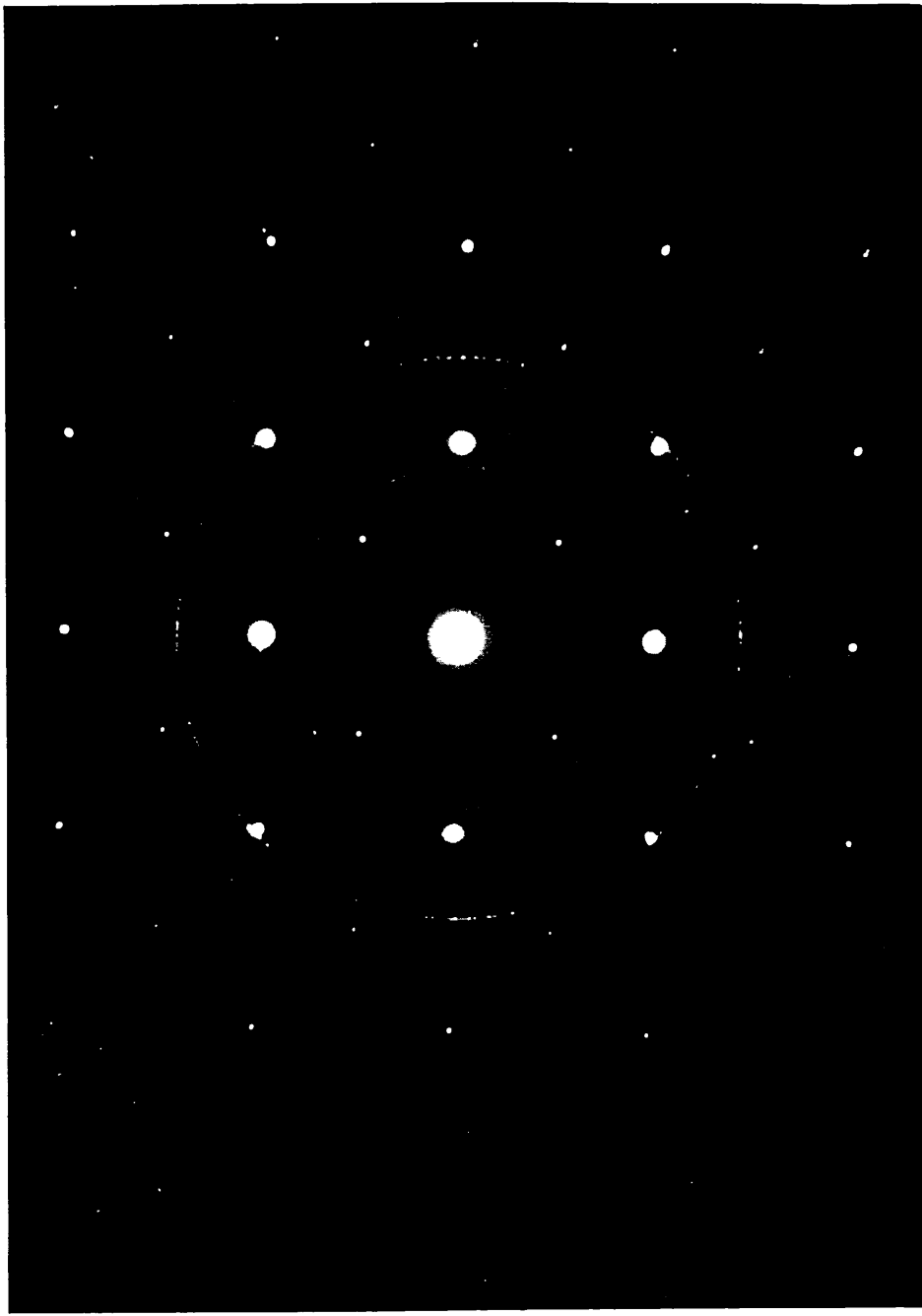


Figure 7.22 (b): A Selected Area Diffraction Pattern (SAED) of the Au overlayer deposited on  $\text{In}_{0.52}\text{Al}_{0.48}\text{As}(100)$  at low temperature (125K).

TEM studies indicated that low temperature In deposition produced an overlayer with a smaller grain size than compared to room temperature deposition.

### 7.3.2 Au-In<sub>0.52</sub>Al<sub>0.48</sub>As interface formation

SXPS studies of Au-In<sub>0.52</sub>Al<sub>0.48</sub>As(100) interface formation at room temperature indicates that as for In deposition, the growth mode is of a layer by layer followed by islanding nature. However, comparison of the attenuation of the Al2p core level intensity for In and Au deposition, shows that the extent of metal overlayer clustering is much less pronounced in the Au deposition case. It is also evident from the attenuation of the core levels that As out-diffuses from the In<sub>0.52</sub>Al<sub>0.48</sub>As(100) substrate into the growing Au overlayer. This is confirmed by the evolution of the As3d core level as a function of Au overlayer thickness, whereby a reacted component is resolved after about 3Å of Au has been deposited. This reacted component completely dominates the As3d lineshape at high Au coverages, and comparison with emission from the elemental As cap suggests that As is present in a form other than elemental As. It is therefore thought that a chemical reaction occurs between the Au and As forming an Au/As compound and producing a perturbed interface that is complex and defected with an excess of In, and As vacancies.

The barrier height obtained by SXPS was  $\sim 0.83 \pm 0.1$  eV which was lower than for the In-In<sub>0.52</sub>Al<sub>0.48</sub>As(100) interface and is in good agreement with reported values of  $\phi_b$  for Au and In diodes on both "as grown" and "As decapped" In<sub>0.52</sub>Al<sub>0.48</sub>As(100) surfaces.

Low temperature Au deposition produced an interface that was virtually identical to that formed at room temperature. TEM studies confirmed the out-diffusion of As into the Au overlayer at both deposition temperatures and also indicated that the Au overlayer formed at low temperature has a reduced grain size compared to that formed at room temperature. The barrier height as determined by SXPS was found to be  $\sim 0.73 \pm 0.1$  eV.

## 7.4 References

- [1] P. Chu, C.L. Lin and H.H. Wieder, *Appl. Phys. Lett.* **53**, 2423 (1988).
- [2] S.A. Clark, S.P. Wilks, J.I. Morris, D.A. Woolf and R.H. Williams, *J. Appl. Phys.* **75**, 2481 (1994).
- [3] L. P. Sadwick, C. W. Kim, K. L. Tan and D. C. Streit, *IEEE Electron Device Lett.* **12**, 626 (1991).
- [4] P. D. Hodson, R. H. Wallis, J. I. Davies, J. R. Riffat and A. C. Marshall, *Semicond. Sci. Technol.* **3**, 1136 (1988).
- [5] H. Ohno, C. E. Wood, L. Rathburn, D. V. Morgan, G. W. Wicks and L. F. Eastman, *J. Appl. Phys.* **52**, 4033 (1981).
- [6] A. Fricke, G. Stareev, T. Kummetz, D. Sowada, J. Mähns, W. Kowalsky and K. J. Ebeling, *Appl. Phys. Lett.* **65**, 755 (1994).
- [7] G.J. Davies, T. Kerr, C.G. Tuppen, B. Wakefield, D.A. Andrews, *J. Vac. Sci. Technol.* **B2**, 219 (1984).
- [8] G. -H. Goetz, D. Bimberg, H. Jürgensen, J. Selders, A.V. Solomonov, G.F. Glinski and M. Razhegi, *J. Appl. Phys.* **54**, 4543 (1983).
- [9] "Practical Surface Analysis, 2<sup>nd</sup> Edition, Volume 1 Auger and x-ray Photoelectron Spectroscopy", edited by D. Briggs and M.P. Seah, John Wiley and Sons (1990).
- [10] J.J. Yeh and I. Lindau, *Atomic Data and Nuclear Tables*, **32**,1 (1985).
- [11] C.J. Spindt, M. Yamada, P.L. Meissner, K.E. Miyano, T. Kendelewicz, A. Herrera-Gomez, W.E. Spicer and A.J. Arko, *Phys. Rev. B*, **45(19)**, 11108-11119 (1992)
- [12] D. Mao, M. Santos, M. Shayegan, A. Khan, G. Le Lay, Y. Hwu, G. Margaritondo, L.T. Flores and J.P. Harbison, *Phys. Rev. B*, **45**, 1273 (1992).
- [13] C.J. Spindt, R. Cao, K. E. Miyano, I. Lindau, W.E. Spicer and Y. -C. Pao, *J. Vac. Sci. Technol.* **B8 (4)**, 974-979 (1990).
- [14] M. Watanabe, T. Kinoshita, A. Kakizaki and T. Ishii, *Journal of the Physical Society of Japan*, **65**, 1730-1733 (1996).
- [15] S.A. Clark, C.J. Dunscombe, D.A. Woolf, S.P. Wilks and R.H. Williams, *J. Vac. Sci. Technol.* **B12**, 551 (1994).
- [16] G. Grenet, E. Bergignat, M. Gendry, M. Lapeyrade and G. Hollinger, *Surf. Sci.* **352-354**, 734 (1996).

- [17] S.A. Clark, S.P. Wilks, J. I. Morris, D.A. Woolf and R.H. Williams, *J. Appl. Phys.* **75**, 2481 (1994).
- [18] J.W. Cairns, PhD Thesis, University of Wales, College Cardiff (1991).
- [19] R. Cao, K.E. Miyano, I. Lindau and W.E. Spicer, *J. Vac. Sci. Technol.* **A8** (4), 3460-3465 (1990).
- [20] H. M. Rosenberg, "The Solid State", Third Edition, Oxford University Press, 1988.
- [21] R.S. Bauer, R.Z. Bachrach, G.V. Hansson and P. Chiaradia, *J. Vac. Sci. Technol.*, **19**(3), 674-680 (1981).
- [22] S.A. Clark, PhD Thesis, University of Wales, College Cardiff (1993).

# Chapter 8

## Discussion and conclusions

### 8.0 Introduction

The III-V materials  $\text{In}_{0.53}\text{Ga}_{0.47}\text{As}$  and  $\text{In}_{0.52}\text{Al}_{0.48}\text{As}$  are currently of technological importance for high speed and optoelectronic devices. A recent study has shown that the Schottky barrier formed at the interface between In and intimate “as grown”  $\text{In}_{0.53}\text{Ga}_{0.47}\text{As}(100)$  may be improved if the metallisation is carried out on a surface held at low temperature [1]. As a consequence, the present study has been undertaken to investigate the fundamental aspects of intimate interface formation between metals and the semiconductors  $\text{In}_{0.53}\text{Ga}_{0.47}\text{As}$  and  $\text{In}_{0.52}\text{Al}_{0.48}\text{As}$  as a function of temperature.

In this chapter, the results obtained in chapters 5, 6 and 7 are summarised and then discussed in the context of current models for Schottky barrier formation as described in chapter 2. Finally conclusions to the study will be drawn, and potential areas of future research that may be undertaken will be considered.

### 8.1 Summary of experimental results

(i) *The clean  $\text{In}_{0.53}\text{Ga}_{0.47}\text{As}(100)$  surface*

Atomically clean MBE grown  $\text{In}_{0.53}\text{Ga}_{0.47}\text{As}(100)$  surfaces have been protected from air contamination by the formation of a protective As cap directly after growth. The clean surface was regenerated in the analysis chamber by the thermal desorption of the As cap under UHV conditions. XPS studies showed that the relative abundance of As on the  $\text{In}_{0.53}\text{Ga}_{0.47}\text{As}(100)$  surface decreased as the annealing temperature increased (300°C - 475°C), indicating the preferential desorption of As from the sample surface with increasing temperature. The As cap was removed at ~350°C and after annealing at a temperature of 390°C the intensity ratio between the In and Ga at the sample surface was greater than that observed in the bulk of the material. This indicated the likelihood of In surface segregation during the MBE growth process. Subsequent LEED studies at

Daresbury SRS showed that As capped  $\text{In}_{0.53}\text{Ga}_{0.47}\text{As}(100)$  samples annealed at  $390^\circ\text{C}$  exhibited a  $(3\times 1)$  surface reconstruction that closely replicated that of “as grown” samples.

(ii) *Metal-  $\text{In}_{0.53}\text{Ga}_{0.47}\text{As}(100)$  interface formation*

SXPS studies of the deposition of In onto decapped  $(3\times 1)$  reconstructed surfaces have shown that for evaporation at room temperature there is no evidence of layer by layer growth and that the growth mode is dominated by islanding. The attenuation of the As3d core level signal indicates that there may also be out-diffusion of As into the growing In overlayer, with the possibility of a predominantly InAs rich overlayer. Examination of the evolution of the As3d and In4d core level with increasing In overlayer thickness concurs with the notion that As diffuses into the In film to form InAs. It is concluded therefore that the In- $\text{In}_{0.53}\text{Ga}_{0.47}\text{As}(100)$  interface formed at room temperature is non-abrupt and reacted with the possibility of As vacancies and In-In bonds. The deposited In overlayer is likely to be a mixture of metallic In and InAs. The band bending that could be resolved due to the shift in As3d bulk peak position was observed to be  $\sim 0.25$  eV which is in good agreement with the value of barrier height recorded for In diodes formed on “as grown”  $\text{In}_{0.53}\text{Ga}_{0.47}\text{As}(100)$  at room temperature [1].

Deposition of In onto  $\text{In}_{0.53}\text{Ga}_{0.47}\text{As}(100)$  surfaces held at low temperature showed a striking difference to the room temperature case. The initial  $\sim 5\text{\AA}$  of In were deposited in a layer by layer fashion. Above this thickness an islanding mode of growth tends to dominate. No significant chemical reactions were resolved from the As3d core level evolution and hence it is believed that the interface formed at low temperature is relatively abrupt and unreacted. However band bending of  $\sim 0.5$  eV was observed in the bulk As3d component which is once again in good agreement with I-V measured barrier heights for In diodes formed at low temperature [1]. The In4d core level evolution showed a chemical shift which was interpreted as a transition from emission from covalently bonded In in the semiconductor material to metallic In in the overlayer. TEM studies of the interfaces formed at both temperatures concurred with the SXPS results, showing a less ordered overlayer for room temperature In deposition. It is concluded therefore that low temperature deposition of In reduces the amount of overlayer clustering and also appears to inhibit the out-diffusion of As into the In overlayer.

SXPS studies of Au deposition onto decapped (3×1) reconstructed  $\text{In}_{0.53}\text{Ga}_{0.47}\text{As}(100)$  surfaces at room temperature show that the deposited layer has a layer by layer mode of growth for the first  $\sim 7\text{\AA}$  of Au. After  $\sim 7\text{\AA}$  Au is deposited, islanding tends to dominate, and the attenuation of the As3d signal is much slower than that of the In4d and Ga3d signals. This tends to suggest that as in the case of In deposition, As out-diffuses into the metal overlayer, with the added possibility of Au/In/Ga alloy formation. The evolution of the As3d core level indicates the growth of a reacted component that dominates the emission spectra at high Au coverages. The energy of this reacted component implies that it is not As in an elemental form, and therefore the component is attributed to emission from As in an Au/As compound.

Low temperature deposition of Au results in a layer by layer mode of growth for the first  $\sim 15\text{\AA}$  of Au deposition, with islanding once again becoming significant after this thickness. After  $15\text{\AA}$  Au has been deposited, the As3d signal again attenuates at a slower rate than the Ga3d and In4d signals, indicating As out-diffusion even at the reduced temperature. This is confirmed by the observation of a reacted component in the low temperature, As3d core level evolution spectra, similar to that observed at room temperature. No resolvable binding energy shift of the bulk core level components was observed for either low or room temperature Au deposition, hence Au deposition brought about no significant band bending. The resulting barrier heights formed at low and room temperature Au- $\text{In}_{0.53}\text{Ga}_{0.47}\text{As}(100)$  interfaces, determined by SXPS, were deemed to be "Ohmic". This is in good agreement with I-V measurements of Au diodes formed on "as grown"  $\text{In}_{0.53}\text{Ga}_{0.47}\text{As}(100)$  surfaces [1]. In conclusion, deposition of Au at room temperature results in a layer by layer followed by islanding mode of growth accompanied by the out-diffusion of As from the  $\text{In}_{0.53}\text{Ga}_{0.47}\text{As}(100)$  into the metal overlayer resulting in the formation of an Au/As compound. Low temperature Au deposition has little effect on the formation of the interface or the overlayer other than to reduce metal clustering. The interface environment for both room and low temperature formation is believed to be non-abrupt and reacted consisting of As vacancies and an excess of In possibly bonded to Au.

(iii) *Metal- $\text{In}_{0.52}\text{Al}_{0.48}\text{As}(100)$  interface formation*

SXPS studies of In deposition onto decapped  $\text{In}_{0.52}\text{Al}_{0.48}\text{As}(100)$  have shown that for evaporation at room temperature the initial monolayer ( $\sim 3\text{\AA}$ ) of In is of a

laminar nature. Above this thickness, a three dimensional mode of growth dominates producing the formation of In clusters. The attenuation of the As3d and Al2p core levels indicates that the out-diffusion of substrate species into the growing In overlayer does not take place.

No significant chemical reactions were resolved from the As3d core level evolution, however a shift in the bulk As3d core level energy of  $\sim 0.3$  eV was observed. The size of the resulting Schottky barrier formed at the In-In<sub>0.52</sub>Al<sub>0.48</sub>As(100) interface as determined by SXPS was found to be  $\sim 0.88 \pm 0.1$  eV, consistent with I-V measured values of  $\phi_b$  for In diodes formed on intimate In<sub>0.52</sub>Al<sub>0.48</sub>As(100) surfaces [2]. A larger shift was observed in the In4d core level energy and this was attributed to the transition of emission from covalently bonded In in the semiconductor to emission from the metallic In overlayer. The absence of chemically reacted components tends to suggest that the In-In<sub>0.52</sub>Al<sub>0.48</sub>As(100) interface is relatively abrupt.

Reducing the temperature of the substrate appears to have little effect on the formation of the In-In<sub>0.52</sub>Al<sub>0.48</sub>As(100) interface other than to reduce the effect of In overlayer clustering. TEM studies indicated that low temperature In deposition produced an overlayer with reduced clustering and a smaller grain size than compared to room temperature deposition. It is thought that this may be a consequence of a reduction in the surface mobility of the In atoms as they arrive at the semiconductor surface. The barrier height obtained by SXPS was found to be  $\sim 0.76 \pm 0.1$  eV.

SXPS studies of Au-In<sub>0.52</sub>Al<sub>0.48</sub>As(100) interface formation at room temperature indicates that as for In deposition, the growth mode is of a layer by layer followed by islanding nature. However comparison of the attenuation of the Al2p core level intensity for In and Au deposition, shows that the extent of metal overlayer clustering is much less pronounced in the Au deposition case. It is also evident from the attenuation of the core levels that As out-diffuses from the In<sub>0.52</sub>Al<sub>0.48</sub>As(100) substrate into the growing Au overlayer. This is confirmed by the evolution of the As3d core level as a function of Au overlayer thickness, whereby a reacted component is resolved after about 3Å of Au has been deposited. This reacted component completely dominates the As3d lineshape at high Au coverages, and comparison with emission from the elemental As cap suggests that As is present in a form other than elemental As. It is thought therefore that an Au/As phase is formed, producing a perturbed interface that is complex and defected with an excess of In, and As vacancies. The barrier height obtained by SXPS was  $\sim 0.83 \pm 0.1$  eV which was lower than for the In-In<sub>0.52</sub>Al<sub>0.48</sub>As(100) interface and is in good

agreement with reported values of  $\phi_b$  for Au and In diodes on both “as grown” and “As decapped”  $\text{In}_{0.52}\text{Al}_{0.48}\text{As}(100)$  surfaces [2].

Low temperature Au deposition produced an interface that was virtually identical to that formed at room temperature. TEM studies confirmed the out-diffusion of As into the Au overlayer at both deposition temperatures and also indicated that the Au overlayer formed at low temperature has a reduced grain size compared to that formed at room temperature. The barrier height as determined by SXPS was found to be  $\sim 0.73 \pm 0.1$  eV.

## 8.2 Discussion: Schottky barrier formation

Previously reported I-V studies of the Schottky barriers formed at metal- $\text{In}_{0.53}\text{Ga}_{0.47}\text{As}(100)$  and  $\text{In}_{0.52}\text{Al}_{0.48}\text{As}(100)$  interfaces have shown that barriers are not governed by the Schottky-Mott model [1,2]. The SXPS results presented in this study have shown that band bending occurs at the metal- $\text{In}_{0.53}\text{Ga}_{0.47}\text{As}(100)$  interfaces, in good agreement with the barrier heights recorded by I-V for corresponding metal-semiconductor contacts. Similarly band bending occurs at the metal- $\text{In}_{0.52}\text{Al}_{0.48}\text{As}(100)$  interface. However the magnitude of the band bending was not of the order of the barrier heights observed for equivalent metal- $\text{In}_{0.52}\text{Al}_{0.48}\text{As}(100)$  barrier measured by I-V. The most logical conclusion then, is that the Fermi level at the metal- $\text{In}_{0.53}\text{Ga}_{0.47}\text{As}(100)$  interfaces examined in this study is pinned as a result of metal deposition, whereas for the metal- $\text{In}_{0.52}\text{Al}_{0.48}\text{As}(100)$  interfaces, band bending has occurred before metallisation and is further adapted by the presence of the metal.

### (i) *Metal- $\text{In}_{0.53}\text{Ga}_{0.47}\text{As}(100)$ barrier formation*

I-V studies have shown that for intimate In- $\text{In}_{0.53}\text{Ga}_{0.47}\text{As}(100)$  contacts, the barrier height increases, as the temperature at which the interface is formed is reduced [1]. Photoemission studies of metal interface formation with As-decapped  $\text{GaAs}(100)$  surfaces held at low temperature predict that barrier heights on these surfaces are a result of pinning of the Fermi level by gap states arising from chemically induced defects, incorporated following the reaction of the deposited metal with the semiconductor surface [3,4]. It has been proposed that the use of low substrate temperatures ( $\approx 100\text{K}$ ) inhibits these chemical reactions and under these conditions the

barrier heights should approach the Schottky limit. The validity of this hypothesis has been examined using the  $I$ - $V$  technique for diodes formed on "as grown"  $\text{In}_{0.53}\text{Ga}_{0.47}\text{As}(100)$  surfaces at room and low temperatures, and no correlation between metal work function and  $\phi_b$  was found [1]. Furthermore SXPS results presented here of  $\text{Au-In}_{0.53}\text{Ga}_{0.47}\text{As}(100)$  interface formation at room and low temperature have shown that a reaction takes place between out-diffused As and Au in the growing overlayer regardless of interface formation temperature. It is possible, however, that the alteration of the nature of the  $\text{In-In}_{0.53}\text{Ga}_{0.47}\text{As}(100)$  interface brought about by the use of different metallisation temperatures can influence the Fermi level pinning behaviour and hence the size of the resulting Schottky barrier.

The results presented here indicate that the use of low temperatures for In deposition can reduce metal clustering and inhibit As out-diffusion. It is reasonable then, to propose that the corresponding change in the geometry of the interface may alter the distribution of surface states in the gap, so leading to a different pinning position. The out-diffusion of As observed for RT deposition will inevitably result in a more complex and reacted interface, in comparison with LT deposition. This may be a contributing factor in the lower barrier height observed, as there is a distinct possibility that the differences in the chemical bonding at the RT and LT interfaces will result in different pinning positions. It should be noted that for the case of  $\text{Au-In}_{0.53}\text{Ga}_{0.47}\text{As}(100)$  interface formation where As out-diffusion was observed for both temperatures, the resulting contacts were found to be "Ohmic". This indicates a possible correlation between As out-diffusion and the production of low Schottky barriers for the metal- $\text{In}_{0.53}\text{Ga}_{0.47}\text{As}(100)$  system.

(ii) *Metal-  $\text{In}_{0.52}\text{Al}_{0.48}\text{As}(100)$  barrier formation*

The Schottky barrier heights measured by SXPS for In and Au- $\text{In}_{0.52}\text{Al}_{0.48}\text{As}(100)$  interfaces formed at room temperature were found to be  $0.88 \pm 0.1$  eV and  $0.83 \pm 0.1$  eV respectively. These values correspond to Schottky barriers measured by the  $I$ - $V$  technique for intimate contacts, where In diodes produced barriers of 0.91 eV and Au diodes, barriers of 0.82 eV [2]. The results presented here indicate that the As decapping procedure does not significantly modify the electrical characteristics of the  $\text{In}_{0.52}\text{Al}_{0.48}\text{As}(100)$  surface. The Fermi shifts of  $\Delta E_F \approx 0.3$  eV and 0.25 eV observed during the formation of In- and Au- $\text{In}_{0.52}\text{Al}_{0.48}\text{As}(100)$  interfaces,

respectively, are well below the Schottky barrier heights. Hence it is deduced that band bending occurs at the clean (3×1) reconstructed  $\text{In}_{0.52}\text{Al}_{0.48}\text{As}(100)$  surface and that the pinning position is subsequently adapted upon metallisation. Although little is known about the nature of the surface states on clean  $\text{In}_{0.52}\text{Al}_{0.48}\text{As}(100)$ , as the bulk epilayer is *n*-type, the surface pinning states can be expected to have acceptor-like character. For *n*-type InAs, it is well understood that "Ohmic" contacts may be readily formed, as the charge neutrality level is located in the conduction band [5]. Conversely, Al-AlAs interfaces exhibit barriers, which are consistent with Fermi level pinning close to the middle of the energy gap [6]. One might therefore expect that the Fermi level at these metal- $\text{In}_{0.52}\text{Al}_{0.48}\text{As}(100)$  interfaces will be pinned in the region between mid-gap and the conduction band. This in fact seems to be the case, as examination of the Fermi edge and valence band maximum at the clean  $\text{In}_{0.52}\text{Al}_{0.48}\text{As}(100)$  surface at room temperature shows that the Fermi level lies in a region of  $0.58\text{-}0.68 \pm 0.1$  eV below the conduction band minimum. The mid gap point being  $\sim 0.7$  eV below the conduction band minimum.

Metallisation of the  $\text{In}_{0.52}\text{Al}_{0.48}\text{As}(100)$  surface appears to adapt the density and distribution of states at the interface, so leading to a new Fermi level pinning position. This may be related to the introduction of extrinsic interface states emanating from the quantum mechanical coupling of semiconductor and metal wavefunctions, following the "metal induced gap states" (MIGS) model [7]. Alternatively, the "unified defect model" predicts that similar states are created by the introduction of deep defect levels when the metal contact is made [8]. For both In- and Au- $\text{In}_{0.52}\text{Al}_{0.48}\text{As}(100)$  interfaces, there is a distinct possibility that MIGS may result in an adaptation of the pinning position. For the particular case of the In- $\text{In}_{0.52}\text{Al}_{0.48}\text{As}(100)$  interface, in which no chemical reactions or inter-diffusion have been resolved, the validity of the application of the UDM to interpret the observed adaptation of pinning position remains an open question. On the other hand, the Au- $\text{In}_{0.52}\text{Al}_{0.48}\text{As}(100)$  interface appears complex and reacted; with As diffusing from the substrate into the Au overlayer to form an Au/As compound. The  $\text{In}_{0.52}\text{Al}_{0.48}\text{As}(100)$  onto which the Au is deposited is predominantly InAs rich. Furthermore, as the bond energies of In-As and Al-As are 1.41 eV and 1.98 eV, respectively, it is highly likely that the majority of the out-diffused As will come from this surface region leaving a combination of defects and an excess of In [9,10]. Therefore, the probability that deep level defects will alter the density of states at the Au- $\text{In}_{0.52}\text{Al}_{0.48}\text{As}(100)$  interface is significantly greater in this case. This may account for the observed differences in  $\phi_b$  and  $\Delta E_F$  for In- and Au- $\text{In}_{0.52}\text{Al}_{0.48}\text{As}(100)$  interfaces

formed at room temperature. It should also be noted that once more the lower barriers were observed at interfaces where As out-diffusion has taken place.

Low temperature metal deposition appears to have little effect on the nature of the interface formed for either of the two metals in question; a slight reduction in overlayer clustering was observed in both cases. However the barrier heights observed by SXPS for both metals showed a reduction in  $\phi_b$  of  $\sim 0.1$  eV compared to metallisation at room temperature. This difference in  $\phi_b$  is of the order of the error in barrier height measurement by SXPS and hence it is difficult to say with confidence that there is a change in Schottky barrier height for low temperature metal deposition. It would be beneficial to correlate these findings with I-V measurements of In and Au diodes formed on  $\text{In}_{0.52}\text{Al}_{0.48}\text{As}(100)$  at room and low temperatures. Unfortunately it was not possible to conduct low temperature I-V experiments during the period of research, and this should be the subject of future investigation.

### 8.3 Conclusions

The effect of cryogenic processing on the Schottky barrier heights of intimate metal- $\text{In}_{0.53}\text{Ga}_{0.47}\text{As}(100)$  and  $\text{In}_{0.52}\text{Al}_{0.48}\text{As}(100)$  interfaces have been studied for the first time by SXPS and TEM. I-V studies have shown that the low Schottky barriers ( $\phi_b \approx 0.3$  eV) at intimate In- $\text{In}_{0.53}\text{Ga}_{0.47}\text{As}(100)$  interfaces formed at room temperature can be increased ( $\phi_b \approx 0.45$  eV) if the In is deposited onto the  $\text{In}_{0.53}\text{Ga}_{0.47}\text{As}(100)$  surface held at low temperature. However, Au deposition onto clean  $(3\times 1)$  reconstructed  $\text{In}_{0.53}\text{Ga}_{0.47}\text{As}(100)$  at both room and low temperature produced barriers that were "Ohmic" in nature [1]. Room temperature I-V studies of In and Au diodes formed on clean  $(3\times 1)$  reconstructed  $\text{In}_{0.52}\text{Al}_{0.48}\text{As}(100)$  have shown that Schottky barriers for In diodes ( $\phi_b \approx 0.91$  eV) were larger than those obtained for Au diodes ( $\phi_b \approx 0.83$  eV) in direct contrast to the Schottky-Mott model [2].

The SXPS results presented here indicate that the use of low temperature deposition appears to inhibit As out-diffusion for the In- $\text{In}_{0.53}\text{Ga}_{0.47}\text{As}(100)$  interface resulting in a more abrupt interface compared to room temperature formation. However the reduction in metallisation temperature fails to deter Au from perturbing the interface with either  $\text{In}_{0.53}\text{Ga}_{0.47}\text{As}(100)$  or  $\text{In}_{0.52}\text{Al}_{0.48}\text{As}(100)$ , resulting in interfaces that are reacted, and As out-diffusion into the Au overlayer to form an Au/As compound. The

In-In<sub>0.52</sub>Al<sub>0.48</sub>As(100) interface was found to be relatively abrupt for both room and low temperature deposition.

Comparison of the barrier heights measured by the I-V technique with those measured by SXPS indicate that barriers to In<sub>0.53</sub>Ga<sub>0.47</sub>As(100) are determined by pinning of the Fermi level by defect related or metal induced states brought about by the deposition of the metal onto the semiconductor surface. The Fermi level at the clean In<sub>0.52</sub>Al<sub>0.48</sub>As(100) surface however, appears to be pinned prior to metal deposition by similar states and subsequently adapted further, upon metallisation. Furthermore SXPS results have shown that As out-diffusion was evident at the majority of interfaces examined. Schottky barriers at interfaces where As out-diffusion was prevalent tend to produce lower barriers than the more abrupt interfaces. It is highly likely then that the incorporation of defects and the change in stoichiometry at these reacted interfaces will result in an adaptation of the Fermi level pinning position which may be detrimental to the height of the Schottky barrier formed. Low temperature deposition appeared to reduce metal overlayer clustering in all cases and it is assumed that this is a consequence of a reduction in surface mobility of the metal adatoms on the semiconductor surface. The resulting overlayers at low temperature had a smaller grain size (as examined by TEM) than those formed at room temperature, showing a tendency towards a more amorphous yet laminar mode of growth.

#### 8.4 Future work

Although there has been a clear correlation between the barrier heights observed on As decapped and “as grown” In<sub>0.53</sub>Ga<sub>0.47</sub>As(100) and In<sub>0.52</sub>Al<sub>0.48</sub>As(100) surfaces, it is possible that surface damage and non-uniformities may occur due to the decapping technique. This may result in defect related states in the forbidden gap which will pin the Fermi level prior to metallisation. To fully evaluate the significance of these factors, a technique such as Scanning Tunnelling Microscopy (STM) would be ideal, and this should be the focus of a future study.

The photoemission technique has been utilised in this study to corroborate the values of I-V measured Schottky barrier heights observed for In and Au contacts to clean (3x1) reconstructed In<sub>0.53</sub>Ga<sub>0.47</sub>As(100) formed at room and low temperature and also In and Au diodes on clean (3x1) reconstructed In<sub>0.52</sub>Al<sub>0.48</sub>As(100), formed at room temperature. The barrier heights at In- and Au-In<sub>0.52</sub>Al<sub>0.48</sub>As(100) interfaces formed at

low temperature have been reported for the first time by SXPS, to the best knowledge of the author. However the accuracy of barrier height determination from photoemission measurements is rather limited, being  $\sim \pm 0.1$  eV in favourable cases [10]. Hence for the case of In and Au diodes formed on  $\text{In}_{0.52}\text{Al}_{0.48}\text{As}(100)$  at low temperature, it would be useful to conduct I-V measurements to provide more accurate values for the Schottky barriers formed.

It has been shown that cryogenic processing offers a degree of control of the interfacial properties of metal- $\text{In}_{0.53}\text{Ga}_{0.47}\text{As}(100)$  and  $\text{In}_{0.52}\text{Al}_{0.48}\text{As}(100)$  systems. Extending this study to other metals and semiconductor materials would offer a broader picture of the effect of its validity as a tool in device processing.

## 8.5 References

- [1] S.A. Clark, S.P. Wilks, A. Kestle, D.I. Westwood and M. Elliott, *Surf. Sci.* **352-354**, 850 (1996)
- [2] S.A. Clark, S.P. Wilks, J. I. Morris, D.A. Woolf and R.H. Williams, *J. Appl. Phys.* **75**, 2481 (1994)
- [3] R.E. Vitturo, S. Chang, J.L. Shaw, L.J. Brillson, P.D. Kirchner and J.M. Woodall, *J. Vac. Sci. Technol.* **B7**, 1007 (1989)
- [4] S. Chang, J.L. Shaw, R.E. Vitturo, L.J. Brillson, P.D. Kirchner and J.M. Woodall, *J. Vac. Sci. Technol.* **A8**, 3803 (1990)
- [5] L.J. Brillson, M.L. Slade, R.E. Vitturo, M.K. Kelly, W. Pache, G. Margaritondo, J.M. Woodall, P.D. Kirchner, G.D. Petit and S.L. Wright, *J. Vac. Sci. Technol.* **B4**, 919 (1986)
- [6] M. Missous, E.H. Rhoderick, K.E. Singer and W.S. Truscott, *J. Cryst. Growth*, **111**, 116 (1991)
- [7] J. Tersoff, *Phys. Rev. Lett.* **52**, 465 (1984)
- [8] W.E. Spicer, I. Lindau, P. Skeath and C.Y. Su, *J. Vac. Sci. Technol.* **17**, 1019 (1980)
- [9] E.H. Parker, Ed., "The Physics and Technology of Molecular Beam Epitaxy", Plenum, New York, 1985.
- [10] E.H. Rhoderick and R.H. Williams, "Metal-Semiconductor Contacts", Clarendon Press, Oxford (1988) and references therein.